Ultrafast excited state dynamics and dispersion studies of optical nonlinearities in Porphycenes, Naphthobipyrroles, Phthalocyanines, and Porphyrins

A Thesis Submitted for the degree of
Doctor of Philosophy in Physics

by

DEBASIS SWAIN

Under the supervision of

Dr. Soma Venugopal Rao

Advanced Centre of Research in High Energy Materials (ACRHEM)
University of Hyderabad
Hyderabad 500046

March 2014

Dedicated to

My parents and family…

&

My thesis supervisor

DECLARATION

I hereby declare that the matter embodied in the thesis entitled "**Ultrafast excited state dynamics and dispersion studies of optical nonlinearities in Porphycenes, Naphthobipyrroles, Phthalocyanines, and Porphyrins**" is the result of investigation carried out by me in ACRHEM, University of Hyderabad, India, under direct supervision of Associate Prof. Soma Venugopal Rao.

HYDERABAD **(DEBASIS SWAIN)**

DATE

CERTIFICATE

This is to certify that the work described in this thesis entitled **"Ultrafast excited state dynamics and dispersion studies of optical nonlinearities in Porphycenes, Naphthobipyrroles, Phthalocyanines, and Porphyrins"** has been carried out by Debasis Swain, under my direct supervision and this has not been submitted for any degree or diploma at this or any other University.

Place: Hyderabad
Date:

Supervisor **Director, ACRHEM**

(S. Venugopal Rao)

ACKNOWLEDGEMENTS

A number of people are involved directly or indirectly to make this Ph.D. thesis in the final shape. I express my deep sense of gratitude and profound thanks to my thesis supervisor, S. Venugopal Rao, for his inspiring guidance and constant encouragement throughout the course of these research findings. I have been able to learn a great deal in this fascinating field of research through his inspiring and thought provoking discussions, and I consider my association with him a rewarding experience. His guidance to me goes even beyond science and he has helped me to grow as a strong individual. In my 5 years and 9 months as a doctoral student at advanced centre of research in high energetic materials (ACRHEM) in university of Hyderabad (UoH), I have learned a great deal about both science and life. The journey has been challenging as well rewarding. I am grateful to my thesis advisor for the lesson he taught me about ultrafast optics, research journals browsing technique and life as a scientist. He changed my view that science is above any religion. He consistently encourages me to progress with the time. I cannot forget his trust on me in my lifetime. I am a proud member to be in his research team (Gopala Krishna, Sreedhar, Hamad, Anusha, Sreeja, Nageswar, Ajay, Kalam and Mounika, Radhakant, Benoy). I thank all the non-teaching staff (Venkata Subbaiah garu, Satyanarayana garu, Rajeswar garu, Subhash garu, Ananta Rao garu, Mahesh, Nagaraj, Pravin, Gopal, Prabhakar) of ACRHEM for their assistance on various occasions during my Ph.D.. Defence Research Development Organization (DRDO) through ACRHEM, India is gratefully acknowledged for providing me a fellowship (JRF/SRF).

I thank present Director (Dr. K. Venkateswara Rao) for encouraging me to focus in study. I also thank former director Dr. D. K. Setua and Prof. M. Durga Prasad for giving some useful comments/suggestions regarding useful tips to shape the thesis in present form. I thank also Prof. Surya P. Tewari, founder Director of ACRHEM, and associate faculties of ACRHEM for their co-operation in providing experimental facilities. I should also express my sincere thanks to Dr. G. Manoj Kumar and Dr. Anil Kumar Chaudhary for their constant support as doctoral committee members in the development of femtosecond pump-probe experimental set up at ACRHEM. I thank a lot to Dr. P. Prem Kiran for analysis of Z-scan and pump-probe results. I am

also thankful to Dr. G. Vaitheeswaran for giving me constant moral support and fruitful discussions about theoretical research.

My association with Dr. Sai Santosh, School of physics has been very rewarding and heartfelt sincere thanks to him. I also express my appreciation for Dr. N.K.M. Naga Srinivas, UCL, London for providing feedback on few chapters of my thesis. Research scholars (Dipak, Alee, Sriramulu, Kuladeep, Balu) along with of Prof. D. Narayana Rao helped me a lot in knowing ultrafast optics with valuable discussions. I would like to thank Dr. L. Giribabu (IICT, Hyd.) and his students (Varun, Krishna), for providing me the phthalocyanines sample molecules for the multi-photon/pump-probe studies. I would like to thank Dr. Pradeepta Kumar Panda (School of chemistry, UoH) and his students (Tridib, Anup, Nandakishore) for providing me the molecules of porphycenes, cyclo[4]naphthobipyrroles and porphyrins for multiphoton/pump-probe studies. I thank Mr. O. E. Jagadesh and Arun Kumar of Laser Science for his constant support of laser facility for my experiments. Special words of appreciation to all my associations with physics students at ACRHEM such as Vijayalakshmi madam, Dr.Sudha, Sita Lakshmi, Balaji, Leela, Silpa, Ramesh, Bheem, Kondaiah, Ramaiah, Ashwin, Anubham, Bharat, Nagendra, Ramakant, Fahem, Venkatesh, Konda, Rakesh, Manikanta, Sai Shiva, Vinod, Venkateswarulu, Sachin, Ravi, Yedukondalu, Ganesh for constantly encouraging and supporting me throughout my time at UoH to accomplish the research goal. Without the support of these guys this thesis work wouldn’t have been successful.

I express my sincere gratitude to Dr. Narayan Sethi for his inspiring words of wisdom in early days at UoH. My stay on this campus has been pleasant with the association of many other students whose list cannot be mentioned due to lack of space. I would like to thank T. Shuvan Prashant of SSSU (now at NUS, Singapore) for learning/writing the LabVIEW code for data acquisition. I thank Dr. J. Clark (University of Cambridge), Dr. N. Sri Ram Gopal (now faculty at HCU), Dr. N. Kamaraju (IISc, Bangalore) and Dr. J. Jayabalan (RRCAT, Indore) for giving very valuable suggestions regarding development of femtosecond pump-probe experiments.

The unconditional love of my Maa, Baba, Sasu, Sasur, Aja, Aie, Dada, Khudi and in the memory of late Bou and Nana, Budha bapa for their blessings, made me what I am today and I owe everything to them. A Special word of thank to my two little sweet sisters (Sasmita and Namrata) for having faith on me to complete this thesis. I owe my special thanks to my beloved wife (Trupti) and my daughter (Debishree) for their sacrifices to make this possible. I would like to thank all my family members (Amar mamu, Rosy, Omi, Avinash, Jagu, Guddu, Gungun, Uttam) and relatives (Ganesh Bhaina and Koko nani, Bablu, Didi, Bhaina, Muna Bhai, Phukuna bhai, Ayush, Khusi, Tezas, Sidhu, Srimukta, Sai Saranya, Narayan) for their support and guidance throughout my life. At this juncture, I should extend my sincere thanks and deep appreciation to all my friends (Durga, Gyan, Laxmi, Sanjib, Kartik, Ramesh, Pravat, Satchi, Gopal, Parameswar, Maya, Pradip, Bijaya, Basu, Pramila, Suchitra, Minashkhi and Urmishree) and my seniors Akhyaya bhai, Biswajit bhai, Jhasa bhai and Sumant bhai for being my strength right through the course of my Ph.D. days. I wish to all my facebook friends for their moral support throughout the research career.

This Thesis/dissertation is a culmination of all the efforts of my teachers, right from childhood to Ph.D. As a final note, I would like to express my love and gratitude to Swami Vivekananda, who is my source of inspiration, and who taught me the basic principles of life. I thank him for giving me patience and perseverance to endure challenges in my life. I dedicate this thesis to his lotus feet.

Arise, Awake, and Stop not till goal is achieved.

List of Figures

Chapter 1

Chapter 2

Chapter 5

List of Tables

TABLE OF CONTENTS

Chapter 1

Introduction and Motivation

1.1 Ultrashort Laser Pulses and Energetic Materials

LASER is the acronym of Light Amplification by Stimulated Emission of Radiation. Theodore Maiman demonstrated the first working laser [1] in 1960. A laser can be classified as operating in continuous wave (cw) or pulsed mode. A solid state pulsed laser such as Titanium-doped sapphire (Ti: sapphire) produces a highly tunable infrared laser, commonly used in spectroscopy. Ultrashort laser pulses are being used for basic as well as applied research in frontier laboratories, hospitals, metrology, communications, spectroscopy, terahertz science, medicine, material processing and defense technological applications in recent times [2]. Ultrafast lasers based research and development has been an active area for probing light and matter interaction. One can use short pulsed lasers with high peak power to measure dynamical behavior in sample on extremely fast timescales. Such time-resolved measurements capture snapshots of an event as it happens, which can built up into a full sequence, mapping out exactly what is going on at any given time. In this thesis we have focused our research to study the interaction between light and matter at femtosecond (fs), picosecond (ps) and nanosecond (ns) time scales. It is a major tool used for the determination of quantum energy levels in atoms, molecules, semiconductors, etc. For example, molecules possess vibrational and rotational degrees of freedom. Such motion is quantized, i.e., only motion corresponding to discrete rotational, vibrational/electronic energies is allowed. Spectroscopy, which investigates transitions between these quantized states, is the primary tool in elucidating the energy-level spacing. In nature we have a lot of phenomena that take place in a very short time scales (ps and fs time scales) such as electron-phonon scattering, chemical reactions and photo dissociations. These short time intervals cannot be time resolved by our fastest available electronic instruments such as fast detectors and oscilloscopes. Therefore, to resolve such phenomena that occur in ultrafast time scale, we need a technique called as “pump-probe technique”. Fs technology is a significant achievement since in this regime, the movement of light seems insignificant i.e. in one fs light travels only 300 nm. Broadly one can envisage two powerful applications of fs pulses in optics - in probing processes on a fs time scale and creating high intensity photons. The latter has generated further interest in studying the interaction of fs pulses with optically transparent materials because at such high peak intensities even these materials absorb laser radiation through multi-photon processes.

An energetic material is a substance which stores a large amount of energy and can be initiated to undergo rapid decomposition, usually accompanied with generation of high pressure, heat or light and sound. The first application of explosives in human's history could be dated back to the invention of black powder in 9^{th} the century in China. The invention of nitroglycerine (NG), dynamite and gelignite in 19^{th} century marked a breakthrough in the explosive field, due to greater power and improved safety of those materials. Since World War II, two new explosives, RDX and HMX, have been extensively utilized in both sectors of military and industry. High Energetic materials (HEMs such as explosives, propellants and pyrotechnics) are extensively used for both civilian and military applications. Worldwide various research programmes are going on to develop pyrotechnics with reduced smoke and new explosives and propellants with higher performance or enhanced insensitivity to thermal or shock insults. Decomposition of energetic materials is a complex dynamical process involving events that span a wide range of time scales. Elementary intra-molecular motions including those involved in molecular vibrations, bond breakage, and bond formation occur in 10 to 100's of fs. Elementary collective motions including those that mediate lattice vibrations, intermolecular collisions, and shock front propagation between neighboring lattice sites occur on the hundreds of fs time scale. While macroscopic shock front propagation, build-up of energetic primary reaction products, and detonation occur on much slower time scales, elucidation of the elementary events is crucial to understand the microscopic mechanisms of energetic material decomposition. It has recently been suggested [3] that molecular excited states may play a decisive role in ignition of detonation. It is then very important to observe the characteristics and the behavior of molecular excited states. Comparison of excited state properties of explosive and non-explosive molecules may indeed allow understanding the specificity of explosive molecules and, finally, the key of the ignition of explosion and detonation processes. However, excited state lifetimes may be very short and these states, after excitation, may evolve and be transformed on a sub-ps time-scale. It is necessary to observe these excited states with a sub-ps time-resolution. With fs time resolution, one can freeze atoms in motion and study the evolution of molecular structures as reactions unfold and pass through their transition states, thus providing a motion picture of the transformation. Nelsons group at Massachusetts Institute of Technology [4-5] performed fs time

resolved study of Tri-Nitro Azetadine (TNAZ). Decomposition of HEMs can be initiated by different processes, including sparks, arcs, shocks, compression waves and light. These events induce electronic excitation in energetic molecules. In principle, a number of photochemical and photophysical processes can occur following electronic excitation of an energetic molecule: these include radiative transitions, such as fluorescence and phosphorescence, non-radiative transitions, such as internal conversion (IC), intersystem crossing (ISC) and excited state photochemistry. Among these IC is particularly important since it initiates the decomposition of energetic molecules via transferring electronic energy to the vibrational degrees of freedom of the excited electronic state potential energy surface (PES). The basic idea behind the present research problem is that energetic materials are excited electronically ($S_0 \rightarrow S_n$) upon shock, spark, plasma, laser, etc. ignition event, and these excited electronic states are the initiators of the decomposition process in which an energetic molecule releases its energy. The initial step in this process releases small radical molecules, such as NO, N_2, NH_3, etc., and this process occurs rapidly, of the order of 100 fs. The mechanisms for this release of energy involve radiation less and non-adiabatic electronic state interactions and transition involving conical intersections between potential energy surfaces. Reed et al. [6] performed the first atomistic simulation of an azide energetic material (HN_3) from beginning to the end of chemical evolution and discovered that the time scale for complete decomposition was ~10 ps, orders of magnitude shorter than that of secondary explosives and approaching the fundamental limiting time scale for chemistry; i.e., vibrational time scale. Strachan et al. [7] utilized reactive force field (ReaxFF) to describe the high energy nitramine RDX and used it with molecular dynamics (MD) to study its shock-induced chemistry. Their simulations show clearly that the primary reactions leading to NO_2, OH, NO, and N_2 occur at very early stages. They also found that although the barrier for the pathways leading to NO_2 and HONO was essentially the same, NO_2 was the main product for low shock velocities (<6 km/s), in agreement with experimental data. However, there is little known literature available about the coupling between the mechanical loading and detonation initiation in HE materials. Such a fundamental understanding is critical for the design of next-generation materials with improved performance and sensitivity.

Fs laser pump-probe techniques were successfully utilized in understanding the dynamics of photo dissociation in HMX, RDX from excited electronic states at 230 nm, 228 nm, 226 nm to monitor the time evolution of the NO product [8]. Decomposition studies of RDX in the gas phase at ~225 nm generate NO as initial product. The generated nascent NO is vibrationally hot (T_{vib} ~1800 K) and rotationally cold (~20 K). The dynamics of NO formation is faster than 180 fs. Bernstein's group [8-14] from Colorado state university has extended efforts towards understanding of the critical role of non-adiabatic couplings in the initial steps of the excited electronic state decomposition of energetic materials. This group focused on understanding the mechanism, dynamics of decomposition of HEMs. Different decomposition channels were observed for model compound like dimethylnitramine (DMNA) with different experimental conditions. These experiments provide a potentially useful methodology for accurate and predictive determination, design, and synthesis of new energetic materials. Nitro-group stretching modes lifetimes of few ps for several energetic molecules at room temperature have been evaluated [15]. Pump pulse creates a non-stationary medium while the probe pulse propagates in medium and absorbs. The production of fs optical pulses to investigate induced nuclear motion in molecules and in a medium. Duration of pump pulse is shorter than periods of some vibrational modes of molecule. The speed of atomic motion is ~1 km/s and, therefore, to record atomic scale dynamics over a distance of ~1 A^o, average time required is ~100 fs.

Nano-sized energetic materials offer the potential of high heat release rates, increased combustion efficiencies, tailored burning rates, and reduced sensitivity. Nano-energetic materials can provide a significant enhancement in the rate of energy release as compared with micro-scale materials. The ability to control the temporal pulse-intensity profile leads to greater control over the effects of ablative heating and the resulting shockwave propagation. Nano-energetic materials such as nano-aluminum are a fast-growing research area in explosives and propellants because of the high heat release and fast reaction. However, determination of the nano-material heat release rate is a challenge because of the short reaction time scale. Prof. Dlott's research group (at the University of Illinois) focused on different aspects of ultrafast spectroscopy of nano-energetic materials and shock induced chemistry [16-19]. They had also performed some pioneering experiments on one of the simplest HEM,

Nitromethane (NM) [20]. NM is an insensitive explosive liquid, the simplest of nitro-organic molecular explosives. It is believed that vibrational energy plays key roles in both shock initiation and detonation processes. When an initiating shock wave is present translational energy from the shock front must be driven into NM vibrations, a process termed "multiphonon up-pumping". Once these reactions have been initiated and exothermic chemistry begins, energy from the excited vibrations of hot nascent molecular species such as HONO and HCN must be converted into translational energy for driving the detonation wave. IR-Raman measurements of NM-h_3 with CH-stretch excitation demonstrated that vibrational cooling (VC) occurred in three different stages. In the first stage parent excitation decayed within ~3 ps simultaneously populating all lower-frequency vibrations. These excited daughter vibrations could be divided into a midrange tier (1600-1000 cm^{-1}) and a lower-frequency tier (1000-480 cm^{-1}). In the second stage, excitations in the midrange tier decayed into the lower-frequency tier in ~20 ps. The lower frequency tier thus became excited in two stages, the first lasting ~3 ps and the second ~15 ps. In the third stage, excitations of the lower-frequency tier decayed into the bath in 30-50 ps. The initial CH-stretch excitation became thermalized on the ~100 ps time scale. The instantaneous populations of most of the fifteen NM vibrations were determined with good accuracy. Figure 1 shows a typical energy level diagram depicting all the vibrational relaxation times of NM.

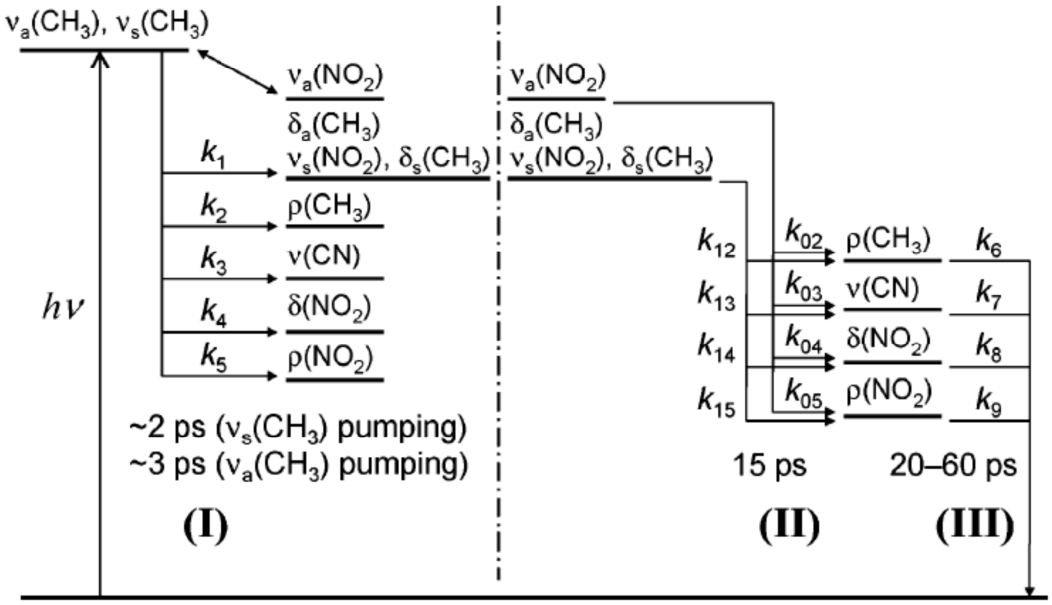

Figure 1 Energy level diagram showing the kinetic model with three stages of vibrational relaxation used to fit the NM-*h*3 data. Figure is adapted from reference [20a]

Energetic materials can explode only by shock ignition in condensed phase. The shearing of crystal planes can cause large electric fields ~10^8 V/cm that can generate excited atoms, ions and radicals, all of which can be highly chemically reactive. Ignition processes involving sparks, shock, lasers, and arcs can all initiate the decomposition reaction of energetic material by generating excited electronic states. Decomposition of energetic materials following electronic state excitation has been experimentally proven to play an important role in their overall decomposition mechanisms and kinetics. Final decomposition products are characterized by their rotational, vibrational, and electronic state populations. Since decomposition of energetic materials occurs within the fs time scale, experimental identification of the intermediates and their decomposition dynamics offers a number of challenges. We anticipate that decomposition mechanisms of simple model systems, if understood, will help us to understand some of the complex reactions that are involved in the decompositions of energetic materials. Though limited in their absolute structural resemblance to the energetic materials, the model systems can provide a point of departure and a baseline comparison for the study of the excited electronic state decomposition mechanisms of the complex energetic materials. The field of energetic materials is now maturing through innovative methods such as fs spectroscopy and enabling the diagnostics of energy release rates or measurements of reaction products via fs spectroscopy. The aforesaid spectroscopy extends the investigation of hot spot formation of microsecond durations, combustion rates from few meters to detonations at few km/s and deformations from drop-weight impacts to shock wave loading. Creation of biomedical skeletal structures, shell casings, metal foam structures, environmentally attractive igniters or cartridge primers, and missile components are providing a new dimension for many touted applications of energetic materials. Knowledge of the optical absorption properties of nano-metallic particles will redound to an understanding of the ignition energy and time, thereby allowing materials to be tailored for specific applications. Time dependence of steady state energy levels show some limitation to pump-probe processes as theoretically suggested by Fain et al. [21].

Kuklja et al. [22] performed a combined theoretical and experimental study to understand the initiation of chemistry process in high explosive crystals. In particular,

they were investigating the relationship between defect-induced deformation of electronic structure of solids, electronic excitations, and chemical reactions under shock conditions. Moore's group [23a] achieved exquisite time synchronicity between shock and diagnostics (needed to unravel chemical events occurring in picoseconds) using a shaped ultrafast laser pulse to both drive the shocks and interrogate the sample via a multiplicity of optical diagnostics. The shaped laser drive pulse produced well-controlled shock states of sub-ns duration with sub-10 ps rise times, sufficient for investigation of fast reactions or phase transformations in a thin layer with ps time resolution. They also investigated ultrafast laser generated shocks [23b] using electronic absorption spectroscopy in the range 400–800 nm to address the extent to which electronic excitations are involved in shock induced reactions. They presented the data on shocked Polymethylmethacrylate (PMMA) thin films and single crystal pentaerythritol tetranitrate (PETN). Their group also measured the Hugoniot and shocked refractive index of cyclohexane subject to shock loading using ultrafast dynamic ellipsometry and transient absorption spectroscopy [23c, 23d]. The same group also studied shock to detonation transition of NM by using ultrafast experiments recently [23e]. Roy et al. [24] performed spatially and temporally resolved temperature measurements behind an expanding blast wave using picosecond N_2 coherent anti-Stokes Raman scattering (CARS) technique following laser flash heating of mixtures containing Al nanoparticles embedded in ammonium-nitrate oxidant. It is evident from the above mentioned works that ultrafast events occurring in the decomposition/detonation of HEMs is not clearly understood. Therefore, there is a necessity to develop ultrafast spectroscopic techniques to study such processes (in the sub-ps time scales) so as to enable us to understand the energy dissipation/distribution during detonation/decomposition processes and further utilize this information, probably, to develop superior energetic materials.

1.2 Historical development of time-resolved phenomena

High-speed photography is the science of taking pictures of very fast phenomena. Muybridge (photographer) was the first to perform the time-resolved experiments could able to resolve events of the order of 1 ms with fast photography during 1878 [25]. This concept was extended to laser-based time-resolved experiments to study physical, chemical, and biological processes. A first intense

pulse (called pump pulse) is used to initiate dynamics in the system under scrutiny. Then a second laser pulse interacts with the system, becoming encoded with information about its properties at the moment of arrival. Thus by changing the relative time delay between the pulses a series of snapshots are observed. This technique is the heart of the pump-probe experiment. In order for these snapshots to be of any use, regardless of the century, they need to clearly resolve what they are measuring. Muybridge experiments with "Horse in Motion" (1878) set the platform for time-resolved experiments. Topler performed the first known pump–probe experiment [26]. He used a 2 μs spark to initiate a sound wave and then photographed the propagation using a second spark triggered with an electrical delay. The first photograph of a supersonic flying bullet was taken by the Austrian physicist Peter Salcher in 1886, a technique that was later used by Ernst Mach in his studies of supersonic motion. German weapons scientists applied the techniques in 1916. High speed camera can capture different fast events such as explosions, ballistic research and aircraft propeller disintegration in various temporal scales.

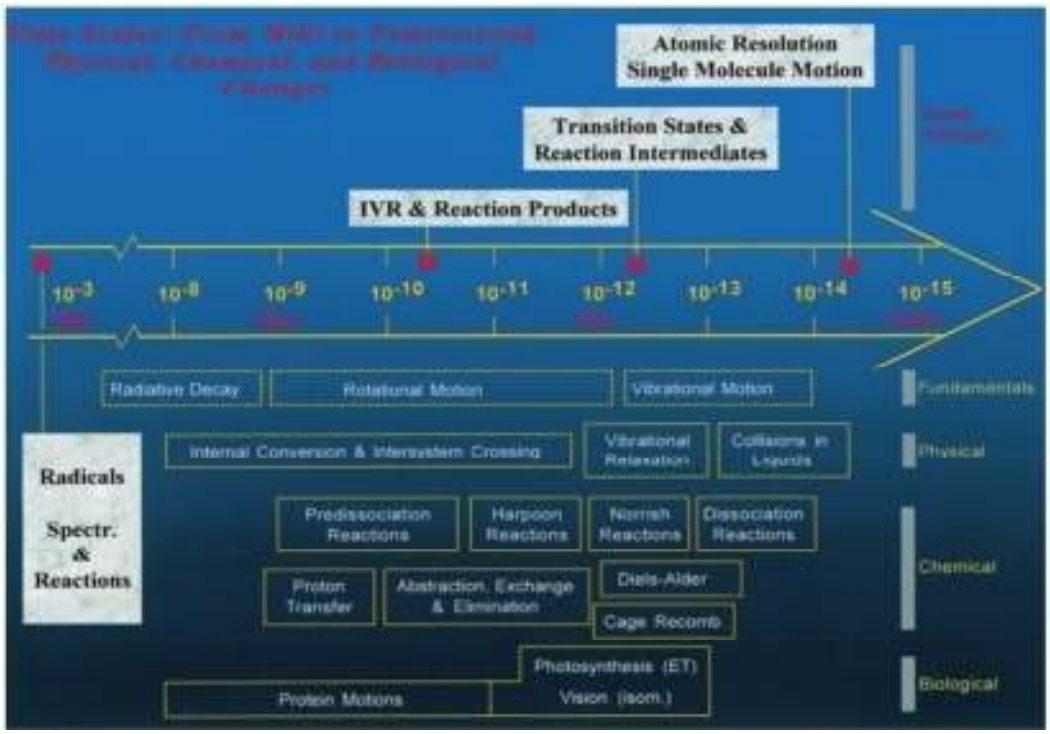

Figure 2 explaining the different timescales involved in various physical, chemical and biological processes. Adapted from Ahmad H. Zewail from Nobel lecture Dec 8, 1999/ J. Phys. Chem. A **104** (2000) 5660.

With the advent of time and technology one could able to resolve the events μs/ns with the electronics available. Ippen and Shank were improved the pump–probe

experimental technique using ultra-short light pulses [27, 28]. Time-resolved science has garnered two Nobel Prizes, marking important milestones in the speed with which dynamical events can be recorded. In 1967, the Nobel Prize in Chemistry was awarded to Manfred Eigen, Ronald G.W. Norrish, and George Porter "for their studies of extremely fast chemical reactions, effected by disturbing the equilibrium by means of very short pulses of energy" [29]. They were able to monitor chemical reactions taking place on microsecond (10^{-6} seconds) and nanosecond (10^{-9} seconds) timescales. The rapid growth in fs technology in the 80's and 90's paved the way for the second prize, awarded to Ahmed Zewail in 1999 "for his studies of the transition states of chemical reactions using fs spectroscopy" [29]. By using light in a manner similar to that described earlier, Zewail's group was able to capture reactions taking place on picosecond (ps, 10^{-12} seconds) and fs (fs, 10^{-15} seconds) timescales. Processes occurring on such short timescales are referred to as 'ultrafast' processes. They include not only chemical reactions, but also many operations taking place in different systems, where the nature of interactions gives rise to ultrafast events. Figure 2 depicts some of processes of importance with the different timescales involved in various fundamental, physical, chemical and biological phenomena.

The continuing development of ultrafast laser sources, and ever shorter probes they provide, has enabled a great progress in observing and understanding these fundamental processes, extending the approach of Zewail in new and exciting directions. In addition to underlying interactions studies, ultrafast technology has opened up the ability to control matter in new ways. Using laser radiation, material systems can be driven into new non-equilibrium states, inaccessible by more traditional methods. The properties of these new meta-stable phases can be controlled and altered by varying the properties of the driving laser, suggesting a wealth of potential technological applications based on short-lived or rapidly-changing effects. The investigation of ultrafast microscopic process such as intra molecular energy transfer in the light harvesting complexes in chlorophyll; intra-molecular electron, proton transfer, as in the reaction of photosynthesis; radiative decay of excited energy levels; dissociation and isomerization of excited molecule opens the way to understand the primary of chemical reactions. A thorough knowledge of these dynamical processes is of fundamental importance in many branches of physics, chemistry and biology. In order to study these natural process experimentally, one

needs sufficient high temporal resolution, which means that the resolvable minimum time interval must be shorter than the time scale of the process under investigation. The development of ultrafast laser pulses and new detection techniques permits achieve a very high temporal resolution [in the fs and attosecond (10^{-18}s) range] to study extremely fast process in nature. Tremendous progress in the generation, amplification, measurement of ultrashort light sources ensures that commercial sources are available at the moment to perform such studies.

The short duration of fs pulses makes them ideal tool to investigate the ultrafast process. One drawback is that the available electronic detectors are not fast enough to measure these ultrafast processes. This problem can be overcome by employing the pump-probe technique, called ultrafast pump-probe spectroscopy. The advantage of using ultra-short pulses is that they open the door to investigating the dynamics of the system directly, i.e., the movement of individual particles such as electrons or atoms. From the perspective of classical mechanics, a short pulse whose duration is on the same time scale as the motion of a particle in a confined system could be used to probe the dynamics of the particle directly. For typical atomic speeds of the order of 10000 m/s (= 0.1 A^o/fs), laser pulses 10 fs in duration achieve l A^o spatial resolution, a range that is of great scientific interest in physics and chemistry. In principle, fs time-resolved spectroscopy permits direct observation of the fast events of interest. However, there are several pre-requisites that must be satisfied. The most daunting challenge is posed by the irreversible destruction of the sample during the process under study. Ultrafast spectroscopy as it is normally conducted involves the use of an excitation pulse to initiate the events of interest and a temporally delayed probe pulse to monitor the sample at a particular time after excitation. This measurement, with the probe delay time held constant, is typically repeated many times to optimize signal/noise levels. The probe delay is then changed and iterations were continued to determine the sample response at a second delay time. This procedure is repeated with many different pump-probe delay times until the entire time-dependent sample response is mapped out. The entire procedure typically involves many thousands or millions of pump-probe repetitions. If the sample is a liquid or a gas, then irreversible change induced by the excitation pulse can be managed through continuous flow of fresh material into the irradiated region. For a solid-state sample, however, flow is not an option. Rastering of different sample

regions into the pump-probe beam path may be practical for a highly uniform semiconductor or polymer sample, but for energetic single crystals, often obtained as small and irregular pieces, this is rarely if ever possible. Thus, new methods must be developed that provide the entire ultrafast sample response in a single laser shot. On ps and slower time scales, the necessary time resolution is offered through fast electronic apparatus including streak cameras and digitizing oscilloscopes. On fs time scales, all optical methods must be developed.

To observe the behavior of molecular excited states with sub-ps time-resolution two main techniques are available. The first one is "pump-probe" experiments in which one excites the sample with a laser pulse and observes its behavior, after excitation, by means of a probe pulse. This method mainly involves electronic transitions occurring between excited states. At certain wavelengths, corresponding to electronic transitions between excited states, the probe pulse can be absorbed by the different excited species present in the sample after excitation. Other technique involves observing the transmission characteristics (dynamic and spectral) of the probe pulse through the excited sample providing information on the behavior of excited states. Apart from observing the behavior of a sample under excitation through changes of electronic transitions, it is also important to use spectroscopic methods to study the behavior of certain vibrational modes of the sample. When a molecule is excited we may expect to observe, for example, the disappearance or the evolution of its vibrational characteristics.

The production of fs optical pulses is to investigate induced nuclear motion in molecules and in a medium. Duration of pump pulse is shorter than periods of some vibrational modes of molecule. First one "pump" creates an event by applying a laser pulse that induces an excitation in the sample. The sample is disturbed from its equilibrium and returns to its initial state after some time. We keep pumping the sample at regular intervals that are longer than the response of the sample to ensure that there is no overlap of excitation events from the current pump and the previous pump. While the sample is changing, the response of the system to the excitation event that you created is probed by the other pulse. To come up with a complete picture, probing of the system over the entire cycle of the systems response to the event has been carried out.

Conversion	Space	Time
1	0.3 nm	1 attosecond (as)
2	0.3 μm	1 fs
3	1 μm	3.33 fs
4	10 μm	33 fs
5	1 mm	333 fs
6	1 cm	3.33 ps
7	1 m	3.33 ns

Table1 Space time conversion

The pump and the probe come from the same source. Part of the main beam from the laser is split off by a beam splitter and sent off to travel down a different path. This path includes a "delay line" which is a device that lengthens the optical path of the light relative to the pump beam. There is a retro on a motorized translation stage. The retero-reflector was positioned on the rail which can be navigated by the motion controller. If the retro reflector moves backwards and lengthens the path, it takes much longer time for the light to reach the sample than the pump beam. For example: If you move the retro-reflector back 1mm then the path is lengthened by 2 mm which provoke the probe pulse to travel (2×10^{-3} m /3.0×10^{8} m/s = 6.66 ps) an extra 6.66 ps to reach the sample. This means you can probe the sample ~ 7 ps after it has been pumped. If you keep doing that you can probe it at nearly 0, 7, 14, … etc ps after it has been pumped. Time and Space relative measures are given in table 1. This gives you the time evolution of some property of the system at one point on the surface of the sample as a function of time.

Pump-probe experiments with fs pulses are one of the most widely used approaches for extracting the information of carrier dynamics. In this experiment, a non-degenerate setup is preferred because it can provide more information about carrier flow among different energy states. A broad spectrum of the probe (WLC) can give the data of time-resolved spectral evolution for clearly demonstrates the whole carrier relaxation scenarios. For this purpose, usually a super-continuum generator or an optical parametric oscillator (pumped by a regenerative amplified mode-locked Ti:sapphire laser) is used. Here, we have used cross polarization for pump and probe for the study to avoid the pump induced contribution to the probe. Modification of pump-probe spectroscopy (similar to transient absorption spectroscopy) requires

differential amplifier with lock-in amplifier makes the system easy to detect the (ΔT/T) measurement ready. There may be presence of two component carrier relaxation process. The initial rapid processes occur at the time scale comparable to pulse duration, while the slower process occur on ps time scale. Theoretical fit to the data provides the respective relaxation time. We have calculated (ΔT/T) of liquid samples and (ΔR/R) measurement for solid samples.

In addition to those methods of control mentioned above, the properties of a material can also be perturbed using light. Unlike those methods, photo-excitation is a non-adiabatic process, shaking the system up in a highly non-equilibrium fashion. The effects of photo-excitation can vary depending on the material properties and nature of the light used, and range from simple carrier excitation to photo-induced structural and electronic phase transitions. Many different types of dynamics can arise from photo-excitation, and studying them can reveal a lot about the nature of the underlying interactions in the solid. Photo-excitation has been used in semiconductors for a long time to understand carrier relaxation and early-timescale dynamics in both absorption spectroscopy [30, 31] and terahertz (THz) spectroscopy [32]. The parallels between photo-excitation and chemical doping have led to the process often being described as 'photo-doping' [33]. Light is also frequently used for controlling the behavior of a material through photo-induced phase transitions [34]. In these types of transition, excitation of electrons upsets the interplay between degrees of freedom, driving the system into a new regime where its properties can become quite different: structural relaxation can take place, shifting the positions of ions towards some new symmetry position [35–37], the optical properties can undergo large scale changes [38], and metallic states can be formed [39]. All of these effects last for only fractions of a second, with the system eventually relax back to its equilibrium state. Spectroscopy of time-dependent process is an invaluable tool for the investigation of chemical and physical dynamics, facilitating comprehension of fundamental processes in nature otherwise inaccessible to frequency resolved techniques. Ultrafast pump-probe spectroscopy affords experimentalists the ability to observe dynamics in real-time, limited only by the spectral and temporal resolution of their instruments. Early absorption techniques with limited temporal resolution still permitted investigation of kinetic processes in chemistry due to the inherent sensitivity of the absorption of light at a given wavelength to the concentration of a chemical species.

The range of tools available for studying ultrafast processes has blossomed in the last couple of decades. The frontiers of ultrafast science continue to explore ever shorter timescales, studying effects on the scale of a few fs [40, 41] and pushing on into the as regime [42]. Observing the collapse of gaps after photo-excitation on the fastest timescales and clocking the rate at which processes occur can reveal a great deal of information on the formation of states in complex materials. These endeavors provide insight into the fundamental timescales and electronic interactions, there is still the important task of characterizing the dynamics of photo-induced phases in solids. In the same way that it is important to determine the equilibrium properties of a material by studying its electrodynamic response over a broad energy range, a full understanding of photo-induced phenomena can only be attained by looking across different energy scales. This requires an array of different ultrafast probes covering large portions of the electromagnetic spectrum, from terahertz (THz, 10^{12} Hz) frequencies, up through the infrared and visible spectrum, and into the ultraviolet and X-ray regions. Electronic motion has been explored in semiconductor systems. The key is that the duration of the laser pulses must be shorter than the time scale of the dynamics that one wants to observe.

1.3 Development of Nonlinear optical (NLO) phenomena

Broadly one can envisage two powerful applications of fs pulses in optics (a) in probing processes on fs time scale and (b) creating high intensity photons. The latter has generated further interest in studying the interaction of fs pulses with optically transparent materials because at such high peak intensities even these materials absorb laser radiation through multi-photon processes. Manifestation of such mechanism is the observation of numerous novel nonlinear optical (NLO) phenomena. The interaction of high intense laser with matter lead to the new field of physics i.e. Nonlinear Optics. In the linear regime, electric field strength is less than intra atomic field and also the refractive index is independent of intensity. If $E_{field} > E_{atom}$ ($E_{atom} \sim 2\times10^{7}$e.s.u.) then we are in the nonlinear domain and it is intensity dependent process [42]. NLO field is an active branch that studies light-matter interaction in presence of strong electromagnetic field after the discovery of ultra-short laser pulses. Z-scan method was used because it is not only a very simple

method, but also a very accurate technique for retrieving the quantities of the nonlinear absorption coefficient as well as the nonlinear refractive index of a material. The measurements of two-photon absorption coefficient and nonlinear refractive index can be easily performed using the standard and well developed Z-scan technique [43, 44]. This technique is based on the variation of light intensity by altering geometrical parameters of light-matter interaction. This is achieved by scanning or moving a sample along the axis of propagation (Z) of a focused laser beam through its focal plane and measuring the transmission (T) of the sample for each Z position. As the sample experiences different electric field strengths at different Z positions, the recording of the transmission as a function of the Z coordinate provides accurate information about the nonlinear effects present in the sample. Ultrafast Z-Scan experiments are standard experiments for measuring nonlinear refractive index/nonlinear absorption of materials and in turn can determine the real/imaginary parts of third order NLO susceptibility. The primary goal of performing Z-scan experiments for the molecules investigated in this thesis is the information it can provide (especially the open aperture data) about various excited state absorption mechanisms at different wavelengths of interest.

1.4 Fundamentals of femtosecond laser pulses

Fs laser pulses are electromagnetic wave packets and as such are fully described by the time and space dependent electric field. In the frame of a semi-classical treatment the propagation of such fields and the interaction with matter are governed by Maxwell's equation with the material response given by the macroscopic polarization. The real electric field corresponding to an ultrashort pulse oscillates at an angular frequency ω_0 corresponding to the central wavelength of the pulse. To facilitate calculations, a complex field $\tilde{E}(t)$ is defined. It is defined as the analytic signal corresponding to the real field. The central angular frequency ω_0 is explicitly written in the complex field, which may be separated as an intensity function I(t) and a phase function ψ(t):

$$\tilde{E}(t) = \sqrt{I(t)}\exp(i\omega_0 t)\exp[i\psi(t)] \qquad (1)$$

The expression of the complex electric field in the frequency domain is obtained from the Fourier transform of $\tilde{E}(t)$:

$$\tilde{E}(\omega) = F\left(\tilde{E}(t)\right) \tag{2}$$

Because of the presence of the $\exp(i\omega_0 t)$ term, $\tilde{E}(t)$ is centered around ω_0 , and it is a common practice to refer to $\tilde{E}(\omega-\omega_0)$ by writing just $\tilde{E}(t)$. Just as in the time domain, intensity and a phase function can be defined in the frequency domain:

$$\tilde{E}(\omega) = \sqrt{S(\omega)}\exp\left[i\phi(\omega)\right] \tag{3}$$

The quantity $S(\omega)$ is the spectral density (or simply, the spectrum) of the pulse, and $\phi(\omega)$ is the spectral phase. The intensity functions $I(t)$ and $S(\omega)$ determines the time duration and spectral bandwidth of the pulse.

1.5 Relationship between pulse duration and spectral width

We define the pulse duration τ_p as the full width at half maximum (FWHM) of the intensity profile $\left|\tilde{E}(t)\right|^2$ and the spectral width $\Delta\omega_p$ as the FWHM of the spectral intensity $\left|\tilde{E}(\omega)\right|^2$. C_B is the time bandwidth product.

Shape	**Intensity profile [$I(t)$]**	**Spectral profile [$S(\omega)$]**	c_B
Gauss	$e^{-2(t/\tau_G)^2}$	$e^{-\left(\frac{\omega\tau_G}{2}\right)^2}$	0.441
Sech	$\sec h^2(t/\tau_s)$	$\sec h^2\frac{\pi\omega\tau_s}{2}$	0.315
Lorentz	$\left[1+(t/\tau_L)^2\right]^{-2}$	$e^{-2\lvert\omega\rvert\tau_L}$	0.142
Asym. sech	$\left[e^{t/\tau_a}+e^{-3t/\tau_a}\right]^{-2}$	$\sec h\frac{\pi\omega\tau_s}{2}$	0.278
Square	1 *for* $\lvert t/\tau_r\rvert\le 1$ 0 *elsewhere*	$\sin c^2(\omega\tau_r)$	0.443

Table 2 Examples of standard pulse profiles. (Table adapted from ref.[50])

Because the temporal and spectral characteristics of the field are related to each other through Fourier transforms, the bandwidth $\Delta\omega_p$ and the pulse duration τ_p cannot vary

independently of each other. There is a minimum duration-bandwidth product given by:

$$\Delta\omega_p\tau_p = 2\pi\Delta\upsilon_p\tau_p \geq 2\pi c_B \quad (4)$$

where c_B is a numerical constant on the order of 1, depending on the actual pulse shape. Some examples are shown in Table 2. The classical physical relationship eq. (4), which leads to the quantum-mechanical time-energy uncertainty principle, has several important consequences in the field of ultrashort light pulses. The transform limit is usually understood as the lower limit for the pulse duration which is possible for a given optical spectrum of a pulse. A pulse at this limit is said to be transform limited. The condition of being at the transform limit is essentially equivalent to the condition of a frequency-independent spectral phase, and basically implies that the time–bandwidth product is at its minimum i.e. no chirp. The minimum time–bandwidth product depends on the pulse shape, and is e.g. ≈ 0.315 for bandwidth-limited sech^2-shaped pulses and ≈ 0.441 for Gaussian-shaped pulses. (These values hold when a full-width-at-half-maximum criterion is used for the temporal and spectral width.)

1.6 Basic NLO processes

1.6.1. Self-focusing

The year 2013 marked the 51st anniversary of the first published prediction by Askaryan of the self-focusing phenomenon in light beams [45]. The change in the refractive index or spatial distribution of the refractive index of a medium due to the presence of intense optical field is called as nonlinear refractive index (n_2). The refractive index of air n in the presence of an intense electromagnetic field does not only depend on its frequency, but also on the space and time dependent intensity $I(r,t)$ of the laser according to the law:

$$n=n_0+n_2I(r,t) \quad (5)$$

The coefficient n_2 is usually positive, leading to an increase of the refractive index in the presence of intense radiation. Assuming monochromatic incident laser beam with a Gaussian-beam intensity profile given:

$$n = n_0 + n_2 I_0 \exp\left(\frac{-2r^2}{\omega_0^2}\right), I(r,t) = I_0 \exp\left(\frac{-2r^2}{\omega_0^2}\right) \quad (6)$$

Implying this can be expanded into infinite series;

Considering only first order term of the infinite series, the intensity of the beam, at the center of the beam is given by

$$\approx n_0 + n_2 I_0 (1 - \frac{2r^2}{\omega_0^2})$$

1.6.2. Self-phase modulation

Self-phase modulation (SPM) is a nonlinear optical effect of light-matter interaction. An ultrashort pulse of light, when traveling in a medium, will induce a varying refractive index of the medium due to the optical Kerr effect. This variation in refractive index will produce a phase shift in the pulse, leading to a change of the pulse's frequency spectrum.

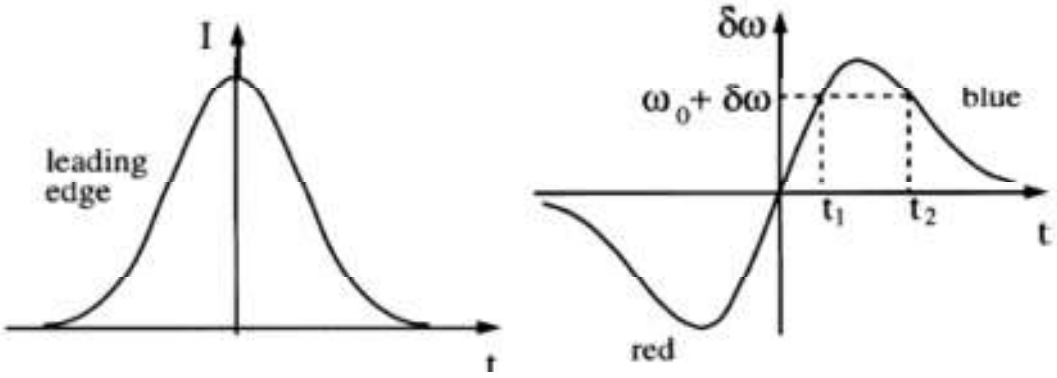

Figure 3 (*Left*) intensity dynamics of a Gaussian light pulse; the earlier times, i.e. the leading edge of the pulse, lie on the left side of the graph. (*Right*), time variation of the central pulsation, which is proportional to negative of the pulse envelope derivative when nonlinear index of refraction is positive (adapted from [50]).

The nonlinear index of material depends on the time dependence of a light pulse intensity envelope, which can be expressed as:

$$n = n_0 + n_2 I(r,t), \quad I(t) = e^{-\Gamma t^2} \quad (7)$$

To examine the influence of this time varying index on the frequency of the light, we simplify our analysis by considering a plane wave propagating in a nonlinear medium:

$$E(z,t) = E_0 \cos(\omega_0 t - kz), \text{ where } k = (\omega_0 / c) n(t) \tag{8}$$

The instantaneous frequency, being the time derivative of the phase, can be written as

$$\omega(t) = \frac{\partial}{\partial t}\Phi(t) = \omega_0 - \frac{\omega_0}{c}\frac{\partial n(t)}{\partial t} z \tag{9}$$

and the frequency variation can be written as

$$\delta\omega(t) = \omega(t) - \omega_0 = -\frac{\omega_0 n_2}{2c} z \frac{\partial I(t)}{\partial t} \tag{10}$$

Figure 3 shows a graphical elucidation of the above relation in case of the considered pulse of Gaussian phase variation. As a consequence of the Fourier duality between time and frequency, an application of periodic amplitude or phase modulation to a periodic signal results in creation of new components in its frequency spectrum. In the self-phase-modulation process, with n_2 positive, new low frequencies are created in the leading edge of the pulse envelope and new high frequencies are created in the trailing edge. These new frequencies are not synchronized, but are still created inside the original pulse envelope. Self-phase-modulation is not a dispersive effect in itself, but a pulse does not remain transform-limited when it crosses a transparent material.

1.6.3. Nonlinear absorption (NLA)

Nonlinear absorption refers to the change of transmittance of a material as a function of intensity or fluence. The high intensities associated with fs pulses can induce profound changes in the optical properties of a material leading to a nonlinear response originates from real and imaginary parts of polarization. The imaginary part of the nonlinear polarization is associated for instance with multiphoton transitions and will exhibit a n-photon resonance when two level of an atomic or molecular system can be connected by n optical quanta.

At sufficiently high intensities, the probability of a material absorbing more than one photon before relaxing to the ground state can be greatly enhanced. As early as 1931 Göppert-Mayer derived the two-photon transition probability in a system using the second order quantum perturbation theory [45]. With the availability of high

intensities with fs pulses, in addition to numerous investigations into this phenomenon of the simultaneous absorption of two photons, multiphoton (>2) absorption has also been widely studied. Multiphoton absorption processes are highly promising for a number of processes including optical limiting [46], 3D microfabrication [47], optical data storage [48], and biomedical applications [49].

The shorter the pulse duration than the ps and fs scale the more is its peak power (~1 TW/cm^2). Thus the non-linear effects are prominent at these power scales. To understand the non-linear optical phenomenon one has to keenly observe the interaction at interface of laser and matter. When one or more electromagnetic wave packets propagate in a material, the atoms and molecules oscillates not only at frequencies of electric field applied but also at different combination of those frequencies as a response of the medium. The charge particles of the medium are displaced from their equilibrium positions, so that positive charged particles (nuclei) move in the direction of the field, while the negative charged particles (electrons) move in the direction opposite to the direction of the applied electric fields. Dipole moments are created because of the displacement between positive and negative charges, and the dipole moment per unit volume describes the induced polarization of the medium. For small field strengths this induced polarization is proportional to the applied electric field. When an electromagnetic wave propagates through a dielectric medium, the electric displacement can be written as,

$$D=\varepsilon E \tag{11}$$

where ε is the permittivity tensor and E is the electric field. The electric displacement, electric field and polarization are vector quantities. However, for the sake of simplicity, they are considered as scalar quantities in the following discussion. The permittivity tensor can be written in terms of the permittivity of free space (ε_0) and relative permittivity (ε_r) as,

$$\varepsilon = \varepsilon_0 \varepsilon_r \tag{12}$$

The electric displacement can also be written as,

$$D = \varepsilon_0 E + P \tag{13}$$

Where P is the electric polarization (electric dipole moment density). From the above equations, we can write,

$$P = \varepsilon_0(\varepsilon_r - 1)E = \varepsilon_0 \chi E \tag{14}$$

Where $\chi = (\varepsilon_r - 1)$, is called the electric susceptibility tensor (or simply electric susceptibility) of the medium. In the nonlinear regime, the expression for the Polarization can be expanded in power series form

$$P = \varepsilon_0(\chi^{(1)}E + \chi^{(2)}EE + \chi^{(3)}EEE + \cdots) \quad (15)$$

Where, $\chi^{(1)}$, $\chi^{(2)}$, and $\chi^{(3)}$ are the linear, quadratic (second-order), and cubic (third order) susceptibility tensors, respectively. Substitution of equation 15 into Maxwell's equations leads to a set of nonlinear differential equations that involve terms with high-order-powers of the optical electric field strength. These terms are responsible for various observed coherent optical frequency-mixing effects. In other words, in the nonlinear case, the re-radiation coming from the dipoles do not faithfully reproduce the sinusoidal electric field that generates them. Third-order nonlinear optical interactions, which are described by the term $\chi^{(3)}$, can occur in any material. Real part of $\chi^{(3)}$ is related to the nonlinear index of refraction and imaginary part is related to nonlinear absorption. In nonlinear optics, the product of two or more oscillating fields generates oscillations at different combinations of the incident frequencies. In order to account for this and to have a complete description of the process, the following notation is used:

$$P(\omega) = \chi^{(1)}(-\omega;\ \omega)\, E(\omega) + \chi^{(2)}(-\omega_3 ;\ \omega_1 ,\ \omega_2).\ E(\omega_1).\ E(\omega_2) + \chi^{(3)}(-\omega_4;\ \omega_1,\ \omega_2,\ \omega_3).E(\omega_1).\ E(\omega_2).\ E(\omega_3) + \ldots \quad (16)$$

The above notation also reflects the conservation of energy in each nonlinear process

$\omega_3 = \omega_1 + \omega_2 = \omega$ [for $\chi^{(2)}$] (17)

$\omega_3 = \omega_1+\omega_2 +\omega_3= \omega$ [for $\chi^{(3)}$] (18)

The macroscopic nonlinear polarization expression can be rewritten as

$$P_i(\omega) = \chi_{ij}^{(1)}(-\omega;\ \omega).\ E_j(\omega) + \chi_{ijk}^{(2)}(-\omega_3 ;\ \omega_1 ,\ \omega_2)\ .\ E_j(\omega_1).E_k(\omega_2) + \chi_{ijkl}^{(3)}(-\omega_4;\ \omega_1 ,\ \omega_2 ,\ \omega_3)\ E_j(\omega_1).\ E_k(\omega_2).\ E_l(\omega_3) + \ldots = P_i^{(1)} + P_i^{(2)} + P_i^{(3)} + \ldots \quad (19)$$

We have investigated novel organic molecules and confine ourselves to energy level structure of such molecules. A typical organic molecule consists of singlet and triplet states. The nonlinear absorption mechanism in such molecules varies drastically depending on (a) the wavelength of input light used (resonant/non-resonant) (b) input peak intensity (c) concentration of the molecules used (d) lifetimes

of high lying excited states etc. Figure 4 shows most of the possible nonlinear absorption mechanisms:

Saturable Absorption (SA):

Saturable absorption is a property of any material where the absorption of light decreases with increasing light intensity. At sufficiently high incident light intensity, atoms or molecules in the ground state of a saturable absorber material become excited into an upper energy state at such a rate that there is insufficient time for them to decay back to the ground state before the ground state becomes depleted, and the absorption subsequently saturates.

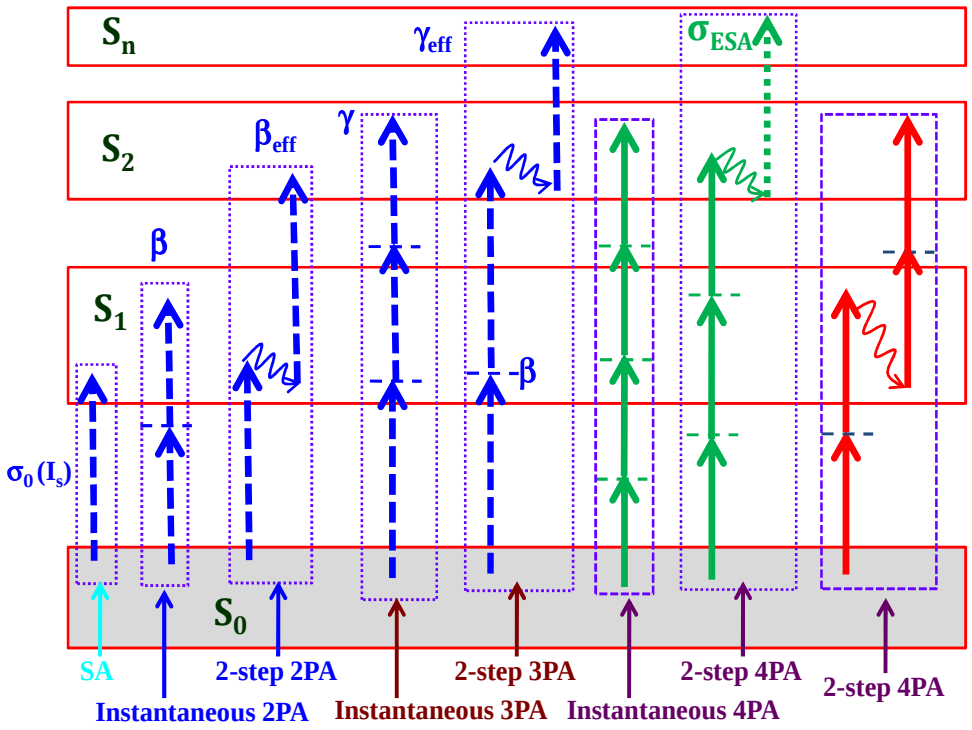

Figure 4 Various possible nonlinear absorption processes in organic macromolecules.

A simple kinetic model can often be used when the saturation is considered in terms of depletion of the ground state concentration. Thus, under the steady state,

$$\frac{dN}{dt} = \frac{\sigma I}{h\nu}\left(N_g - N\right) - \frac{N}{\tau} = 0 \qquad (20)$$

Where N is the concentration of excited state molecules, N_g is the undepleted ground state concentration, σ is the absorption cross section, $h\nu$ is the photon energy, and τ is

the lifetime of the excited state population. Assuming that the absorption coefficient α is proportional to the ground state population, $\alpha = \sigma\left(N_g - N\right)$ we get the following equation describing the saturation,

$$\alpha = \alpha_0 \frac{1}{1+\left(\tau\sigma I/_{h\nu}\right)} = \alpha_0 \frac{1}{1+\left(I/_{I_s}\right)} \tag{21}$$

Where $I_s = h\nu/_{(\sigma\tau)}$ is the saturation intensity and $\alpha_0 = \sigma N_g$ is the linear absorption coefficient. The case described by the above equation is often referred to as homogeneous saturation. In the case of a two-level system with inhomogeneously broadened states and hole burning, it has been found that the saturation can be described by,

$$\alpha = \alpha_0 \frac{1}{\left(1+\left(I/_{I_s}\right)\right)^{0.5}} \tag{22}$$

The main applications of saturable absorbers are in passive mode locking and Q-switching components of lasers, i.e., in the generation of short pulses. The key parameters for a saturable absorber are its wavelength range (where it absorbs), its dynamic response (recovery time), and its saturation intensity and fluence (at what intensity or pulse energy it saturates). Saturable absorbers are also useful for purposes of nonlinear filtering outside laser resonators, e.g., cleaning up pulse shapes, and optical signal processing.

Reverse Saturable Absorption (RSA):

Reverse saturable absorption (RSA) is a two-step, sequential one-photon absorption process. In this case the medium has linear absorption for the incident laser wavelength, and some of the molecules in the ground state are excited to an excited state 2. For a properly chosen medium, it is possible that the excited molecules make another transition from the excited state 2 to a higher excited state 3 via one-photon absorption. (In polyatomic molecules in fact a 5-level model may be considered, which involves both singlet and triplet states). The possibility of this process depends on the number of molecules N_2 at the first excited state 2, the incident intensity I, and the excited state absorption cross sectionσ_{21}. On the other hand N_2 is related to N_1 and I by the relation,

$$N_2 \propto \sigma_{12} N_1 I \tag{23}$$

where σ_{12} is the cross-section of the transition from the ground state to state 2. As can be seen from this relation, the number of molecules in state 2 (N_2) continuously grows with the incident intensity I and the one-photon sequential absorption from state 2 to state 3 becomes more significant, provided that the cross section σ_{23} of this transition is considerably larger than σ_{12}. Under the steady-state condition, the intensity change of the laser beam in the nonlinear medium along its propagation direction can be expressed as,

$$\frac{dI}{dz} = -\sigma_{12}(N_1 - N_2)I - \sigma_{23} N_2 I \tag{24}$$

In the simplest case, it can be assumed that $N_1 \gg N_2$, $N_3 = 0$, and $N_1 = N_0$ where N_0 is the number density of the absorbing molecules. Then according to equation 1.24, the above equation can be rewritten as,

$$\frac{dI}{dz} = -\sigma_{12} N_0 I - b\sigma_{12}\sigma_{23} N_0 I^2 \tag{25}$$

or

$$\frac{dI}{dz} = -\alpha_0 I - \beta' I^2 \tag{26}$$

where b is a proportionality coefficient, and the linear absorption coefficient α_0 and nonlinear absorption coefficient β are defined as,

$$\alpha_0 = \sigma_{12} N_0 \tag{27}$$

$$\beta' = b\sigma_{12}\sigma_{23} N_0 \tag{28}$$

Two-photon Absorption (2PA): When two photons are simultaneously absorbed via a virtual state and population is transferred between two real (quantum) states it is defined as instantaneous 2PA. However, if a photon excites the population from ground state to higher state (single photon transition) and there it relaxes back to the lowest vibrational state (in the excited state manifold), there is a possibility of absorbing another photon to reach further higher states. This is termed as two-step 2PA.

In non-resonant TPA two photons combines to bridge an energy gap larger than energies of each photon individually. If there is an intermediate state in the gap,

this could happen via two separate one photon transition in a process described as "resonant TPA", sequential TPA, 1+1 absorption. Non-resonant TPA transition occurs without the presence of intermediate state. This can be viewed as being due to a virtual state created by the interaction of photons with the molecule. The intermediate level being virtual, the two photons should be simultaneously absorbed making the process sensitive to the instantaneous optical intensity of the incident radiation. The two-photon absorption process is proportional to the square of the input intensity. The propagation of laser light through the system describing the optical loss is given by,

$$\frac{dI}{dz} = -\alpha I - \beta I^2 \tag{29}$$

where α is the linear absorption coefficient (which can be very small) and β the two-photon absorption coefficient. β is a macroscopic parameter that characterizes the material and is related to the individual molecular two-photon absorption cross section σ_2 through,

$$\sigma_2 = \frac{\hbar\omega\beta}{N} \tag{30}$$

where N is the number density of the molecules in the system and ω is the incident radiation frequency. It is the imaginary part of the third-order nonlinear susceptibility of the system that determines the strength of the two-photon absorption.

Three Photon Absorption (3PA): When three photons are simultaneously absorbed via virtual states and population is transferred between two real (quantum) states it is defined as instantaneous 3PA. However, if two photons excite the population from ground state to higher state (two photon transition) and there it relaxes back to the lowest vibrational state (in the excited state manifold), there is a possibility of absorbing another photon to reach further higher states. This is termed as two-step 3PA. The relaxation within the vibrational states occurs, typically, in a few ps time scale. Therefore, if the pulse duration is <100 fs the excitation can be considered as an instantaneous process.

3PA is a fifth-order nonlinear process, and the propagation equation for a medium having significant three-photon absorption is given as,

$$\frac{dI}{dz} = -\alpha I - \gamma I^3 \tag{31}$$

where α is the linear absorption coefficient, which can be typically small, and γ is the three-photon absorption coefficient.

Four Photon Absorption (4PA):

When four photons are simultaneously absorbed via virtual states and population is transferred between two real (quantum) states it is defined as instantaneous 4PA. However, if two photons excite the population from ground state to higher excited state (two photon transition) and there it relaxes back to the lowest vibrational state (in the excited state manifold), there is a possibility of absorbing another two photons to reach further higher states. This is termed as two-step 4PA. Another possibility is absorption of 3+1 photons wherein the population relaxes within the vibrational states after absorption of three photons and before absorbing the fourth photon. In all the above case instantaneous 2PA/3PA/4PA [50] can occur via real states only when the input pulse duration is much shorter than the relaxation time of population within the vibrational states. Instantaneous processes are intensity dependent while multi-step processes are fluence dependent. In the present thesis we dealt with either ps or fs pulses and, therefore, we neglect any transitions from singlet to triplet states via intersystem crossing.

Free Carrier Absorption (FCA)

Free carrier absorption (FCA) occurs when a material absorbs a photon and a carrier is excited from a filled state to an unoccupied state (in the same band). This is different from interband absorption in semiconductors because the electron being excited is a conduction electron (i.e. it can move freely). In interband absorption, the electron is being raised from a valence (non-conducting) band to a conducting one. When excitation is into the absorption band we see saturation type behavior .At higher intensities we observe RSA behavior even at these wavelengths.

1.7 Nonlinear refraction (NLR)

Change in the refractive index of the medium due to presence of optical wave called nonlinear refractive index (NRI). Nonlinear refraction has led to a variety of fascinating applications. It is also central to many fundamental investigations.

$$n = n_0 + n_2 I \quad (32)$$

where n is the total refractive index, n_0 is the linear refractive index, n_2 is the nonlinear refractive index and I is intensity of the light. Different physical phenomena could be responsible for NRI. Some of them are discussed below.

1.7.1 Electronic polarization

Electronic polarization is the slight relative shift of positive and negative electric charge in opposite directions within an insulator, or dielectric, induced by an external electric field. Polarization occurs when an electric field distorts the negative cloud of electrons around positive atomic nuclei in a direction opposite the field. This slight separation of charge makes one side of the atom somewhat positive and the opposite side somewhat negative. One of the measures of polarization is electric dipole moment, which equals the distance between the slightly shifted centers of positive and negative charge multiplied by the magnitude of either of the charges. Polarization *P* in its quantitative meaning is the amount of dipole moment *p* per unit volume *V* of a polarized material, $P = p/V$.

1.7.2 Optical Kerr effect

Optical Kerr effect is change in the refractive index of a material in response to an applied electric field. The Kerr effect is distinct from the Pockel's effect in which the induced index change is directly proportional to the square of the electric field instead of varying linearly with it. The optical Kerr effect is the case in which the electric field is due to the light itself. This causes a variation in index of refraction which is proportional to the local irradiance of the light. This refractive index variation is responsible for the nonlinear optical effects of self-focusing, self-phase modulation and modulational instability, and is the basis for Kerr-lens mode locking. This effect only becomes significant with very intense beams those are from pulsed lasers.

1.7.3 Self-focusing and Self-defocusing

If light gets intense enough, its electromagnetic field can affect the optical properties of the matter it is passing through. One such effect is increase of index of refraction at higher light intensities .If the laser beam is more intense in the middle,

this means the index of refraction provided by the center of the beam is higher than at the edges. This makes even uniform matter act like a lens to focus the beam. When this happens, the beam is said to be self focused. This effect only becomes apparent at very high power levels. In air, self focusing can be observed at ~1×10^{10} W. Note that the intensity does not matter; contrary to what intuition might tell you, it is the total power of the beam that matters, not how tight the beam is.

1.8 Theory of ultrashort pulse propagation

With short pulses, one has to account for the combined effects of the broad spectral bandwidths and the frequency dependence of the refractive index (dispersion). This is usually seen through the definition of the propagation constant:

$$\beta(\omega) = \frac{\omega}{c} n(\omega) \tag{33}$$

The propagation constant can be rewritten in a Taylor expansion around a central carrier frequency ω_0 as:

$$\beta(\omega) = \beta(\omega_0) + \frac{d\beta(\omega_0)}{d\omega}(\omega-\omega_0) + \frac{1}{2!}\frac{d^2\beta(\omega_0)}{d\omega^2}(\omega-\omega_0)^2 + \frac{1}{3!}\frac{d^3\beta(\omega_0)}{d\omega^3}(\omega-\omega_0)^3 + \ldots \tag{34}$$

The first order term of the expansion is related to phase velocity v_p, which measures the propagation velocity of the single frequency line ω_0. However, different frequency lines travel with different phase velocities as the system's dispersion dictates. Therefore, the pulse envelope travels with a group velocity v_g, which appears in second term of the above equation. Higher order terms are related to higher order dispersion. In particular, the third term represents group velocity dispersion (GVD), which is responsible for changes in the shape of the temporal pulse envelope. The last term in the proceeding equation (third order dispersion) as well as higher order terms can be neglected to a first approximation for pulses exceeding ~50 fs in duration. Table 3 depicts the exact expressions for these quantities. All the quantities depend on the refractive index profile of the material.

$v_\phi \left[\frac{m}{s}\right]$	$\left[\frac{\beta(\omega_0)}{\omega_0}\right]^{-1} = \frac{c}{n(\omega_0)}$
$v_g \left[\frac{m}{s}\right]$	$\left[\frac{d\beta(\omega)}{d\omega}\Big\|_{\omega_0}\right]^{-1} = \left[\frac{1}{c}\left(n(\omega_0) + \omega_0 \frac{dn(\omega)}{d\omega}\Big\|_{\omega_0}\right)\right]^{-1}$
GVD $\left[\frac{fs^2}{m}\right]$	$\frac{d^2\beta(\omega)}{d\omega^2}\Big\|_{\omega_0} = \frac{1}{c}\left(2\frac{dn(\omega)}{d\omega}\Big\|_{\omega_0} + \omega_0 \frac{d^2n(\omega)}{d\omega^2}\Big\|_{\omega_0}\right) = \frac{\lambda_0^3}{2\pi c^2}\frac{d^2n(\lambda)}{d\lambda^2}\Big\|_{\lambda_0}$
TOD $\left[\frac{fs^3}{m}\right]$	$\frac{d^3\beta(\omega)}{d\omega^3}\Big\|_{\omega_0} = \frac{1}{c}\left(3\frac{d^2n(\omega)}{d\omega^2}\Big\|_{\omega_0} + \omega_0 \frac{d^3n(\omega)}{d\omega^3}\Big\|_{\omega_0}\right)$

Table 3 Units and expressions for the phase velocity v_p, group velocity v_g, group velocity dispersion (GVD) and third order dispersion (TOD).

1.9 GVD and GVM

Nonlinear pulse propagation in bulk media can lead to substantial modifications in the temporal, spectral or spatial characteristics of a given input pulse. It has been realized earlier that when a pulse propagates in a Kerr-type medium there is a perfect analogy between the spectro-temporal behaviors of the pulse shape with the spatial behavior of the pulse spatial profile. The Kerr effect leads to the self-phase modulation (SPM) of a pulse, which affects its spectral width by broadening it, without affecting the pulse temporal duration. The amount of spectral broadening depends on the pulse intensity, interaction length and the nonlinear index of refraction, n_2, which can be positive or negative and is a characteristic of the medium. When acting on the spatial domain, the Kerr effect leads to self-focusing, if $n_2 > 0$, or self defocusing, if $n_2 < 0$, of a beam propagating in a nonlinear material. Inherent effect acting on the beam profile is the diffraction, which always broadens the beam width. In the time domain, the group velocity dispersion is responsible for the pulse width broadening, and even though it can be positive or negative, always leads to pulse broadening. NLO crystals are frequently used in generation of new frequencies with ultrashort pulses. During the frequency conversion process the maximum

achievable pulse duration is often limited by the group velocity mismatch between fundamental and the second harmonic pulses. A phase shift which varies linearly with frequency corresponds to a time delay, without any change of temporal shape of the pulse. Higher order phase shifts, however, tend to modify pulse shape are thus of relevance for the formation of short pulses and frequency conversion experiments. Due to the large bandwidth associated with these ultrashort pulses dispersion compensation is an important phenomenon [50-56]. We are progressing towards studying the process of the ultrafast dynamics of high energy materials using pump-probe techniques. We are interested in generating new wavelengths in the UV-visible spectral region by converting the fs pulses in the IR spectral region. Beta Barium Borate (β-BaB_2O_4, BBO) has been identified as the potential nonlinear optical crystal and has been investigated extensively for frequency conversion. We attempt to study the ultrashort pulse ($\leq$50 fs) broadening effects due to group velocity mismatch in this crystal along with the propagation properties of these pulses in various media. We compare our simulations with the autocorrelation data obtained from BBO crystal using ~40 fsec, 800 nm pulses from an optical parametric amplifier. A variety of pumps/ probes are essential to perform these studies and the knowledge (a) generating ultrashort UV-visible pulses from IR pulses (b) their properties after passing through various optical components is necessary in such endeavors.

BBO is a nonlinear optical crystal which combines a number of unique features including wide transparency and phase matching ranges, large nonlinear coefficient, high damage threshold and excellent optical homogeneity. Frequency-doubling and tripling of ultrashort-pulse lasers are the applications in which BBO shows superior properties to KDP and ADP crystals (d_{11} = 2.3 pm/V). An ultrashort laser pulse of even 10 fs can be efficiently frequency-doubled with a thin BBO, in terms of both phase-velocity and group-velocity matching. BBO's relatively narrow angular acceptance bandwidth (especially in the UV) may limit its usefulness in certain applications involving lasers with less than diffraction limited beam quality. BBO has a relatively large d_{eff} (2.01 pm/V at 1060 nm, 1.99 pm/V at 780 nm) but also a large walk-off which reduces the conversion efficiency. Furthermore, BBO is hygroscopic, which limits the lifetime of the crystal.

In the context of nonlinear frequency conversion with use of ultrashort pulses, a number of issues related to the above quantities have to be addressed. First of all,

matching the phase velocities of the interacting waves is required for the process to build up in useful material lengths. However, even under perfect phase matching conditions the interaction length is limited by mismatch of the group velocities of the interacting pulses. Evidently, the group velocity mismatch (GVM) between two pulses with central frequencies $v_g(\lambda/2)$ and $v_g(\lambda)$ is given by:

$$GVM\ [s/m] = \frac{1}{v_g(\lambda/2)} - \frac{1}{v_g(\lambda)} \tag{35}$$

Group velocity mismatch (or temporal walk-off) as defined above measures the time separation of the two pulses after a unit length of propagation in the dispersive medium. This can be used to define the actual interaction length, as the length L over which the two pulses of duration $\Delta\tau$ do not overlap any more:

$$L = \frac{\Delta\tau}{GVM} \tag{36}$$

In turn, group velocity dispersion is responsible for temporal broadening of the pulse by introducing a linear phase chirp across the pulse. This can be understood as follows: Form table 3 it is clear that GVD can be written as:

$$GVD = \frac{d}{d\omega}\left(\frac{1}{v_g}\right) = -\frac{1}{v_g^2}\frac{dv_g}{d\omega} \tag{37}$$

Equation (3) suggests that the value of GVD is positive when the group velocity decreases as frequency increases. In this case, blue components travel slower and therefore can be found in the trailing edge of the pulse (normal dispersion). Thus, the instantaneous frequency increases in time, suggesting that the pulse is positively chirped ($\beta > 0$). Applying similar argumentation, one can easily conclude that in presence of negative GVD (abnormal dispersion) the pulse is negatively chirped ($\beta < 0$). The pulse broadening of an initially transform limited, un-chirped pulse with duration $\Delta\tau$, after propagation of length z in a dispersive medium, can be quantified as:

$$\Delta\tau_z = \Delta\tau \cdot \sqrt{1 + \frac{z^2}{z_D^2}} \tag{38}$$

where $\Delta\tau_z$ is the pulse duration at z and z_D is referred to as the dispersion length given by:

$$z_D = \frac{\Delta\tau^2}{4\ln(2)}(GVD)^{-1} \quad (39)$$

It should be noted that in eqns. 33 and 39 the second power of GVD and the chirp parameter β are involved. Therefore, a pulse travelling in a dispersive medium (irrespectively of the sign of GVD) faces a two-fold effect: a) it experiences temporal broadening and b) it departs from the transform limit value of the bandwidth-duration product.

1.10 Scope and Organization of the thesis

One of the fundamental goals of our centre (ACRHEM) is to understand the detailed mechanisms occurring at various time scales (especially in the sub-picosecond time domain) during decomposition of energetic materials (i.e. during the release of their stored energy), and to apply this knowledge to create/synthesize improved/novel energetic species. Achieving this goal will enable the production of new specific systems for better and more stable fuels, explosives, and mobile energy sources. Our main objective is to capture the ultrafast events occurring in HEMs such as RDX, HMX, TNAZ, CL-20 and DMNA etc.. In this pursuit we started with setting up of (a) degenerate pump-probe experiments with ps and fs pulses (b) improvise these to non-degenerate pump-probe and pump-white light probe experiments (c) finally establish near-IR pump/visible probe experiments for understanding the dynamics of energetic materials in a controlled fashion. We were successful in setting up pump-probe experiments with ps and fs pulses, investigate a few novel organic materials, which are also potential candidates for photonics applications. This thesis deals with (a) setting up of pump-probe experiments with fs pulses (b) investigation of simple organic molecules which are third order nonlinear optically active materials (c) understand the decay dynamics with the presence/absence of nonlinear absorption in such molecules. The decay dynamics depend on the input (pump) peak intensities exciting these molecules into high lying states. Further thesis chapters are organized as follows:

Chapter 2 is devoted for discussion on instrumentation details of experiments of fs/ps degenerate pump-probe spectroscopy and fs/ps Z-scan. The ps/fs pulses were characterized using external autocorrelation in BBO crystal and a single shot

Autocorrelator (SSA). Furthermore, the fs (1 kHz) pulses were characterized using Silhouette (Coherent). Initial pump-probe results on a few phthalocyanine thin films are presented.

Chapter 3 present results from the detailed investigations of metal free base and metal substituted dinapthoporphycenes using fs pump-probe and ps Z-scan experiments. These compounds exhibited 2PA and 3PA with different input peak intensities with 800 nm excitation. At lower energies (or peak intensities) there is possibility of 2PA while at higher peak intensities 3PA was observed since both these processes are intensity dependent. Our detailed studies indicated that at lower peak intensities (typically <100 GW/cm^2) 2PA prevailed and at higher peak intensities (typically >100 GW/cm^2) 3PA was the dominant mechanism. The order and magnitude of 2PA and 3PA cross-section were also calculated. Fs pump-probe data indicated photo-induced absorption at 600 nm resulting from two-photon/single photon excitation, whereas ps pump-probe data demonstrated photo-bleaching.

Chapter 4 presents results from the ps NLO studies of three novel cyclo[4]naphthobipyrroles (octaisopropyl cyclo[4]naphthobipyrrole, octa-n-propyl cyclo[4]naphthobipyrrole, and octa-n-pentyl cyclo[4]naphthobipyrrole) at wavelengths of 600 nm, 640 nm, 680 nm, and 800 nm by Z-scan technique. The excited state decay dynamics were investigated using degenerate pump-probe experiments with ~70 fs pulses near 600 nm. The process of ultrafast relaxation is depicted with the help of Jablonski diagram.

Chapter 5 presents the detailed investigation of both metal free base and metal substituted phthalocyanines (Pc-1, Pc-2, and Pc-3) using Z-scan with ps pulses. Two novel sterically demanded phthalocyanines (Pc-1, Pc-2) were synthesized and characterized. Nonlinear optical (NLO) properties were evaluated at wavelengths of 600 nm, 640 nm, 680 nm, and 800 nm using ps pulses and further studies with fs (~140 fs) pulses at 800 nm have been performed. Two-photon absorption (2PA) and saturable absorption (SA) were the dominant nonlinear absorption mechanisms observed with ps/fs excitation at different wavelengths. NLO coefficients were extracted from ps/fs closed and open aperture Z-scan measurements. The excited state decay dynamics were investigated using degenerate pump-probe experiments with ~70 fs pulses near 600 nm. Double exponential fits of the pump-probe data

suggested two decay times for both the molecules investigated. Similar experiments were performed with a novel Thio-Zinc phthalocyanines (Pc-3) dissolved in THF. NLO coefficients were calculated and the excited state dynamics were evaluated.

Chapter 6 demonstrate results from the detailed investigation of 3,8,13,18-tetrachloro-2,7,12,17-tetramethoxyporphyrin and its metallo-derivatives by using fs/ps Z-scan and pump-probe techniques. The free-base molecule is unique owing to the presence of an electron donating methoxy group and electron withdrawing chloro-group on the adjacent β- positions of each pyrrole moiety. We discuss the NLO response of metal free and metal (Zn, Ni) substituted porphyrins in chloroform using Z-scan technique with ~40 fs and ~2 ps, 800 nm laser pulses. Excited state dynamics were investigated using pump-probe experiments with fs pulses near 600 nm. Such molecules have been demonstrated to detect explosives using florescence quenching methods. Some of these porphyrins have been used for explosives sensing in the liquid state using fluorescence quenching method [57].

Chapter 7 consists of the future prospects and the potential of investigated macromolecules and summarizes the results obtained in this thesis. Some discussion on the nature and lifetimes of various energetic molecules will be presented. Decomposition mechanisms of new energetic materials in excited electronic states will be discussed. Future directions for upgrading the present experiments to investigate simple HEMS are outlined. Newly synthesized novel organic macro molecules which have comparable (to visible excitation) gap between ground state and excited state were usually selected for time resolved study. Moreover, nonlinear optical processes (third order) are prominent in these molecules for studying multi-photon processes. We have investigated NLO properties of organic macromolecules with different pulse width and different wavelength interactions are observed.The ultimate goal of our group at ACRHEM is (a) to perform ultrafast spectroscopic measurements during the detonation/decomposition of HEMs (b) to develop techniques using ultrashort pulses for standoff detection of explosive molecules [see for e.g. 58].

1.11 References

1. T. H. Maiman, Nature **187** (1960) 493.
2. J. Hecht, Appl. Opt. **49** (2010) F99
3. C. Rajchenbach, G. Jonusauskas and C. Rulliere, J. DE PHYSIQUE IV Colloque C4, supplkment au Journal de Physique, **5** (1995) 111.
4. L. Dhar, J. A. Rogers, K. A. Nelson, Chem. Rev. **94** (1994) 157.
5. G.P. Wakeham, D.D. Chung, K.A. Nelson, Thermo. Acta **384** (2002) 7.
6. E.J. Reed, A.W. Rodriguez, M.R. Manaa, L.E. Fried, C.M. Tarver, Phys. Rev. Lett. **109** (2012) 038301 .
7. A. Strachan, A.C.T. van Duin, D. Chakraborty, S. Dasgupta, W.A. Goddard, Phys. Rev. Lett. 91 (2003) 098301.
8. M. Greenfield, Y.Q. Guo, E.R. Bernstein, Chem. Phys. Lett. **430** (2006) 277.
9. (a) A. Bhattacharya, Y. Guo, E.R. Bernstein, Acc. Chem. Res. **43** (2010) 1476 (b) E.R. Bernstein, Adv. Quant. Chem. **69** (2014) 31–69, Chapter 2.
10. (a) A. Bhattacharya, Y. Guo, E.R. Bernstein, J. Chem. Phys. **136** (2012) 024321 (b) B. Yuan, Z. Yu, E. R. Bernstein, J. Chem. Phys. **140** (2014) 034320 (c) Z. Yu, E. R. Bernstein, J. Phys. Chem. A **117** (2013) 1756 (d) Z. Yu, E. R. Bernstein, J. Chem. Phys. **137** (2012)114303 (e) Z. Yu, E. R. Bernstein, J. Chem. Phys. **135** (2011) 154305.
11. (a) Y Guo, A. Bhattacharya, E. R. Bernstein, J. Phys. Chem. A **115** (2011) 9349, (b) A. Bhattacharya, E. R. Bernstein, J. Phys. Chem. A **115** (2011) 4135 (c) Y. Q. Guo, A. Bhattacharya, E. R. Bernstein, J. Chem. Phys. **134** (2011) 024318 .
12. (a) H.S. Im and E. R. Bernstein, J. Chem. Phys. **113** (2000) 7911 (b) D. P. Taylor, C. F. Dion, and E. R. Bernstein, J. Chem. Phys. **106** (1997) 3512 (c) D. P. Taylor and E. R. Bernstein, J. Chem. Phys. **103** (1995) 10453.
13. (a) Y. Q. Guo, M. Greenfield, A. Bhattacharya, E. R. Bernstein, J. Chem. Phys. **27** (2007) 154301 (b) Y. Q. Guo, A. Bhattacharya, E. R. Bernstein, J. Chem. Phys. **128** (2008) 034303.
14. (a) A. Bhattacharya, Y.Q. Guo, E.R. Bernstein, J. Phys. Chem. A **113** (2009) 811 (b) A. Bhattacharya, Y. Q. Guo, E. R. Bernstein, J. Chem. Phys. **131** (2009) 194304 (c) Y. Q. Guo, A. Bhattacharya, and E. R. Bernstein, J. Phys. Chem. A **113** (2009) 85 (d) Y. Q. Guo, M. Greenfield, E. R. Bernstein, J. Chem. Phys. **122** (2005) 244310 (e) E.R. Bernstein, In *Overviews of Recent Research on*

Energetic Materials; D. Thompson, T. Brill, R. Shaw, R., Eds.; World Scientific, Hackensack, NJ, 2004.

15. C.M. Aubuchon, K.D. Rector, W. Holmes, M.D. Fayer Chem. Phys. Lett. **299** (1999) 84.
16. (a) Y. Yang, Z. Y. Sun, S. F. Wang, D. D. Dlott, J. Phys. Chem. B **107** (2003) 4485 (b) X. Zheng, A.D. Curtis, W.L. Shah, D.D. Dlott, J. Phys. Chem. C **117** (2013) 4866 (c) S. Wang, Y. Yang, Z. Sun, D.D. Dlott, Chem. Phys. Lett. **368** (2002) 189.
17. (a) Y. Yang S. Wang, Z. Sun, D. D. Dlott, J. Appl. Phys. **95** (2004) 3667 (b) Y. Yang, S. Wang, Z. Sun, D. D. Dlott, Appl. Phys. Lett. **85** (2004) 1493.
18. (a) R.W. Conner, D.D Dlott, J. Phys. Chem. A **114** (201) 6731 (b) M.A. Zamkov, R.W. Conner, D.D Dlott, J. Phys. Chem. C **111** (2007) 10278 (c) R.W. Conner, D.D. Dlott, Chem. Phys. Lett. **512** (2011) 211 (d) R.W. Conner, D.D. Dlott, J. Phys. Chem. C **116** (2012) 2751 (d) R.W. Conner, D.D. Dlott, J. Phys. Chem. C **116** (2012) 14737
19. (a) X. Hong, S. Chen, D.D. Dlott, J. Phys. Chem. **99** (1995) 9102 (b) J.C. Deàk, L.K. Iwaki, D.D. Dlott, J. Phys. Chem. A **103** (1999) 971 (c) D.D. Dlott, Annu. Rev. Phys. Chem. **62** (2011) 575 (d) H. Kim, S.A. Hambir, D.D. Dlott, Shock Waves **12** (2002) 79 (e) M.A. Zamkov, R.W. Conner, D.D. Dlott, J. Phys. Chem. C **111** (2007) 10278 (f) Ch. Leela, P. Venkateshwarlu, R.V. Singh, P. Verma, P. P. Kiran, Opt. Exp. **22** (2014) A268.
20. (a) S. Shigeto, Y. Pang, Y. Fang, D.D. Dlott, J. Phys. Chem. B **112** (2008) 232 (b) Y. Sun, B.C. Pein, D. D. Dlott, J. Phys. Chem. B **117** (2013) 15444.
21. B. Fain, S. H. Lin, V. Khidekel, Phy. Rev. A **47** (1993) 3222.
21. (a) M.M. Kuklja, Advances in Quantum Chemistry, Volume **69,** 2014, Pages 31–69, Chapter 3 (b) M.M. Kuklja, B.P. Aduev, E.D. Aluker, V.I. Krasheninin, A.G. Krechetov, A.Y. Mitrofanov, J. Appl. Phys. **89** (2001) 4156.
23. (a) D.S. Moore, AIP Conf. Proc. **1195** (2009) 287 (b) S.D. McGrane, D.S. Moore, V.H. Whitley, C.A. Bolme, D.E. Eakins, AIP Conf. Proc. **1195** (2009) 1301 (c) C.A. Bolme, S.D. McGrane, D.S. Moore, V.H. Whitley, and D.J. Funk, Appl. Phys. Lett. **93** (2008) 191903 (d) N. C. Dang,C. A. Bolme, D. S. Moore,S. D. McGrane J. Phys. Chem. A **116 (**2012) 10301 (e) K. E. Brown, S. D. McGrane, C. A. Bolme, D. S. Moore, J. Phys. Chem. A (2014) Just Accepted DOI: 10.1021/jp4125793.

24. S. Roy, N. Jiang, H.U. Stauffer, J.B. Schmidt, W.D. Kulatilaka, T.R. Meyer, C.E. Bunker, J.R. Gord, J. Appl. Phys. **113** (2013) 184310.
25. E. Muybridge. Muybridge's Complete Human and Animal Locomotion (Dover Publications, 1979).
26. A. Topler, Ann. Phys. Chem. **131** (1867) 180.
27. D. H. Auston and C. V. Shank, Phys. Rev. Lett. **32** (1974) 1120.
28. E. P. Ippen, C. V. Shank, A. Lewis, and M. A. Marcus, Science **200**(1978) 1279.
29. Nobel Prize Website (2010). http://nobelprize.org.
30. (a) N. Dean, Jesus College, Oxford (2010) (b) J. Orenstein and G. L. Baker, Phys. Rev. Lett. **49** (1982) 1043.
31. C.V. Shank, R. Yen, R.L. Fork, J. Orenstein, G.L. Baker, Phys. Rev. Lett. **49** (1982) 1660.
32. M.C. Beard, G.M. Turner, C.A. Schmuttenmaer, Phys. Rev. B **62** (2000) 15764.
33. G. Yu, C.H. Lee, A.J. Heeger, N. Herron, E.M. McCarron, Phys. Rev. Lett. **67** (1991) 2581.
34. S. Koshihara, S. Koshihara, Y. Tokura, T. Mitani, G. Saito, T. Koda, Phys. Rev. B **42** (1990) 6853.
35. A. Cavalleri, Cs. Tóth, C. W. Siders, J. A. Squier, F. Ráksi, P. Forget, J. C. Kieffer, Phys. Rev. Lett. **87** (2001) 237401.
36. K. Sokolowski-Tinten, C. Blome, J. Blums, A. Cavalleri, C. Dietrich, A. Tarasevitch, I. Uschmann, E. Förster, M. Kammler, M. Horn-von-Hoegen, D. von der Linde, Nature **422** (2003) 287.
37. A. Cavalleri, Th. Dekorsy, H. H. W. Chong, J. C. Kieffer, R. W. Schoenlein, Phys. Rev. B **70** (2004) 161102.
38. M. Chollet, L. Guerin, N. Uchida, S. Fukaya, H. Shimoda, T. Ishikawa, K. Matsuda, T. Hasegawa, A. Ota, H. Yamochi, G. Saito, R. Tazaki, S. Adachi, S. Koshihara, Science **307** (2005) 86.
39. K. Miyano, T. Tanaka, Y. Tomioka, and Y. Tokura. Phys. Rev. Lett. **78** (1997) 4257.
40. D. Polli, M. Rini, S. Wall, R. W. Schoenlein, Y. Tomioka, Y. Tokura, G. Cerullo, A. Cavalleri, Nat. Mater. **6** (2007) 643.
41. S. Wall, D. Prabhakaran, A. T. Boothroyd, A. Cavalleri, Phys. Rev. Lett. **103** (2009) 097402.

42. A. L. Cavalieri, N. Müller, Th. Uphues, V. S. Yakovlev, A. Baltuska, B. Horvath, Schmidt, L. Blümel, R. Holzwarth, S. Hendel, M. Drescher, U. Kleineberg, P. M. Echenique, R. Kienberger, F. Krausz, U. Heinzmann, Nature **449** (2007) 1029. (b) Nonlinear Optics, Robert W. Boyd, 2nd Edition (2003).
43. M. Sheik-Bahae, A. A. Said, E.W. Van Stryland, Opt. Lett. **14** (1989) 955.
44. M. Sheik-Bahae, A.A. Said, T. Wei, D. J. Hagan and E. W. Van Stryland, IEEE J. Quant. Electron. **26** (1990) 760.
45. (a) G.A. Askaryan, Sov. Phys. JETP-USSR **15** (1962) 1088 (b) M. Göppert-Meyer, Ann. Phys. **9** (1931) 273 (c) R. S. S. Kumar thesis, University of Hyderabad February (2009).
46. (a) G.S. He, L.S. Tan, Q. Zheng, and P. N. Prasad, Chem. Rev. **108** (2008) 1245 and references there in,(b) N. Venkatram L. Giribabu , S. Venugopal Rao and D. N. Rao, Appl. Phys. B, 91, 149 (2008) (c) P. P. Kiran, D. R. Reddy, B. G. Maiya, A. K. Dharmadhikari, G. R. Kumar, and D. N. Rao Appl. Opt. **41** (2002) 7631 (d) G. S. He, G. C. Xu, P. N. Prasad, B.A. Reinhardt, J.C. Bhatt, R. McKellar, and A.G. Dillard, Opt. Lett. **20** (1995) 435.
47. (a) S. Maruo, O. Nakamura, and S. Kawata, Opt. Lett. **22** (1997) 132 (b) B.H. Cumpston, S.P. Ananthavel, S. Barlow, D.L. Dyer, J.E. Ehrlich, L.L Erskine, A.A. Heikal, S. M. Kuebler, I.Y. S. Lee, D. McCord-Maughon, J. Qin, H. Röckel, M. Rumi, X.-L. Wu, S.R. Marder, J.W. Perry, Nature **398** (1999) 51 (c) S. Kawata, H.-B. Sun, T. Tanaka, K. Takada, Nature **412** (2001) 697 (d) W. H. Zhou, S. M. Kuebler, K.L. Braun, T.Y. Yu, J.K. Cammack, C.K. Ober, J.W. Perry, and S.R. Marder, Science **296** (2002) 1106.
48. (a) D. A. Parthenopoulos, P.M. Rentzepis, Science **245** (1989) 843 (b) J. H. Strickler, and W. W. Webb, Opt. Lett. **16** (1991) 1780 (c) A.S. Dvornikov, and P.M. Rentzepis, Opt. Commun. **119** (1995) 341 (d) K.D. Belfield, K.J. Schafer, Chem. Mater. **14** (2002) 3656.
49. (a) M. F. Yanik, H. Cinar, H. N. Cinar, A. Gibby, A. D. Chisholm, Y. Jin, and A. Ben-Yakar, IEEE Journ. Quantum Electron. **12** (2006) 1283 (b) P.N. Prasad, Introduction to Biophotonics, Chapter-12, Wiley-Interscience, New Jersey (2003) (c) A. Karotki, M. Khurana, J. R. Lepock and B. C. Wilson, Photochem. Photobio. **82** (2006) 443 (d) I.G. Meerovich, V. M. Derkacheva, G.A. Meerovich, N.A. Oborotova, Z.S. Smirnova, A.P. Polozkova, I.Y. Kubasova, E.A. Lukyanets, and A.Y. Baryshnikov, Proc. of SPIE **6427** (2007) 64270X.

50. (a) C. Rullière (ed.), Femtosecond Laser Pulses, 2nd Ed. Springer (2005) (b) B. Gu, W. Ji, X. Q. Huang, P. S. Patil, S. M. Dharmaprakash, J. Appl. Phys. **106** (2009) 033511 (c) B. Gu, W. Ji, X. Q. Huang, P. S. Patil, S. M. Dharmaprakash, Opt. Express **17** (2009) 1126 (d) B. Gu, W. Ji, P. S. Patil, S. M. Dharmaprakash, H. T. Wang, Appl. Phys. Lett. **92** (2008) 091118 (e) B. Gu, Y. Sun, W. Ji, Opt. Express **16** (2006) 17745 (f) B. Gu, K. Lou, H.-T. Wang, W. Ji, Opt. Lett. **35** (2010) 417.
51. F. Wagner, M Feuerhake, P Simon, Opt. Quant. Electron. **29** (1997) 811.
52. (a) M. Ghotbi, M. Ebrahim-Zadeh, A. Majchrowski, E. Michalski, I. V. Kityk, Opt. Lett. **29** (2004) 2530 (b) M. Ebrahim-Zadeh, Proc. SPIE **6118** (2006) 611809 (c) M. Ebrahim-Zadeh Proc. SPIE **6451** (2007) 645106.
53. S. Venugopal Rao, J. Opt. A. **6** (2004) 569.
54. K. Moutzouris, Thesis, University of St. Andrews, 2003.
55. Rick Trebino, Lecture Slides, Georgia Tech. University, USA. http://frog.gatech.edu/lectures.html
56. D. Swain, S. Venugopal Rao**,** in Emerging Trends in Laser & Spectroscopy and Applications, (ISBN # 978-81-8424-626-1)**,** Eds. A.K. Rai, I.M.L. Das, K.N. Uttam, Allied Publishers Pvt. Ltd., 272-276, 2010.
57. A. Rana, P. K. Panda, RSC Adv. **2** (2012) 12164.
58. (a) O. Katz, A. Natan, S. Rosenwaks, Y. Silberberg, Appl. Phys. Lett**. 92** (2008) 171116 (b) O. Katz, A. Natan, S. Rosenwaks and Y. Silberberg, OPN December 2008, 47.

Chapter 2

Experimental Details, Theory of Pump-Probe and Z-Scan Techniques

2.1 Ultrafast Laser Sources

High power pulsed lasers are attractive due to their potential applications in a diversified fields such as defense, communications, lithography, biomedical research etc.. At present kW to PW (peak power) lasers are commercially available in the market for various technological applications. Phenomena such as Q-Switching, Mode-locking and Chirp Pulse Amplification (CPA) assist the production of high energy pulses (ns to fs). One of the most common current ultrafast pulsed lasers include Ti-sapphire lasers. Generally, these short pulse laser sources aim to be cost effective, robust, and technologically simple. In 1982 researchers at Lincoln Laboratory operated a tunable laser based on Ti: Al_2O_3 for the first time [1a]. The most recent advances in the field of ultrashort pulse generation have been around the development of titanium-doped aluminum oxide (Ti^{3+}:Al_2O_3) as a gain medium. Ti:sapphire was introduced in 1986 and is the most favored gain medium, producing ultrashort pulses with good beam quality and high output power. The larger Ti^{3+} ion replaces 0.1% of Al^{3+} ion in the sapphire structure a few percent to progress in crystal growth. The ionic radius of the titanium ion is 26% larger than the aluminum one it replaces; induces a strong local distortion in the titanium ion, which then creates a strong local electric field. This means the absorption band is abnormally wide in the blue-green part of the spectrum. Under influence from the generated local electric field the absorption at these visible wavelengths excites electrons from a $2T_g$ ground state to a $2E_g$ excited level, which then splits into two sublevels 200000 cm^{-1} apart. The vibrational modes of the sapphire matrix are strongly coupled with the ground and excited states of the Ti^{3+} ion, which induces strong homogenous broadening.

Some of the special properties of the Ti:sapphire gain medium [1b] are:

- Sapphire (monocrystalline Al_2O_3) has an excellent thermal conductivity, lessening thermal effects even at high laser powers/intensities.
- Ti^{3+} ion has a very large gain bandwidth, permitting the generation of ultrashort pulses combined with wide tunability in wavelength. The maximum gain, laser efficiency are obtained near 800 nm. The possible tuning range is

~ 650-1100 nm, but different mirror sets are normally required for covering this huge range. The number of mirror sets required can be reduced by using ultra broadband chirped mirrors, which have been developed by various groups recently.

- There is also a wide range of possible pump wavelengths, which however are located in the green spectral region (typically 532 nm), where powerful laser diodes are not available. In the majority of cases, several watts of pump power was used, sometimes even 20 W (in our laser we use a 10 W pump laser). Originally, Ti:sapphire lasers were in most cases pumped with 514-nm argon ion lasers, which are powerful, but very inefficient, expensive to operate, and bulky. Other kinds of green lasers are now available, and frequency-doubled solid-state lasers based on neodymium-doped gain media are widely used. The pump wavelength is then typically 532 nm, with a slightly reduced pump absorption efficiency compared with 514 nm.
- The upper-state lifetime of Ti:sapphire is short (~3.2 μs), and the saturation power is very high. This suggests that the pump intensity has to be high, so that a strongly focused pump beam and thus a pump source with high beam quality will be essential.
- Despite the huge emission bandwidth, Ti:sapphire has relatively high laser cross sections, which reduces the tendency of Ti:sapphire lasers for Q-switching instabilities.
- Ultrashort pulses from Ti:sapphire lasers can be generated with passive mode locking which utilizes kerr lens effect as principle phenomena usually in the form of Kerr lens mode locking.
- Ti:sapphire is also used for multi-pass/regenerative amplifiers. Particularly with chirped-pulse amplification, such devices can reach enormous output peak powers of several terawatts (TW), or in large facilities even petawatt (PW).

Fs pulses [2] are now commonly available in numerous laboratories for employing pump probe techniques to understand chemical reactions on a ps/fs time scales. Detailed knowledge of temporal intensity profile of such laser pulses is important in many experiments. In addition it is often necessary to properly align the

laser system so that optimized (in terms of duration and energy) pulses are delivered. An improperly aligned grating compressor will not compress the pulse to desired pulse length. Due to non-availability of fast photo detectors to measure the pulse length several techniques such as Single Shot Autocorrelator (SSA) [3-5], Frequency Resolved Optical Gating (FROG) [6], GRating-Eliminated No-nonsense Observation of Ultrafast Incident Laser Light E-fields (GRENOUILLE) [7], and Spectral Phase Interferometry for Direct Electric-field Reconstruction (SPIDER) [8] have been invented over the last two decades. Some of the methods just provide the temporal information whereas others provide detailed information about the short pulses (temporal and phase). With detailed information about the input laser pulses one can (a) determine the temporal resolution of an experiment (b) determine whether a pulse can be made even shorter (c) understand various media: the better we know the light in and light out, the better we know the medium (d) use shaped pulses for possible applications in chemical reactions.

The classical method of second order intensity autocorrelation consists of crossing two pulses in non linear crystal and measuring the second harmonic light beam produced when the temporal delay between the two initial pulses varies. However this technique gives information about the pulse duration and yields no information about the temporal shape of the pulses. This method can, therefore, only be applied to lasers with good stability and not for amplified ultrashort lasers which work at low repetition rate because the pulse stability is poor. Consequently, it is necessary to use single shot measurements. The principle of an autocorrelator is to transform temporal information into spatial information which is easier to record. In this chapter we describe the various laser sources used in different experiments for studying the ultrafast response of organic molecules. The oscillator, amplifier, and OPA were commercial systems (MICRA, LEGNED, TOPAS). Furthermore, we also present the basic theory of various techniques utilized in the present studies such as degenerate pump-probe technique and Z-scan. Pump-probe studies were performed with both ps (800 nm) and fs (~600 nm) pulses. Z-scan studies were performed using ps (600 nm -800 nm, 1 kHz) and fs pulses (800 nm, 80 MHz and 1 kHz)

2.2 Micra Layout

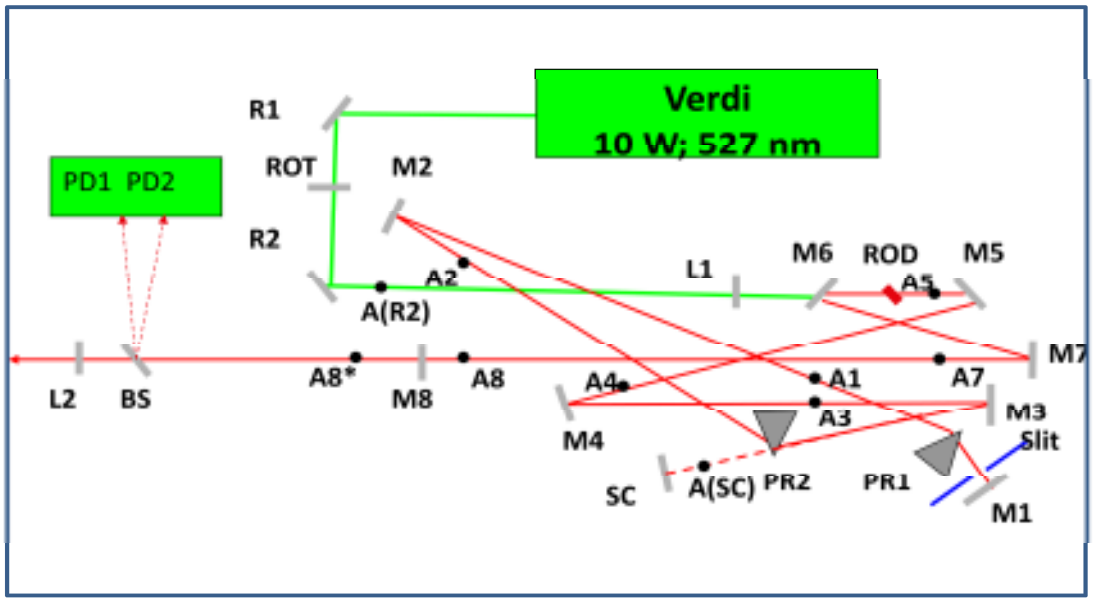

Figure 1 Optical layout of MICRA [9].

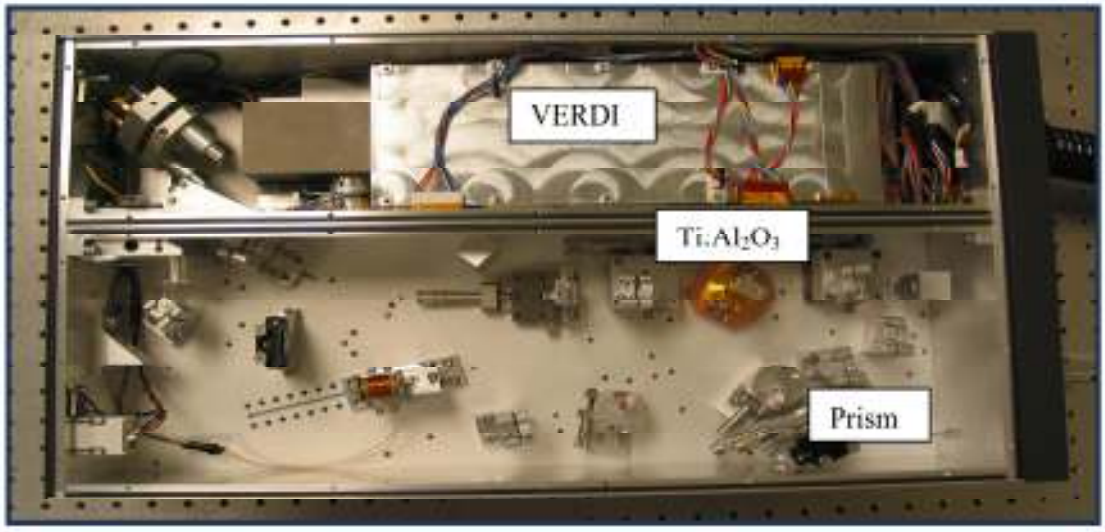

Figure 2 Inside view of MICRA [9].

MICRA (oscillator) optical layout and the inside view (actual) are shown in figures 1 and 2, respectively. MICRA is a compact broadband mode-locked ultrafast laser oscillator producing >100 nm bandwidth pulses centered near 800 nm gain peak of Ti:sapphire. The Micra (one box-design) combines stability of an integrated Verdi pump laser, along with bandwidth and centre wavelength tenability. Typical Micra

operation with a 10W Verdi pump laser at 532 nm generates 500-800 mW output power with bandwidth 40-60 nm.

2.3 Fs amplifier (LEGEND) Layout

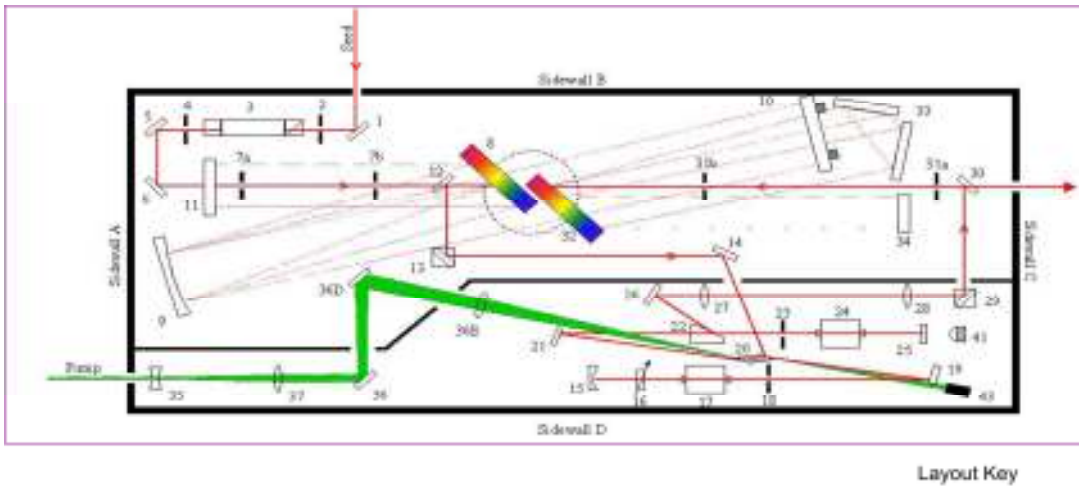

Figure 3 Inside view of LEGEND amplifier (Coherent Inc.) [10].

Legend (Ultrashort Pulse, USP) is a scientific and industrial regenerative amplifier CPA laser system as shown in figure 3 using all-solid–state technology and is capable of producing femtosecond pulses with an average energy of ~2.5 mJ at 800 nm delivering pulses at 1 kHz repetition rate. Legend consists of three assemblies (a) pulse stretcher (b) Ti:Al_2O_3 regenerative amplifier and (c) a pulse compressor. The sapphire rod is pumped by the 20W pump source (Evolution, Nd:YLF) at 527 nm. Legend (USP) uses regenerative amplification rather than complex multi-pass technology. Regenerative amplification provides better beam quality, stability, and simplicity of use for the <40 fs operating range.

2.4 TOPAS-C (Travelling wave Optical Parametric Amplifier Super fluence) layout

TOPAS-C is pumped by a fundamental harmonic of Ti:sapphire lasers and covers wavelength range from 1150 to 2600 nm. With optional frequency mixers this range can be extended from 189 nm to 20 μm. TOPAS-C (schematic/inside view is shown in the figure 4) is a two-stage parametric amplifier of white-light continuum. Its basic configuration comprises of several subunits: pump beam delivery and splitting optics, white-light continuum generator (WLG), a pre-

amplifier or first amplification stage (PA1), a signal beam expander-collimator (SE) and a power amplifier or second amplification stage (PA2). These subunits are arranged in a single compact unit. The device employs computer controlled translation and rotation stages that allow for a fast and precise optimization of positions of certain optics when tuning the output wavelength of TOPAS-C.

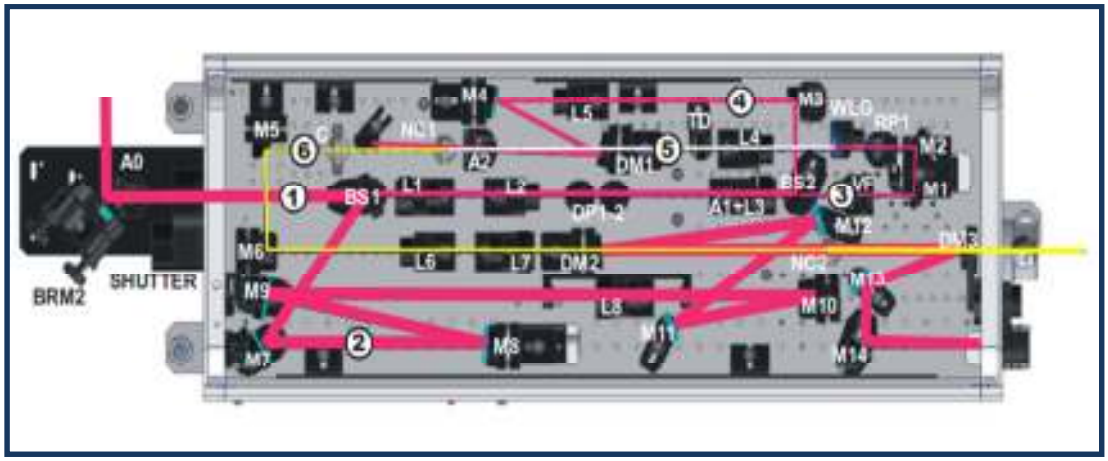

Figure 4 Inside view of TOPAS-C [11].

Small fraction (~1-3 μJ) of pump pulses at 800 nm is used to produce a white light continuum (WLC) in sapphire plate. The WLC beam and another fraction (30-50 μJ) of the pump beam are focused into the pre-amplifier crystal. The pulses are timed and overlapped noncollinearly inside the nonlinear crystal, where parametric amplification takes place. A non-collinear geometry is used for easy separation of the amplified signal beam. The residual pump and idler beams are blocked by a beam blocker after the crystal. The signal beam is expanded and collimated by a lens telescope, and transported into the second amplification stage. The power amplifier is usually pumped by the bulk of the input pump beam. The pump beam size is reduced to achieve necessary pump intensity by a lens-mirror telescope. The beam is kept collimated after the telescope. The pump and signal beams are overlapped collinearly in the second nonlinear crystal. As a result the TOPAS-C outputs collinear well collimated signal and idler beams. Optional frequency mixers can be used at TOPAS-C output to extend the tuning range into visible, ultraviolet and/or infrared. The wavelength tuning in the pre-amplifier stage is achieved by changing the delay of the white-light pulse with respect to the first pump pulse and adjusting

the crystal angle for optimal phase-matching. The wavelength tuning in the power-amplifier is achieved by first adjusting the pre-amplifier wavelength and then optimizing the second crystal angle and signal delay with respect to the second pump beam. The wavelength can be changed easily through a computer using a dedicated software package WinTOPAS.

2.5 Measurement of fs/ps pulses spectra

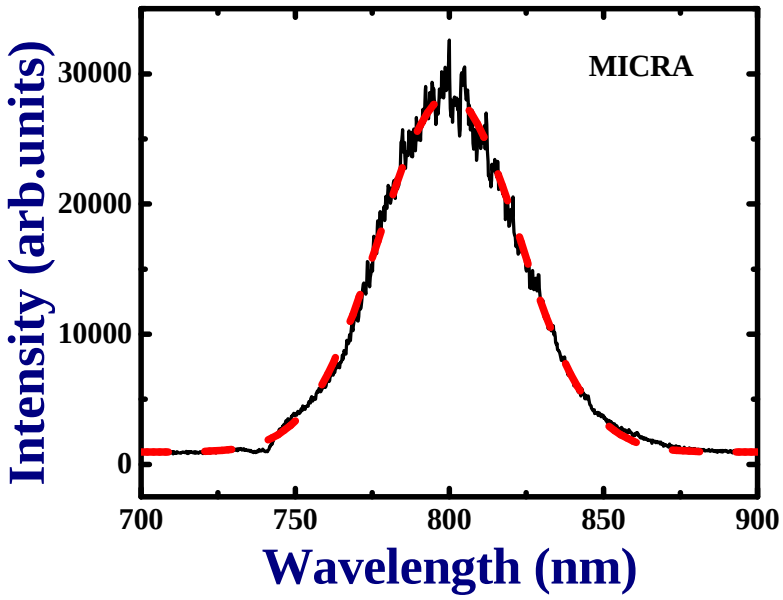

Figure 5 Output of MICRA (femtosecond oscillator) as measured by Ocean optics spectrometer (USB 4000). Bandwidth (FWHM) of output was found to be ~40 nm at 800 nm. Dotted line is the fit while black line is the data.

MICRA (oscillator) seeds both the fs and ps amplifiers. Approximately 20% (of ~600 mW) from MICRA output goes in to LEGEND (USP) while 80% seeds a ps amplifier (LEGEND, ~2 ps). Figure 5 shows a typical spectrum obtained from MICRA. The output pulse duration (and hence the bandwidth) can be tuned by adjusting the prisms inside MICRA. The pulse duration can be adjusted from ~12 fs to ~100 fs with corresponding bandwidth adjustment possible from ~90 nm to ~10 nm. Typically a bandwidth of 50-55 nm (FWHM) is required and utilized for stable operation of the fs amplifier. The ps amplifier does not require such bandwidth. However, the lasers were designed such that both the amplifiers can work

simultaneously with single seed. Figure 6 shows a typical output spectrum from fs amplifier (~25 nm FWHM). Fully compressed pulses had a FWHM of ~28 nm).

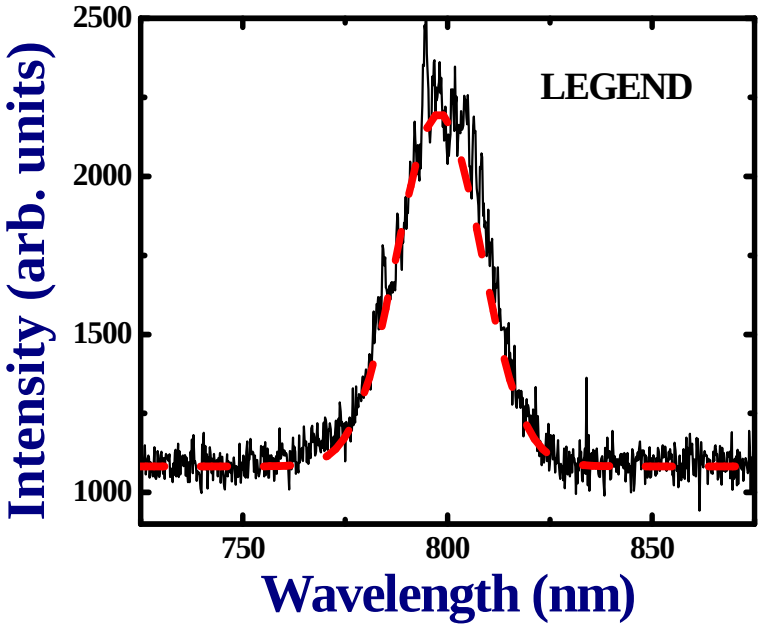

Figure 6 Output of fs amplifier measured by a spectrometer (USB 4000). Band width was found to be (FWHM) ~25 nm at 800 nm. Dotted line is the fit while black line is the data.

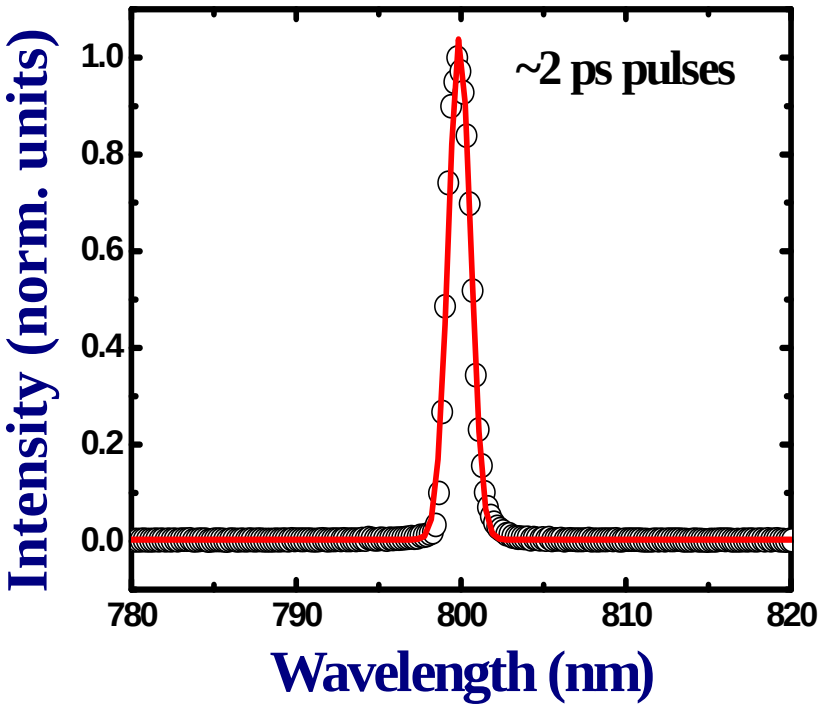

Figure 7 Output of LEGEND ps amplifier measured at 800 nm by Ocean optics spectrometer (USB 4000). Band width was found to be FWHM ~ 1.5 nm.

The bandwidth can be adjusted by changing compressor position in the amplifier. An optimized bandwidth (shortest pulse duration) was obtained each time by looking at the plasma generated in air or optimizing the output of TOPAS C (maximum output occurs only for shortest and compressed pulses). Figure 7 shows a typical spectrum from ps amplifier (~1.5 nm FWHM). The pulse duration in both fs and ps case were measured using autocorrelation techniques (both external and using a single shot autocorrelator).

2.6 Intensity autocorrelation

Intensity autocorrelation $A^{(2)}(\tau)$, is an attempt to measure the pulse intensity vs. time. It is the result of pulse used to measure itself in time domain. It involves splitting the pulse into two and delaying temporally and spatially overlapping them onto the non linear second harmonic generating (SHG) crystal. A SHG crystal will produce the twice the frequency of input light with a field that is given by

$$E_{sig}^{SHG}(t,\tau) \propto E(t)E(t-\tau) \tag{1}$$

Where τ is the delay between two pulses. The resultant field intensity is proportional to the product of intensities of two input pulses:

$$I_{sig}^{SHG}(t,\tau) \propto I(t)I(t-\tau) \tag{2}$$

Intensity autocorrelation or autocorrelation is given by

$$A^{(2)}(\tau) = \int_{-\infty}^{\infty} I(t)I(t-\tau)dt \tag{3}$$

The autocorrelation trace yields a rough measure of the pulse intensity width and, for very complex pulses, a rough measure of the pulse spectral width. But this is all that it yields. It says nothing of the actual spectrum or the intensity structure. Thus, a pulse intensity shape and phase must typically be assumed when using any type of autocorrelation. The resulting pulse length will depend sensitively on the shape chosen. A relative delay of one pulse length will typically reduce the SHG intensity by a factor of two.

2.7 External Autocorrelation with BBO

Due to the large bandwidth associated with ultrashort pulses dispersion is an important phenomenon that needs to be understood and countered [12-17]. BBO is a potential nonlinear optical crystal for frequency conversion in the UV-visible region. During initial stages we performed autocorrelation measurements externally using a 2-mm BBO crystal (type I critically phase matching for SHG, 29.1^0 cut). Figure 8 shows the schematic of the non-collinear external autocorrelation experiments performed on ~40 fs/~1.5 ps pulses at 800 nm.

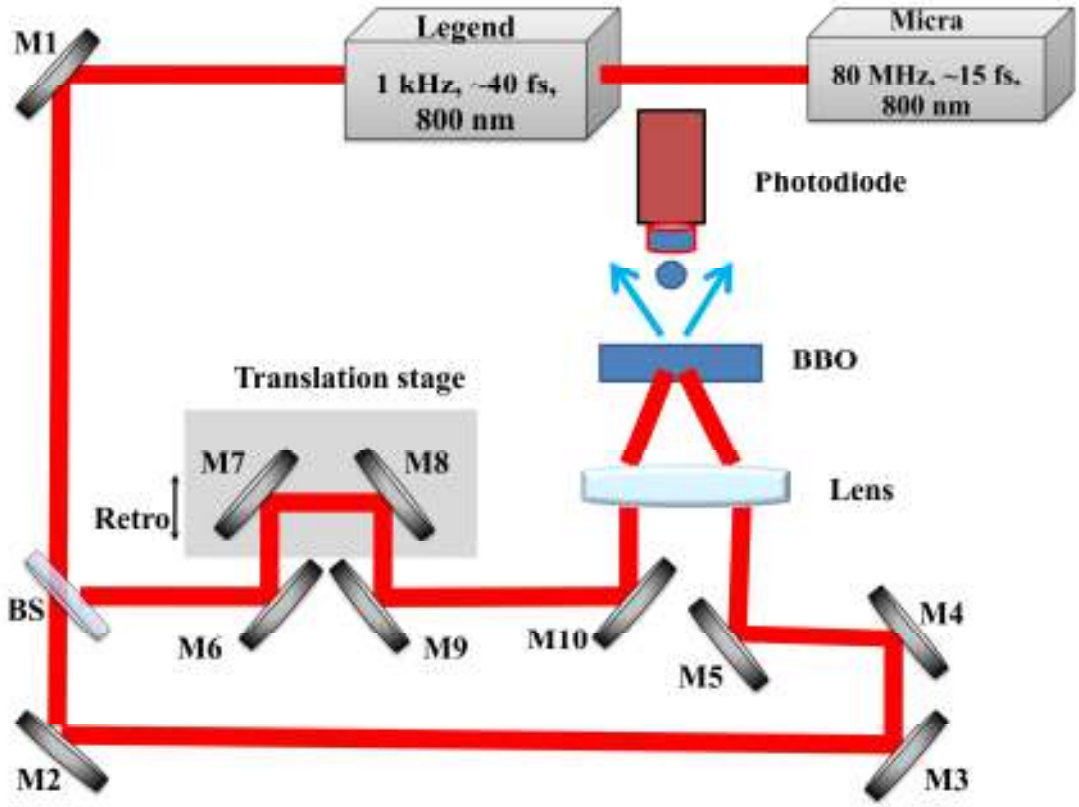

Figure 8 External autocorrelation measurements of fs pulses using BBO.

Figure 9 shows typical autocorrelation data for ps pulses at 800 nm. The pulse width obtained from the experiments was ~1.55 ps. Throughout the thesis we assumed the ps pulses duration to be ~1.5 ps. However, depending on the MICRA alignment and the ps amplifier alignment we expect the pulse duration to be in the range of 1.5-2.0 ps. We also studied the pulse broadening effects due to group velocity mismatch in both these crystals along with the propagation properties of

these pulses in various media. We compared our simulations with the autocorrelation data obtained from BBO crystal using ~40 fs, 800 nm pulses. BBO or beta-BaB_2O_4 is a NLO crystal possessing wide transparency and phase matching range, large nonlinear coefficient, high damage threshold and excellent optical homogeneity. Figure 10 illustrates the autocorrelation data of ~40 fs pulses. The pulse duration retrieved was ~432 fs.

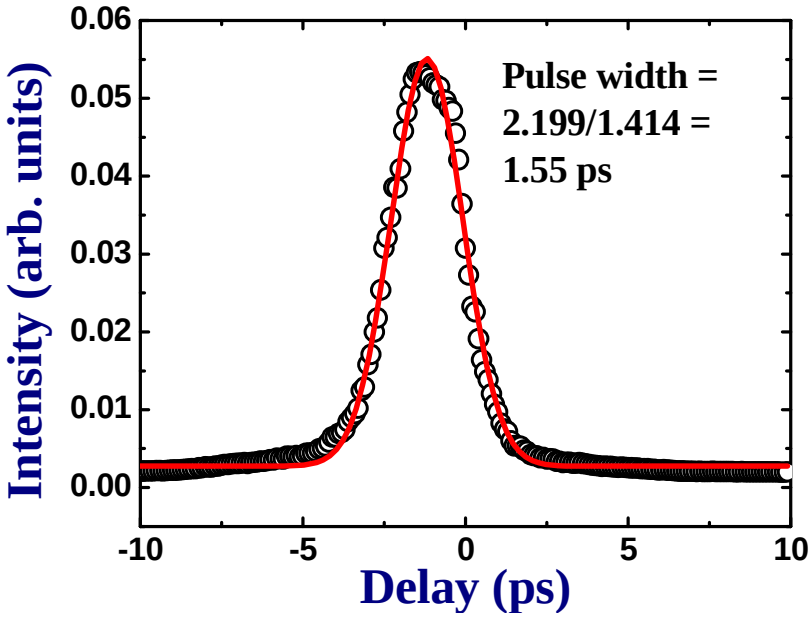

Figure 9 ps autocorrelation measurement depicting a pulse width of ~1.55 ps. SHG of 800 nm radiation was used for these studies.

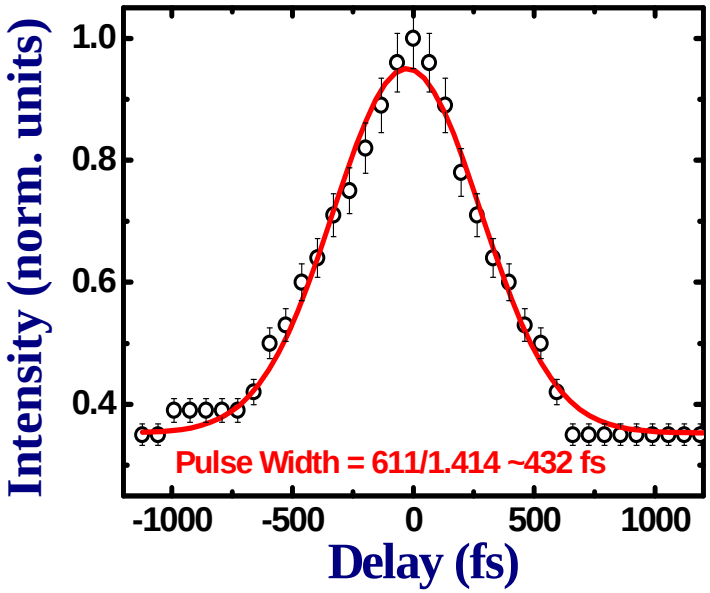

Figure 10 Fs autocorrelation (pulse width) measurements using BBO crystal (800 nm to 400 nm SHG)**.**

Experiments, Simulations and Results:

The group velocity mismatch (GVM) and group velocity dispersion (GVD) were calculated using the equations (36,37) as explained section 1.9 .

Sellmeier equation for BBO:

$n_o^2(\lambda_0) = 2.7359+0.01878/(\lambda_0^2 -0.01822)-0.01354\ \lambda_0^2$

$n_e^2(\lambda_0) = 2.3753+0.01224/(\lambda_0^2-0.01667)-0.01516\ \lambda_0^2$

At λ_0= 800 nm $V_g(\lambda_0/2) = 1.6830 \times 10^8$ m/s, $V_g(\lambda_0) = 1.7810 \times 10^8$ m/s &

GVM = 194 fs/mm GVD at 800 nm is 74.735 fs^2/mm for BBO.

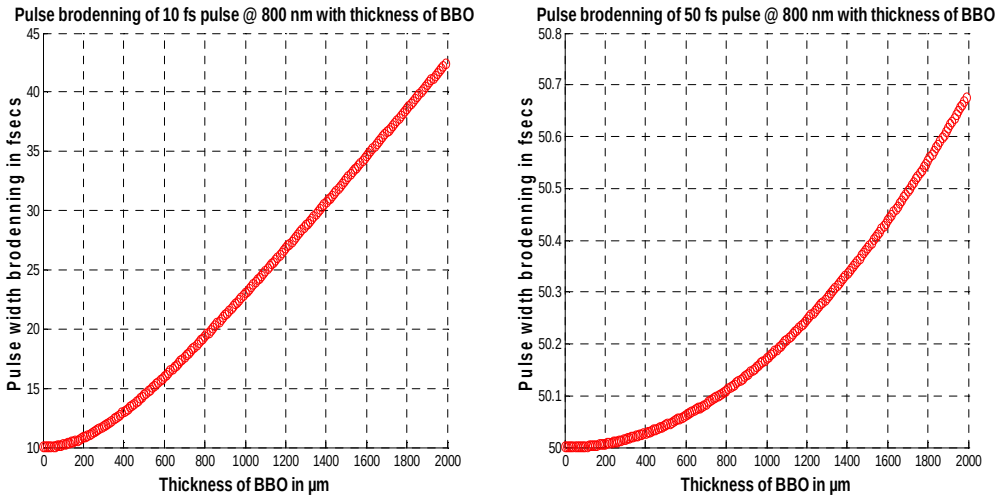

Figure 11 Pulse broadening as a function of crystal length for (a) 10 fs pulse (b) 50 fs pulse.

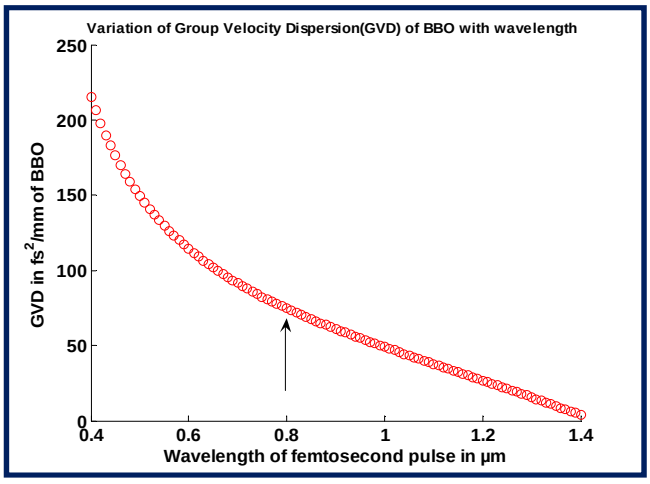

Figure 12 GVD in BBO as a function of wavelength.

Figure 11 illustrates the pulse broadening effects of 10 fs and 50 fs pulses when passed through BBO. Figure 12 demonstrates the variation of GVD in BBO as a function of wavelength. Group velocity mismatch (GVM) for 800 nm SHG (to 400 nm) in BBO was estimated to be ~ 194 fs/mm. From these simulations we have extracted the pulse duration after travelling the BBO crystal (~2 mm) to be ~388 fs (GVM × L = 194 fs/mm × 2 mm) [17]. Our experimental value observed was ~432 fs. Thus the experimental and theoretical pulse width values were ~432 fs and ~388 fs, respectively, which matched reasonably well. Table summarizes the values of group velocity and group velocity dispersion (GVD) of common optical materials and crystals which will be helpful in estimating the pulse broadening.

Material	**R.I. @ 800 nm**	**Group velocity (v_g) m/s**	**Group Velocity Mismatch (GVM) (fs/mm) for SHG of 800 nm**	**Group Velocity Dispersion (fs^2/mm)**
Quartz	1.4533	2.04×10^8	-	36.13
SF10	1.7113	1.71×10^8	-	158.9
Sapphire	1.7602	1.68×10^8	-	58.06
Calcite	1.6487	1.68×10^8	-	76.20
BBO	1.6606 (n_o)	1.78×10^8	194.0	74.73
BiBO	1.9191 (n_1)	1.52×10^8	592.9	164.22
LBO	1.5692	1.68×10^8	123.0	40.33
LiNbO3	2.2552	1.61×10^8	3736.4	429.58
KD*P	1.5543	1.43×10^8	7654	1334.8
KTP	1.7487	1.67×10^8	981.8	201.44
KDP	1.5015	1.68×10^8	77.0	27.33

Table 1 Dispersion parameters calculated for typical materials used in various experiments.

2.8 Single Shot Autocorrelator (SSA)

SSA provides complete temporal characterization (sans phase information) of ps/fs pulses. Laser pulses are split into two beams, which are then non-collinearly frequency doubled in a non-linear crystal (KD*P). Figure 13 shows the layout of SSA. The relative wave front tilt produces a spatial time delay in the frequency-doubled signal, resulting in an autocorrelation of the temporal intensity profile of the pulse. The autocorrelation is detected by a CCD array that is read out on a standard laboratory oscilloscope or captured with a computer DAC. A variable delay line is included, which provides accurate, calibrated synchronization of the two beams.

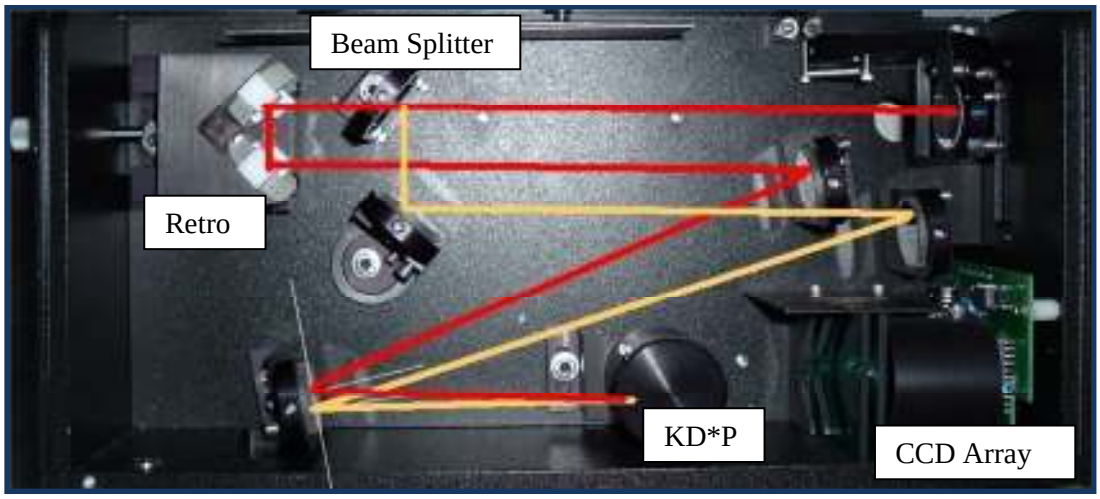

Figure 13 Inside view of a single shot autocorrelator.

In fs mode, the geometric wave front tilt introduced by non-collinearly crossing the beams in the crystal is sufficient to measure sub-picosecond pulses. One can measures temporal pulse widths ranging from 30 fs to 20 ps. It covers wavelengths in between 530 nm to 1600 nm. The autocorrelation signal was detected by CCD array that read out on Tektronix 1320B series oscilloscope as explained in section 2.2. A single shot autocorrelation trace (data shown in figure 14) is obtained by mapping the delay onto position and spatially resolving the autocorrelation signal using camera or array detector. This involves crossing of two beams in the nonlinear-optical crystal at large angle, so that on the left, one pulse precedes the other, and, on the right, the other precedes the one. In this manner, the delay ranges from a negative value on one side of the crystal to a positive value on the other. Typical pulse duration measured using SSA was ~54 fs. Depending on

the compressor position within the amplifier and the number of optics the fs laser pulses are passing through the pulse duration (originally fully compressed pulses duration was ~36 fs) the measured pulse duration will vary.

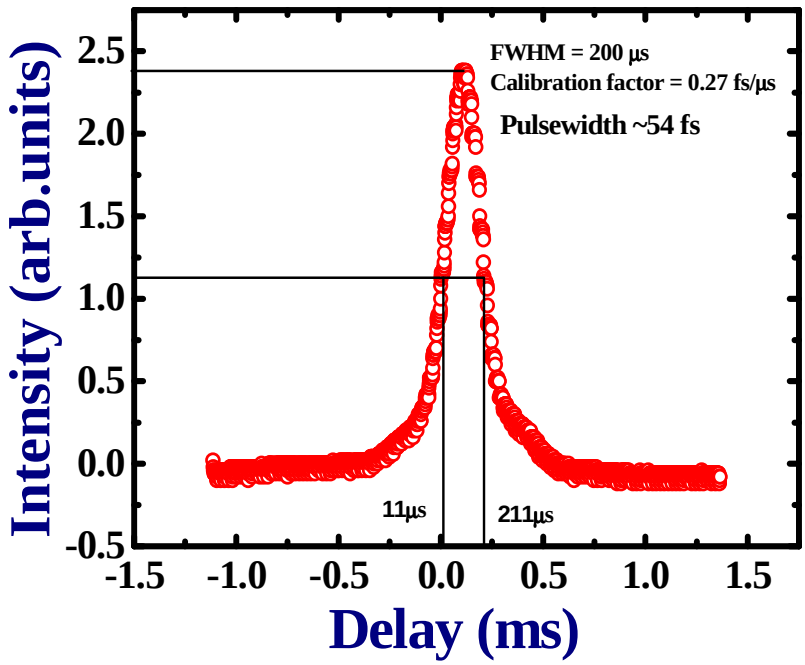

Figure 14 Output of a Single Shot Autocorrelator.

2.9 Pump-probe transmission

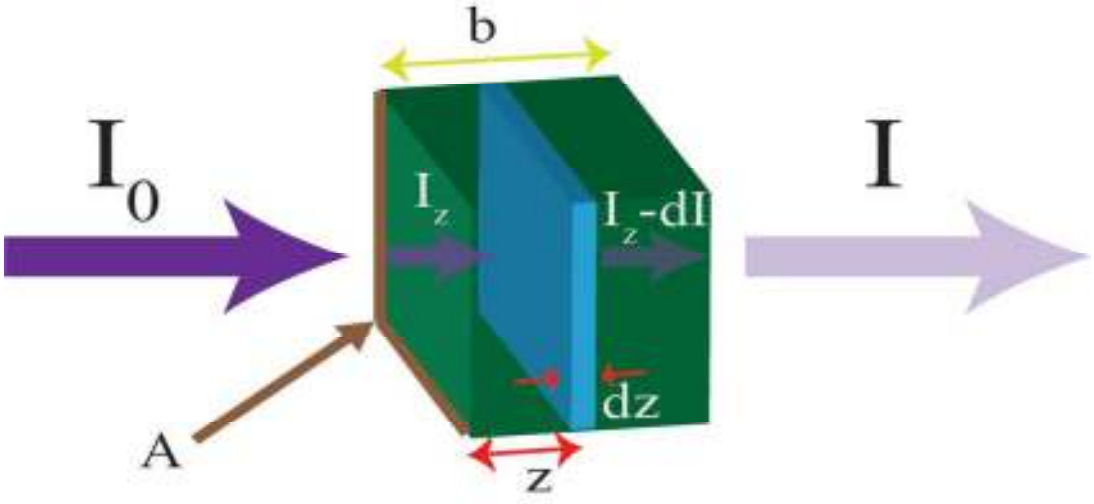

Figure 15 Typical absorption schematic according to the Beer-Lambert Law. Initially, radiation of intensity *I* is incident on a sample of length *b* and total area *A*. For a subsection of the sample of width *dz*, *z* deep into the sample along the propagation axis of the incident light (arriving at *z* now with intensity I_0), a certain amount of light (*dI*) is absorbed by the sample [*n(z)* particles] with absorption cross section *s*. Finally, the light emerges from the sample with intensity *I*. (adapted from thesis of Erik Robert Hosler [23c]).

We can see from figure 18 the various processes at sample position. Absorption by a sample may be derived starting with a small subsection of the total sample. Given that light of initial intensity *I* is incident on a sample of interaction length *b*, over an incremental section *dz*, *dI* light is absorbed from the initially incident light intensity, I_0 (at some position (*z*) within the sample such that some light has already been absorbed from *I*), on the subsection of area *A*

$$\frac{dI}{I_z} = -\sigma * n(z) * dz \tag{4}$$

The total number of absorbers illuminated by the incident light source within the subsection of volume *Adz* is *n(z)* and each absorber has a cross-section for absorption of σ. Then, integrating over the total volume of the sample illuminated by the light source the total change in the absorption may be calculated:

$$\int_{z=0}^{z=b} \frac{dI}{I_z} = -\int_{z=0}^{z=b} \sigma * n(z) * dz$$

$$\ln[I] - \ln[I_0] = \ln\left[\frac{I}{I_0}\right] = -\sigma * n_{eff} * b \tag{5}$$

Here, the effective number density, n_{eff}, accounts for the pressure gradient encountered in the gas phase experiments across the aperture of the target cell. Essentially, n_{eff}, reflects the total analyte molecules along the path length of the incident light, which are more accurate than the absolute number density. The total absorbance of the sample in terms of the incident and transmitted light intensities is then:

$$Absorbance = ln\left[\frac{I}{I_0}\right] = \sigma * n_{eff} * b \tag{6}$$

Where transmittance is given as:

$$Transmission = e^{-\sigma * n_{eff} * b} \tag{7}$$

The optical density of the sample may then be written as:

$$OD_{measured}(E) = -log_{10}\left[\, e^{-\sigma * n_{eff} * b} \right] \quad (8)$$

By utilizing the Beer-Lambert law optically density in base$_{10}$ a direct comparision may be made between the absorbed light and the incident light i.e.if a sample of given density and the absorption section initially has an optical density of 0.5 and subsequently has an optical density of 0.25 after the pertubation. Therefore, absorption spectroscopy provides a unique method for monitoring chemical dynamics in real-time given sufficient temporal resolution relative to the investigated phenomena.

2.10 Theory of Pump-Probe spectroscopy

To describe a pump-probe experiment [18, 19], let us consider a situation in which the sample is illuminated by two pulses: a pump pulse, centered at time zero, $I_{pu}(t) = I_1(t)$, and a probe pulse delayed by a time τ, $I_{pr}(t) = I_2(t - \tau)$. Calling α_0 the linear optical absorption coefficient of the sample, the pump pulse perturbs it inducing a variation given by

$$\Delta\alpha(t) = \int_{-\infty}^{t} I_1(t')A(t - t')dt' = I_1(t) * A(t) \quad (9)$$

where the symbol * stands for convolution and A(t) is the impulse response of the medium, whose determination is usually the object of the experiment. The probe pulse intensity changes by

$$\Delta I_{Pr}(t) = I_{pr}(t)e^{-\alpha_0 d}(e^{-\Delta\alpha(t)d} - 1) \approx I_{pr}(t)e^{-\alpha_o d}\Delta\alpha(t) \quad (10)$$

where d is the sample thickness, and the perturbation induced by the pump pulse is assumed to be small ($\Delta\alpha d \ll 1$).

The pump induced variation of probe energy is

$$\Delta E_{pr}(\tau) = \int_{-\infty}^{+\infty} \Delta I_{pr}(t')dt' \tag{11}$$

$$= k \int_{-\infty}^{+\infty} I_2(t' - \tau)dt' \int_{-\infty}^{+\infty} I_1(t^{"})A(t' - t^{"})$$

$$dt^{"} = kI_2(t) \otimes [I_1(t) * A(t)] \tag{12}$$

where the symbol $\otimes$ stands for cross-correlation. By a change of variables, equation 24 can be cast in the form

$$\Delta E_{pr}(\tau) = A(t) * [I_1 \otimes I_2] = A(t) * C(t) \tag{13}$$

where $C(t) = \int_{-\infty}^{+\infty} I_1(t)I_2(t + \tau)dt'$ is the cross-correlation of pump-probe intensity profiles. The pump-probe signal is thus given by convolution of system response with cross-correlation of pump and probe pulses. Equation (4) highlights the need to use very short pump and probe pulses to resolve fast temporal dynamics. All dynamical processes taking place on the time scale much shorter than the pump-probe cross-correlation are averaged out by the experiment.

For time delays τ much longer than the duration of pump-probe cross-correlation, when pump and probe pulses are not temporally overlapped, one can simplify equation (3) to $\Delta E_{pr} = -\Delta\alpha(\tau)de^{(-\alpha_0 d)} \int_{-\infty}^{+\infty} I_{pr}(t)dt$
so that the normalized probe energy variation becomes

$$\frac{\Delta T}{T} = \frac{\Delta E_{Pr}}{E_{Pr}} = -\Delta\alpha(t)d \tag{14}$$

To calculate the absorption change Δα, let us assume that the system under study consists of *n* electronic states, with populations N_j, which are changed by the pump pulse by an amount ΔN_j. One can then write

$$\Delta\alpha(\nu, \tau) = \sum_{i,j=1}^{n} \sigma_{ij}(\nu)[\Delta N_i(\tau) - \Delta N_j(\tau)] \tag{15}$$

Where σ_{ij} is the frequency-dependent cross section for the transition between state N_i and state N_j. The resulting differential transmission change is

$$\frac{\Delta T}{T}(\nu,\tau) = -\Delta\alpha d = \sum_{i,j=1}^{n} \sigma_{ij}(\nu)[\Delta N_i(\tau) - \Delta N_j(\tau)] \quad (16)$$

$\Delta T/T$ signal depends on both pump-probe delay and probe frequency ν, at each frequency the signal can be the result of the overlap of several transitions, each weighted with its cross-section.

2.11 Physical processes involved in pump-probe spectroscopy

The differential transmission ($\Delta T = T_{Pump,ON} - T_{Pump.OFF}$) is observed by measuring the probe transmission when sample is pumped on and pumped off. It is possible to find information about excited state molecules or atoms at a specific time after excitation. The time resolution and information about the kinetics of the molecules or atoms can be obtained by measuring the delay between pump and probe. When sample absorbs a photon from pump beam it is promoted to excited state. Three important physical processes can occur.

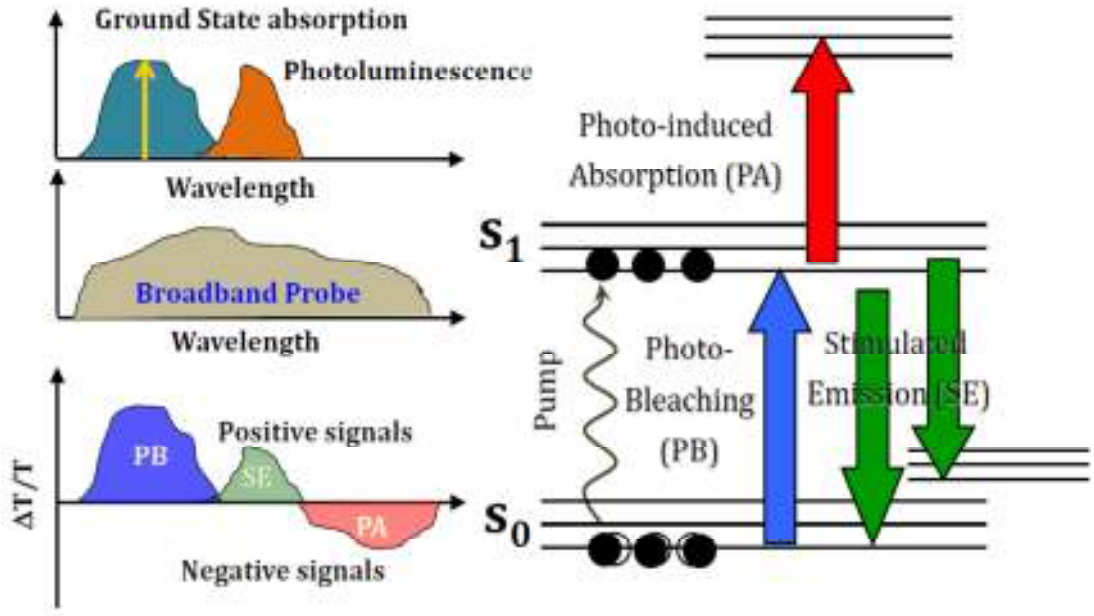

Figure 16 Physical processes in Pump-probe spectroscopy.

2.11.1 Ground state bleach or photo-bleach (GSB/PB)

Pump excites the molecules to higher states which results in reduced number of molecules in the ground state. There will be an increase in transmission at the wavelength where molecules absorb in the ground state. A positive signal of ($\Delta T>0$) is obtained in this case.

2.11.2 Stimulated Emission (SE)

Pump populates the excited state in such a way that the probe can stimulate those molecules at excited state to return back to ground state and photon identical to an excited photon will be released. The quantity of photo releases will increase thus increase in the differential transmission ($\Delta T >0$).

$$\frac{\Delta T(t)}{T} = y_0 + A_1 e^{-(t-t_0)/\tau_1} + A_2 e^{-(t-t_0)/\tau_2} + A_3 e^{-(t-t_0)/\tau_3} \quad (17)$$

The signal is caused by the excited state population which can be excited further to higher energy level by probe pulse. There will be increase of the absorption by probe beam thus decrease in transmission by the probe beam ($\Delta T <0$). [20]

2. 11.3 Excited State Absorption (ESA)

Pump pulses reduces the number of absorbing molecules in ground state inducing, at probe frequencies equal to or higher than the ground state absorption, an absorption decreases; this is so called ground state bleaching (PB), giving rise to a transmission increases ($\Delta T/T >0$). At the same time, pump pulses populate the excited state, so that a probe photon can stimulate emission (SE) signal, also causing a transmission increase ($\Delta T/T >0$) occurs at probe frequencies equal or lower than ground state absorption. For some probe frequencies PB and SE overlap, while for other pure SE signal is observed. Finally, the excited state populated by the pump pulse can absorb to some other higher-lying level; this so-called photo-induced absorption (PA) causes a transmission decrease ($\Delta T/T <0$). PA can occur at any probe frequency, depending on the energy level structure of the molecule under study; in particular, it can sometimes spectrally overlap the PB and SE signals and even overwhelm them.

2.12 Femtosecond pump-probe experiments at 600 nm

All the fs degenerate pump-probe experiments [18-22] were performed near 600 nm. The liquid samples were taken in a 5 mm thick glass cuvette. The samples were excited with pulses from 1 kHz optical parametric amplifier (TOPAS-C, Light Conversion, Coherent) delivering pulses of ~70 fs duration pumped by a Ti:sapphire regenerative amplifier. The pulse-width at the sample in our fs experiments was estimated (taking into account the optics and lenses involved) to be ~70 fs. Pump pulses in the energy range of 5–50 µJ were used. The probe beam diameter was ~2 mm, and pump beam diameter was ~4 mm.

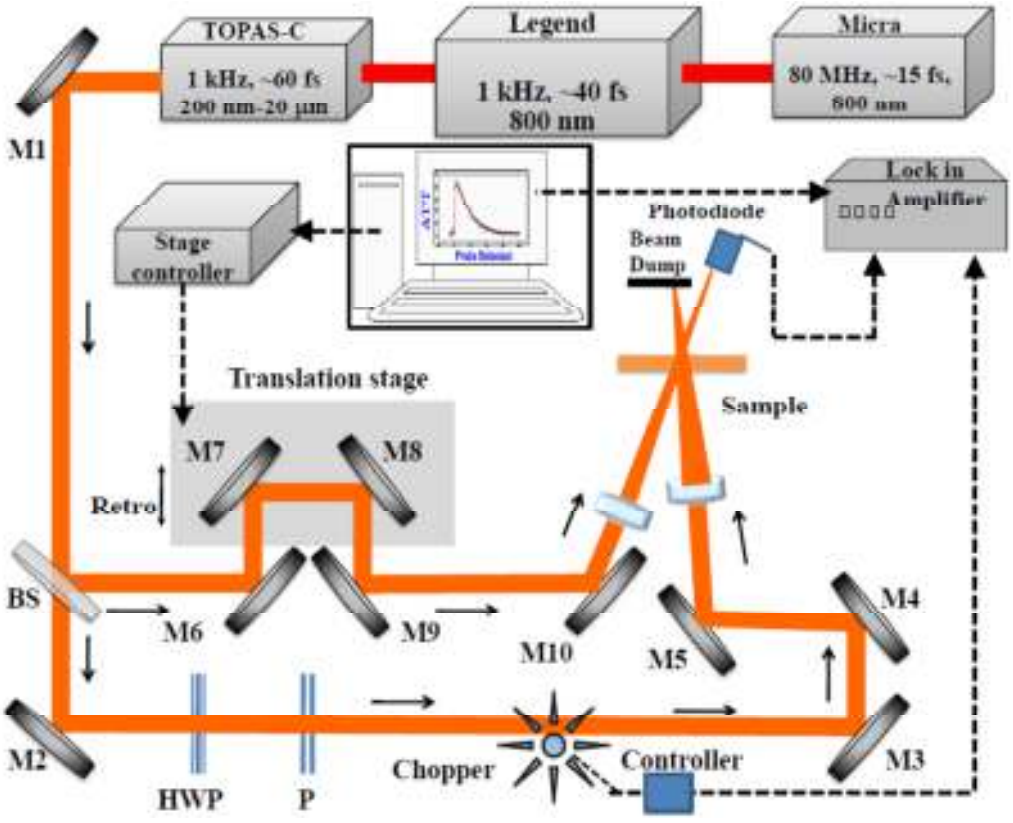

Figure 17 Typical arrangement of fs pump-probe experiment at 600 nm.

The pump beam was focused using a 150 mm lens, while the probe beam was focused using a longer focal length lens (500 mm). The ratio of pump to probe intensities was > 20. The pump beam was modulated at 109 Hz with the help of a chopper and the change in transmitted probe intensity was measured using a combination of a photodiode (SM05R/M, Thorlabs) and lock-in amplifier (7265,

Signal Recovery). The polarization of pump/probe beams was perpendicular to avoid coherent artefacts [23]. Schematic and actual fs experimental set up can be seen from the data presented in figures 17 and 18. The crucial aspect in pump-probe experiments is the maximum overlap between pump-probe at the sample. The zero delay is adjusted properly to tune both side i.e. +ve and –ve sides. The variation of pump-probe diameter was also optimized. The ratio of pump power to probe power was 50:1 or better. Dispersion less mirrors are used for the experiments. Angle of overlap between pump and probe (~5^0) was optimized to achieve better signal noise ratio. The crucial zero delay is the key issue in pump-probe experiment. All efforts were made for both spatial and temporal overlap of the beams meet at the sample. Polarization of the beam was modified using a half wave plate and Brewster polarizer combination. Sufficient care was taken for achieving stability of input laser beam throughout the scan. Laser TTL pulses can be seen as yellow lines and chopper output at 500 Hz in the figure 19. It was observed that chopper square wave pulse drifts with triggered TTL laser pulse. Therefore, we have taken care so that frequency of the chopper should not be multiple of line frequency 50 Hz. Later on we have taken an optimized chopper frequency of 109 Hz and the observed TTL pulse was quite stable. We had collected average of 10 pulses per second for achieving superior signal to noise ratio.

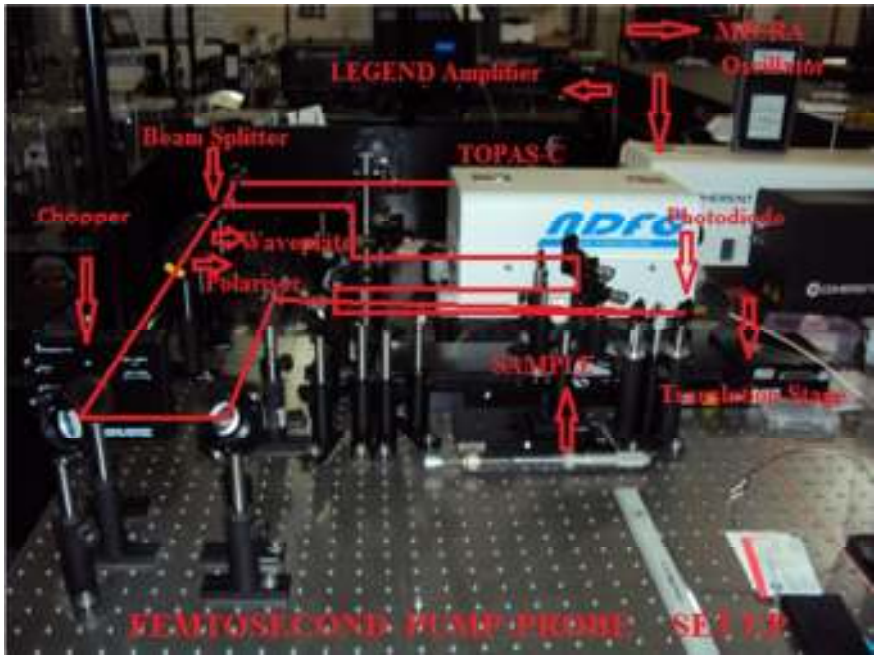

Figure 18 Photograph of the actual fs pump-probe experimental set up.

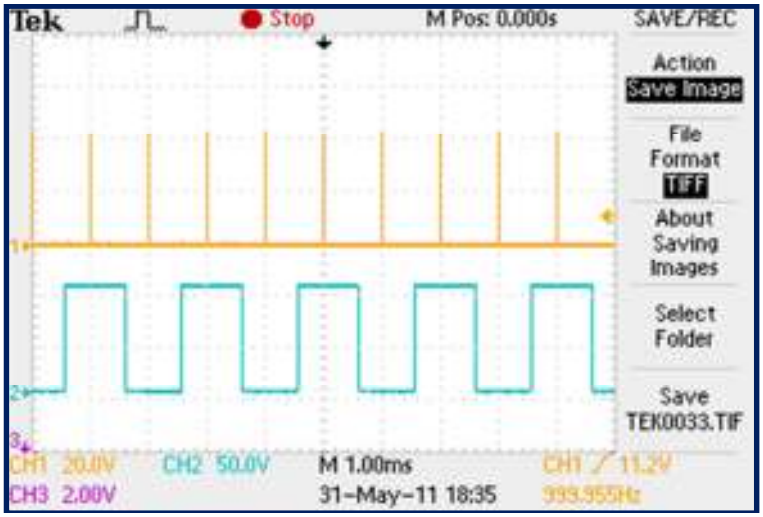

Figure 19 Output of oscilloscope with chopper output given by blue lines and yellow lines given by laser 1 kHz pulses.

2.13 Ps pump-probe experiments at 800 nm

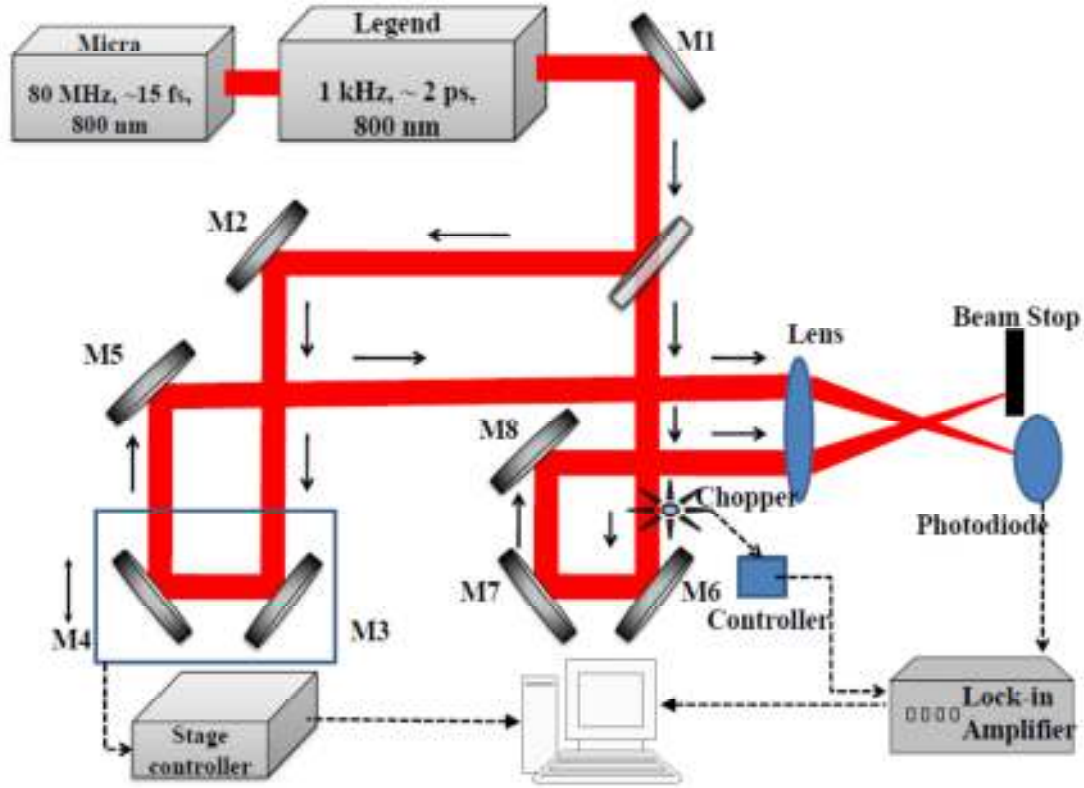

Figure 20 Typical arrangement of a ps pump-probe experiment at 800 nm.

In the ps pump-probe set up, pump and probe beam diameters were ~4 mm, ~2 mm, respectively. The molecules were excited by pulses from 1 kHz Ti:sapphire regenerative amplifier (LEGEND, Coherent) delivering pulses of ~1.5 ps duration. The pump and probe beams were focused using single 200 mm lens. Typical peak intensities of pump and probe beams were ~150 GW/cm^2 and ~2–4 GW/cm^2, respectively. The ratio of pump to probe intensities was at least 75. The focusing was such that the probe beam diameter was ensured to be slightly smaller than the pump beam diameter. The schematic of experimental set up is illustrated in figure 20.

2.14 Z-scan experimental setup

The technique of Z-scan [24] has been used in time range of fs [24] to ms [25] to measure the nonlinear optical parameters. The changes due to the absorptive nonlinearity give rise to saturable absorption (SA) and reverse saturable absorption (RSA) effects in Z-scan profiles. On the other hand, changes in nonlinear refraction appear as peak-valley or valley-peak in the Z-scan profiles. In this technique the transmitted energy is measured as a function of the sample position. Information on nonlinear absorption (NLA) and nonlinear refraction (NLR) are determined by keeping in view of the geometry of the experimental setup. To obtain information on the NLA, the open aperture (OA) geometry is used in which all the transmitted energy is collected. In the case of NLR the transmitted energy is collected through the aperture centered on the beam in the far field (known as the closed aperture (CA) Z-scan) [26].

2.14.1 Ps Z-Scan experiments (800 nm)

Z-scan measurements [27-30] were performed using ~2 ps, 800 nm pulses with a repetition rate of 1 kHz from an amplified Ti:sapphire system (Legend, Coherent) as shown in figure 21. The pulses were nearly transform limited and this was confirmed from the bandwidth and pulse duration measurements using an external auto-correlation experiment in a BBO crystal. The amplifier was seeded

with pulses of duration 15 fs (spectral bandwidth of 55 nm) from the oscillator (Micra, Coherent Inc.).

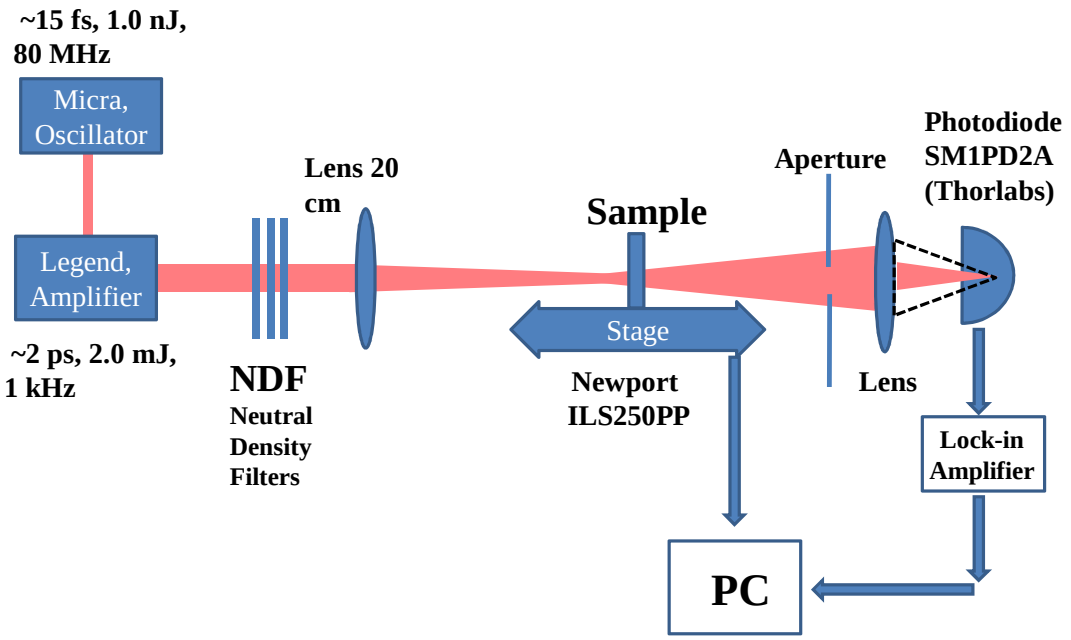

Figure 21 Experimental schematic of ps Z-Scan at 800 nm.

A quartz cuvette (1-mm thick) containing the sample solution was traversed in the focusing geometry enabled by an achromat lens of 200 mm focal length. The beam waist ($2\omega_0$) at focal plane was estimated to be ~80 µm with a corresponding Rayleigh range (Z_r) of ~6.0 mm ensuring the validity of thin sample approximation. The Z-scan was performed over a distance of $10Z_r$ using a high-resolution linear translation stage (Newport ILS250PP) by recording the sample transmittance using a sensitive power sensor (Coherent PS19). A LabVIEW program was written and used for automating the data acquisition of all the Z-scan experiments. The experiments were performed with peak intensities in the range of 50–400 GW/cm^2. The closed aperture scans were performed at low peak intensities (<100 GW/cm^2) to ensure that higher order nonlinear effects are minimal.

2.14.2 Ps Z-Scan at other than 800 nm

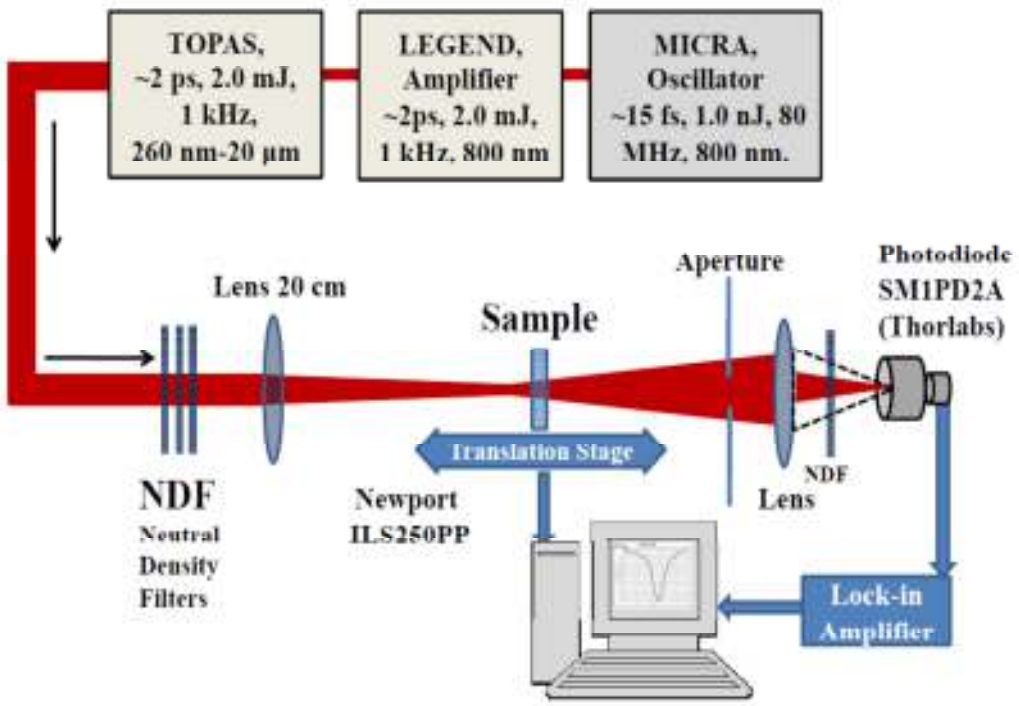

Figure 22 Experimental schematic of ps Z-Scan at other than 800 nm (using TOPAS).

Z-scan measurements [5] were performed at 560 nm, 580 nm, and 600 nm, 640 nm, 680 nm, 700 nm using ~1.5 ps (FWHM) pulses with a repetition rate of 1 kHz from TOPAS (Light Conversion) pumped with an amplified Ti:sapphire system (LEGEND, Coherent). The amplifier was seeded with pulses of duration ~15 fs (FWHM of ~60 nm) from an oscillator (Micra, Coherent). A quartz cuvette (1 mm thick) containing the sample solution was traversed in the focusing geometry enabled by an achromat lens of 200 mm focal length. The beam waist ($2\omega_0$) at focal plane was estimated to be 60±4 µm ($FW1/e^2M$) with a corresponding Rayleigh range (Zr) of 3.5±0.4 mm ensuring the validity of thin sample approximation.

2.14.3 Femtosecond Z-Scan experiments (1 kHz excitation)

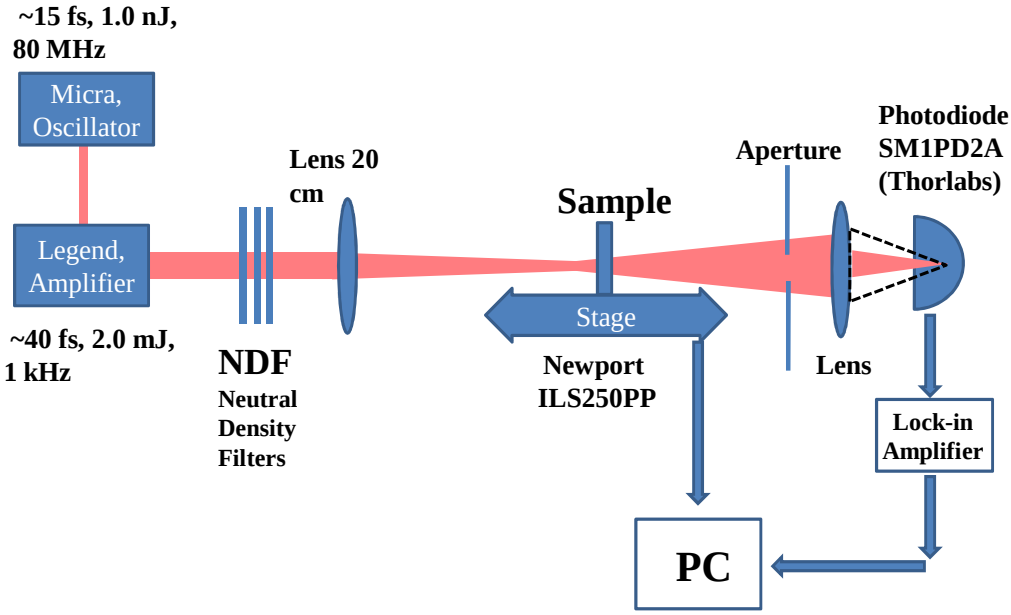

Figure 23 Experimental schematic of fs Z-Scan at 800 nm

The amplifier was seeded with pulses of duration ~15 fs (FWHM) with a spectral bandwidth of 55-60 nm (FHHM) from the oscillator (Micra, Coherent). A quartz cuvette (1-mm thick) containing the sample solution was traversed in the focusing geometry enabled by an achromat lens of 200 mm focal length. The beam waist ($2\omega_0$) at focal plane was estimated to be 60 µm ($FW1/e^2M$) with a corresponding Rayleigh range (Z_r) of ~3.5 mm ensuring the validity of thin sample approximation. Typically <1 µJ energy pulses were used for the experiments. The sample was translated using a high resolution stage (Newport, ILS250PP) and the transmitted light was collected using a lens and a photodiode (Thorlabs, SM1PD2A) combination. An aperture was placed in front of the lens for closed aperture scans and total light was collected during open aperture scans. The photodiode output was fed to a lock-in amplifier (7265, Signal Recovery). Several neutral density filters were used to cut down the input intensity before the sample and also the intensity reaching photodiode. The translation stage and the photodiode/lock-in were controlled by a personal computer using a LabVIEW program. Since the ultrashort pulses passed through several optical elements before entering the sample pulse

duration was estimated (theoretically) to be ~60 fs and this value was used for peak intensity calculations. Fresnel losses from the optics were considered during these calculations. The Z-scan measurements were performed using ~40 fs (FWHM), 800 nm pulses with a repetition rate of 1 kHz delivered by an amplified Ti:sapphire system (Legend, Coherent)[31,32]. Details of experiments were shown in figure 23.

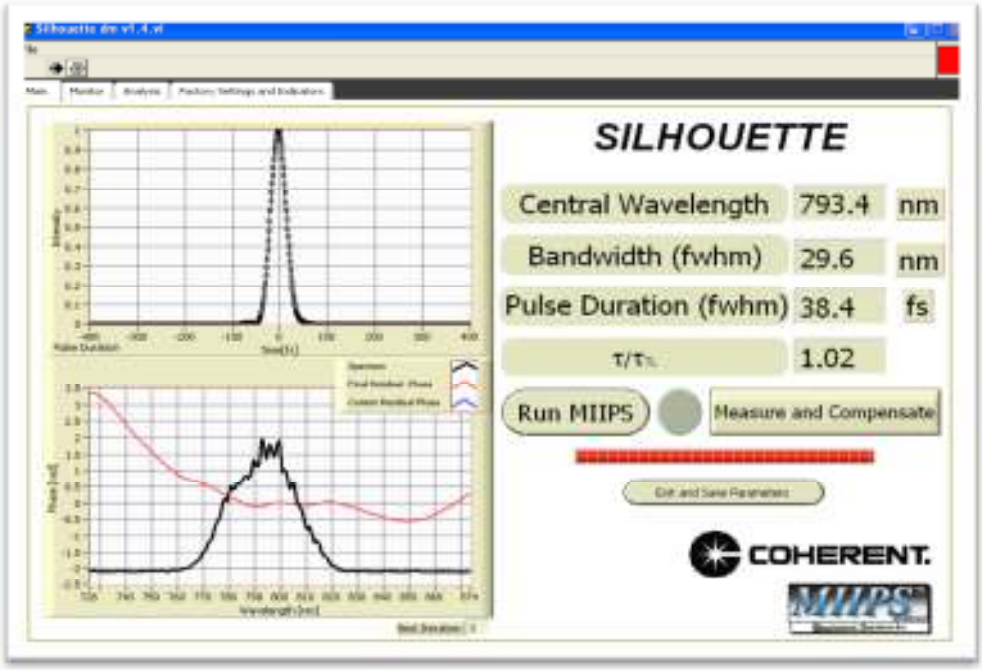

Figure 24 Typical MIIPS data obtained for femtosecond amplified pulses using the MIIPS (Multiphoton Intrapulse Interference Phase Scan) technique and Silhouette (Coherent)[33].

The pulses were nearly transform limited and this was confirmed from the MIIPS (Multi-photon intra-pulse interference phase scan) measurements using Silhouette (Coherent) as observed in figure 24 [33]. The amplifier was seeded with pulses of duration ~15 fs (FWHM) with a spectral bandwidth of 55-60 nm (FWHM) from the oscillator (Micra, Coherent). A quartz cuvette (1-mm thick) containing the sample solution was traversed in the focusing geometry enabled by an achromat lens of 200 mm focal length. The beam waist ($2\omega_0$) at focal plane was estimated to be 52±2 µm with a corresponding Rayleigh ranges (Z_r) of 2.65±0.2 mm. Typically <1 µJ energy pulses resulting in 0.1-1 TW/cm^2 peak intensities were used for the experiments.

2.14.4 Fs Z-Scan experiments (80 MHz excitation)

The laser source used for the measurement was Ti: sapphire oscillator (Chameleon) pumped with Nd:YVO_4 produces pulses of pulse duration 140 fs, and 80 MHz repetition rate at central wavelength of 800 nm. This is a tunable laser oscillator which ranges from 720 nm to 950 nm. The sample was scanned along the Z-direction through the focus of the 100 mm focal length lens. Several neutral density filters were used to cut down the input intensity before the sample and also the intensity reaching photodiode. The translation stage moved mechanically step size 1mm and corresponding transmittance reading is taken with the power meter. The transmitted intensity was recorded as a function of the sample position using Power Max sensor. The beam waist ($2\omega_0$) at focal plane was estimated to be 30-40μm (FW1/e^2M) with a corresponding Rayleigh range (Z_r) of ~2 mm ensuring the validity of thin sample approximation. Typically <30 nJ energy pulses were used for the experiments. The input beam was spatially filtered to obtain a pure Gaussian profile in the far field. The sample was placed on a 10 μm resolution translation stage and the detector (Thermal Sensor, Field-Max) and data collected manually. The closed aperture scans were performed at intensities where the contribution from the higher order nonlinear effects is negligible (the value of $\Delta\varphi$ estimated in all the cases was $<\pi$) [34, 35].

2.15 Theory of Z-Scan

Open aperture Z-scan is performed by collecting all the transmittance of the sample using a lens in loose focus before the sensor. This measurement gives the nonlinear absorption of the sample under investigation. In the Closed Aperture z-scan, an aperture before the detector allows only the center of the Gaussian beam to enter the detector. The Kerr lens effect exhibited by the sample due to its nonlinear refractive index changes its transmittance prior to focus and post focus. This measurement indicated the sign of nonlinearity and enables us to calculate the nonlinear phase shift ($\Delta\varphi$). $\Delta\varphi$ in turn gives the intensity dependent refractive index of the sample.

2.15.1 Theoretical Formulae

The nonlinear processes like multi-photon absorption (MPA) coefficient are generally measured by conventional Z-scan experiments. By using both thin samples approximation and slowly varying envelope approximation (SVEA), the wave equation can be separated into two equations: one for the nonlinear phase and the other for the irradiance.

$$\frac{d\Delta\emptyset}{dz'} = kn_2 \sum_{m=2} I^{m-1} \tag{18}$$

$$\frac{dI}{dz'} = -(\alpha_0 + \sum_{m=2} \alpha_m I^{m-1})I \tag{19}$$

where k is the magnitude of the wave vector in free space; α_{2m-2} is the nonlinear index of refraction (m = 2 for the third-order nonlinearity, m = 3 for the fifth-order nonlinearity, and m = 4 for seventh order nonlinearity and so on). α_0 is the linear absorption coefficient, m=α is the MPA coefficient (m= 2 for 2PA; m = 3 for 3PA, m= 4 for 4 PA); and I is the irradiance within the sample.

2.15.2 Open aperture for Z-scan measurements:

If we want to keep the 2PA term and ignore all other terms on the right side of Eq. (30), we can analytically solve Eq. (2) for OA Z-scans on two-photon absorbers. Similarly, by keeping the 3PA term and ignoring the other terms, we can have an analytical expression for OA Z-scans on three photon absorbers. By assuming a spatially and temporally Gaussian profile for incoming laser pulses, the normalized energy transmittance, $T_{\mathrm{OA}}(z)$, for 2PA and 3PA can be derived as Eq.(31) and Eq. (32), respectively [24].

$$T_{OA}(z) = \frac{1}{\pi^{1/2} q_0} \int_{-\infty}^{+\infty} \ln[1 + q_0 \exp(-x^2)]dx \tag{20}$$

$$T_{OA}(z) = \frac{1}{\pi^{1/2} p_0} \int_{-\infty}^{+\infty} \ln\{[1 + {p_0}^2 \exp(-2x^2)]^{\frac{1}{2}} + p_0 \exp(-x^2)\}dx \tag{21}$$

Where $q_0 = \alpha_2 I_0 L_{eff,}\ p_0 = 2\alpha_3 {I_0}^2 L'_{eff}$, $I = {I_{00}}/{(1 + {z^2}/{{z_0}^2})}$ is the excitation intensity at position z.

$L_{eff} = [1 - \exp(-\alpha_0 L)]/\alpha_0$ and

$L'_{eff} = [1 - \exp(-2\alpha_0 L)]/2\alpha_0$ are the effective sample lengths for 2PA and 3PA processes, respectively; and L is the sample length.

3PA Z scans are considerably different from 2PA Z-scans.
Which is mathematically described only for 2PA? If q_0 <1 or p_0 <1, eqn. (20) or (21) can be expanded in a Taylor series as

$$T_{OA} = \sum_{m=0}^{\infty} (-1)^m \frac{{q_0}^m}{(m+1)^{3/2}}$$

$$T_{OA} = \sum_{m=0}^{\infty} (-1)^m \frac{{p_0}^{2m-2}}{(2m-1)!\,(2m-1)^{1/2}} \quad (22)$$

If higher order terms are ignored, we obtain

$$T_{OA} = 1 - \alpha_2 I L_{eff}/2^{3/2} \quad (23)$$

$$T_{OA} = 1 - \alpha_3 I^2 L'_{eff}/3^{3/2} \quad (24)$$

Here for our convenience we have used $\alpha_2 = \beta\ and\ \alpha_3 = \gamma$. These two expressions enable us to identify whether the nonlinear absorption process is a pure 2PA or 3PA process.

2.15.3 Closed aperture for Z-Scan measurements

In this Z-scan experiment, one thing must bear in mind that a purely refractive non-linearity was considered assuming that no absorptive nonlinearity (such as multi-photon absorption) are present qualitatively. The sensitive to nonlinear refraction is entirely due to the aperture, and removal of the aperture completely eliminates this effect.

In the case of the cubic nonlinearity and negligible nonlinear absorption,

Solve the eqs (1) and (2), we get

$$\Delta\emptyset(\boldsymbol{z},\boldsymbol{r},\boldsymbol{t}) = \Delta\emptyset_{\boldsymbol{0}}(\boldsymbol{z},\boldsymbol{t})\boldsymbol{exp}\left(-\frac{\boldsymbol{2r^2}}{\boldsymbol{w(z)^2}}\right) \tag{25}$$

With $\Delta\emptyset_{\boldsymbol{0}}(\boldsymbol{z},\boldsymbol{t}) = \frac{\Delta\emptyset_{\boldsymbol{0}}(\boldsymbol{t})}{\boldsymbol{1+\frac{z^2}{z_0^2}}}$

Where $\Delta\emptyset_{\boldsymbol{0}}(\boldsymbol{t})$ is the phase shift at the focus, is defined as

$$\Delta\emptyset_{\boldsymbol{0}}(\boldsymbol{t}) = k\,\Delta n_0(t) L_{eff} \tag{26}$$

where $\Delta n_0(t) = n_2 I_0(t)$

$I_0(t)$ is the irradiance on the axis at the focus (i.e., z=0)

The resultant field at aperture is given by

$$\boldsymbol{E_a(z,r,t) = E(z,r,t)e^{\frac{-\alpha L}{2}}\sum_{m=0}^{\infty}\frac{(\Delta\emptyset_0(z,t))^m}{m!}\frac{w_{m0}}{w_m}exp\left(-\frac{r^2}{w_m{}^2}-\frac{ikr^2}{2R_m}-i\theta_m\right)} \tag{27}$$

In the limit of small non-linear phase change $|\Delta\emptyset_{\boldsymbol{0}}| \ll \boldsymbol{1}$

The Normalized transmittance is given by

$$\boldsymbol{T(z,\Delta\emptyset_0) = 1 - \frac{4\Delta\emptyset_0}{(x^2+9)(x^2+1)}x} \tag{28}$$

Where $x = {}^{z}/_{z_0}$

If I_s is higher than $I_{00,}$ peak intensity, SA is considered to be a third order process and β can be substituted as $-\alpha_0/I_s$. From the value of β we can calculate Im $\chi^{(3)}$.

The 2PA coefficient, β, can be expressed in terms of 2PA cross section (σ_2) as:

$$\sigma_2(cm^4 s/photon) = \frac{\beta h\nu}{N_0} \tag{29}$$

We have evaluated the three photon cross-section (σ_3) using the relation

$$\sigma_3 = \frac{(\hbar\omega)^2}{N}\gamma \tag{30}$$

where ω is the frequency of the laser radiation, and N is the number density. 'hν' is the incident photon energy and N_0 is the number density of the sample in solution. σ_2 can also be written in the units of GM as: $1GM=10^{-50}$ cm^4s/photon.

The real and imaginary parts of the third order susceptibility is given by

$$\mathrm{Re}(\chi^3)(esu) = 10^{-4}\varepsilon_0 c^2 n_0{}^2 n_2 (cm^2/W) \quad (31)$$

$$\mathrm{Im}(\chi^3)(esu) = \frac{10^{-2}\varepsilon_0 c^2 n_0{}^2 \lambda\beta(cm/W)}{4\pi^2} \quad (32)$$

2.16 Initial pump-probe results of phthalocyanine thin films

2.16.1 Structures of phthalocyanine

Our initial pump-probe experimental set up was tested using two phthalocyanine thin films. Figures 25(a) and 25(b) show the structures of two samples studied viz. zinc tetra tert-butyl Phthalocyanine (denoted as SPc) and 2-(3-(Butane-1,4-dioic acid)-9(10),16,(17),23(24)-tri *tert*-butyl phthalocyanine zinc(II) (denoted as USPc).

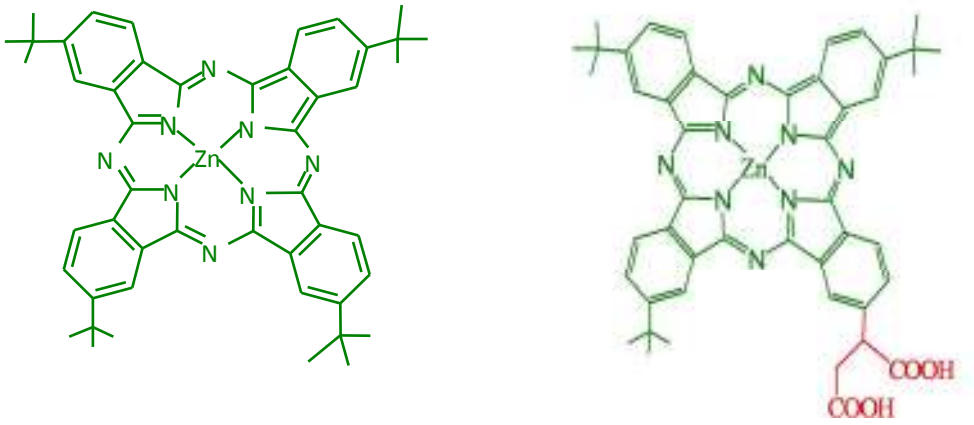

(a) **(b)**

Figure 25 Structures of (a) symmetric (b) unsymmetrical phthalocyanines used for study.

Both the Pc's were doped in PMMA and spin coated on a glass substrate. Typical thickness of the films obtained was ~15-20 μm. We had obtained better data [in terms of signal to noise ratio (SNR)] with 590 nm-610 nm as pump and probe since these molecules absorb strongly in that spectral region. The probe transmission was detected using a sensitive power meter (Coherent). The pump beam diameter was larger (~5 mm) than the probe beam diameter (~2 mm) and both the beams were

not focused. Typically 15-50 μJ energies were used for the pump beam while probe beam energy was a fraction of that. Figure 26 shows typical emission spectrum of SPc indicating a peak near 700 nm and an absorption peak near 650 nm.

2.16.2 Absorption and emission spectra of Phthalocyanine film

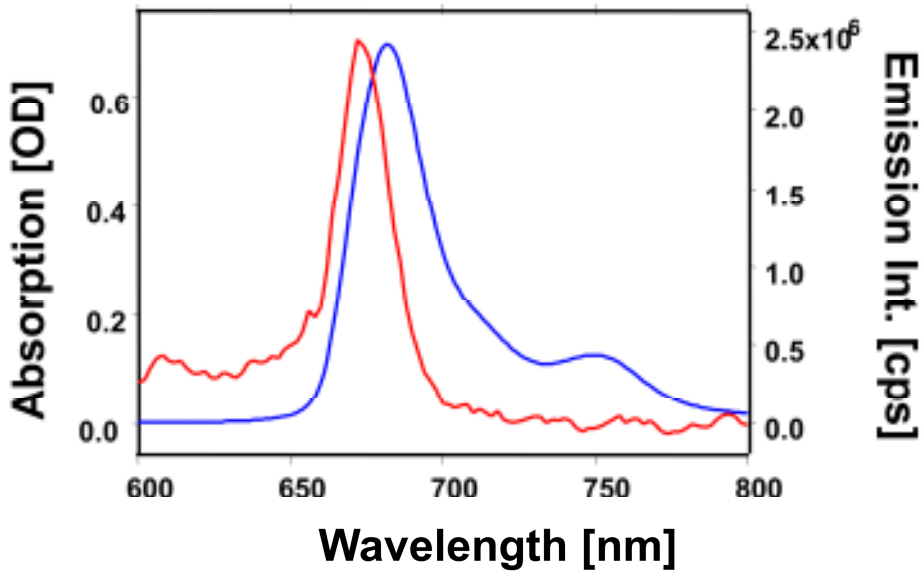

Figure 26 Emission spectrum (blue, right) and absorption spectrum (red, left) of the symmetric Zn-phthalocyanine studied.

2.16.3 Pump-probe spectroscopy of phthalocyanine films

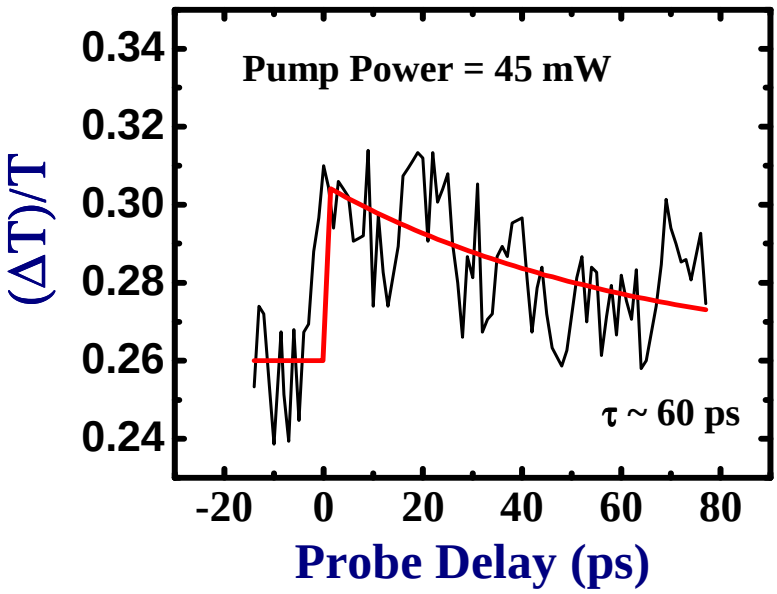

Figure 27 Pump probe data for unsymmetrical ZnPc (USPc) with an input pump power (unfocused) of ~45 mW. The lifetime obtained from the best fit was ~60 ps.

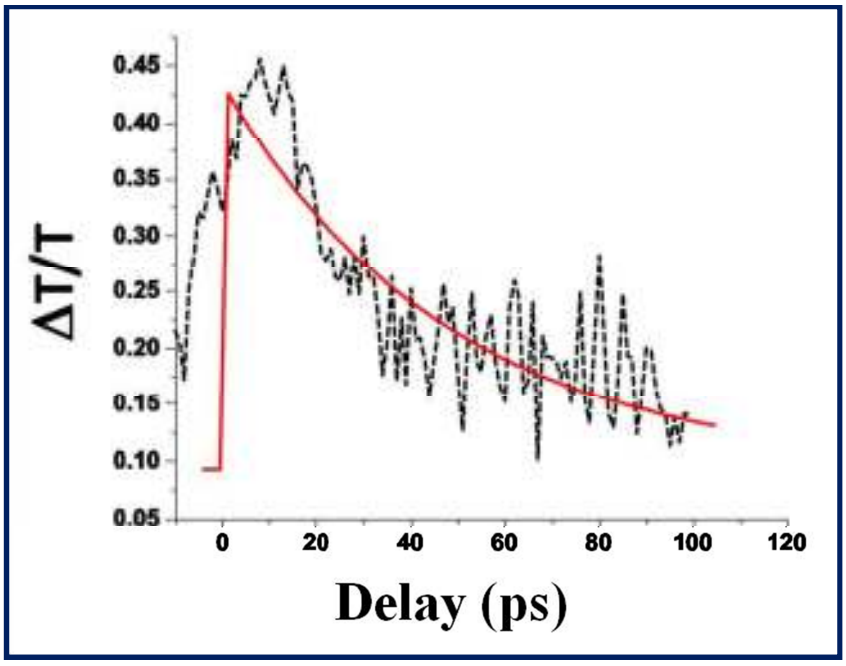

Figure 28 Pump probe data for the same sample with an input pump power of ~16 mW. The lifetime was ~50 ps. Both the data were recorded at 590 nm.

Figure 27 shows a typical pump-probe data for a thin film of USPc doped in PMMA with a pump power (unfocused) of 45 mW. A clear decay was observed post the coherence spike (zero delay) and the data was reproducible. The lifetime achieved using the single exponential fit was ~60 ps. Figure 28 depicts the pump probe data obtained with lower average powers (~16 mW) and the lifetime obtained from the best fit to the experimental data was ~50 ps. We expect the small difference arising from the experimental errors (delays, calibration of power meter, fitting errors etc.). Figure 29 shows the pump-probe data for SPc recorded at 610 nm. The lifetime achieved from the best fit was ~30 ps indicating faster response compare to USPc. We can draw the following conclusions from our data: (a) signal to noise ratio (SNR) is still poor with lot of scattering in the data. Though the data is noisy, the lifetimes were reproducible within an experimental error of ±20%. We improving the SNR through a better detection system of sensitive photo-diode and lock-in amplifier combination (b) these data provide us with order of magnitude for the excited state relaxation mechanism (c) the data was achieved without focusing the laser pulses so as to achieve better overlap of the pulses and at the same time interrogate larger area of the samples.

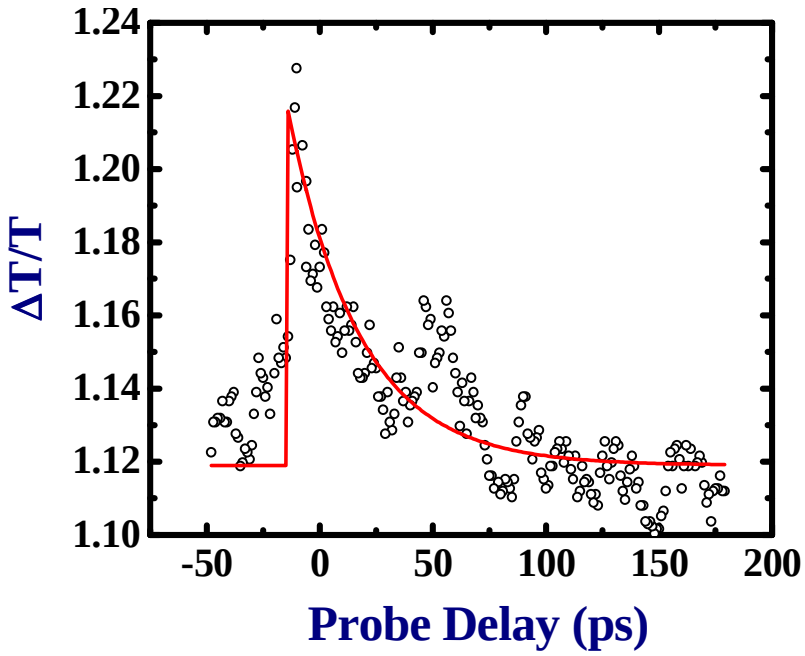

Figure 29 Pump probe data for symmetric ZnPc (SPc) with an input pump power (unfocused) of ~20 mW recorded at 610 nm.

In the solid state, phthalocyanine molecules tend to aggregate making the Q-band broader than that of the monomer in solution form [36-40]. In addition, due to the interaction between molecules in the films or because of molecular distortion, the two-fold degeneracy of the lowest unoccupied molecular orbital (LUMO) band is lifted into two bands with finite oscillator strength [41]. Several other phthalocyanines in thin film form were studied [20, 42-44] for their excited state dynamics and lifetimes of few ps to few tens of ps were observed. Ma et al. [42] observed three lifetimes from their ultrafast studies and attributed the shortest (<1 ps) to electron-phonon interaction, the 130 ps lifetime to the intersystem crossing, and the ns lifetime to the radiative transition from S_1 to S_0. Mi et al. [20] found strong wavelength dependence of the Q-band excited state dynamics. They too observed three different timescales in magnesium phthalocyanine thin film and attributed the 1 ps component to exciton-exciton annihilation, 16.5 ps component to the intersystem crossing rate and the longest component of 300 ps to the non-radiative relaxation process.

2.17 References

1. (a) P. F. Moulton, J. Opt. Soc. B **3** (1986) 125 (b) http://www.rp-photonics.com/titanium_sapphire_lasers.html.
2. T. Brabec and F. Krausz, Rev. Mod. Phys.**72** (2000) 545.
3. F. Salin, P. Georges, G. Roger, and A. Brun, Appl. Opt., **26** (1987) 4528.
4. R. Danielius, A. Stabinis, G. Valiulis and A. Varanavieius, Opt. Commun. **105** (1994) 67.
5. M. Raghuramaiah, A.K. Sharma, P.A. Naik, P. D. Gupta, R.A. Ganeev, Sadhana **26** (2001) 603-611.
6. Rick Trebino, *"Frequency-Resolved Optical Gating: The Measurement of Ultrashort Laser Pulse,"* Kluwer Academic Publisher, 2000.
7. P. O'Shea, M. Kimmel, X. Gu, and R. Trebino, Opt. Lett. **26** (2001) 932.
8. M.E. Anderson, A. Monmayrant, S.P. Gorza, P. Wasylczyk, and I.A. Walmsley, Laser Phys. Lett. **5** (2008) 256.
9. Micra-10 Operator's Manual of Coherent Inc. http://www.coherent.com/
10. Legend femtosecond Amplifier Operator's Manual of Coherent Inc http://www.coherent.com/
11. TOPAS-C Operator's Manual of Coherent Inc http://www.coherent.com/
12. Claude Rulliere, Femtosecond laser pulses (Second edition), Springer, 2005.
13. F. Wagner, M Feuerhake, P Simon, Opt. and Quant. Electron. **29** (1997) 811.
14. M. Ghotbi, M. Ebrahim-Zadeh, A. Majchrowski, E. Michalski, and I. V. Kityk Opt. Lett. **29** (2004) 2530; Ebrahim-Zadeh, M., Proc. SPIE **6118** (2006) 611809; Ebrahim-Zadeh, M., Proc. SPIE **6451** (2007) 645106.
15. S. Venugopal Rao, J. Opt. A. **6** (2004) 569.
16. Moutzouris, K., Ph.D. Thesis, University of St. Andrews, 2003.
17. (a) V. Petrov, M. Ghotbi, O. Kokabee, A. Esteban-Martin, F. Noack, A. Gaydardzhiev,I. Nikolov, P. Tzankov, I. Buchvarov, K. Miyata, A.Majchrowski, F. Rotermund, E. Michalski, and M. Ebrahim-Zadeh, I. V. Kityk, Laser & Photon. Rev. **4** (2010) 53 (b) Juli Thesis, Albert-Ludwigs-Universität Freiburg, page 33 (2007).
18. A. A. Maznev, T. F. Crimmins, and K. A. Nelson, Opt. Lett. **23** (1998) 1.

19. G. Cerullo, C. Manzoni, L. Luer, D. Poli, Photochem. Photobio. Sci. **6** (2007) 135.
20. (a) J. Mi, L. Guo, Y. Liu, W. Liu, G. You, S. Qian, Phys. Lett. A **310** (2003) 486 (b) D. Swain, P.T. Anusha, T. Shuvan Prashant, S.P. Tewari, T. Sarma, P.K. Panda, S. Venugopal Rao, Appl. Phys. Lett. **100** (2012) 141109 (c) K.P. Unnikrishnan, J. Thomas, V. P. N. Nampoori, C.P.G. Vallabhan, Opt. Commun. **217** (2003) 269 (d) K. Venkata Saravanan, K.C. James Raju, M.G. Krishna, Surya P. Tewari, S. Venugopal Rao, Appl. Phys. Lett. **96** (2010) 232905.
21. B. Gu, W. Ji, Opt. Exp. **16** (2008) 10208. (b) J. He, Y. Qu, H. Li, J. Mi, W. Ji, Opt. Express **13** (2005) 2548 (b) T. Wang, N. Venkatram, J. Gosciniak, Y. Cui, G. Qian, W. Ji, and D. T. H. Tan, Opt. Express **21** (2013) 32192 (c) D. Luo, Q.G. Du, H.T. Dai, H.V. Demir, H.Z. Yang, W. Ji, and X.W. Sun, Scientific Reports, **2** (2012) 627 (d) R.S. Singh, V. Nalla, W. Chen, A.T.S. Wee, and W. Ji, ACS Nano **5** (2011) 5969 (e) H. Yang, X. Feng, Q. Wang, H. Huang, W. Chen, A.T.S. Wee, and W. Ji, Nano Lett. **11** (2011) 2622 (f) B. Gu, K. Lou, J. Chen, Y.N. Li, H.T. Wang, W. Ji, Opt. Express **18** (2010) 26843 (g) H.I. Elim, Ph.D. Thesis, National University of Singapore, (2005).
22. (a) B. Gu, Wei Ji, P. S. Patil, S. M. Dharmaprakash, H.T Wang, Appl. Phys. Lett. **92** (2008) 091118 (b) G. Xing, Wei Ji, Y. Zheng and J. Y. Ying, Appl. Phys. Lett. **93** (2008) 241114 (c) X. B. Feng, G. C. Xing, W. Ji, J. Opt. A: Pure Appl. Opt. **11** (2009) 024004 (d) N. Venkatram, S. K. Batabyal, L. Tian, J. J. Vittal, W. Ji, Appl. Phys. Lett. **95** (2009) 201109 (e) B.Gu, H.T. Wang, W. Ji Opt. Lett. **34** (2009) 2769. (f) X. Feng and W. Ji Opt. Express **17** (2009) 13140 (g) B. Gu, Y. Wang,W. Ji, John Wang, Appl. Phys. Lett. **95** (2009) 041114 (h) B. Gu and W. Ji, Opt. Express **16** (2008) 10208 (i) B. Gu, K. Lou, H.-T. Wang, W. Ji, Opt. Lett. **35** (2010) 417 (j) Q. Yingli, Ph.D. Thesis, National University of Singapore (2009).
23. (a) H. Okamoto, S. Matsumoto, A. Maeda, H. Kishida, Y. Iwasa, T. Takenobu, Phys. Rev. Lett. **96** (2006) 019706 (b) N. Kamaraju, S. Kumar, B. Karthikeyan, A. Moravsky, R.O.Lutfy, A.K. Sood, Appl. Phys. Lett. **93** (2008) 091903 (c) E.R. Hosler Thesis, University of California, Berkeley (2013).

24. (a) M. Sheik-Bahae, A.A. Said, T.H. Wei, D.J. Hagan, and E.W. Van Stryland, IEEE J. of Quant. Electron. **QE-26** (1990) 760 (b) M. Sheik-Bahae, A.A. Said, and E.W. Van Stryland, Opt. Lett. **14** (1989) 955.
25. T.D. Krauss and F.W. Wise, Appl. Phys. Lett. **65** (1994) 1739.
26. L.C. Oliveira and S.C. Zilio, Appl. Phys. Lett. **65** (1994) 2121.
27. S. Venugopal Rao, P.T. Anusha, T.S. Prashant, D. Swain, S. P. Tewari, Mater. Sc. Applns. **2** (2011) 299.
28. S. Venugopal Rao , T. S. Prashant, T. Sarma, P.K. Panda, D. Swain, S. P. Tewari, Chem. Phys. Lett., **514** (2011) 98.
29. D. Swain, P.T. Anusha, T. Sarma, P.K. Panda, S. Venugopal Rao. Chem. Phys. Lett. **580** (2013) 73.
30. S. Hamad, Surya P. Tewari, L. Giribabu, S. Venugopal Rao, J. Porphy. Phth. **16** (2012) 140.
31. D. Swain, A. Rana, P. K. Panda, S. Venugopal Rao, Proc. SPIE, **8258**, 82581B, 2012.
32. D. Swain, P.T. Anusha, T. S. Prashant, S.P. Tewari, Tridib Sarma, P.K. Panda, S. Venugopal Rao, AIP Conf. Proc. **1391** (2011) 674.
33. (a) B. Xu, J. M. Gunn, J. M. Dela Cruz, V. V. Lozovoy, M. Dantus, J. Opt. Soc. Am. B **23**, 750-759 (2006). (b) M. Dantus, V. V. Lozovoy, and I. Pastirk, Laser Focus World **43** (2007) 101.
34. D. Swain, R. Singh, V.K. Singh, N.V. Krishna, L. Giribabu, S. Venugopal Rao, J. Mater. Chem. C, **2** (2014) 1711.
35. D. Swain, V.K. Singh, N.V. Krishna, L. Giribabu, S. Venugopal Rao J. Porphy. Phth., DOI:10.1142/S1088424614500035 (2014)
36. (a) M. Tian, S. Yanagi, K. Sasaki, T. Wada, H. Sasabe, J. Opt. Soc. Am. B **15** (1998) 846 (b) S. Venugopal Rao,Debasis Swain, Surya P. Tewari, Proc. of SPIE Vol. **7599** (2010) 75991P-1.
37. A. Terasaki, M. Hosoda, T. Wada, H. Tada, A. Koma, A. Yamada, H. Sasabe, A. F. Garito, T. Kobayashi, J. Phys. Chem. **96** (1992) 10534.
38. L. K. Chau, C. D. England, S. Chen, N.R. Armstrong, J. Phys. Chem. **97** (1993) 2699.
39. J. Mizuguchi, S. Matsumoto, J. Phys. Chem. A **103** (1999) 614.

40. M.M. El-Nahass, A.A. Atta, H. E. A. El-Sayed, E. F. M. El-Zaidia, Appl. Surf. Sci. **254** (2008) 2458.
41. A. Endo, S. Matsumoto, J. Mizuguchi, J. Phys. Chem. A **103** (1999) 8193.
42. G. Ma, J. He, C.-H. Kang, S.H. Tang, Chem. Phys. Lett. **370** (2003) 293.
43. J. Savolainen, D. van der Linden, N. Dijkhuizen, J.L. Herek, J. of Photochem. Photobio. A: Chem. **196** (2008) 99.
44. R.Y. Zhu, Y. Chen, J. Zhou, B. Li, W. M. Liu, S.X. Qian, M. Hanack, Y. Araki, O. Ito, Chem. Phys. Lett. **398** (2004) 308.

Chapter 3

Study of ultrafast excited state dynamics and NLO properties of Dinapthoporphycenes

3.1 Introduction

Tetrapyrrolic macrocycles encompass intriguing physical, chemical, and biological properties. In biological processes, Fe-porphyrins are found in hemoglobin, myoglobin, and cytochromes, whereas chlorophylls are used in photosynthetic systems. These tetrapyrrolic macrocycles play a significant role in vital biological processes such as (a) photosynthesis (chlorophyll) (b) oxygen transport (hemoglobin), (c) oxygen activation (cytochrome) because of which they are termed as "pigments of life"[1] and have attracted the scientific community for over few decades. The biological significance of porphyrins arises from their properties and as chromophores they have captured the imagination of spectroscopists. Their molecular design and structural variability have made them particularly attractive in a variety of applications such as photodynamic therapy (PDT) [2]. Three main features characterize porphyrins: they are macrocyclic, highly colored, and aromatic in nature. To understand and extend above characteristics has inspired considerable interest in the preparation of new porphyrin analogues. The name porphycene arises from its similarity to both porphyrins and acenes. Porphycene is a structural isomer of porphyrin and act as photosensitizers. With the synthesis of porphycene: a tetrapyrrolic structural isomer of porphyrin, a new type of porphyrinoid system became complexes (metalloporphycenes) with many metal ions, although their coordination cavity is noticeably smaller than that of the porphyrins. As a general method of synthesis of porphycenes has since been developed, allowing these compounds to be made in great structural variety, a physical and chemical comparison between porphycenes and porphyrins suggests itself.

Isomers of porphyrins are generally used in the study of multi-photon absorption (MPA). These class of organic materials find specific applications in the fields of imaging, lithography, memory based devices, optical limiting, and PDT to name a few [3-6]. Porphyrins (chapter 6), phthalocyanines (chapter 5), their metallated derivatives, and other similar molecules with large number of de-localized π electrons, are recognized to comprise large third-order nonlinearities enabling them for photonic and opto-electronic applications [7-21]. Despite a number of recent studies reporting novel molecules with large two-photon absorption (2PA) and three-photon absorption (3PA) coefficients/cross-sections, each of them using different

pulses and at different wavelengths, auxiliary advances in this field are essential. Furthermore, it is imperative to thoroughly appraise the structure-property relationship of such molecules, using pulses of varying duration and over a broad spectral range, for understanding their photo-physical behavior and enhancing their potential for practical applications [22-28]. Porphycenes, the constitutional isomers of widely researched porphyrins, were first synthesised by Vogel and co-workers in 1986 and subsequently many derivatives were reported [29-33]. Recently, large enhancement of two photon absorption (2PA) cross section [$\sigma^{(2)}$] was discovered in the case of conjugated porphyrin dimers, directly linked fused porphyrin dimers and even expanded porphyrins [17-18]. Particularly, aromatic core modified porphyrins are reported to have very large values of $\sigma^{(2)}$ [19]. To our knowledge only one report on 2PA studies of porphycenes [34] have been communicated indicating that these organic systems need to be explored further for their tremendous potential in nonlinear optical (NLO) applications. Arnbjerg et al. [34] have established that in the spectral domain of 750-850 nm the 2PA cross sections for two porphycenes (TPPo and PdTPPo) were large compared to that from the porphyrin analogue. These observations are attributed to the fact that, for the porphycenes, the two-photon transition is nearly resonant with a comparatively intense one-photon Q-band transition. In case of benzosapphyrins the extension of π-systems, by fusing the bipyrrole moiety with aromatic ring, has more dramatic effect on the electronic properties of the macrocycle than multiple fusion of benzene rings through the β-positions of respective pyrrole units. We have recently synthesized and studied a new class of porphycenes with interesting photo-physical and NLO properties [35]. In these molecules bipyrrole and naphthalene moieties are involved lending them the name dinapthoporphycenes. We observed that the metallation of the complex leads to significant change in the photo-physical properties of the complexes. Nonlinear optical studies using Z-scan technique with ~1.5 ps pulses at 800 nm have been performed to characterize the dinapthoporphycenes. Closed and open aperture Z-scans were performed to estimate the third order nonlinearities of the molecules.

3.2 Synthesis, Structure and Absorption spectra (Po1-Po5)

To a slurry of low-valent titanium agent, generated by reduction of (1.90 mL, 17.40 mmol) of titanium tetrachloride in dry THF (90 mL) with activated zinc (2.27

g) and CuCl (0.34 g), was added a solution of naphthobipyrroledialdehyde (300 mg, 0.87 mmol) in boiling THF (230 mL). The reaction mixture was heated under reflux for 20 min and then hydrolyzed by slow addition of 10% aqueous potassium carbonate (47 mL). The reaction mixture was filtered through celite to remove the excess metal, washed with dichloromethane and the washings were combined with the organic layer of the filtrate and dried over anhyd. Na_2SO_4 and freed from solvent by rotary evaporator and the solid residue was subjected to chromatography on a neutral alumina column using dichloromethane-hexane (1:1). The blue fraction thus obtained was evaporated to yield the dinaphthoporphycene as a blue solid and re-crystallized from chloroform–hexane mixture. Yield 53 mg (20 %).

The molecular structures of the samples (Po1-Po5) investigated are provided in figure 1. In the metal free dinapthoporphycenes, R in figure 1 denotes n-propyl, i-propyl and n-pentyl groups are the different variations at the periphery of the core are named as Po1, Po2 and Po3 respectively. The nickel coordinated dinapthoporphycenes have only two variations with isopropyl and n-pentyl groups on the periphery of the core named as Po4, Po5 respectively. Solid state structure of Po2 could be derived explicitly from the single crystals obtained via slow evaporation of chloroform/hexane mixture, by X-ray diffraction (XRD) analysis, revealing a near planar geometry (Figure 1b).

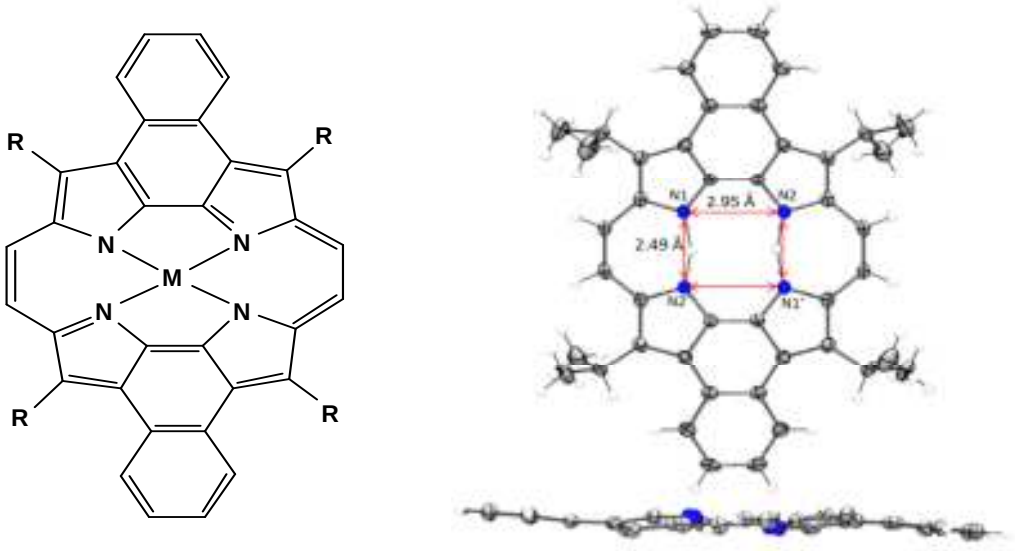

(a) (b)

Figure 1 (a) Structure of the compounds used in present study **(b)** ORTEP of compound Po1

Average deviation of nitrogen atoms from the mean porphycene plane (excluding the isopropyl substituents) is ±0.15 Å. The shortest N-N distance (N1…N2′) in Po2 is 2.49 Å much shorter compared to that of regular Porphycene, while the long (N1…N2) one being 2.95 Å. The absorption spectra resemble those of porphyrins with a Q-band region between 15000cm^{-1} and 23000 cm^{-1}, and a Soret-band region between 25000 cm^{-1} and 30000 cm^{-1}.

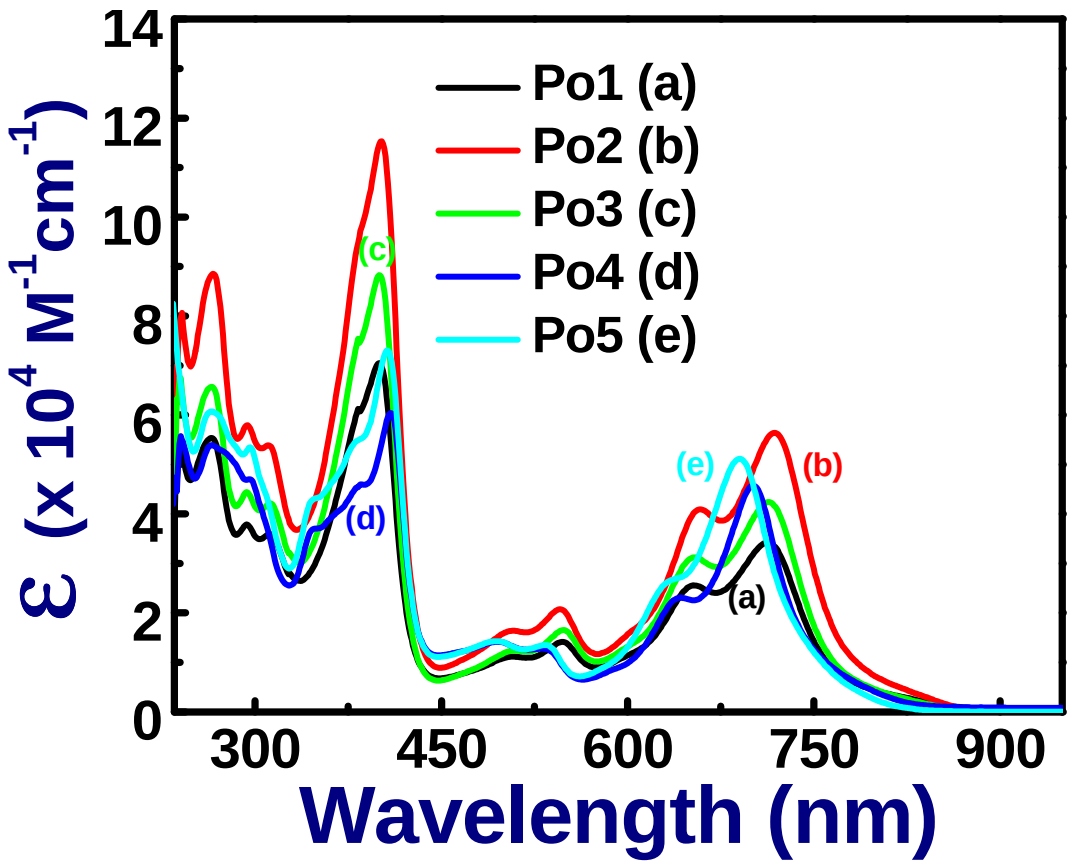

Figure 2 UV-visible absorption spectra of the (Po1-Po5) compounds.

Porphyrin compounds have a weak Q-band around 500-700 nm (1.8-2.5 eV) and a strong Soret-band around 350-400 nm (3-3.5 eV).The Q-band region often exhibits a well-resolved vibrational structure in most of the porphyrins. Despite similarity of the transition energies, this leads to a completely different appearance of the visible part of absorption spectra of two classes of compounds. Similar to porphyrins, the Q as well as the Soret transition pairs are each nearly degenerate [37]. Porphycene, due to its large energy gap between the Soret and Q bands (about 11000 cm^{-1}) is a suitable candidate for investigating intra-molecular electronic relaxation processes. Furthermore, it was well known that for porphycenes and porphyrins the relaxation between excited states occurs in sub-picosecond time domain at room

temperature. For example, in the case of the Zn-tetraphenylporphyrin energy degradation between the Soret and Q bands took place within a time of 60-90 fs [38]. The process of transfer of energy can be showed from the excited molecule into the matrix can be slowed down in comparison with the liquid phase [39-41]. These studies focused on excess energies below 2000 cm^{-1}. The relaxation behavior beyond 2000 cm^{-1} is less understood. Consequently, porphycene which reveals a large energy separation between $S_{1,2}$ and $S_{3,4}$ singlets (11000 cm^{-1}) was used in most of the time–resolved experiments [42]. Absorption spectra of all the molecules (Po1-Po5) are shown in the figure 2. The absorption spectra of metal free porphycenes (Po1, Po2, Po3) have large red shifted absorption bands, lowest energy Q-band (640-750 nm) appear near 715 nm. These porphycenes demonstrate well-defined Soret or B-bands (350-430 nm) peaking near 400 nm. The lowest energy Q-band is relatively more intense than the Soret-band in comparison to other porphycenes [30]. The presence of few UV bands with maxima at 265 nm is attributed to the naphthalene moieties in the macrocycle. The absorption spectra of Po4 and Po5 show a general trend of red-shifted B band and blue-shifted Q-bands. The absorbance at 800 nm was negligible for all the above mentioned compounds with more than 85% linear transmittance. Porphycene has the most intense Q-band, and it was expected to be a suitable basic compound for pigment design. Like dibenzoporphycene, porphycenes Po1-Po3 did not show any fluorescence at room temperature ($< 10^{-4}$)[42].

3.3 Ultrafast dynamics of (Po1-Po5)

It is well established that depending on the excitation wavelength and intensity one can observe 2PA, 3PA, excited state absorption, or a combination of more than one process in such molecules owing to the configuration of their electronic states [9,12,43]. There are various spectroscopic techniques to achieve time-resolved information. However, to understand the decay dynamics of these compounds (Po1-Po5) we have performed degenerate pump-probe experiments with 1 kHz, ~1.5 ps pulses at a wavelength of 800 nm. We have also corroborated our ps data with fs degenerate pump probe data obtained near 600 nm. Furthermore, unfocused pump probe data was also obtained with fs pulses. The complete experimental details of both ps and fs pump probe experiments have been explained in sections 2.12 and 2.13 (figures 17 and 20).

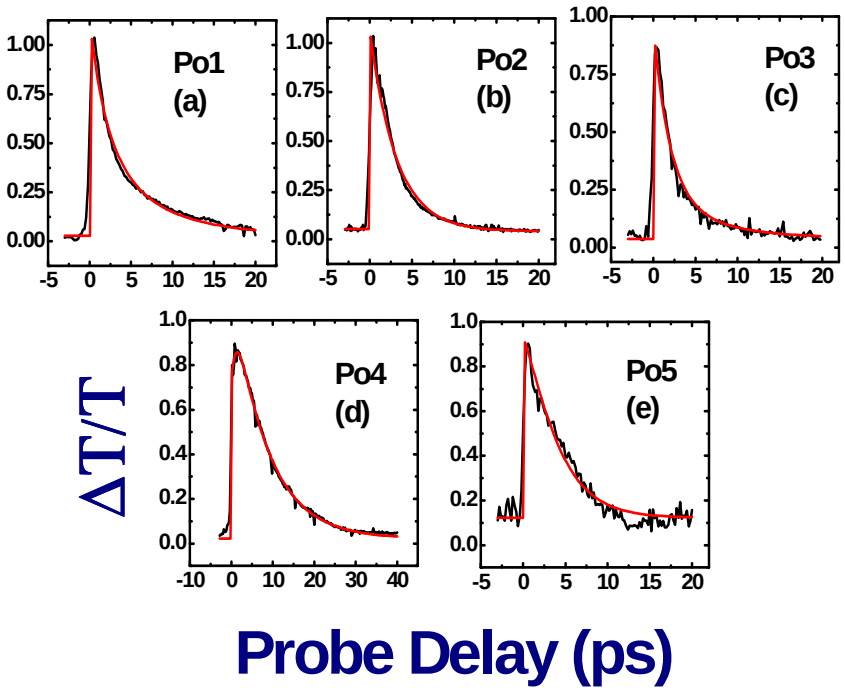

Figure 3 (a)-(e) Excited state dynamics data of Po1-Po5 obtained using 1.5 ps pulses at 800 nm. Black lines represent the experimental data while the red lines are fits to the data.

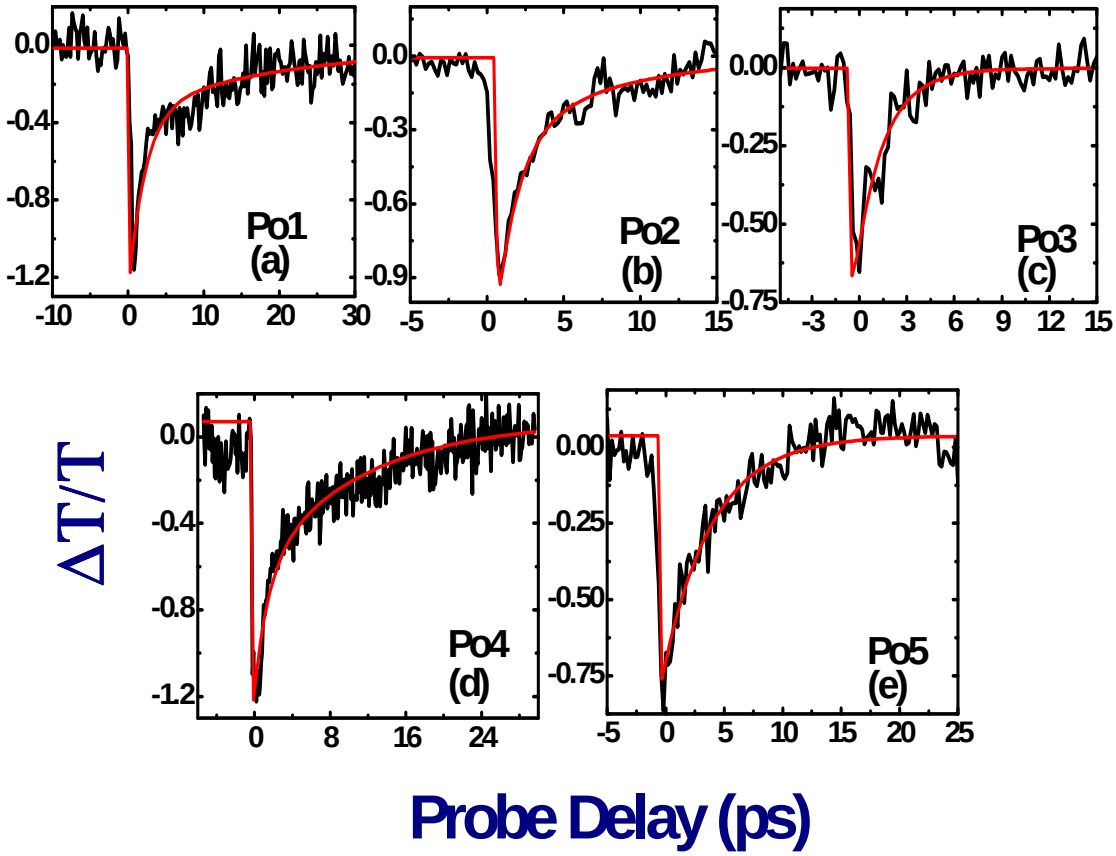

Figure 4 (a)-(e) Excited state dynamics of Po1-Po5 using ~70 fs pulses at 600 nm. The data was obtained using focused pump/probe beams. Black lines represent the experimental data while the red lines are fits to the data.

Typical energies of pump beam used in the experiments was <50 μJ. The pump and probe powers were typically maintained at 20:1 ratio. Depending on the excitation mechanisms and energy levels of these molecules one would expect multi-exponential decays following different excitation mechanisms. Figures 3(a)-(e) illustrates the pump-probe data obtained at 800 nm with ps pulses. The differential transmission was positive. At zero-delay a sharp peak or dip is a typical signature of pump-probe experiments. All the porphycenes (Po1-Po5) depicted similar trend with respect to excited state dynamics. The transmitted probe data was fitted using the equation given below. For the case of single decay observed only τ_1, for double decay τ_1 and τ_2, and for triple exponential decay τ_1, τ_2 and τ_3 were used.

$$\frac{\Delta T(t)}{T} = y_0 + A_1 e^{-(t-t_0)/\tau_1} + A_2 e^{-(t-t_0)/\tau_2} + A_3 e^{-(t-t_0)/\tau_3} \quad (1)$$

$\Delta T(t)$ is the time dependent change in probe transmission, induced by the pump at time 't' after the pump excitation and T is the probe transmission in the absence of pump. The peak intensities (~150 GW/cm^2) used in ps experiments was sufficient to access the three-photon states. The values of A_1, A_2, and A_3 (complete details of these are provided in appendix) dictate the amplitude of the contribution to respective lifetime. The slope of the exponential decay showed different magnitude of lifetimes [43]. We observed photo-bleaching for all the porphycenes studied. The data was fitted with a double exponential decay and two lifetimes were retrieved from the fits. We tried to fit the data for a single exponential but the overall fit was poor. Fast decay retrieved was in the range of 1.8-3.1 ps while the slow component varied from 7 ps to 8.5 ps for different samples. The fast component is attributed to the internal molecular vibration and internal conversion in these molecules whereas the slower one to the non-radiative decay back to the ground state. Similar decay times were observed in Porphycene reported by Fita et al. [44].

We observed photo-induced absorption (PIA) in the ~70 fs pump-probe data collected at 600 nm for all the porphycenes. Details of the experiments can be found in section 2.12 (figures 17 and 18). The negative transmission observed at 600 nm is depicted in figures 4(a)-(e) for all the samples Po1-Po5. The data was obtained with focused pump and probe pulses with pump peak intensities sufficient to excite the

molecules to S_2 states. Probe was absorbed from these states to higher states (S_n) thereby reducing the transmission. That they have been excited to high lying states has been confirmed from the nonlinear absorption measurements. Fits obtained using single/double exponential were not providing perfect match to the experimental data and therefore triple exponential equation was utilized and three different lifetimes were retrieved from the fits. The fastest lifetime observed was in the 100-135 fs which is attributed to the intramolecular vibrational relaxation (IVR) within S_2 states while the slower component of 0.8-1.5 ps could be due to the IC and the slowest one in the 7.3-10.0 ps range again due to non-radiative decay.

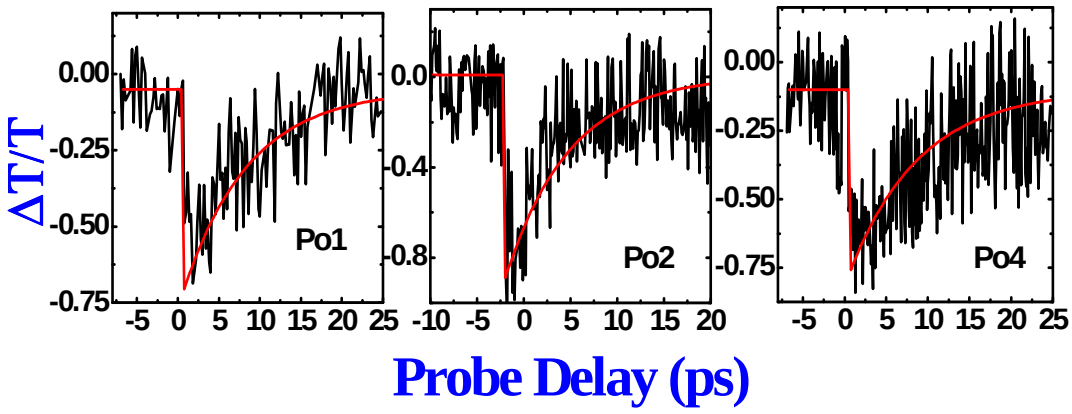

Figure 5 Excited state dynamics of Po1, Po2, and Po4 using ~70 fs pulses at 600 nm using unfocused pump/probe pulses. Black lines represent the experimental data while red lines are fits to the data.

Samples	τ_2 800 nm (ps p-p)	τ_1 800 nm (ps p-p)	τ_3 600 nm (fs p-p)	τ_2 600 nm (fs p-p)	τ_1 600 nm (fs p-p)	τ_1 600 nm (fs p-p unfocused)
Po1	2.0 ps	7.2 ps	120 fs	0.8 ps	8.0 ps	7.5 ps
Po2	3.1 ps	7.6 ps	105 fs	1.4 ps	7.3 ps	7.0 ps
Po3	2.0 ps	7.2 ps	102 fs	1.2 ps	8.2 ps	-
Po4	1.8 ps	8.5 ps	100 fs	1.5 ps	10.0 ps	10.9 ps
Po5	1.8 ps	7.0 ps	135 fs	1.2 ps	8.1 ps	-

Table 1 Lifetimes of porphycenes obtained using ps and fs pump-probe studies.

To ensure that we are indeed exciting the molecules in S_2 states (followed by excitation into S_n states) we performed the fs pump-probe measurements without focusing the pump and probe pulses, thereby ensuring there was no nonlinear absorption. When the beams are not focused the excitation is limited to S_1 states only and therefore induced absorption from S_1 states to S_2 states suggesting decrease in probe transmission. The representative data obtained with unfocused pulses is shown in figure 5 for Po1, Po2, and Po4. The data could be fitted with a single exponential and the lifetimes extracted were 7.5 ps, 7.0 ps, and 10.9 ps for Po1, Po2, and Po4, respectively. Relaxation times extracted for all the samples are enlisted in table 1. The pump-probe data in the ps (800nm) had better signal to noise ratio than fs (600 nm) data. The error bars in pump-probe experimental data for ps case was estimated to be ±5% and for the fs case ±15%.

3.4 NLO studies of Po1-Po5

NLO studies were performed on all the five molecules to assess their nonlinear absorption and nonlinear refraction behavior. Figure 6 shows typical closed aperture data along with their corresponding theoretical fits for solvent (chloroform) and samples Po1-Po5 performed at peak intensities of ~75 GW/cm^2.

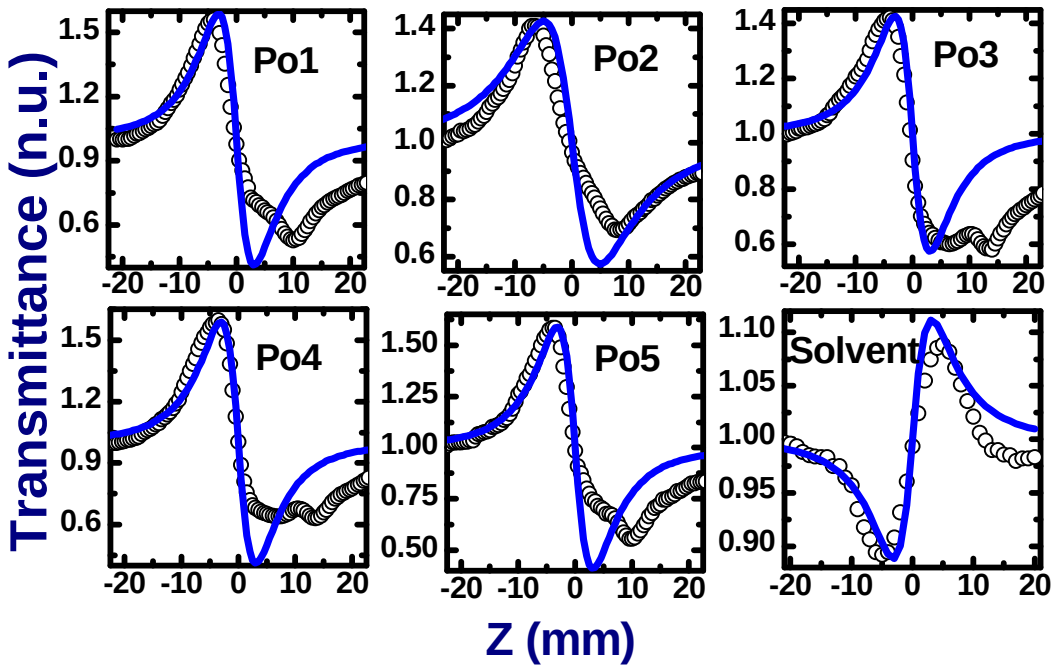

Figure 6 Closed aperture Z-scans of Po1-Po5 and solvent (chloroform) recorded with peak intensities of ~75 GW/cm^2. Open circles represent the experimental data whereas the solid lines are fits.

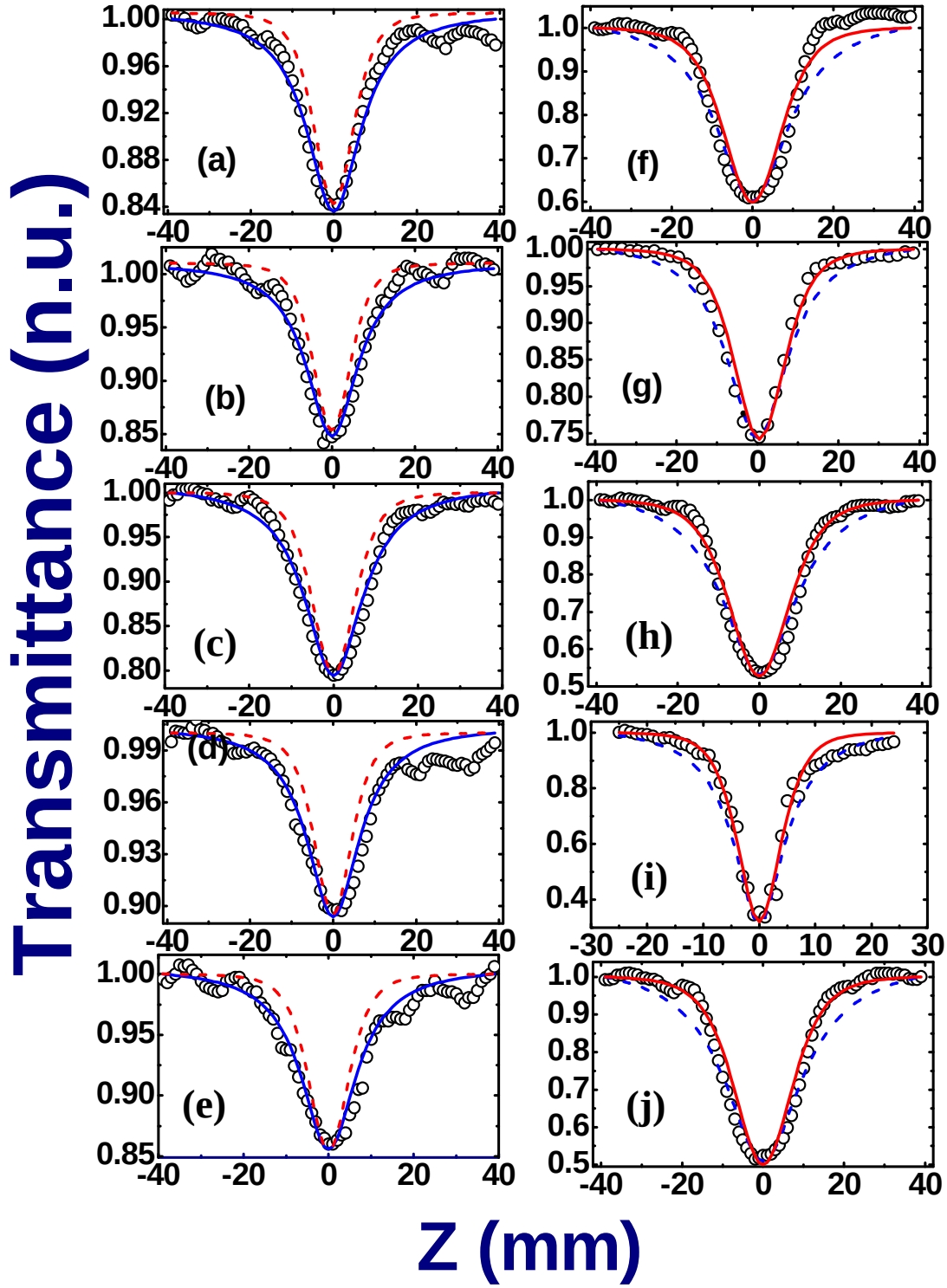

Figure 7 (a)-(j) Open aperture Z-scans of Po1-Po5 at different peak intensities. For low peak intensities 2PA was best fit [blue solid lines are for 2PA and red dotted lines are for 3PA, (a)-(e)] while for high peak intensities 3PA was the best fit [red solid lines are for 3PA and blue dotted lines are for 2PA (f)-(j).

The data were fitted using standard equations [45, 46] to extract nonlinear refractive index (n_2). Details of equations used are discussed in sub-Section 2.15.3 in chapter 2. The samples exhibited large nonlinearities with the formation of annular

rings near focus. This distorted the typical Z-scan curve near the valley reflecting in a slightly asymmetric curve, probably, due to large nonlinear phase-shift. Such behaviour was previously reported by Kouhski et al. [47] and Chen et al. [48]. However, the estimated nonlinear phase shift ($\Delta\varphi$) in our case was less than π for the data presented in figure 6. All the samples possessed negative nonlinearity with the magnitudes of n_2 in the range of $2\text{-}3\times10^{-15}$ cm^2/W and are summarized in table 2 along with their $\chi^{(3)}$ values. The reproduction of the typical closed aperture valley-peak signature for the solvent (chloroform) ruled out the possibility of any misalignment in the setup. Pure solvent exhibited a positive nonlinearity of $\sim0.55\times10^{-15}$ cm^2/W. The solvent contribution being positive clearly suggests that the nonlinearity of the solute (porphycene) is definitely higher than the values quoted here.

Figures 7 (a)-(j) show the open aperture Z-scan data at different peak intensities. The shape of Z-scan curves obtained at lower peak intensities when compared to those obtained at higher intensities were different indicating two different NLO processes occurring at those corresponding intensities. The presence of two resonances in the absorption spectra of these molecules, one near 400 nm (due to the porphycene core) and other near 270 nm (due to the naphthalene moiety), could explain the uncharacteristic nonlinear absorption behaviour of the molecules. 3PA in naphthalene has been ascertained through several earlier studies [49, 50]. For the 800 nm photon these two resonances can act as two-photon (2P) and three-photon (3P) states respectively. Fakis et al. [51] reported similar data in pyrylium chromophores with femtosecond pulses at 760 nm, 790 nm, and 840 nm. In their case higher order effects appeared beyond a certain threshold of peak intensity which resulted in creating a critical population in the first excited state by 2PA process. Sutherland et al. [52] and Anemain et al. [53] also observed similar results and modelled their data using an effective 3PA coefficient. The difference between the *instantaneous* 3PA and *effective* 3PA is the process through which three photons are absorbed by the molecule. In the former case three photons are simultaneously absorbed (via virtual levels of the molecule) whereas in the latter case two photons are absorbed and the molecules are then in an excited state (real state). Depending on the lifetime of the excited state and pulse duration there could be absorption to even higher excited states using another photon (2+1) provided the excited state cross-section is significant. The

effective 3PA can also be termed as two-photon induced excited state absorption. At lower peak intensities (typically <100 GW/cm^2), data presented in figures 7(a)-7(e) was best fitted to 2PA (eqn. 2) indicating that 2PA was the dominant mechanism. At higher peak intensities (typically >110 GW/cm^2), the data presented in figures 3(f)-3(j) was best fitted to effective 3PA (eqn. 3) indicating its dominance in this regime. For Po5, 2PA and 3PA were observed for peak intensities of ~120 GW/cm^2 and ~400 GW/cm^2, respectively. $\chi^{(3)}$ (TPA, Kerr effect etc.) and $\chi^{(5)}$ effects proceed from the combination of the same kind of excited states. There are no different excited schemes separately for $\chi^{(3)}$ and $\chi^{(5)}$. Interference effects related to the phase of the nonlinearity (it is a complex number) can make them appear with different thresholds [55]. In the present case the S_2 state is responsible for both $\chi^{(3)}$ process (2PA) and $\chi^{(5)}$ process (effective 3PA).

$$T_{OA} = 1 - \beta I_0 L_{eff}/2^{3/2} \quad \textbf{(2)}$$

$$T_{OA} = 1 - \gamma {I_0}^2 {L'}_{eff}/3^{3/2} \quad \textbf{(3)}$$

Above equations were obtained from reference 55 and we plotted **ln(Intensity)** vs **ln(1-T_{0A}),** which gave a straight line. A slope of ~1 indicates the presence of 2PA and a slope of ~2 indicates 3PA behavior as shown in figure 8.

The values of ground state absorption cross-section measured for Po1-Po5 were 1.8, 2.4, 2.3, 2.4, 2.7 (× 10^{-17} cm^2) whereas the excited state cross-sections (σ_{ex}) obtained from the fits were 3.9, 6.5, 14.4, 7.4, 11.6 (× 10^{-17} cm^2), respectively. These values were obtained taking lifetime of S_2 state as ~1 ps (see equation 2) and values of β used were obtained from the fits to low intensity data. Table 2 includes 2PA and 3PA cross-sections at different peak intensities for all the five samples. Our measurements were repeated at very low peak intensities (~50 GW/cm^2) for the samples Po2, Po3, and Po4 and the data again confirmed the presence of pure 2PA contribution and rather than 2PA + ESA. However, the 2PA coefficients could have been over-estimated [56] using this technique and other complementary techniques are required to arrive at the exact values. The random experimental errors (arising from estimation of spot size at focus, concentration measurements, input power measurements, data fitting etc.,) result in an overall error of ±20% in our calculations.

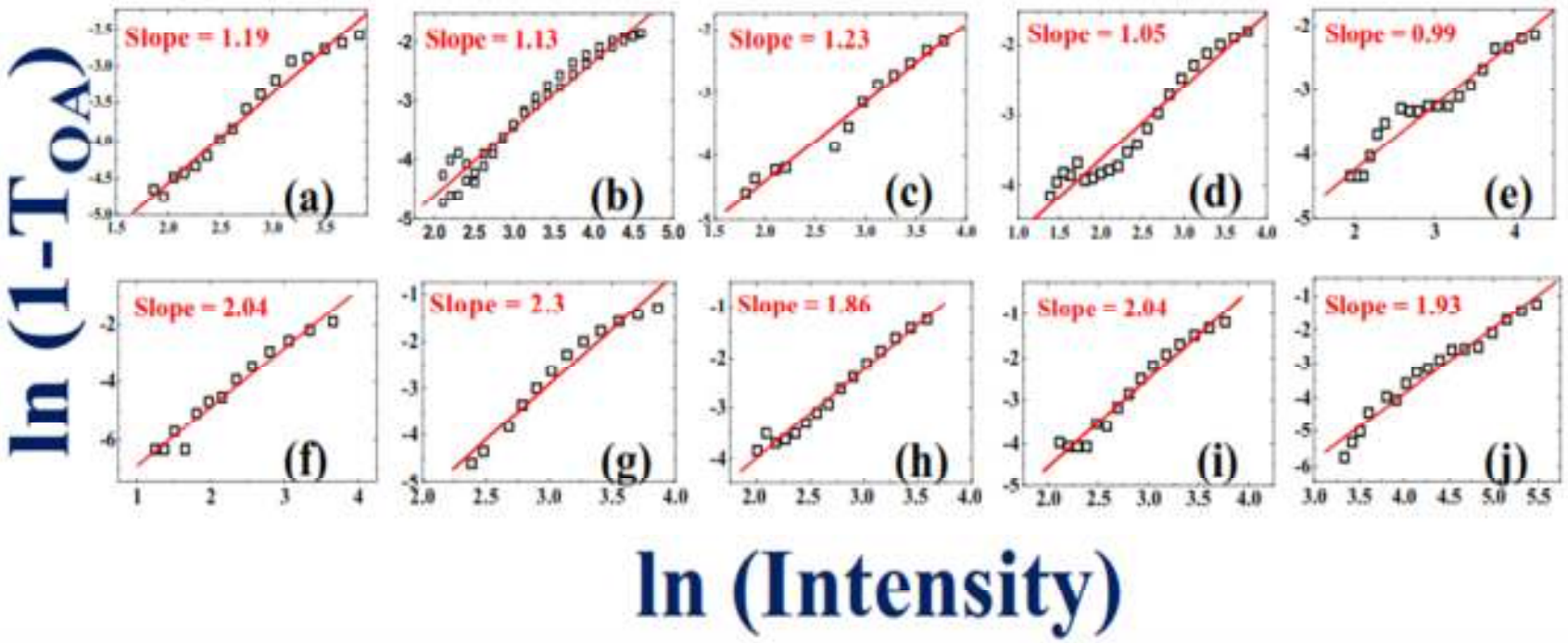

Figure 8 Intensity dependent plots depicting the mechanism to be 2PA (slope 1) or 3PA (slope 2)

Sample	I_{oo} (GW/cm^2)	β (cm/W) × 10^{-11}	$\sigma^{(2)}$ (GM)	α_3 (cm^3/W^2) × 10^{-21}	$\sigma^{(3)}$ (cm^{6}s^2/photon^2) × 10^{-76}	n_2 (m^2/W) × 10^{-19}	Re$\lvert\chi^{(3)}\rvert$ (m^2/V^2) × 10^{-21}	α_2 (m/W) × 10^{-13}	Im$\lvert\chi^{(3)}\rvert$ (m^2/V^2) × 10^{-22}	$\lvert\chi^{(3)}\rvert$ (m^2/V^2) × 10^{-21}	$\lvert\chi^{(3)}\rvert$ (e.s.u.) × 10^{-13}	W	T
Po1	**78**	**5**	**8260**	**-**	**-**								
	118	**-**	**-**	**3.5**	**14.4**	**-3.8**	**4.3**	**5.0**	**3.5**	**4.3**	**3.1**	**1.9**	**1.0**
Po2	**98**	**7**	**11600**	**-**	**-**								
	132	**-**	**-**	**9.0**	**36.9**	**-2.6**	**2.9**	**7.0**	**4.9**	**2.9**	**2.1**	**1.3**	**2.1**
Po3	**74**	**8.8**	**14500**	**-**	**-**								
	117	**-**	**-**	**25.0**	**103.0**	**-2.7**	**3.0**	**8.8**	**6.2**	**3.0**	**2.2**	**1.3**	**2.6**
Po4	**74**	**13**	**21500**	**-**	**-**								
	120	**-**	**-**	**19.5**	**80.1**	**-3.7**	**4.1**	**13.0**	**9.2**	**4.2**	**3.0**	**1.8**	**2.8**
Po5	**120**	**4.8**	**7930**	**-**	**-**								
	407	**-**	**-**	**11**	**45.2**	**-3.5**	**3.9**	**4.8**	**3.4**	**3.9**	**2.8**	**1.8**	**1.1**

Table 2 Summary of the NLO coefficients obtained for Po1-Po5.

Compounds	Sample	σ^2(GM)	τ_p	Ref.
Dye	Cytochrome C	100	150 fs	[16]
HeteroaromaticQuadrupolar Dyes	PEPEP	3130	130 fs	[28]
A-pi-A polymethine dyes	G37 G38 G74 G152	2900 8800 15000 17000	140 fs	[22]
Congeneric Pentapyrrolic Expanded Porphyrins:	Pentaphyrin Sapphyrin Isosmaragdyrin Orangarin	3300 2900 2700 1200	130 fs	[25-27]
Porphyrin -Squaraine - Porphyrin	PoR- SQA-Por	11000	100-140 fs	[23]
Self-Assemblies of Butadiyne-Linked Bis(Imidazolylporphyrin)	Polymer Zn Substituted Bis(Imidazolylprophyrin)	440000	120 fs	[24]
Water Soluble porphyrin dimers	P_2C_2-NMeI P_2C_2-CO_2NH_4 P_2-Suc	17000 14000 10000	300 fs	[25]
Tetra phenyl porphycenes(TPPo)	TPPo PdTPPo mesoTPPo	2280 1750 24	120 fs	[34]
Dinapthoporphycenes	**Po1** **Po2** **Po3** **Po4** **Po5**	**8260** **11600** **14500** **21500** **7930**	**~1.5 ps**	**This work**

Table 3 Summary of NLO coefficients of Po1-Po5 with others reported in literature.

The magnitudes of Im [$\chi^{(3)}$] and $\chi^{(3)}$ were estimated from the nonlinear coefficients and can be found in reference [57, 58]. The figures of merit (FOMs) T and W were evaluated and the data is again shown in table 2. T>1 suggests large nonlinear refraction values suggestive of the potential application of dinapthoporphycenes in photonic-devices. However, the corresponding FOM for nonlinear absorption, W, is >1. W<1 is generally desirable for photonic devices. The 2PA absorption cross-sections are also compared with some of the previously reported molecules and summary of the data is presented in table 3. Cytochrome C [19], PEPEP [33] dyes exhibited low $\sigma^{(2)}$ values of 100 and 3130, respectively. Recently, A-π-A polymethine dyes have demonstrated large cross-sections of the order of 10^4 GM [20]. Porphyrins with expanded rings [26-27] exhibited $\sigma^{(2)}$ values of 1200-3300 GM whereas Porphyrin-Squaraine–Porphyrin assembly has been reported to have $\sigma^{(2)}$ of 11000 GM [21]. For water soluble porphyrins [30], the maximum values reported are of the magnitude ~10^4 GM. However, in comparison to previous molecules, dinapthoporphycenes have large $\sigma^{(2)}$ values with Ni substituted Po4 having $\sigma^{(2)}$= 21500 GM. But self assembled porphyrins reported by Ogawa et al. [24], have larger

$\sigma^{(2)}$ magnitude (~440000 GM) than present work. The nonlinear coefficients presented in this work are obtained with ~1.5 ps pulses and assuming the magnitudes could be larger (due to longer pulses) by one order of magnitude when compared to ~100 fs pulses data, the order of magnitudes for our samples (single monomer molecules) are still comparable to many of the recently investigated molecules (either oligomers or polymers). The fs Z-scan results of Po1-Po5 shows saturable absorption as in the figure 9 (open aperture) and n_2(negative) as observed in figure 10 (closed aperture). The NLO values are extracted and presented in table 4.

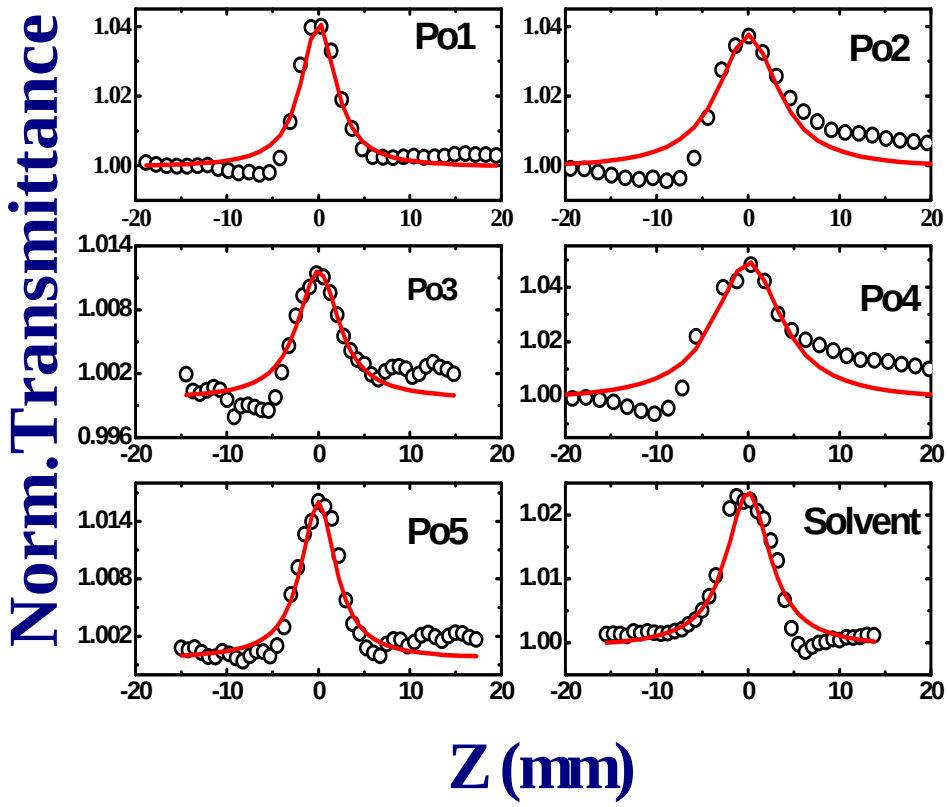

Figure 9 Saturable absorption demonstrated by fs Z-scan in Porphycenes (Po1-Po5) and chloroform (solvent) recorded with ~50 fs pulses (typical peak intensities of 0.6-0.8 TW/cm^2).

Sample	β (fs) (cm/W) × 10^{-13}	n_2 (fs) (cm^2/W) ×10^{-17}
Chloroform	0.50	0.5
Po1	6.00	3.0
Po2	3.10	3.0
Po3	0.95	2.0
Po4	6.00	5.0
Po5	1.15	0.9

Table 4 NLO coefficients of porphycenes at 800 nm obtained using ~50 fs pulses.

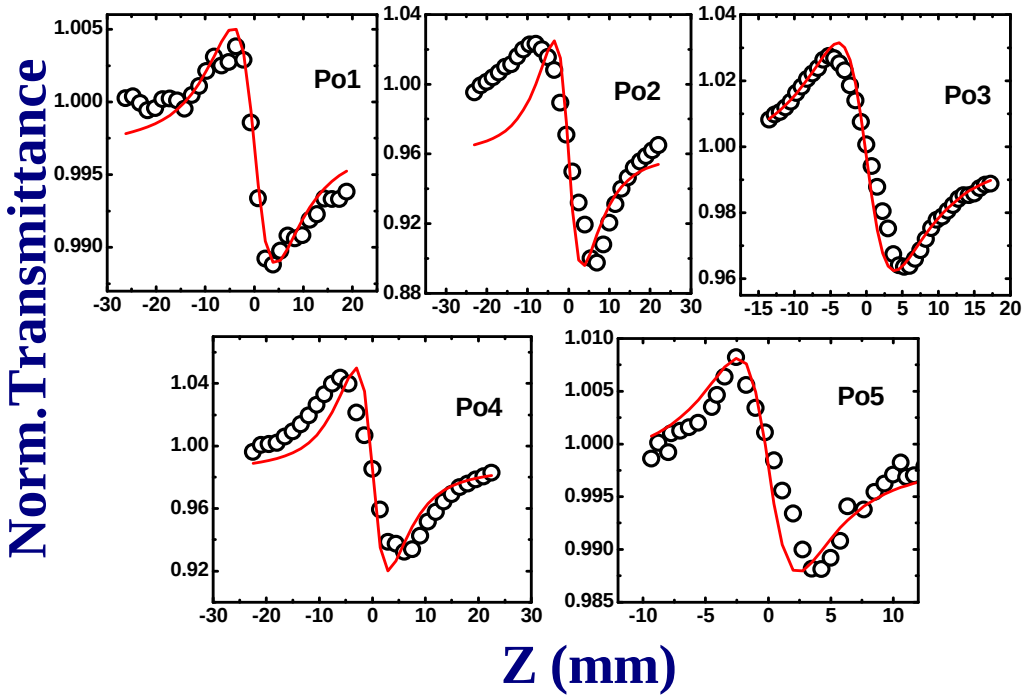

Figure 10 Closed aperture studies of fs Z-scan in Porphycenes (Po1, Po2, Po3, Po4, Po5) recorded with ~50 fs pulses (typical peak intensities of 0.1-0.2 TW/cm^2). Response of solvent (chloroform) can be seen in figure 6.

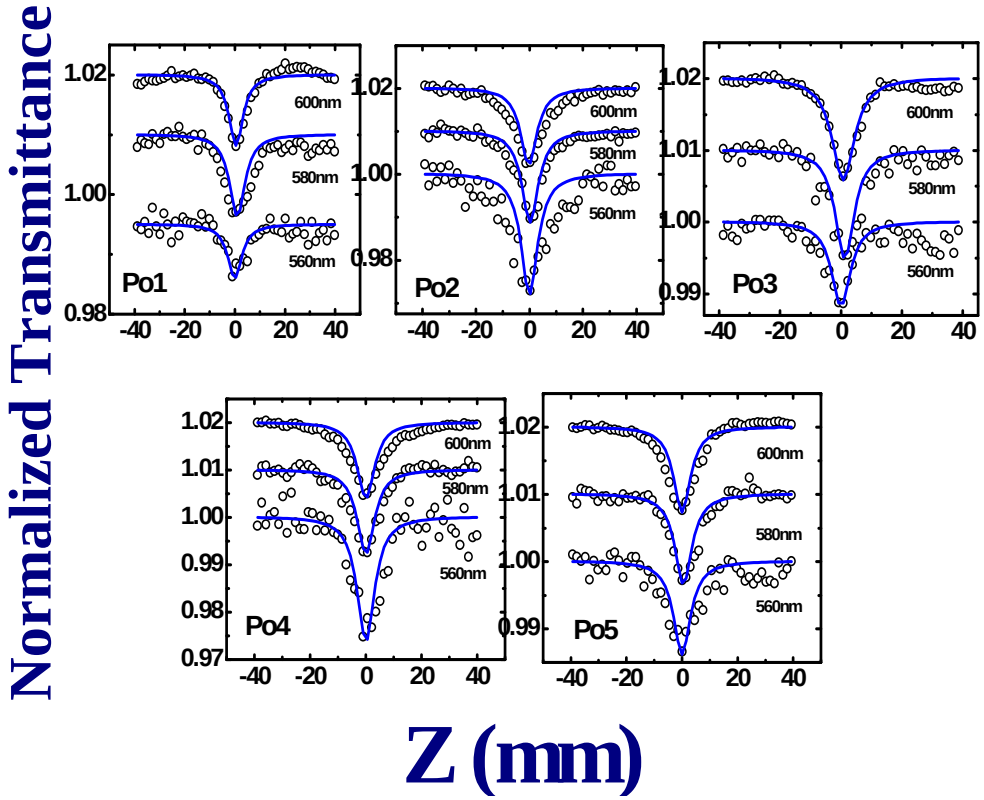

Figure 11 Open aperture Z-scans of Po1-Po5 at different wavelengths at 560 nm, 580 nm, and 600 nm indicating 2PA behavior at peak intensities <100 GW/cm^2 with ~1.5 ps pulses. Some of the plots have been shifted vertically for clarity.

Sample	**β (ps) 560 nm (cm/W) $\times10^{-12}$**	**β (ps) 580 nm (cm/W) $\times10^{-12}$**	**β (ps) 600 nm (cm/W) $\times10^{-12}$**	**n_2 (ps) 560 nm (cm^2/W) $\times10^{-17}$**	**n_2 (ps) 580 nm (cm^2/W) $\times10^{-17}$**	**n_2 (ps) 600 nm (cm^2/W) $\times10^{-17}$**
$CHCl_3$	-	-	-	-	-	-
Po1	2.30	3.50	3.00	8.88	6.58	16.3
Po2	1.10	1.05	8.70	35.3	70.7	78.2
Po3	3.00	4.40	3.75	14.8	7.24	22.7
Po4	7.50	5.00	4.50	7.28	22.4	21.8
Po5	3.50	3.40	3.20	5.12	9.76	10.8

Table 5 NLO coefficients of different porphycenes obtained at wavelengths of 560 nm, 580 nm, and 600 nm.

Reverse saturable absorption (RSA) behavior was observed at 560 nm, 580 nm and 600 nm. The values of two photon absorption coefficients (β) are tabulated above for each case for all the five porphycenes. The absorption spectra illustrate red shifted Soret bands and Q-bands compared to β-alkylated porphycenes, owing to the rigidification and extended-π system resulted by fusion of two naphthalene groups onto the porphycene macrocycle. The absorption spectra (see data presented in figure 2) of free-base porphycene (Po1, Po2, Po3) display relatively intense low energy Q-band (15625 cm^{-1} -12000 cm^{-1}) peaking near 14000 cm^{-1} and well defined Soret or B-bands peaking near 25000 cm^{-1}. Figure 11 shows the open aperture Z-scan data obtained for Po1-Po5 at 560 nm, 580 nm, and 600 nm. We have observed 2PA as the dominant mechanism but one cannot rule out the presence of ESA from S_1 to S_2states. The fits to the data provided the values of an *effective* 2PA coefficient (β) in the range of 1.05×10^{-12} cm/W to 8.70×10^{-12} cm/W. Evidently, these values are an order of magnitude lower than the values reported at 800 nm, which was a resonant two-photon wavelength for these molecules. The values of n_2 in the ps regime recorded for Po1-Po5 were in the range of $5\text{-}35\times10^{-17}$ cm^2/W at 560 nm, $6.5\text{-}71\times10^{-17}$ cm^2/W at 580 nm, $10.8\text{-}78\times10^{-17}$ cm^2/W at 600 nm. Some of this data is presented in Appendix. Interestingly, the n_2 values increased as excitation wavelength changed from 560 nm to 600 nm. This could be attributed to the excited state population near to 600 nm with slight increase in absorption. The values at 560 nm, possibly, represent the true electronic nonlinearity to a great extent since there is minimal absorption at this

wavelength. Po2 had the largest n_2 values for all the wavelengths investigated in this study. Po4 had the largest 2PA values for both fs and ps excitation (except at 600 nm ps excitation). The values of nonlinear coefficients obtained from closed and open aperture data for all the molecules are enlisted in table 5.

3.5 Energy level diagram of Dinaphthoporphycenes

Figure 12 illustrates the possible excitation mechanism in porphycenes with singular nonlinear absorption behaviour. At lower peak intensities 2PA could be from the S_2 states (23250-28500 cm^{-1} with single photon corresponds to 12500 cm^{-1}) of these porphycene molecules while the effective 3PA is a cascaded 2PA and excited state absorption from S_2 state to the S_n states (33300-40000 cm^{-1}). Typical lifetimes of S_2 states in such molecules are reported to be <1 ps [44]. Our pump-probe data was obtained for these molecules after modelling the nonlinear absorption data. A qualitative explanation for relaxation mechanisms in both ps and fs regime (focused and unfocused data) using detailed energy level structure is depicted in figure 13. Some recent studies of the porphycene molecules can be found [57-63].

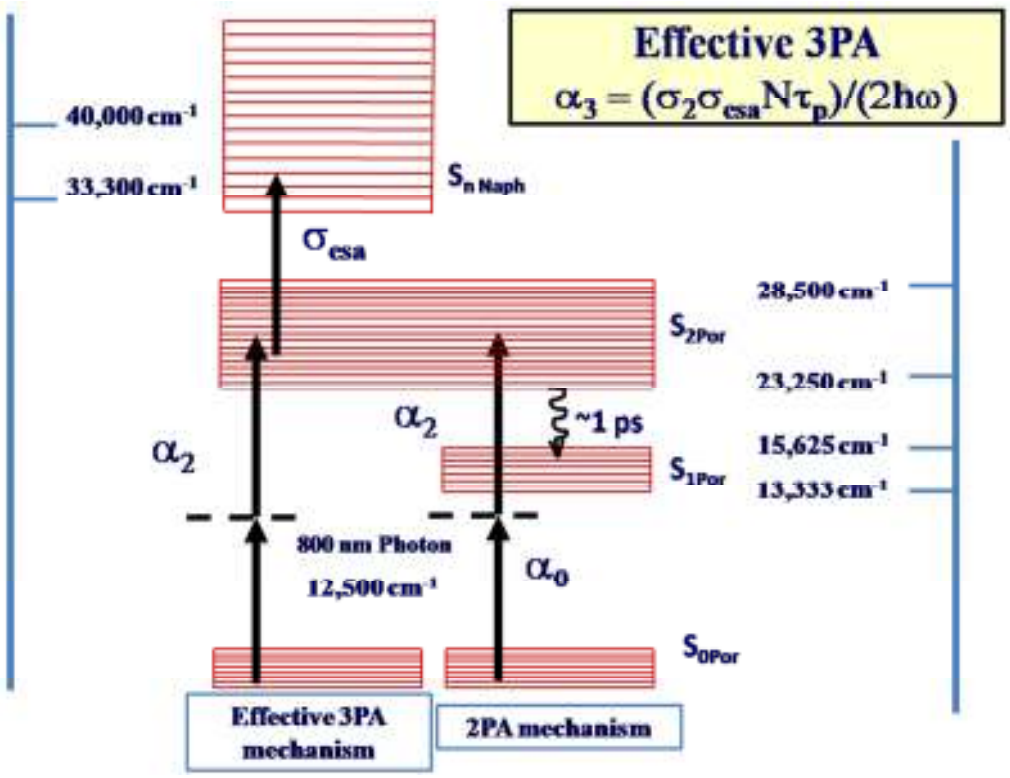

Figure 12 Energy level structures in porphycenes explaining the two resonances for 2PA, 3PA.

An unfocused 600 nm photon (16,667 cm^{-1}) only excites the molecules to S_1 states and consequently single decay time (assigned to S_1-S_0 decay) was observed. Though the scattering is evident from the data we could fit a single exponential decay time and a significant difference in shape of the probe transmission at high peak intensities was seen. At higher peak intensities at 600 nm we could expect the higher lying S_2states (33,333 cm^{-1}) to be populate through two photon absorption (to just below the S_n states) followed by excited state absorption from S_2 to S_n states and one could distinguish three relaxation pathways (IVR, IC, and S_1-S_0).

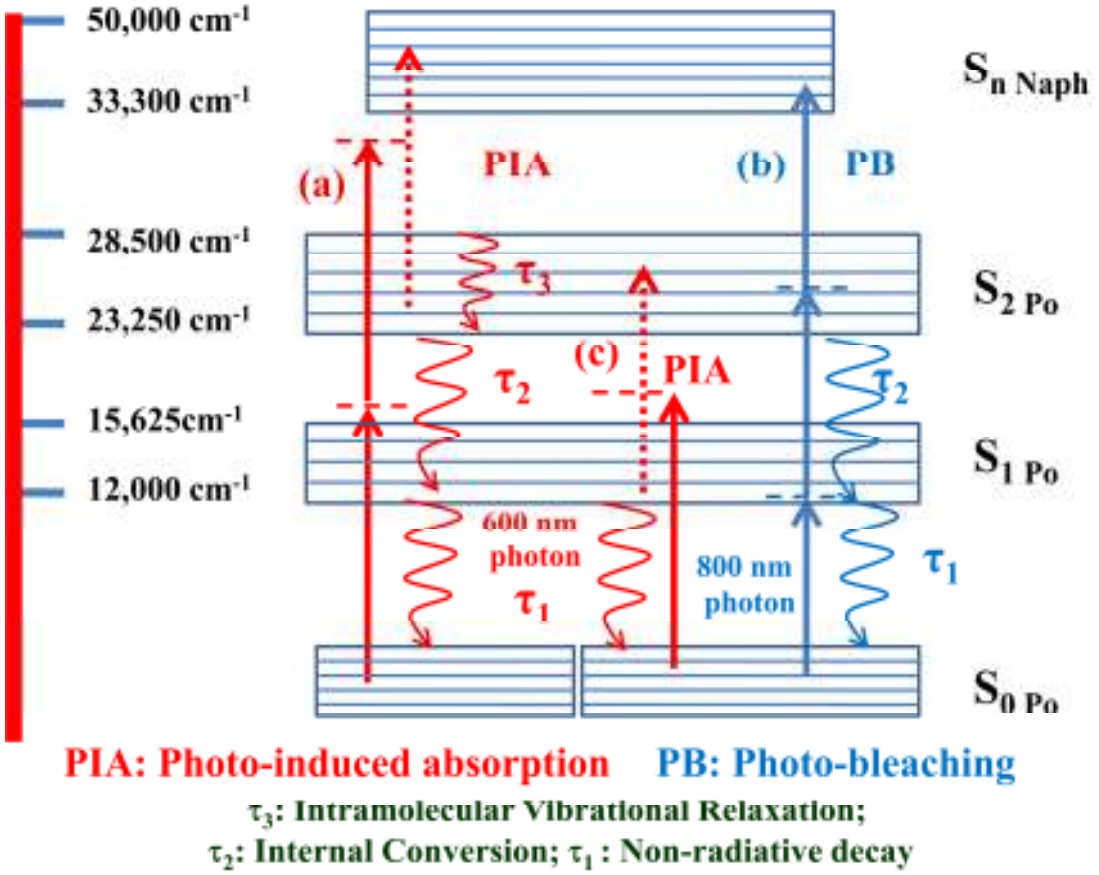

Figure 13 Typical energy level diagram of Po1-Po5 depicting the various relaxation times from different excited states (a) fs pulses, focused pump and probe data, 600 nm (b) ps pulses, focused pump and probe data, 800 nm (c) fs pulses, unfocused pump and probe data, 600 nm.

When excited with ps pulses at 800 nm we observed two distinct lifetimes which are attributed to the S_2-S_1 transition (IC) and S_1-S_0 transition (slowest component). The values presented in table 1 confirm that the fs data and ps data are corroborating each other, within experimental errors, and support our arguments about

different excitation schemes. Since these are non-fluorescent molecules we feel that the lifetimes observed are due to non-radiative transitions (thermalization processes). The errors (from experiments and fitting procedures) in these measurements were estimated to be ~15% for the focused data and ~20% for unfocused data.

3.6 Conclusions

In summary, we have studied excited state dynamics degenerate pump-probe using ~70 fs at 600 nm and ~1.5 ps laser pulses centred at 800 nm of five different dinaphthoporphycenes. Our NLO ps Z-scan results clearly demonstrate 2PA at all the above wavelengths. Two component carrier relaxation dynamics with the fast time constant in the range of 1.8-3.1 ps and the slower one in 7.0-10.0 ps range were observed with ps excitation. We could observe three decay time constants of 100-120 fs, 0.8-1.5 ps, and 7.3-10.0 ps in the fs pump-probe data. The lifetimes observed were similar in both the ps and fs cases. The fastest lifetime is attributed to IVR in the S_2 states while the intermediate lifetime to the S_2 to S_1 states de-excitation (IC). The longest life time is characteristic of the S_1 to S_0 non-radiative decay. The present results demonstrate the strong nonlinear absorption properties of dinaphthoporphycenes combined with ultrafast response times may find possible applications in photonics. Even though general structural and spectral patterns are qualitatively similar in the two isomers, quantitative differences may sometimes be immense. For instance, the lowest electronic transition (Q-band) in porphycene is more than an order of magnitude stronger than that in porphyrin and also significantly red-shifted. Such a pattern, combined with other photophysical characteristics, makes porphycene a potentially much better agent for photodynamic therapy than parent porphyrin and its derivatives. This prediction has been firmly corroborated, using various substituted porphycenes in the treatment of tumors and in photo-inactivation of bacterial strains. Their photo-physics have been widely studied and proposed as attractive second-generation agents for photodynamic therapy (PDT). This is due to their ability to absorb red light and photosensitize singlet oxygen. In order to control their photophysical and other properties, insertion of functionalities into the periphery of the porphycene macro-cycle is essential.

3.7 References

1. (a) R. Chandra, M. Tiwari, P. Kaur, M. Sharma, R. Jain, S. Dass, Ind. J. Clin. Biochem. **15** (2000) 183 (b) A. R. Battersby, Nat. Prod. Rep. **17 (**2000) 507.
2. (a) V. V. Roznyatovskiy, C.H. Lee, J. L. Sessler, Chem. Soc. Rev. **42** (2013) 1921 (b) J.C. Stockert, M. Cañete, A. Juarranz, A. Villanueva, R.W. Horobin, J.I. Borrell, J. Teixidó, S. Nonell, Curr. Med. Chem. **14** (2007) 997 (c) Z. Huang, Technol. Cancer Res. Treat. **4** (2005) 283.
3. (a) M. Pawlicki, H. A. Collins, R.G. Denning, H. L. Anderson, Angew. Chem. **48** (2009) 3244 (b) K. Ogawa, Y. Kobuke, Org. Biomol. Chem. **7** (2009) 2241.
4. M. Albota, D. Beljonne, J. L. Brédas, J. E. Ehrlich, J. Y. Fu, A. A. Heikal, S. E. Hess, T. Kogej, M. D. Levin, S. R. Marder, D. McCord-Maughon, J. W. Perry, H. Röckel, M. Rumi, G. Subramaniam, W.W. Webb, X.L. Wu, C. Xu, Science **281** (1998) 1653.
5. (a) G. S. He, L. S. Tan, Q. D. Zheng, P. N. Prasad, Chem. Rev. **108**, (2008) 1245 (b) M. Rumi, J. W. Perry, Adv. Opt. Photon. **2** (2010) 451.
6. K. D. Belfield, K. J. Schafer, Y. Liu, J. Liu, X. Ren, E. W. Van Stryland, J. Phys. Org. Chem. **13** (2000) 837.
7. (a) M.O. Senge, M. Fazekas, E. G. A. Notaras, W. J. Blau, M. Zawadzka, O. B. Locos, E. M. N. Mhuircheartaigh, Adv. Mater. **19** (2007) 2737 (b) S. Gawinkowski, G. Orzanowska, K. Izdebska, M.O. Senge, J. Waluk, Chem. A Eur. Journal **17** (2011)1003 (c) S. Gawinkowski, Ł. Walewski, A. Vdovin, A. Slenczka, S. Rols, M.R. Johnson, B. Lesyng, J. Waluk, Phys. Chem. Chem. Phys. **14** (2012) 5489 (d) J. Waluk, W. Vogel, J. Phys. Chem. **98** (1994) 4530 (d) K. B. Anderson, E. Vogel, J. Waluk, Chem. Phys. Lett. **271** (1997) 341.
8. G. de la Torre, P. Vazquez, F.A. Lopez, T. Torres, Chem. Rev. **104** (2004) 3723.
9. R. S. S. Kumar, S. Venugopal Rao, L. Giribabu, D. Narayana Rao, Chem. Phys. Lett. **447** (2007) 274.
10. S. Venugopal Rao, N. K. M. N. Srinivas, L. Giribabu, B. G. Maiya, D. N. Rao, R. Philip, G. R. Kumar, Opt. Commun. **182** (2000) 255.
11. P. P. Kiran, D. R. Reddy, B. G. Maiya, A. K. Dharmadhikari, G. R. Kumar, D. N. Rao, Opt. Commun. **252** (2005) 150.
12. N. Venkatram, D. N. Rao, L. Giribabu, S. Venugopal Rao, Chem. Phys. Lett. **464** (2008) 211.

13. M. Morisue, K. Ogawa, K. Kamada, K. Ohta, Y. Kobuke, Chem. Commun. **46** (2010) 2121.
14. M. Samoc, J. P. Morrall, G. T. Dalton, M. P. Cifuentes, M. G. Humphrey, Angew. Chem. Int. Ed. **46** (2007) 731.
15. K. Ogawa, A. Ohashi, Y. Kobuke, K. Kamada, K. Ohta, J. Amer. Chem. Soc. **125** (2003) 13356.
16. A. A. Andrade, N. M. B. Neto, L. Misoguti, L. De Boni, S.C. Zilio, C.R. Mendonca, Chem. Phys. Lett. **390** (2004) 506.
17. M. Drobizhev, Y. Stepanenko, Y. Dzenis, A. Karotki, A. Rebane, P. N. Taylor, H. L. Anderson, J. Phys. Chem. B **109** (2005) 7223.
18. H. Rath, V. Prabhuraja, T.K. Chandrashekar, A. Nag, D. Goswami, B.S. Joshi, Org. Lett. **8** (2006) 2325.
19. H. Rath, J. Sankar, V. Prabhuraja, T. K. Chandrashekar, A. Nag and D. Goswami, J. Am. Chem. Soc. **127** (2005) 11608.
20. S. L. Oliveira, D. S. Corrêa, L. Misoguti, C. J. L. Constantino, R. F. Aroca, S. C. Zilio, C.R. Mendonça, Adv. Mater. **17** (2005) 1890.
21. L. De Boni, J. J. Rodrigues Jr., D.S. Dos Santos Jr., C.H.T.P. Silva, D.T. Balogh, O.N. Oliveira, S.C. Zilio, L. Misoguti, C.R. Mendonça, Chem. Phys. Lett. **361** (2002) 309.
22. L. A. Padilha, S. Webster, O. V. Przhonska, H. H. Hu, D. Peceli, T. R. Ensley, M. V. Bondar, A.O. Gerasov, Y. P. Kovtun, M. P. Shandura, A. D. Kachkovski, D. J. Hagan, E.W. Van Stryland, J. Phys. Chem. A **114** (2010) 6493.
23. S. Webster, S. A. Odom, L. A. Padilha, O. V. Przhonska, D. Peceli, H. H. Hu, G. Nootz, A. D. Kachkovski, J. Matichak, S. Barlow, H. L. Anderson, S. R. Marder, D.J. Hagan, E.W. Van Stryland, J. Phys. Chem. B **113** (2009) 14854.
24. K. Ogawa, A. Ohashi, Y. Kobuke, K. Kamada, K. grOhta, J. Phys. Chem. B **109** (2005) 22003.
25. M.K. Kuimova, H.A. Collins, M. Balaz, E. Dahlstedt, J.A. Levitt, N. Sergent, K. Suhling, M. Drobizhev, N.S. Makarov, A. Rebane, H.L. Anderson, D. Phillips, Org. Biomol. Chem .**7** (2009) 889.
26. Z. S. Yoon, D. G. Cho, K. S. Kim, J. L. Sessler, D. Kim, J. Amer. Chem. Soc. **130** (2008) 6930.
27. J.M. Lim, Z. S. Yoon, J. Y. Shin, K. S. Kim, M. C. Yoon, D. Kim, Chem. Commun. **3** (2009) 261.

28. R. Signorini, C. Ferrante, D. Pedron, M. Zerbetto, E. Cecchetto, M. Slaviero, I. Fortunati, E. Collini, R. Bozio, A. Abbotto, L. Beverina, G.A. Pagani, J. Phys. Chem. A **112** (2008) 4224.
29. E. Vogel, M. Kocher, H. Schmickler, J. Lex, Angew. Chem. Int. Ed. Engl. **25** (1986) 257.
30. D. Sanchez-Garcia, J. L. Sessler, Chem. Soc. Rev. **37** (2008) 215.
31. J. L. Sessler, A. Gebauer, E. Vogel, "Porphyrin Isomers" In Porphyrin Handbook, Vol. **2**, Ch 8, (2000); The Porphyrin Hand Book, Eds. K. M. Kadish, K. M. Smith, R. Guilard, Academic Press, New York, 2000.
32. O. Arad, J. Morros, X. Batllori, J. Teixido, S. Nonell, J. I. Borrell, Org. Lett. **8** (2006) 847.
33. (a) L. Cuesta, E. Karnas, V. M. Lynch, P. Chen, J. Shen, K.M. Kadish, K. Ohkubo, S. Fukuzumi, J.L. Sessler, J. Am. Chem. Soc. **131** (2009) 13538 (b) D. Kuzuhara, H.Yamada, S.Mori, T.Okujima, H.Uno, J. Por. Phtha. **15** (2011) 930.
34. J. Arnbjerg, J. B. Ana, J.P. Martin, S. Nonell, J. I. Borrell, O. Christiansen, P.R. Ogilby, J. Am. Chem. Soc. **129** (2007) 5188.
35. T. Sarma, P. K.Panda, P.T. Anusha, S. V. Rao, Org. Lett. **13** (2011) 188.
36. V. Roznyatovskiy, V. Lynch, and J. L. Sessler, Org. Lett. **12** (2010) 4424.
37. J. Waluk, M. Muller, P. Swiderek, M. Kocher, E. Vogel, G. Hohlneicher, J. Michl, J. Am. Chem. Soc. **113** (1991) 5511.
38. G.G. Gurzadyan, T.H. Tran-Thi, T. Gustavsson, J. Chem. Phys. **108** (1998) 385.
39. V. E. Bondybey, S. V. Milton, J. H. English, P. M. Rentzepis, Chem. Phys. Lett., **97** (1983) 130.
40. P. M. Rentzepis, V. E. Bondybey, J. Chem. Phys. **80** (1984) 4727.
41. D. Huppert, V. E. Bondybey, P.M. Rentzepis, J. Phys. Chem. **89** (1985) 5811.
42. (a) J. Dobkowski, Thesis, Institute of Physical Chemistry, Polish Academy of Sciences (2007) (b) J. Dobkowski, V. Galievsky, A. Starukhin, E. Vogel, J. Waluk, J. Phys. Chem. A **102** (1998) 4966.
43. (a)S. Venugopal Rao, T. S. Prashant, D. Swain, T. Sarma, P. K. Panda, and S. P. Tewari, Chem. Phys. Lett. **514** (2011) 98 (b) J. Mi, L. Guo, Y. Liu, W. Liu, G. You, S. Qian, Phys. Lett. A **310** (2003) 486.
44. P. Fita, C. Radzewicz, J. Waluk, J. Phys. Chem. A **112** (2008) 10753.
45. M. Sheik-Bahae, A. A. Said, T. H. Wei, D. J. Hagan, E. W. Van Stryland, IEEE J. Quant. Electron. **26** (1999) 760.

46. R. L. Sutherland, *Handbook of Nonlinear Optics*, New York, (2003).
47. E. Koushki, A. Farzaneh, S. H. Mousavi, Appl. Phys. B **99** (2010) 565.
48. S. Q. Chen, Z. B. Liu, W. P. Zang, J.G. Tian, W.Y. Zhou, F. Song, C.P. Zhang, J. Opt. Soc. Amer. B **22** (2005) 1911.
49. G. P. Srivastava, S. C. Gupta, J. Phys. D.: Appl. Phys. **7** (1974) 169.
50. S. Singh, L.T. Bradley, Phys. Rev. Lett. **12** (1964) 612.
51. M. Fakis, G. Tsigaridas, I. Polyzos, V. Giannetas, P. Persphonis, I. Spiliopoulos, J. Mikroyannidis, Chem. Phys. Lett. **342** (2001)155.
52. R. L. Sutherland, M. C. Brant, J. Heinrichs, J. E. Slagle, D. G. McLean, P. A. Fleitz, J. Opt. Soc. Am. B **22** (2005) 1939.
53. R. Anémian, Y. Morel, P. L. Baldeck, B. Paci, K. Kretsch, J. M. Nunzi, C. Andraud, J. Mater. Chem. **13** (2003) 2157.
54. M. Gil, P. Fita, J. Dobkowski, C. Radzewicz, D. Marks, G.W. Salyga, M. Pietraszkiewicz, M. Glasbeek, N. Urbanska, J. Waluk, P. Borowicz, J. Am. Chem. Soc. **132** (2010) 13472.
55. (a) F. Charra, J. M. Nunzi, J. Opt. Soc. Am. B **8** (1991) 570, (b) J. He, Y. Qu, H. Li, J. Mi, J. Wei, Opt. Exp. **13** (2005) 9235.
56. Z. Suo, M. Drobizhev, C.W. Spangler, N. Christensson, A. Rebane, Org. Lett. **7** (2005) 4807.
57. D. Swain, P. T. Anusha, T. S. Prashant, S.P. Tewari, T. Sarma, P.K. Panda, S.V. Rao**,** AIP Conf. Proc. **1391** (2011) 674.
58. D. Swain, P.T. Anusha, T.S. Prashant, S.P. Tewari, T. Sarma, P.K. Panda, S. Venugopal Rao, Appl. Phys. Lett. **100** (2012) 141109.
59. H. Piwonski, A. Sokolowski, M. Kijak, S. Nonell, J. Waluk, J. Phys. Chem. Lett. **4** (2013) 3967.
60. M. Taneda, A. Tanaka, H. Shimakoshi, A. Ikegami, K. Hashimoto, M. Abe, Y. Hisaeda, Tetrahed. Lett. **54** (2013) 5727.
61. T. Kumagai, F. Hanke, S. Gawinkowski, J. Sharp, K. Kotsis, J. Waluk, M. Persson , L. Grill, Phy. Rev. Lett. **111** (2013) 246101.
62. T. Kumagai, F. Hanke, S. Gawinkowski, J. Sharp, K. Kotsis, J. Waluk, M. Persson , L. Grill, Nat. Chem. **6** (2014) 41.
63. M.K. Abdel-Latif, O. Kuhn, arXiv:1010.5598v1 [physics.chem-ph] 27 Oct 2010.

Chapter 4

Ultrafast excited state dynamics and NLO studies of Cyclo[4]naphthobipyrroles

4.1 Introduction

The 1930 Nobel prize winner in chemistry (Hans Fischer) elucidated the chemical structure of various porphyrins, the pigment responsible for oxygen binding in erythrocytes. Scientific hunt for numerous porphyrin and porphyrin-like bio-molecules attracted attention of several researchers over the last few decades. Another motivation for work in the area of porphyrin research that may allow a more detailed understanding of photosynthesis, cell respiration and oxygen transport processes is effectiveness and ingenuity with which these processes operate in nature. Considerable efforts are in progress to the design of artificial solar cells, water splitting catalysts, etc. that are based on porphyrins and porphyrin analogues. One of the primary goals in synthesizing expanded porphyrin was to get absorption spectra that are bathochromically shifted compared to porphyrin due to its extended π-conjugation. However, larger expanded porphyrin containing 6 or more pyrrole rings often adopts non-planar or figure eight structure there by disrupting the effective conjugation pathway, which proved to be non-aromatic or weakly aromatic in nature. As research in natural porphyrin chemistry has advanced, increased attention has been devoted to expanded porphyrins and their analogs. For example, progress in the synthetic methodology of porphyrins and a greater basic understanding of their properties resulted in the design of sophisticated fully conjugated oligoporphyrin ribbons with large two-photon absorption coefficients and negative first oxidation potentials, properties that rendered this group of molecules promising as materials for use in photo-electronic applications. Similarly, the discovery of relatively easy procedures for the synthesis of annulated pyrroles inspired the porphyrin community to create new pyrrolic chromophores that differ from porphyrins and contain these particular building blocks.

The attractive features of π-extended porphyrins and expanded porphyrins have provided an incentive to create new porphyrin analogues that combine key attributes from both approaches within a single chemical entity. This convergence has led recently to the synthesis of new chromophores that are both expanded and π-extended relative to normal porphyrins. A large variety of expanded porphyrins can be prepared by adding more number of pyrrole or other hetero-aromatic molecules apart from tuning their number of bridging meso-carbons. Several novel organic

moieties with strong two-photon absorption (2PA) and three-photon absorption (3PA) coefficients/cross-sections have been investigated over the last decade due to their impending applications in the fields of photonics, biomedical applications, lithography etc. [1-14]. However, most of those investigations were confined to a single wavelength in the visible spectral region (800 nm or 532 nm) while using single pulse duration [femtosecond (fs) or nanosecond (ns)]. Multi-photon absorption in organic materials typically occurs at longer wavelengths (≥ 800 nm) providing noteworthy advantages such as (a) minimal light losses due to scattering and (b) decrease in superfluous linear absorption. Our group has been working extensively over the last decade investigating several new molecules (e.g. Phthalocyanines, Porphycenes, Corroles etc.) for quantifying their nonlinear optical (NLO) coefficients/cross-sections over a range of wavelengths in the visible spectral region and using cw/ns/ps/fs pulses [15-26]. In the last two decades expanded porphyrins have emerged as a new class of attractive molecules because of their potential applications in near infrared (NIR) dyes, anion sensors, 2PA materials, photosensitizers, and in photodynamic therapy (PDT) [14,17,27]. They are having active role in optical data processing, telecommunications, aerospace, military camouflage. A large array of expanded porphyrins can be prepared by increasing the number of pyrrole or other hetero-aromatic molecules apart from tuning their number of bridging meso-carbons. Furthermore, it is observed that aromatic expanded porphyrins display large third order nonlinear optical response while normal porphyrin monomers exhibit small σ_2 values of <100 GM [12-14]. Similarly, porphycenes (isomers of porphyrins) possess slightly higher σ_2 values compared to the parent isomers i.e. porphyrins [14]. However, upon β-fusion of naphthalene at its periphery, through its constituent bipyrrolic units, we observed a large enhancement of NLO response in dinaphthoporphycenes [15-17]. Therefore, in order to assess the effect of this naphthalene fusion (by both rigidification and π-extension), we chose to explore the NLO response of our recently reported cyclo[4]naphthobipyrroles, a unique class of cyclo[8]pyrroles, which are expanded porphyrins displaying the classic disk like structure of simple porphyrins with 30π electrons [28-29]. The cyclo[8]pyrrole molecule can be derived by replacing all four meso-carbon bridges of porphyrin with four additional pyrrolic rings. Consequently, these molecules contain direct linkage between the α-pyrrolic positions, which imparts rigidity to the molecule

thereby making a near planar arrangement despite having expanded core compared to porphyrins. The significance of these molecules is encompassed in their novel photophysical and NLO properties. The fusion of alternate pyrrole units with naphthalene moieties adds rigidity to cyclo[8]pyrroles along with extended π-conjugation resulting in the formation of cyclo[4]naphthobipyrroles. Sarma et al. [28] reported that the cyclo[4]-naphthobipyrrole moiety is very sensitive to the nature of the substituents at its periphery owing to the involvement of large number of non-bonding interactions. Due to their near planar structure, possessing a large aromatic core (30π-electrons) with extended π-conjugation, they are expected to possess strong third-order optical nonlinearity. The number of π electrons and/or the molecular geometry associated with the static and dynamic polarizability of these molecules can be considered as determining parameters in controlling the NLO susceptibility. Herein, we present results from (a) dispersion studies of nonlinear optical properties (studied using Z-scan technique) at wavelengths of 600 nm, 640 nm, 680 nm, and 800 nm and (b) excited state dynamics (studied near 600 nm using fs pump-probe technique) of three novel cyclo[4]naphthobipyrroles namely, octaisopropylcyclo[4]naphthobipyrrole (5a), octa-*n*-propylcyclo[4]naphthobipyrrole (5b) and octa-*n*-pentylcyclo[4]naphthobipyrrole (5c).

4.2 Synthesis, Structure and Absorption Data

A 1-L round bottom flask was charged with a stirring bar and dichloromethane (500 mL). A solution of $FeCl_3$ (2.7 g, 17 mmol) in aq. 1M H_2SO_4 (100 mL) was then added. The resulting biphasic mixture was stirred at around 300 rpm, while a solution of alkylated naphthobipyrrole (0.3 g, 1 mmol) in dichloromethane (60 mL) was added via a syringe pump over a period of 9 h with the needle submerged into the organic phase. After complete addition the reaction mixture was stirred for 15 h at room temperature. Organic layer was separated and dried over anhyd. sodium sulfate, solvent was evaporated to obtain the crude molecule. The crude product was purified by column chromatography on silica gel using dichloromethane as the eluent. The greenish-yellow band was collected. The solid residue obtained after removal of the solvent was re-crystallized from $CHCl_3$/methanol to yield 5a as a dark green powder 5a and 5c. For 5b and 5c the

amount of $FeCl_3$used was 6.6 equiv. compared to naphthobipyrrole, whereas, the remaining procedure is same as described above for **5a**.

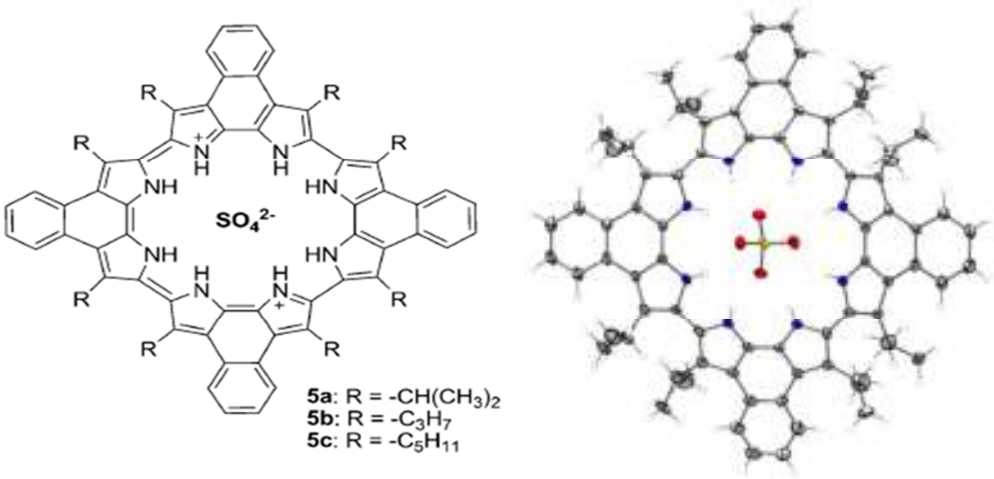

Figure 1 Structures of Cyclo[4]naphthobipyrroles and ORTEP of 5a under study.

The structure of the cyclo[4]naphthobipyrroles 5a, 5b and 5c are shown in figure 1. The synthesis and NLO properties of 5a were studied by Sessler group [29]. They obtained significantly large and practically useful σ_2 values in the range of 1000-2400 GM in the spectral regions of 1800-2400 nm when excited with fs pulses. They also observed fast lifetimes for singlet excited state in their pump-probe/transient absorption measurements. Our group has recently synthesized three molecules with different peripheral substituents and attempted studying their NLO properties. Interestingly, unlike other porphyrinoids, these molecules have strong absorption in the near infrared (1100 nm) wavelengths and comparatively weaker absorption in the UV spectral band (430 nm), which entitles them for niche applications such as optical storage, processing and signaling devices [30]. The understanding of excited states lifetimes in such molecules is essential for various applications such as PDT, optical switching etc. Initial NLO data of sample 5a have been presented in one of our earlier works [31]. Another interesting attribute of cyclo[8]pyrrole derivatives is their formation of supramolecular liquid crystalline adduct with nitro-aromatic molecule. Exposure of dihydrogen sulfate salts of appropriately substituted cyclo[8]pyrrole to electron-deficient acceptor molecules gives discotic liquid crystals stabilized via electron-donor/electron acceptor interaction. TNB (trinitrobenzene) molecules intercalate into stacks of cyclo[8]pyrrole cores coordinated to the sulfate ions making them promising for explosive sensing [32]. The most striking feature about this macrocycle is that it possesses a very strong

near infrared (NIR) [33] absorption band at ~1100 nm (also designated as L band) compared to a weaker Soret type near UV-band at ~430 nm (B band), unlike the other porphyrinoids where the lower energy bands are of feeble intensity.

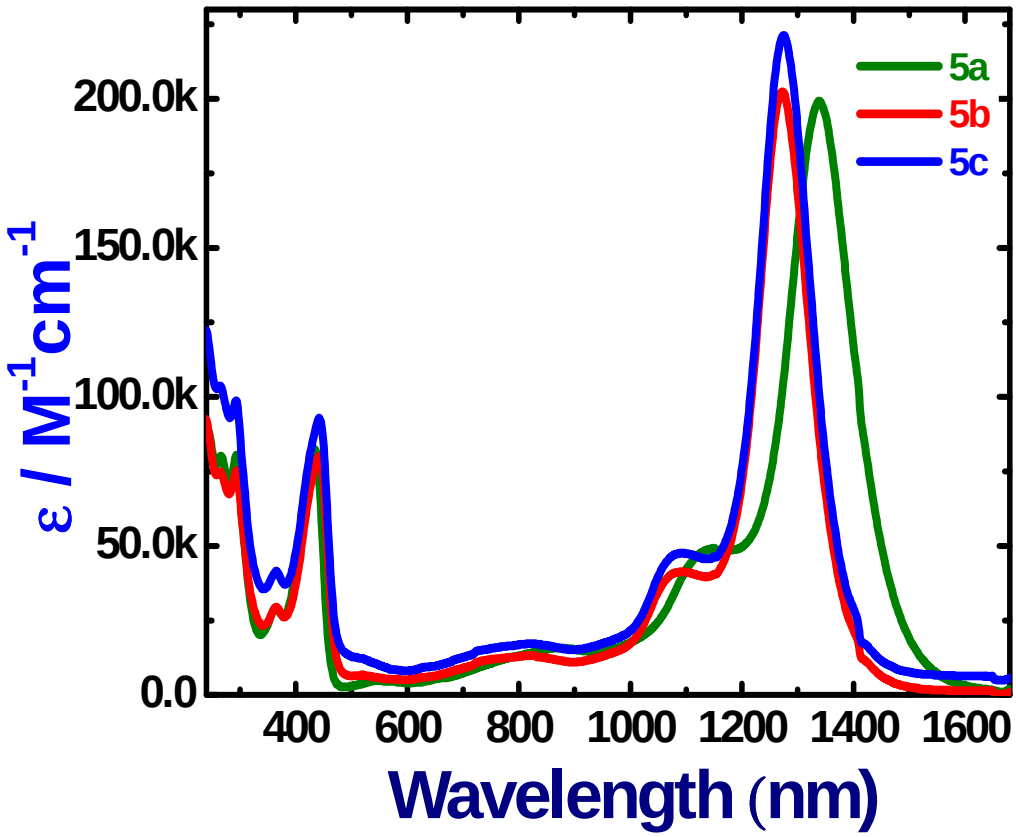

Figure 2 UV-visible-NIR absorption spectra of 5a-5c.

In literature, there are very few cited examples of dyes possessing intense absorption band beyond 1000 nm [34]. This attribute, makes the cyclo[8]pyrrole a promising material for optical data storage and signalling devices [35]. UV-Vis-NIR absorption spectra, depicted in figure 2, consisted of B bands near 433 nm [5] and strong L bands near 1339 nm, which is a characteristic of these molecules. The L-bands are very sensitive to the nature of the substituent in comparison to the B-bands. Fusion of four naphthalene moieties onto the cyclo[8]pyrrole periphery led to marginal red shift (3 – 11 nm). Absorption spectra consisted of L bands at 244 nm, and B bands at 433 nm. Moreover, it has a strong Q bands at 1339 nm which is a characteristic of these molecules. The L-bands are very sensitive to the nature of the substituent in comparison to the B-bands.

4.3 NLO studies using ps pulses

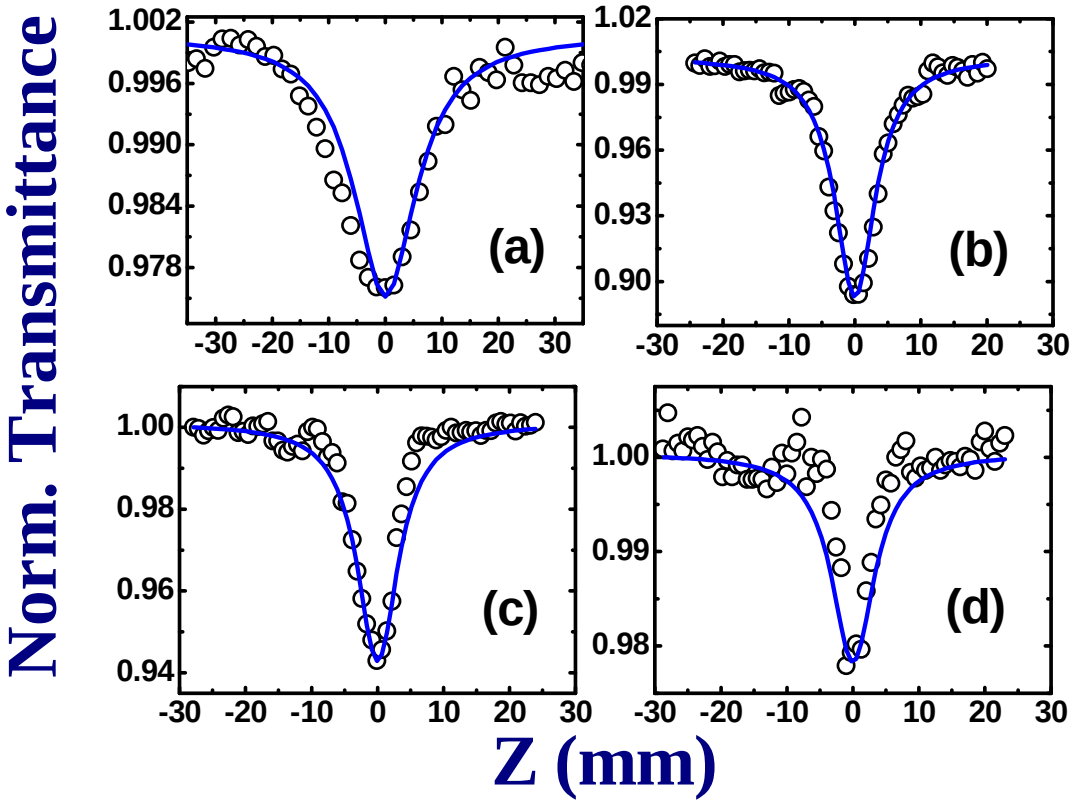

Figure 3 Open aperture Z-scan data of 5a at (a) 800 nm (b) 600 nm (c) 640 nm (d) 680 nm. Open circles are the experimental data while the solid lines are theoretical fits [31].

Figures 3(a)-3(d) shows typical open, closed aperture Z-scan data at (a) 800 nm (b) 600 nm (c) 640 nm (d) 680 nm. All the data showed reverse saturable absorption (RSA). The data was fitted by conventional Z-scan analysis in which the propagation equation was solved [9]. The analysis showed that two-photon absorption (TPA) is the cause of nonlinear absorption. The closed aperture Z-scan data showed that these molecules exhibited negative nonlinearity. The value of n_2 was estimated from the fits. The peak intensity used for closed aperture data avoided higher order contributions. The solvent contribution was minimal at these peak intensities. Nonlinear absorption coefficients were determined from open aperture Z-scan data. Figures 4 and 5 shows typical open aperture Z-scan data obtained at (a) 600 nm (b) 640 nm (c) 680 nm and (d) 800 nm of 5b, 5c, respectively. All the data show reverse saturable absorption kind of behavior with a valley near zero. The analysis shows that two-photon absorption (TPA) is the cause of decrease in the transmittance. The two photon resonance corresponding to 600 nm excitation is 33,333 cm^{-1}. Summary of NLO coefficients obtained from the fits are provided in table 1.

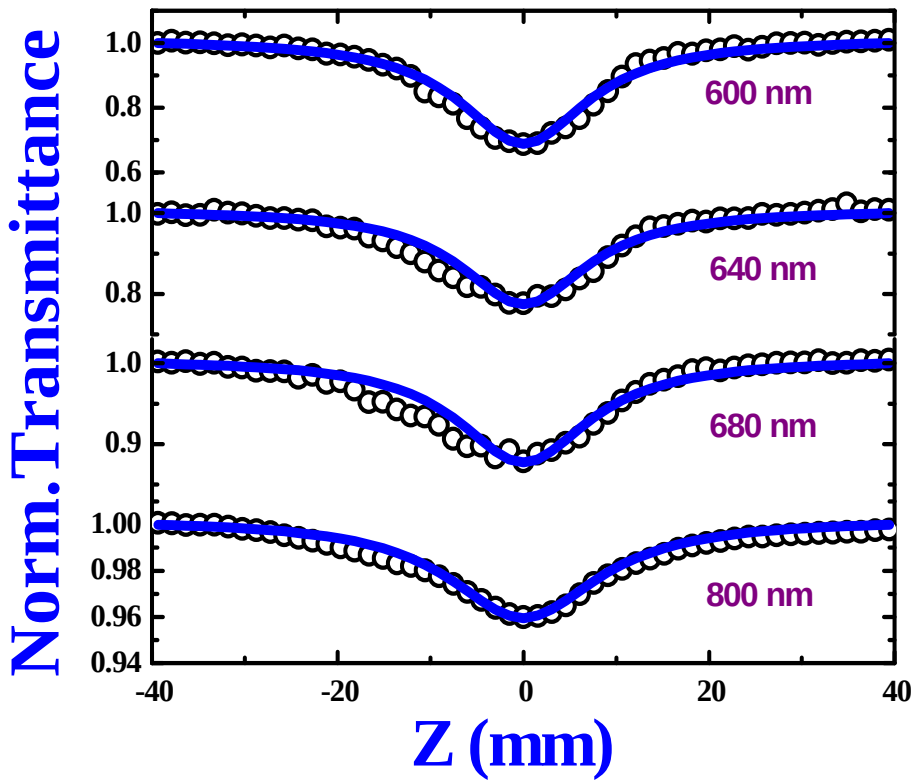

Figure 4 Open aperture Z-scan data of 5b at different wavelengths. Open circles are the experimental data while the solid lines are theoretical fits.

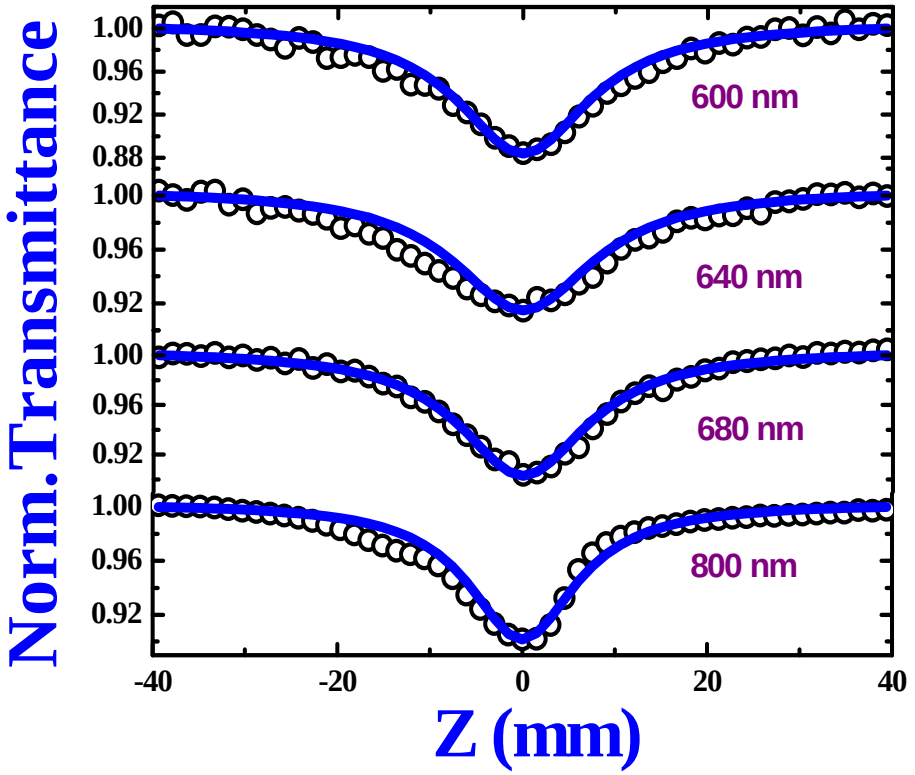

Figure 5 Open aperture Z-scan data of 5c at different wavelengths. Open circles are the experimental data while the solid lines are theoretical fits.

As observed the dip in RSA curve of 5b is more at 600 nm and 640 nm but at 680 nm and 800 nm it is lesser. Similar pattern was observed in 5a also. There is an increase in the linear absorption as we moved from 600 nm to 800 nm. Interestingly RSA dip in 5c was higher at 600 nm than other wavelengths such as 640 nm, 680 nm and 800 nm with replacement in heavier n-pentyl group in 5c. The values of β evaluated for 5b were in the range of 0.11-5.80×10^{-11} cm/W and the corresponding σ_2 values were in the range of 0.22-9.70×10^4 GM. Figure 5 shows the open aperture data of 5c in the 600-800 nm spectral range and the values were in the range of 2.65-5.60 cm/GW and the corresponding σ_2 values were in the range of 3.30-5.20×10^4 GM. The values of β for 5a were in the range of 0.62-3.20 cm/GW and the corresponding σ_2 values were in the range of 0.50-2.9×10^4 GM.

The values of NLO coefficients are at least one order of magnitude higher than those reported by other groups [29]. This could possibly be due to experiments being performed (by us) in the visible spectral region with residual absorption compared to the NIR region (by others). The largest value of σ_2 was observed for 5b at a wavelength of 680 nm. The closed aperture Z-scan data of all the molecules demonstrated that these molecules exhibited negative nonlinearity as demonstrated in figure 6. The peak intensities used were low and avoided higher order contributions. The solvent contribution was minimal (<2%) in the open aperture case at the respective peak intensities. The magnitudes of n_2 were in the range of 1.9-11× 10^{-16} cm^2/W with 5c exhibiting the highest n_2 of 11×10^{-16} cm^2/W at a wavelength of 680 nm. Closed aperture data of the solvent (data presented in figure 7) provided a value of 2.8×10^{-16} cm^2/W but, most importantly, the sign was opposite to that of the solution suggesting that the actual value of solutes could be higher than values estimated and presented here. The closed aperture data of 5a, 5b, and 5c obtained at different wavelengths and the n_2 values retrieved from closed aperture data are summarized in table 1. From n_2 and β we could estimate the real, imaginary, and total magnitude of $\chi^{(3)}$, second hyperpolarizabilities (γ) and the corresponding figures of merit. The values of NLO coefficients presented in this work are within an error of ±15%, which basically arises from (a) estimation of input beam diameter, beam waist, peak intensities (b) calibration of neutral density filters (c) fitting procedures etc.

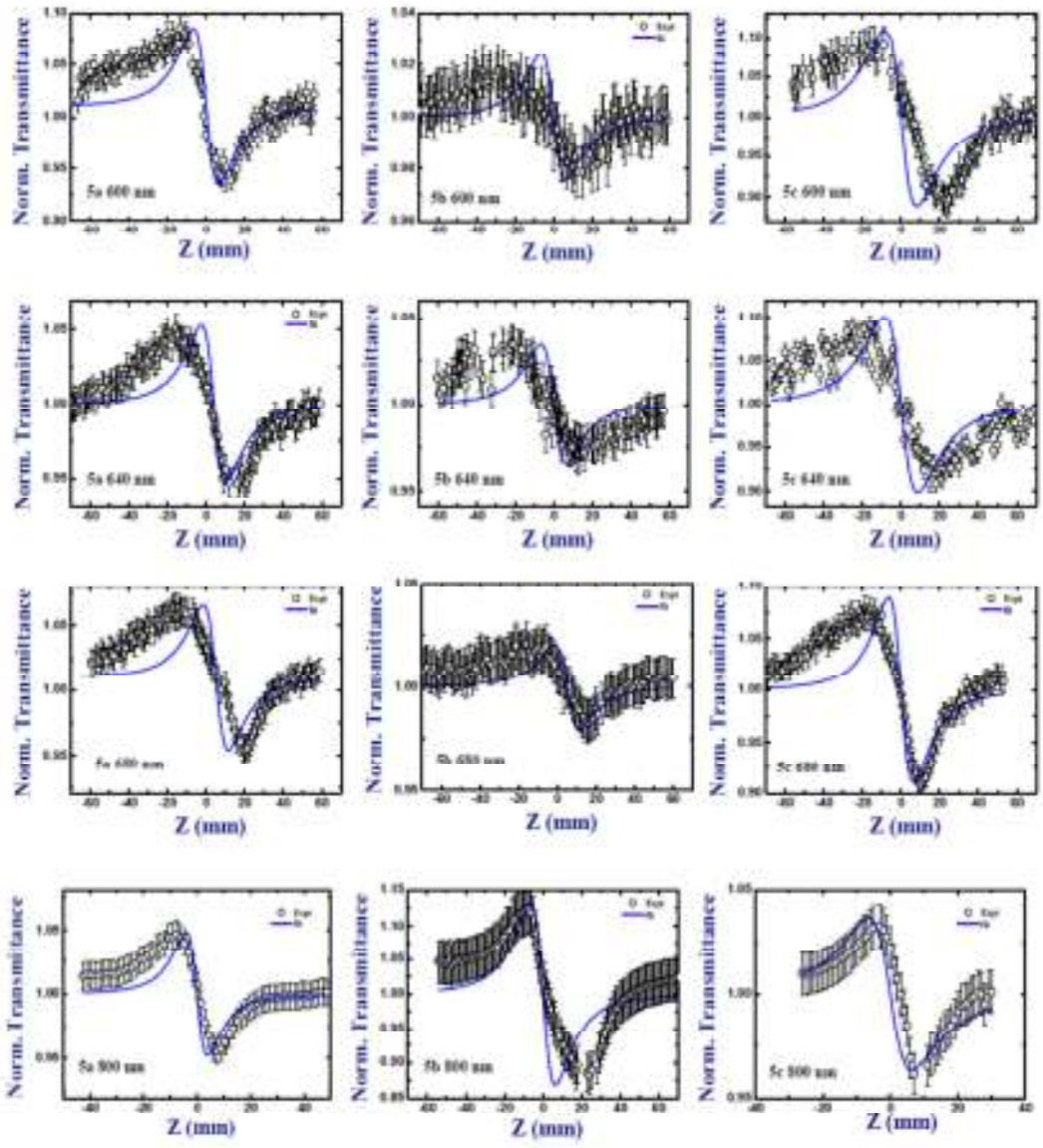

Figure 6 Closed aperture Z-scan data of 5a, 5b, and 5c at 600 nm, 640 nm, 680 nm, and 800 nm. The peak intensities used were ~20-50 GW/cm^2.

The two photon resonance corresponding to 600 nm excitation is ~33,333 cm^{-1} whereas for an 800 nm photon it is 25,000 cm^{-1}. Except for the molecule 5b, variation in β with wavelength was minimal. While 5b exhibited strongest β at 680 nm, 5c exhibited strongest n_2 at 680 nm compared to others. However, 5c exhibited highest β at 600, 640 and 800 nm as compared to 5a and 5b. The difference in the structures is the presence of isopropyl in 5a, n-propyl in 5b, and n-pentyl groups in 5c at the β-pyrrolic positions. The increase in strength of nonlinearity could be attributed to the increased conjugation from 5a to 5c, owing to increased planarity, as the neighbouring isopropyl substituents exert more non-bonding interaction compared to n-alkyl

analogues [28]. The closed aperture behavior of solutions (5a-5c) showed negative nonlinearity and the coefficients calculated are presented in table 2. Figure 8 depicts the spectral dependence of σ_2 in 5a-c. Except for 5b the variation in σ_2 with wavelength was minimal.

Intensity dependent β for 5c at 800 nm at a concentration of ~0.2 mM was found to be constant and is evident from the data presented in figure 9. This suggests that the process involved is purely two-photon and minimal exicted state absorption. The magnitudes of two-photon cross-sections obtained from these studies are comparable to some of the recently reported dinaphtoporphycene molecules (see chapter 3 of this thesis). De Boni et al. [5] investigated perylene derivatives with two-photon cross-sections of typically 200-1200 GM obtained using ~190 fs pulses. Andrade et al. [7] studied cytochrome solutions possessing two-photon cross-sections with a maximum value of 1000 GM using fs pulses. Sarma et al. [15] reported two-photon cross-sections in dinaphthoporphycenes in the range of 10^4-10^5 GM obtained with ps pulses.

	5a		**5b**		**5c**	
λ (nm)	**β (cm/W) $\times 10^{-11}$**	**σ_2 ($\times 10^4$ GM)**	**β (cm/W) $\times 10^{-11}$**	**σ_2 ($\times 10^4$ GM)**	**β (cm/W) $\times 10^{-11}$**	**σ_2 ($\times 10^4$ GM)**
600	3.20 (122)	2.90	0.15 (133)	0.40	3.35 (133)	4.50
640	1.50 (129)	1.30	0.11 (117)	0.22	2.65 (117)	3.30
680	0.62 (114)	5.00	5.80 (103)	9.70	3.65 (103)	4.40
800	1.50 (58)	1.00	2.15 (62)	5.00	5.60 (62)	5.20

Table 1 Summary of NLO coefficients of 5a, 5b, and 5c

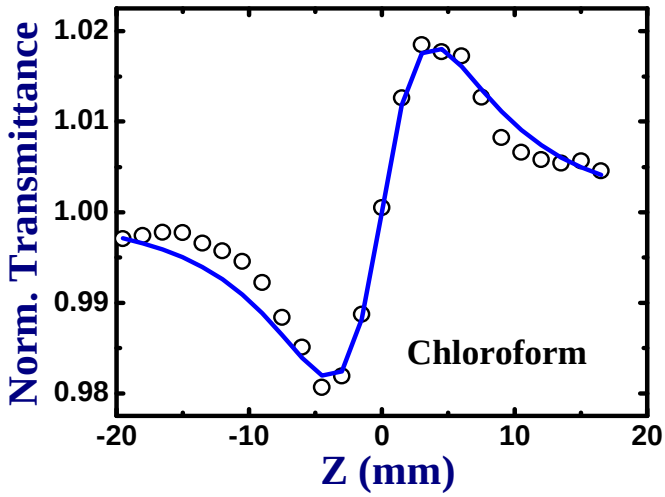

Figure 7 Closed aperture data of solvent chloroform, n_2= 2.8×10^{-16} cm^2/W, I_{00} = 28 GW/cm^2

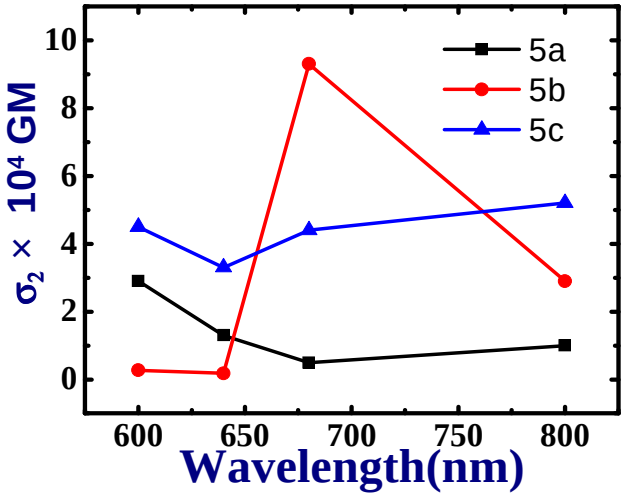

Figure 8 Spectral dependence of σ_2 in 5a-c. Squares represent 5a data, circles represent 5b data and triangles represent 5c data. The solid line is only a guide to the eye.

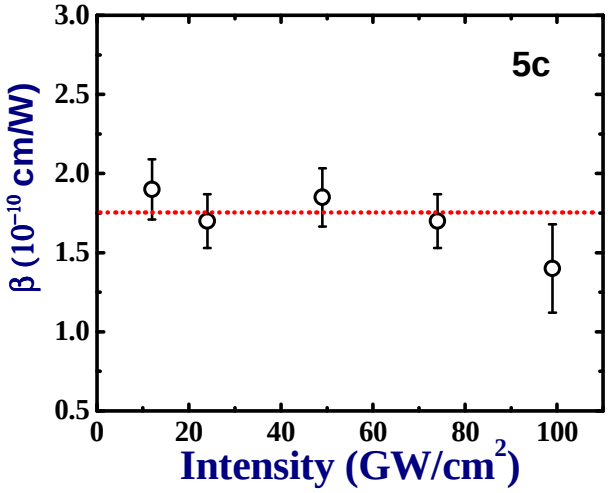

Figure 9 Intensity dependent β for 5c at 800 nm at a concentration of ~0.2 mM.

Even though our present studies were also carried out with ~1.5 ps pulses the values obtained (~10^3-10^4 GM) are superior to many of the recently reported ones. This is corroborated by the fact that values obtained with shorter pulses and at longer wavelengths were in the 10^3 GM range [29]. The variation in total third order NLO susceptibility values (χ^3) with wavelength at for 5a, 5b and 5c did not demonstarte any significant pattern which is evident from data presented in figure 10(a). The values of χ^3 are at the higher side for sample 5c at all the wavelengths. Sample 5c had the highest value of χ^3 at all the available wavelengths confirmed from the data presented in figure 10(a). Figure of merit data for all molecules at different wavelengths is presented in figuer 10(b). Figure of merit T <1 is desirable for any molecule to be used in photonic applications. T value was <1 for (a) 5b at 600 nm (b) 5b 640 nm (c) 5a at 680 nm indicating that these molecules can be used in photonic applications. But 5a and 5c does not have such values at 600 nm, 640 nm and 800 nm. Table 2 summarizes the spectral dependence of n_2 for all the three molecules. Tables 3-6 summarizes the various NLO coefficients retreived for these molecules at wavelengths of 600 nm, 640 nm, 680 nm, and 800 nm. We had confined our studies to these wavelengths only since (a) the absorption spectra have interesting peaks in these spectral regions (b) our ps OPA output was not stable at other wavelengths.

Molecule	**n_2 @ 600 nm cm^2/W**	**n_2 @ 640 nm cm^2/W**	**n_2 @ 680 nm cm^2/W**	**n_2 @ 800 nm cm^2/W**
5a	2.7×10^{-16}	3.6×10^{-16}	4.9×10^{-16}	6.0×10^{-16}
5b	2.6×10^{-16}	1.9×10^{-16}	3.6×10^{-16}	1.5×10^{-16}
5c	4.4×10^{-16}	4.5×10^{-16}	11×10^{-16}	6.0×10^{-16}

Table 2 n_2 values for 5a, 5b, and 5c at different wavelengths.

Molecule	**Re(χ^3) @ 600 nm (m^2/W^2)**	**Im(χ^3) @ 600 nm (m^2/W^2)**	**Total (χ^3) @ 600nm (m^2/W^2)**	**Figure of Merit (T) @ 600 nm**
5a	1.4×10^{-14}	7.6×10^{-15}	1.5×10^{-14}	7.1
5b	1.3×10^{-14}	3.6×10^{-16}	1.3×10^{-14}	0.34
5c	2.2×10^{-14}	8.0×10^{-15}	2.3×10^{-14}	4.5

Table 3 Real, imaginary, and total $\chi^{(3)}$ values of 5a, 5b, 5c recorded at 600 nm.

Molecule	Re(χ^3) @ 640 nm (m^2/W^2)	Im(χ^3) @ 640 nm (m^2/W^2)	Total (χ^3) @ 640nm (m^2/W^2)	Figure of Merit (T) @ 640 nm
5a	1.8×10^{-14}	3.8×10^{-15}	1.8×10^{-14}	2.60
5b	9.5×10^{-15}	2.8×10^{-16}	9.5×10^{-15}	0.37
5c	2.2×10^{-14}	6.7×10^{-15}	2.3×10^{-14}	3.76

Table 4 Real, imaginary, and total $\chi^{(3)}$ values of 5a, 5b, 5c recorded at 640 nm.

Molecule	Re(χ^3) @ 680 nm (m^2/W^2)	Im(χ^3) @ 680 nm (m^2/W^2)	Total (χ^3) @ 680 nm (m^2/W^2)	Figure of Merit (T) @ 680 nm
5a	2.4×10^{-14}	1.7×10^{-15}	2.4×10^{-14}	0.86
5b	1.8×10^{-15}	1.6×10^{-15}	2.4×10^{-14}	10.9
5c	5.5×10^{-14}	9.8×10^{-15}	5.6×10^{-14}	2.25

Table 5 Real, imaginary, and total $\chi^{(3)}$ values of 5a, 5b, 5c recorded at 680 nm.

Molecule	Re(χ^3) @ 800 nm (m^2/W^2)	Im(χ^3) @ 800 nm (m^2/W^2)	Total (χ^3) @ 800nm (m^2/W^2)	Figure of Merit (T) @ 800 nm
5a	3.0×10^{-14}	4.7×10^{-15}	3.0×10^{-14}	2.25
5b	7.5×10^{-15}	6.8×10^{-15}	1.0×10^{-14}	5.60
5c	3.0×10^{-14}	18×10^{-15}	3.5×10^{-14}	8.40

Table 6 Real, imaginary, and total $\chi^{(3)}$ values of 5a, 5b, 5c recorded at 800 nm.

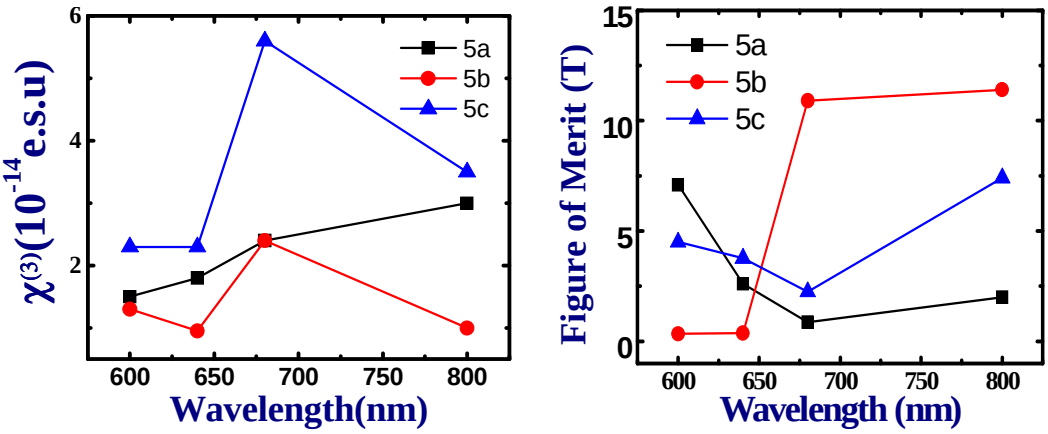

Figure 10 (a) Variation of $\chi^{(3)}$ with wavelength for 5a, 5b, 5c (b) Variation of figure of merit (T) with wavelength for 5a, 5b, 5c.

4.4 Excited State Dynamics of (5a-5c)

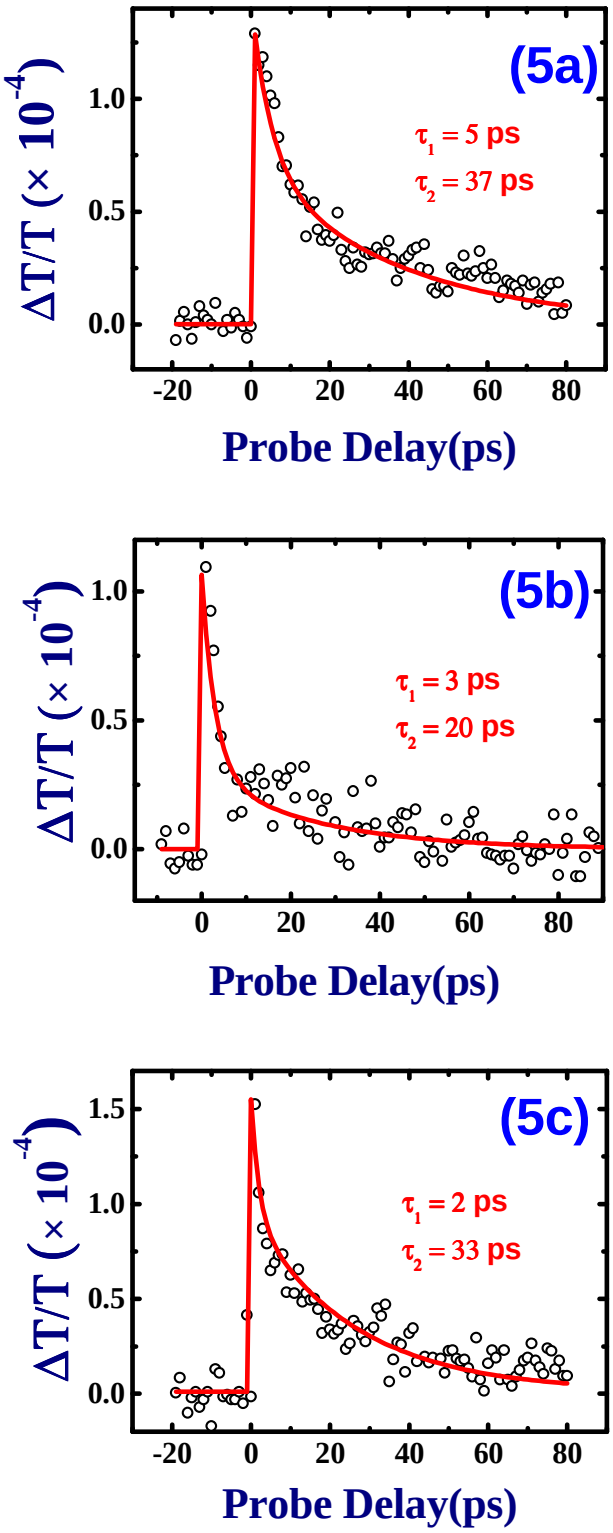

Figure 11 Femtosecond degenerate pump probe data of 5a-c recorded at 600 nm indicating two lifetimes. Open circles are the experimental data while the solid (red) lines are double exponential fits.

The complete experimental details of fs pump probe experiments have been explained in sections 2.12 (figure 17). Figure 11 shows the fs degenerate pump-probe data of 5a-5c obtained at 600 nm using ~70 fs pulses with typical pump energies of ~10 μJ. The data was fitted for a double exponential [17, 20] and two lifetimes (τ_1 and τ_2) were retrieved from each of the fits. The values of τ_1 and τ_2 were ~5 ps and ~37 ps for 5a; ~3 ps and ~20 ps for 5b; and ~2 ps and ~33 ps for 5c, respectively.

4. 5 Energy level diagram of 5a-5c

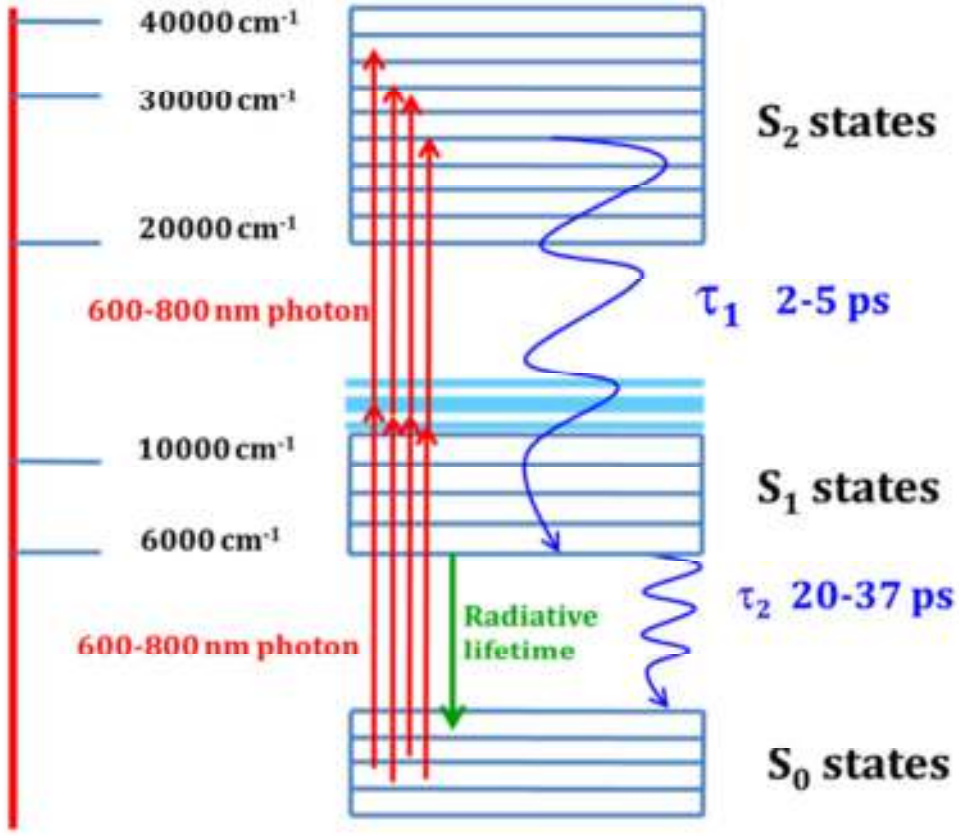

Figure 12 Schematic of energy level diagram of 5a-c explaining the double exponential behavior (τ_1 and τ_2) observed in pump-probe data.

Figure 12 shows a simplified energy level diagram indicating the excitations and decay times for these molecules. Excitation with focused 600 nm photons enables 2PA resulting in populating the S_2 states. The de-excitation mechanism, then, could be from (a) lowest vibrational state of S_2 manifold to highest vibrational states of S_1 manifold (Internal Conversion, IC) followed by intra-molecular vibrational relaxation (IVR) from highest states of S_1 to lowest states of S_1). However, we could not resolve these two lifetimes in our present data while we could in the case of

porphycenes [17]. These are typically fast processes (<1 ps for IC, ~1-3 ps for IVR) and, therefore, the shorter lifetimes observed in pump-probe data (3-5 ps) could be attributed to this relaxation and (b) from the lowest vibrational states of S_1 manifold the molecules relax to ground state via non-radiative mechanism by releasing the energy to solvent (also called as vibrational cooling). This process typically occurs in few tens of ps in such molecules. The longer lifetime can be associated with such a process in 5a-5c. Radiative lifetimes in similar molecules were observed to be typically few ns [20]. The pump-probe studies of 5a were carried out at 0.062 mM while that of 5b and 5c were carried out at 10^{-4} M and at these concentrations we did not observe any aggregation effects (confirmed from absorption spectral studies) and, therefore, we can neglect the inter-molecular contributions to the lifetimes observed. Our initial ESR studies carried out recently suggest that the triplet ground state could be much closer to the singlet ground state and there could be a possible contribution of this to the longer decay times observed. However, further detailed studies (such as non-degenerate pump-probe and transient absorption) are essential to exactly identify the complicated decay dynamics in these molecules.

4.6 Conclusions

There are several studies which identify processes in similar molecules [36-38]. Fita et al. [39, 40] studied few zinc phthalocyanines and observed 10-50 ps time scale dynamics which were characteristic of the vibrational cooling (relaxation to ground state by transfer of heat to the solvent) from the S_1 state. Kullmann et al. [41] working with a bisporphyrin recorded four different lifetimes. The fastest lifetime (~100 fs) was assigned to intramolecular vibrational relaxation within the S_2 states, second fastest lifetime (few ps) to the decay of S_2 states, slower lifetime (few tens of ps) to the cooling dynamics (non-radiative). All NLO and pump-probe data of 5a-5c can be found in reference [42]. These cyclo[4]naphthobipyrroles, particularly 5a (owing to its good solubility), are of great importance for realistic applications as NIR dyes [43-45], apart from their potential utility in light harvesting, dye-sensitized solar cells, bio-imaging, and optical limiting and switching applications. Our future studies will focus on incorporating these molecules in a suitable, transparent polymer and extend the studies of NLO coefficients evaluation and excited state dynamics over the entire visible spectral range.

4.7 References

1. M. Albota, D. Beljonne, J. L. Brédas, J. E. Ehrlich, J. Y. Fu, A. A. Heikal, S. E. Hess, T. Kogej, M. D. Levin, S. R. Marder, D. McCord-Maughon, J.W. Perry, H. Röckel, M. Rumi, G. Subramaniam, W. W. Webb, X. L. Wu, C. Xu, Science **281** (1998) 1653.
2. F. E. Hernandez, K. D. Belfield, I. Cohanoschi, Chem. Phys. Lett. **391** (2004) 22.
3. P. Cronstrand, Y. Luo, P. Norman, H. Agren, Chem. Phys. Lett. **375** (2003) 233.
4. M. Drobizhev, A. Karotki, M. Kruk, A. Rebane, Chem. Phys. Lett. **355** (2002) 175.
5. L. De Boni, C. J. L. Constantino, L. Misoguti, R. F. Aroca, S. C. Zilio, C. R. Mendonça, Chem. Phys. Lett. **371** (2003) 744.
6. L. De Boni, J. J. Rodrigues Jr., D. S. Dos Santos Jr., C. H. T. P. Silva, D. T. Balogh, O. N. Oliveira Jr., S. C. Zilio, L. Misoguti, C. R. Mendonça, Chem. Phys. Lett. **361** (2002) 209.
7. A. A. Andrade, N. M. B. Neto, L. Misoguti, L. De Boni, S. C. Zilio, C. R. Mendonça, Chem. Phys. Lett. **390** (2004) 506.
8. C. E. Powell, J. P. Morrall, S. A. Ward, M. P. Cifuentes, E. G. A. Notaras, M. Samoc, M.G. Humphrey, J. Am. Chem. Soc. **126** (2004) 12234.
9. M. Samoc, G. T. Dalton, J. A. Gladysz, Q. Zheng, Y. Velkov, H. Ågren, P. Norman, M. G. Humphrey, Inorg. Chem. **47** (2008) 9946.
10. M. Samoc, T. C. Corkery, A. M. McDonagh, M. P. Cifuentes, M. G. Humphrey, Aust. J. Chem. **64** (2011) 1267.
11. J. M. Lim, Z. S. Yoon, J. Y. Shin, K. S. Kim, M. C. Yoon, D. Kim, Chem. Comm. **3** (2009) 261.
12. H. Rath, V. Prabhuraja, T. K. Chandrashekar, A. Nag, D. Goswami, B. S. Joshi, Org. Lett. **8** (2006) 2325.
13. Z. S. Yoon, J. H. Kwon, M. C. Yoon, M. K. Koh, S. B. Noh, J. L. Sessler, J. T. Lee, D. Seidel, A. Aguilar, S. Shimizu, M. Suzuki, A. Osuka, and D. Kim, J. Am. Chem. Soc. **128** (2006) 14128.
14. J. Arnbjerg, J. B. Ana, J. P. Martin, S. Nonell, J. I. Borrell, O. Christiansen, P. R. Ogilby, J. Am. Chem. Soc. **129** (2007) 5188.
15. T. Sarma, P. K. Panda, P.T. Anusha, S. Venugopal Rao, Org. Lett. **13** (2010)

188.

16. S. Venugopal Rao, T. S. Prashant, T. Sarma, P.K. Panda, D. Swain, S.P. Tewari, Chem. Phys. Lett. **514** (2011) 98.
17. D. Swain, P.T. Anusha, T. S. Prashant, S.P. Tewari, T. Sarma, P.K. Panda, S. Venugopal Rao, Appl. Phys. Lett. **100** (2012) 141109.
18. S. J. Mathews, S. C. Kumar, L. Giribabu, S. Venugopal Rao, Mater. Lett. **61** (2007) 4426.
19. S. J. Mathews, S. C. Kumar, L. Giribabu, S. Venugopal Rao, Opt. Commun. **280** (2007) 206.
20. P. T. Anusha, D. Swain, S. Hamad, L. Giribabu, T. S. Prashant, S. P. Tewari, S. Venugopal Rao, J. Phys. Chem. C. **116** (2012) 17828.
21. N. Venkatram, L. Giribabu, D. N. Rao, S. Venugopal Rao, Chem. Phys. Lett. **464** (2008) 211.
22. R.S.S. Kumar, S. Venugopal Rao, L. Giribabu, D. N. Rao, Chem. Phys. Lett. **447** (2007)274.
23. P.T. Anusha, L. Giribabu, S.P. Tewari, S. Venugopal Rao, Mat. Lett. **64** (2010) 1915.
24. N. Venkatram, L. Giribabu, D. Narayana Rao, S. Venugopal Rao, Appl. Phys. B **91** (2008) 149.
25. S. Venugopal Rao, N. Venkatram, L. Giribabu, D. Narayana Rao, J. Appl Phys. **105** (2009) 053109.
26. R. S. S. Kumar, S. Venugopal Rao, L. Giribabu, D. N. Rao, Opt. Mat. **31** (2009) 1042.
27. J. L. Sessler, A. Gebauer, S.J. Weghorn, in *The Porphyrin Handbook*, Vol. **2**: (Eds.: K. M. Kadish, K. M. Smith, R. Guilrad), Academic Press, San Diego, 55-124 (2000).
28. T. Sarma, P. K. Panda, Chem. Eur. J. **17** (2011) 13987.
29. V. V. Roznyatovskiy, J. M. Lim, V. M. Lynch, B. S. Lee, D. Kim, J. L. Sessler, Org. Lett. **13** (2011) 5620.
30. D. Seidel, J. L. Sessler, V. Lynch, Angew. Chem. Int. Ed. **41** (2002) 1422.
31. P. T. Anusha, D. Swain, T. Sarma, P. K. Panda, S. Venugopal Rao, in *Nonlinear Optics and Applications VI*, edited by Benjamin J. Eggleton, Alexander L. Gaeta, Neil G. Broderick, Proc. SPIE, **8434** (2012) 84341D.
32. J. Yinon, Anal. Chem., **75** (2003) 99 A.

33. J. Fabian, Chem. Rev., **92** (1992) 1197.
34. A. Tsuda, A. Osuka, Science **293** (2001) 79.
35. J.L. Brédas, C. Adant, P. Tackx, A. Persoons, B.M. Pierce, Chem. Rev. **94** (1994**)** 243.
36. S. Venugopal Rao, J. Mod. Opt. **58** (2011) 1024.
37. L. De Boni, E. Piovesan, L. Gaffo, C.R. Mendonca, J. Phys. Chem. A **112** (2008) 6803.
38. M.G. Vivas, T. Shih, T. Voss, E. Mazur, C.R. Mendonca, Opt. Expr. **18** (2010) 9628.
39. P. Fita, T. Osmalek, T. Goslinski, M. Wierzchowski, J. Mielcarek, J. Photochem. Photobiol. A: Chem. **232** (2012) 44.
40. P. Fita, C. Radzewicz, J. Waluk, J. Phys. Chem. A. **112** (2008) 10753.
41. M. Kullmann, A. Hipke, P. Nuernberger, T. Bruhn, D.C.G. Gotz, M. Sekita, D.M. Guldi, G. Bringmann, T. Brixner, Phys. Chem. Chem. Phys. **14** (2012) 8038.
42. D. Swain, P. T. Anusha, T. Sarma, P. K. Panda, S. Venugopal Rao, Chem. Phys. Lett. **580** (2013) 73.
43. M. Ishida, S. J. Kim, C. Preihs, K. Ohkubo, J. M. Lim, B. S. Lee, J. S. Park, V. M. Lynch, V. V. Roznyatovskiy, T. Sarma, P. K. Panda, C. H. Lee, S. Fukuzumi, D. Kim and J. L. Sessler, Nat. Chem. **5** (2013)15.
44. S.Y. Kee, J. M. Lim, S.J. Kim, J. Yoo, J. S. Park, T. Sarma, V. M. Lynch, P. K. Panda, J. L. Sessler, D. Kim and C. H. Lee, Chem. Commun., **47** (2011) 6813.
45. (a) T. Sarma, P. K. Panda, J. Setsune, Chem. Commun. **49** (2013) 9806 (b) M. Takase, A. Inabe, Y. Sugawara, W. Fujita, T. Nishinaga, K. Nomura, Org. Lett. **15** (2013) 3202.

Chapter 5

Study of ultrafast excited state dynamics and NLO properties of novel Phthalocyanines

5.1 Introduction

Phthalocyanine [derived from Greek words, *naphtha* (rock oil) and *cyanine* (blue)] nomenclature was first used by Linstead in 1933 to describe a new class of organic compounds. Phthalocyanine (Pc) molecules are macro-cyclic compounds extensively studied now due to their potential applications as pigments and dyes and also model systems for important biological system/processes due to their similar functions as porphyrins, hemoglobin and chlorophyll. Pc molecules have also been found to be potential candidates for application in organic solar cells or organic light emitting devices (OLED) and also used as the active elements in chemical sensors (gas sensors) [1]. These molecules have been successfully used in homogeneous and heterogeneous catalysis during a long period for oxidation reactions. Pc's are also used in many different applications such as dye pigments in textiles, p-type organic semiconductors, gas sensors, cancer therapy, organic, light-emitting devices and magnetic switches [2]. The chemical and electronic properties of Pc's may be tuned through variation in the metal center, or through organic functionalization of the macrocycle. Pc's are versatile because they offer enormous structural flexibility with the capacity of hosting 70 different elements in the central cavity. The structure of Pc has been significantly scrutinized for improved chemical and physical properties and it is the elegant modification of Pc structure that has been demonstrated to effectively improve its photochemical and photo-physical properties. Because of diverse redox chemistry, and high thermal/chemical stability, various applications such as semiconductors, electro-chromic displays, chemical sensors, sensitizers in solar cells, photodynamic therapy, and optical properties have motivated the researchers to synthesize various types of Pc's. Due to their planar π-conjugated system they are well suited for third-order nonlinear optical (NLO) response and possess exceptional stability against photo-irradiation. The NLO properties of Pc's and MPc's can be improved by changing the central metal atom, peripheral/axial substitution, and/or its aggregation state. The large optical nonlinearities of Pc's due to delocalized π electrons are envisaged in applications such as optical processing devices, practical optical limiters and all optical switches [3-10]. Various research groups, including our group, have studied in detail the NLO response of a number of Pc's with different central metals and peripheral substitutions [11-26]. The luminescence properties of Pc's are of interest because of their structural similarities to the porphyrins as will be

demonstrated in the data presented in chapter 6. The UV–visible absorption spectra of Pc's demonstrate a Soret band of 360 nm and a Q band at 684 nm without substitution at peripheral positions [27]. Pc's are excellent singlet oxygen generators with a high value of quantum yield of singlet oxygen production of 0.59–0.80 [28] as well as a fluorescence quantum yield production higher than that of porphyrins [29]. Therefore, one has to come up the design of Pc's which render enhanced solubility and anticipated superior properties. The solubility of Pc's in non-polar solvents can be improved by introducing different kinds of bulky groups like alkyl, alkoxy, alkylthio and crown ether groups on the Pc framework [30-32]. To fully explore the photosensitizing qualities of ZnPc, a detailed description of the intramolecular processes, occurring on time scales ranging from femtoseconds to microseconds, is required. Several experimental studies on the photo-physics of ZnPc and similar compounds (derivatives or different MPc's) in solution have been reported [33,34] but so far the results fail to depict a coherent picture of the overall photo-physics. Furthermore, new molecules with high two-photon absorption (2PA) and three-photon absorption (3PA) coefficients and cross-sections are interesting for their potential applications in photonics, biomedical, and lithorgraphic applications [35]. Thiol substituted MPc's show rich spectroscopic and photochemical properties as they absorb at longer wavelengths (>700 nm) than other MPc's [36-39].

The wide range of Pc applications are primarily because of their high molar absorption coefficient ($\varepsilon > 10^5$) in the far end of the visible spectrum, high triplet state quantum yields, long lifetimes, exceptionally high thermal and chemical stability, and rational synthetic routes towards preparation of these compounds [40]. The optical properties of Pc's, of great scientific interest, depend on the solubility as well as aggregation of the macrocycle [41,42]. Owing to the extended π-systems, these complexes show high aggregation tendency in both solution and solid state, less solubility in common organic solvents thus influencing their spectroscopic and photo-physical properties and thereby limiting the application potential [43]. Therefore, many efforts have been directed into designing non-aggregated Pc's in order to control their properties. Essentially, aggregation is due to the co-facial association of the highly planar Pc units even at μM concentration which leads to the low efficiency for device applications [44]. Consequently, if one could get rid of the planarity either by axial ligation of the Pc molecule or use of bulky substituents and π-substitution of the

Pc-molecule, aggregation can be reduced. The most effective way to reduce aggregation is by creating steric crowding over the Pc's macrocycle by use of bulky substituent [45-48]. Based on thermal, photochemical stability, and electrochemical properties Pc's were found to be alternative sensitizers for dye-sensitized solar cell applications [49]. However, because of planarity of the Pc, macrocycle tends to aggregate at μM concentration and results in low efficiency of the device. Recently, we have successfully introduced bulky substituents at peripheral positions of Pc macrocycle and designed several efficient sensitizers for dye-sensitized solar cell applications [50-52]. This approach gave highly soluble and non-aggregated Pc derivatives in dilute solution as well as in the solid state. Pc's are proper choice for effectively harvesting red light due to their strong Q band light absorption properties near 700 nm. Thus, Pc-sensitized solar cells for use as photovoltaic window transmit part of the visible light and harvest in the red/near-IR part of the spectrum [53]. MPc's are characterized by intense B and Q-bands centered near 350 and 670 nm, respectively. Strong absorbance in the far red region of the UV/visible spectrum was thus retained upon introduction of the fluorous peripheral substituent [54]. Recently, we have successfully introduced bulky substituents at peripheral positions of phthalocyanine macrocycle by adopting '*push-pull*' concept and designed several efficient sensitizers for dye-sensitized solar cell applications. These phthalocyanines are having bulky either alkyl or alkoxy groups, which acts as electron releasing ('*push*'), and it also having carboxyl groups which acts as electron withdrawing ('*pull*'). This approach gave highly soluble and non-aggregated Pc derivatives in dilute solution as well as in the solid state. Phthalocyanines are proper choice for effectively harvesting red light due to their strong Q band light absorption properties near 700 nm.

In order to achieve aforementioned properties, one has to design Pc's such that the macrocycle is soluble in all common organic solvents, display minimum aggregation (at μM concentration) and also further shift the absorption of Q bands towards the red region of the absorption spectrum. Herein, we have designed and prepared two sterically hindered Zn-Pc's by introducing 3,4-dimethoxy (Pc-1) and 2,6-dimethoxy (Pc-2) phenyl groups at the peripheral positions of Pc-molecule. By introducing these bulky substituents at peripheral positions of Pc macrocycle, one can expect to improve the solublity but also minimizes its aggregation. Thiol substituted

metallophthalocyanines show rich spectroscopic and photochemical properties as they absorb at longer wavelengths (>700 nm) than other metallophthalocyanines.The further red-shift in Q band absorption Pc can be achieved by introducing thiol substituted groups at non-peripheral positions of macrocycle. In the present chapter, we have also designed Pc molecule having eight *tert*-butylphenyl thio substituents at the non-peripheral positions. The detailed photophysical and photochemical studies along with their ultrafast NLO responses have been studied for both arylalkoxy and *tert*-butylphenyl thio substituted zinc phthalocyanines (Pc-3).

5.2 Structures of Pc-1, Pc-2 and Pc-3

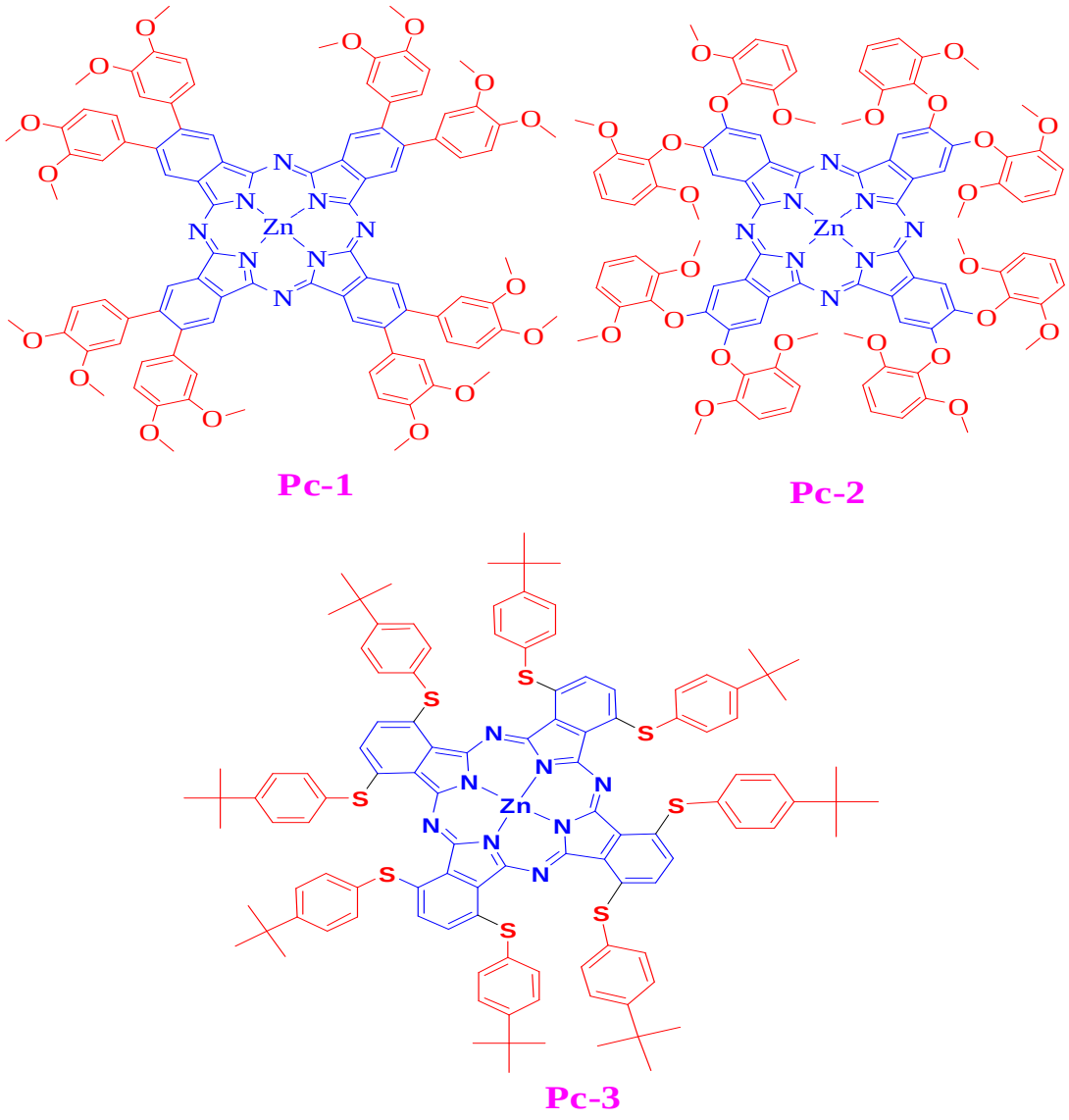

Figure 1 Structure of Sterically hindered Zn-Pc (Pc-1, Pc-2) and Thio-ZnPc (Pc-3) used for the study.

The structures of sterically hindered Zn-Pc's (Pc-1, Pc-2) and Thio-Zn-Pc (Pc-3) are illustrated in figure 1. Pc's are 18 electron hetrocyclic aromatic systems derived from porphyrins. The more systematic name is therefore, tetra-aza-tetra-benzo-porphyrins. These comprise of four isoindole unit at four identical corners, linked together through their 1,3-position by aza bridges. The IUPAC names of Pc-1 and Pc-2 are 2,3,9,10,16,17,23,24-octakis (3,4-dimethoxyphenyl) Zn(II)Pc and 2,3,9,10,16,17,23,24-octakis (2,6-dimethoxyphenyl) Zn(II)Pc, respectively. The IUPAC name of Thio-Zn-Pc is 1,4,8,11,15,18,22,25-octakis (4-*tert*-butylthiophenyl) Zn(II)Pc and is termed as Pc-3 throughout this chapter. The molecule is able to coordinate hydrogen and metal cations in its center by coordinate bonds with the four iso indole nitrogen atoms. The central atoms can carry additional ligands. 3,4 dimethooxy (Pc-1) and 2,6 dimethoxy (Pc-2) phenyl groups at the peripheral position of Pc-molecule. Most of the elements have been found to be able to coordinate to the Pc's macrocycles. Therefore, a variety of Pc's complexes exist. A disadvantage of Pc's is the extreme insolubility of the parent compound. In order to increase the solubility in common organic solvents, a number of functional groups have been added to the Pc's core at the benzene rings on the periphery of these micro cycles. The physical, chemical and electronic properties of Pc's may also be improved by the addition of appropriate substituent's and functional group to the molecule such as alkyl chains, higher order aromatics, ethers, amines, thiols or halides.

5.3 UV-Vis Absorption spectra of Pc-1, Pc-2, Pc-3

The electronic absorption spectra of Pc-1 and Pc-2 revealed characteristic features of the Pc. They show a low intense Soret band (B band) in the range of 300–400 nm and a relatively intense Q band in the range of 600–800 nm (figures 2a and 2b). Considerable intensity of this band has been a result of π-π^* transitions from the macrocyclic system. UV-visible absorption spectroscopy is a very valuable technique which can be used to study the aggregation phenomena of Pc's in both solution and solid state. The extent and the nature of the molecular packing can also be deduced from the interpretation of UV-visible absorption spectrum (Q band). The insolubility of Pc's in most organic solvents is due to the planarity structure and leads to aggregate by forming π-π stacking. As frequently encountered in most of Pc's, the shoulder on the high energy side of the Q band indicates the presence of aggregated species.

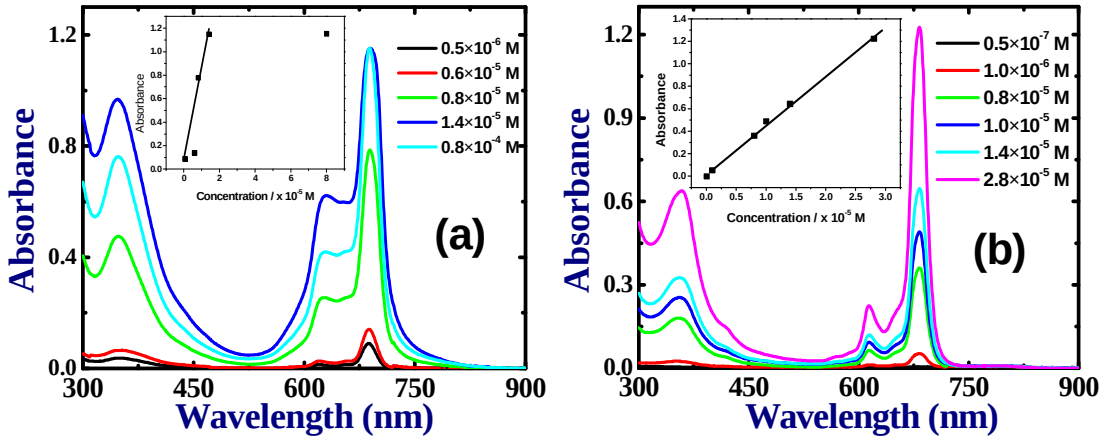

Figure 2 Absorption spectra of **(a) Pc-1 (b) Pc-2** in CH_2Cl_2 at different concentrations.

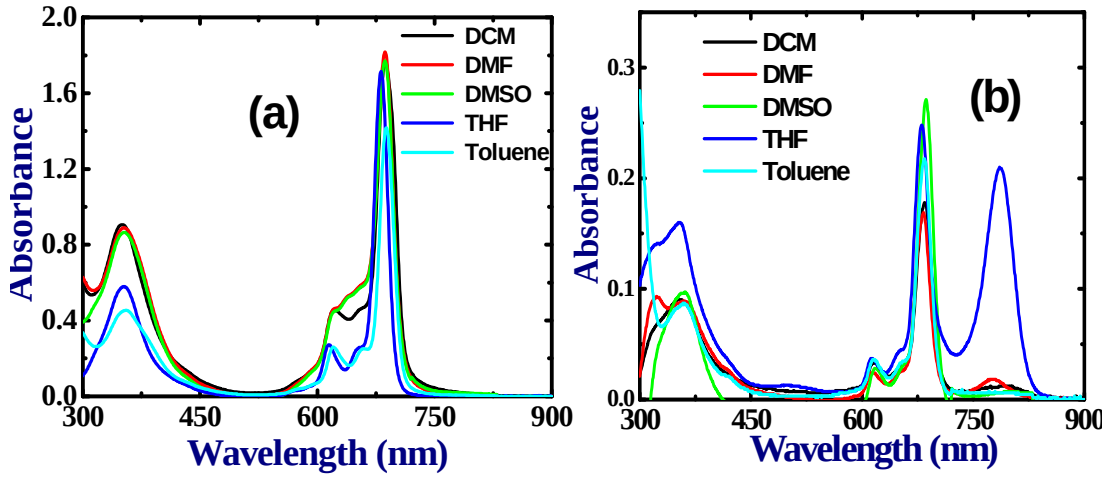

Figure 3 Absorption spectra of **(a)** Pc-1 and **(b)** Pc-2 in various solvents (DCM, DMF, DMSO, THF, and Toluene).

The solubility and aggregation problem can be overwhelmed by introducing bulky aryloxy groups at peripheral positions of both Pc's. As anticipated, both Pc's have shown no evidence of aggregation in solution as demonstrated by the sharp unperturbed single Q band, typical of metallated Pc complexes with D_{4h} symmetry. For example, as shown in figure 3b, the absorption spectrum of Pc-2 showed a single sharp Q band at 686 nm in dichloromethane solvent, which is a typical non-aggregated species as evaluated from its position and shape. The concentration dependence of absorption spectra of these derivatives was further assessed in order to prove the absence of aggregation. It has been found that both the complexes exhibited a monomeric form (i.e., no new blue-shifted band due to aggregation) as deduced from the recorded absorption spectra in different concentrations. Its apparent molar extinction coefficient remains almost constant indicating a pure monomeric form,

which obeys the Beer–Lambert Law in the outlined range of concentration. Similar non-aggregated properties were also observed in the case of Pc-1 (figure 3a). The introduction of bulky aryloxy groups at the peripheral positions of Pc cannot cause any significant shift of the Q band absorption maxima. Figures 3a and 3b illustrate the absorption studies of both Pc-1and Pc-2 in various solvents (DCM, DMF, DMSO, THF, and Toluene). From the data presented in figure 3 it is evident that as the solvent polarity increased, the shape and absorption maxima of both B band and Q band did not change. Similar absorption behavior was also observed in Pc-2, except in THF and DMSO solvents. In both THF and DMF solvents, Q band was split into two bands at 684 nm and 775 nm, respectively. The split in Q band is probably due to the axial coordination of the Zn(II) ion by solvent molecules [55]. Typical Pc complex is known to exhibit two strong absorption bands arising from their orbital interactions and symmetry, one of them in the UV region at around 300-400 nm arising from deeper π-levels to LUMO transition and the other in the visible part around 700 nm attributed to HOMO to LUMO transition (π-π*) of the Pc-2 ring. These intense band systems can be shifted or broadened depending on peripheral substitution, metallation and aggregation of the molecules.

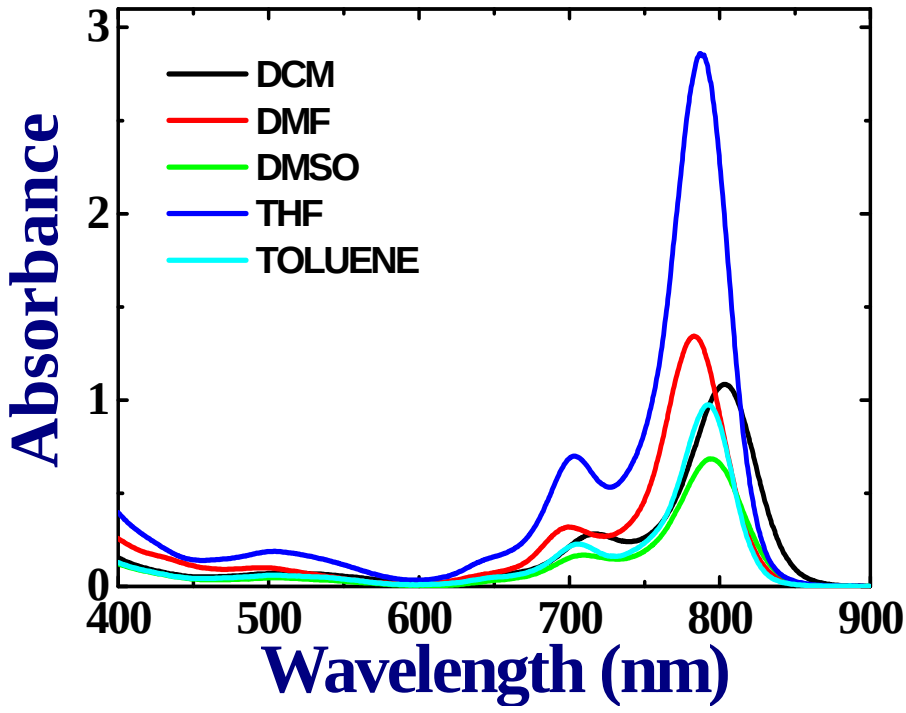

Figure 4 Absorption spectrum of Pc-3 in different solvents.

Substitution with strongly electron donating or electron withdrawing groups potentially provides a method of tuning the Q-band absorption. The UV-Vis spectrum of the Pc-3 complex in various solvents, including DCM, is shown in figure 4. Pc-3 exhibited a Q band near 796 nm and a B band near 354 nm in DCM. A new absorption peak was observed at 510 nm, a similar band appeared in thio substituted Pc's reported in literature [56]. The spectra depicted monomeric behavior evidenced by a single narrow Q band, typical of metallated Pc's [57]. The Q band was considerably shifted to near IR region attributed mainly to the substitution of Pc ring at eight α-positions with arylthio substituents.

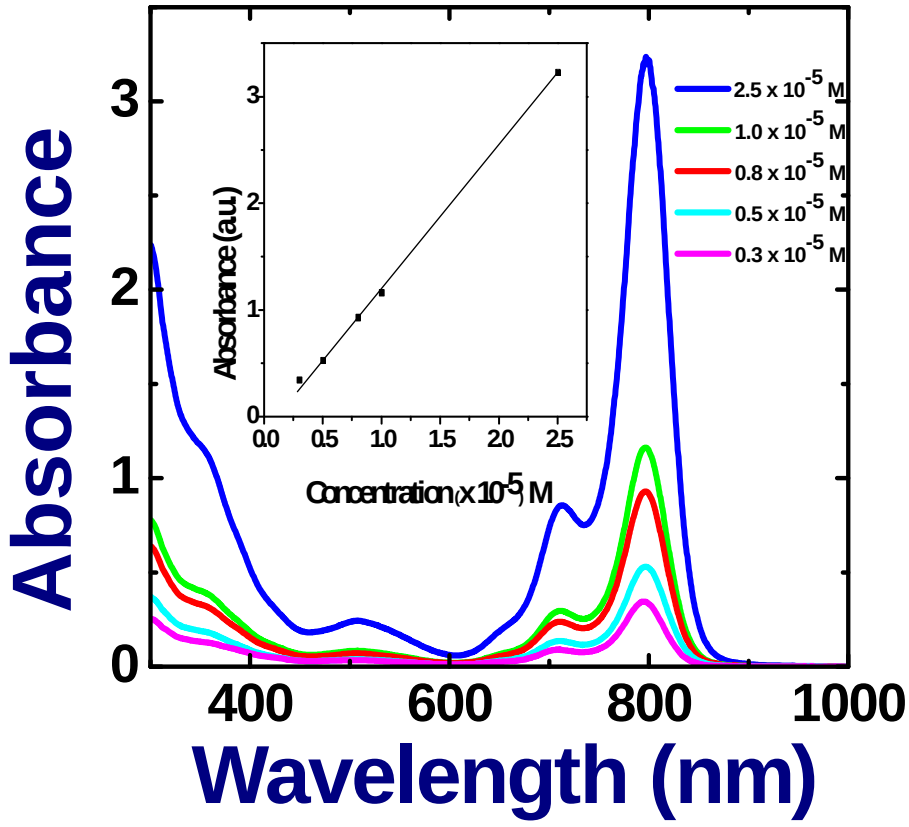

Figure 5 Absorption spectral changes of **Pc-3** in DCM at different concentrations:(a) 0.3×10^{-5} (b) 0.5×10^{-5} (c) 0.8×10^{-5} (d) 1.0×10^{-5} (e) 2.5×10^{-5} M. Inset shows the plot of absorbance versus concentration.

The presence of sulphur atoms further helps to red shift the absorption. The observed red spectral shift is typical of Pc's with substituents at the non-peripheral positions [58,59] and has been explained to be due to linear combinations of atomic orbitals (LCAO) coefficients at the non-peripheral positions of the HOMO being greater than those at the peripheral positions. As a result, the HOMO level is

destabilized more at the non-peripheral position than it is at the peripheral position. Resultantly, the energy gap between the HOMO and the LUMO becomes smaller, consequently in a bathochromic shift. Aggregates are undesirable not only for analytical purposes, for their absorbance spectra overlaps with that of the monomer, but also for practical device applications. The aggregation depends on concentration, solvent, substituents, complexed metal ions and temperature [60]. For many non-bulky or electron rich benzo substituted complexes, aggregation occurs readily, even at low concentrations, typically, used to record absorption spectra, making the spectral data more difficult to interpret. In dilute solutions Pcs exist as single molecule and are surrounded by solvent molecules but with increasing concentration Pc molecules aggregate. In the aggregated state electronic structure of complex Pc rings are perturbed thereby altering the ground and excited state electronic structures [61]. Keeping this in mind, we have carried out the aggregation studies of Pc-3 at different concentrations in DCM and the data is shown in figure 5. The complex clearly followed Beer-Lambert's law (figure 5 inset) for the monomeric species present in the solution since no aggregation tendency was observed evident from linear change of absorbance in the Q band maxima.

5.4 Pump-probe studies of Pc-1,Pc-2 and Pc-3

The complete experimental details of fs pump probe experiments have been explained in sections 2.12 (figure 17). Figure 6 shows the degenerate pump-probe data of Pc-1 and Pc-2 (in DCM) obtained near a wavelength of 600 nm using ~70 fs pulses with typical pump energies of 10 μJ. Positive $\Delta T/T$ in the pump-probe data indicted photo-bleaching prevailed. The experimental data was fitted with a double exponential function and two lifetimes (τ_1 and τ_2) were retrieved from each of the fits. The values of τ_1 and τ_2 were ~3 ps and ~40 ps for Pc-1 whereas the values were ~2 ps and ~500 ps for Pc-2. Qualitative evaluation of emission, including quantitative analysis of the fluorescence spectra and determination of the quantum yields (ϕ) was performed for Pc-1 and Pc-2. The emission spectra of both phthalocyanines were collected by exciting both phthalocyanines at 680 nm as observed in figure 7. The steady state fluorescence spectra of both the complexes are almost similar except the different emission maxima.

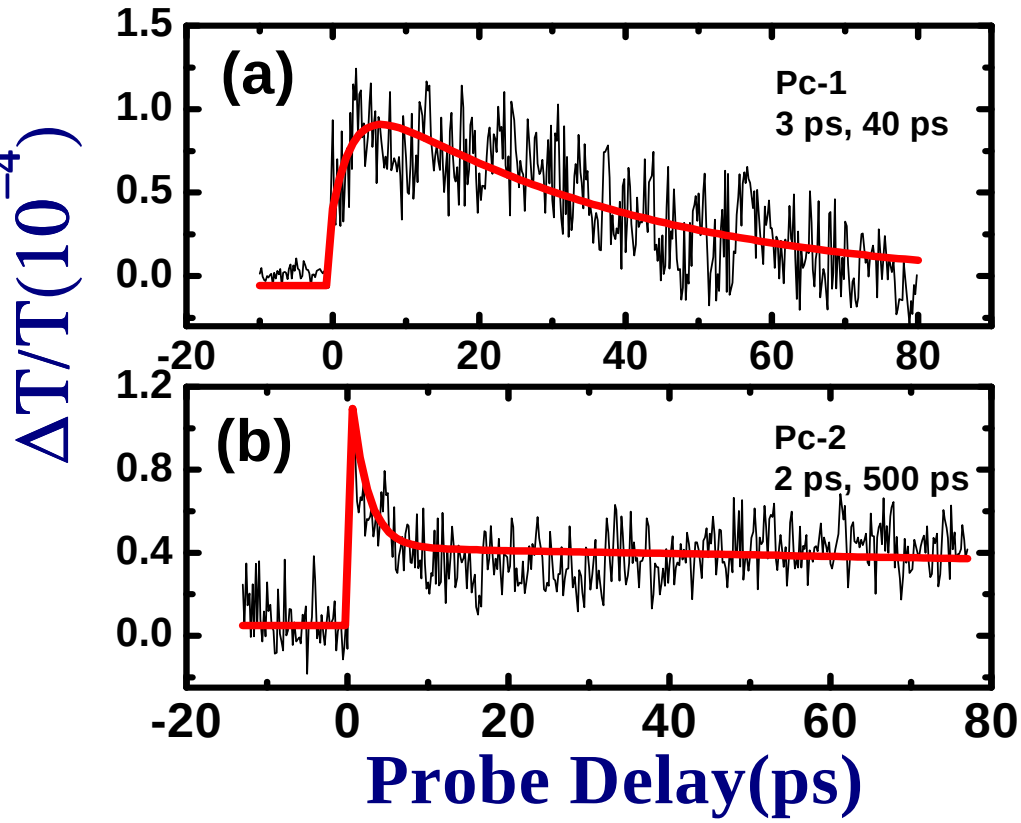

Figure 6 Degenerate pump-probe data of **(a) Pc-1 and (b) Pc-2** obtained with ~70 fs pulses near 600 nm. Red solid lines are theoretical fits using the equations as explained in Chapter 2.

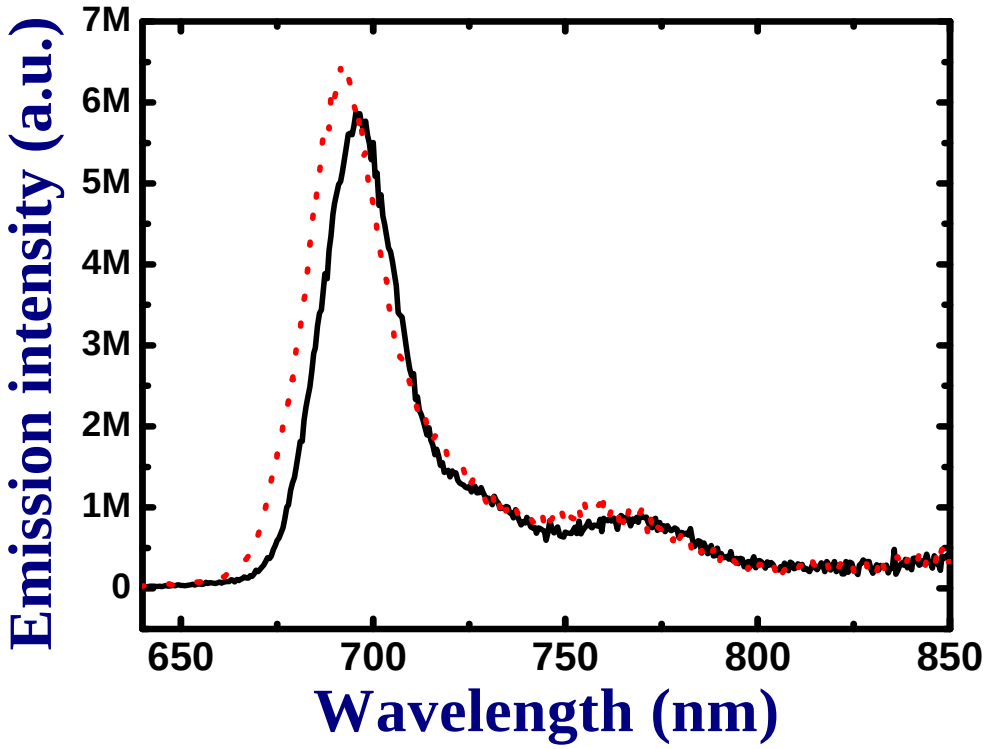

Figure 7 Emission spectrum of **Pc-1** (—) & **Pc-2** (----) in DCM at λ_{exc} = 680 nm.

Figure 8 presents the fluorescence decay data of Pc-1 and Pc-2 in DCM. Figures 9 and 10 present the fluorescence decay data of Pc-1 and Pc-2 in various solvents. It is evident from the data presented in figures 8-10 that the emission spectra of Pc-1 and Pc-2 were consistent with both the Stokes rule and the rule of mirror symmetry between the absorption and fluorescence bands. The emission properties of Pc-1 and Pc-2 in DMSO were evaluated by comparison with those of ZnPc possessing no peripheral substituents. For ZnPc the Stokes shift was small ($\Delta\lambda$ = 7 nm) which confirmed that the geometry of molecule in the singlet excited state S_1 does not differ much from that in the ground state. The Stokes shift in the emission spectra of phthalocyanines possessing peripheral substituents was somewhat greater. Fluorescence quantum yields (ϕ_f) were determined by the comparative method according to

$$\emptyset_{Sample} = \frac{F_{sample} \times Abs._{standard}}{F_{stanadard} \times Abs._{sample}} \times \emptyset_{f,standard}$$

where $\emptyset_{Sample}$ is the fluorescence quantum yield of sample; $\emptyset_{f,standard}$ is fluorescence quantum yield of the standard; F_{sample} is fluorescence intensity of the sample; $F_{Standard}$ is fluorescence intensity of the standard; $Abs._{sample}$ is absorbance of the sample at the excitation wavelength; and $Abs._{standard}$ is the absorbance of the standard at the excitation wavelength. The emission spectra of both Pc-1 and Pc-2 were measured in different solvents and corresponding quantum yield data is presented in table 1. From table 1 data it is apparent that as the polarity of the solvent increased, the emission maxima slightly blue shifted by 3-5 nm and quantum yield was reduced in both the phthalocyanines. This might be due to increase of aggregation in polar solvents, which reduces the possibility of radiative deactivation *i.e.*, fluorescence through dissipation of energy by the aggregates. The quantum yields were greatly reduced in un-substituted phthalocyanines. This in turn effect on the singlet excited life time. As in steady state emission, lifetimes were also affected with polarity of the solvents used.

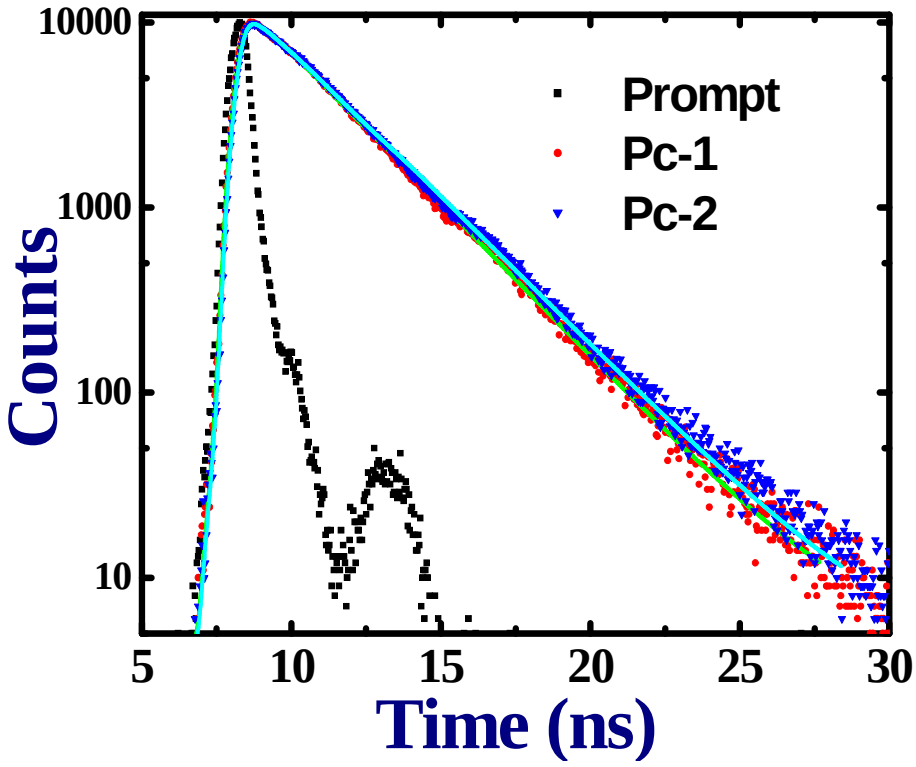

Figure 8 Fluorescence decay signals of **Pc-1** & **Pc-2** in DCM. The detection wavelength was at 690 nm. Solid lines are fits to the experimental data

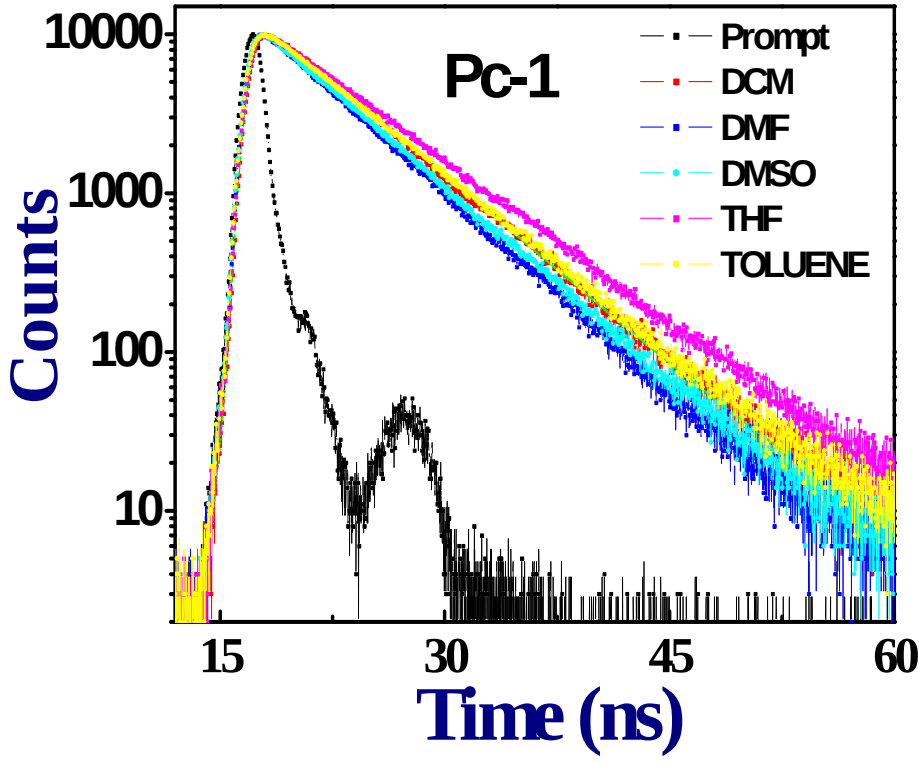

Figure 9 Lifetime spectra of **Pc1** in different solvents

Sample	Solvent	λ_{max}, nm (log ε) $M^{-1}cm^{-1}$	$\lambda_{em.\ max.}$ nm	ϕ_f	τ_f (ns)
Pc-1	Toluene	688 (4.85)	696	0.32	2.73
	DCM	690 (4.76)[a]	696	0.31	2.60
	THF	682 (4.64)	691	0.29	2.97
	DMF	686 (4.61)	695	0.28	2.40
	DMSO	688 (4.59)	698	0.26	2.50
Pc-2	Toluene	685 (4.84)	693	0.27	2.81
	DCM	684 (4.56)[b]	691	0.26	2.70
	THF	680 (4.37)	689	0.25	3.18
	DMF	682 (4.19)	691	0.24	2.60
	DMSO	685 (4.14)	693	0.22	2.91

Table 1 Summary of absorption, emission data of **Pc-1** and **Pc-2** in different solvents.

a log ε value is recorded for DCM only
b log ε value is recorded for DCM only

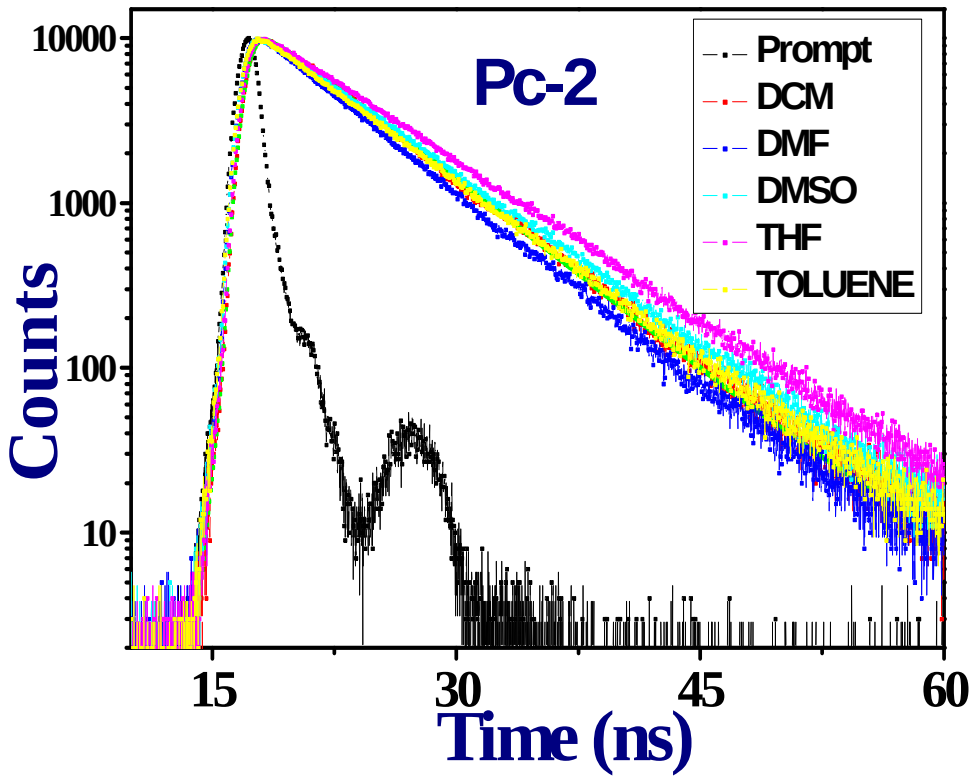

Figure 10 Lifetime spectra of **Pc-2** in different solvents.

Figure 11 depicts the fs degenerate pump-probe data of Pc-3 recorded near the wavelength of 600 nm. It is evident from the data presented that ΔT/T was negative suggesting the presence of photo-induced absorption with a single exponential decay. The lifetime recovered from the fit to experimental data was a long one of ~309 ps. Pc-3 is a radiative molecule with lifetimes of ~few ns as seen from the data presented in figure 12 and rediative lifetimes are summarized in table 2. Therefore, the ~309 ps lifetime observed cannot be from the radiative transitions. Excitation with 600 nm pump photon could have excited the molecule to first excited singlet state due to small linear absorption at that wavelength. With strong pump inentisites (>100 GW/cm^2) two-photon absorption (2PA) is possible where as the data is presented depicting 2PA in this molecule at 600 nm with stronger pumping and SA at weaker pumping). In the present case of pump-probe measurements the peak intensity of pump was much lower than 100 GW/cm^2. Once excited into high lying states the molecules can come down to ground state via radiative and/or non-radiative mechanisms. The ~309 ps lifetime could be attributed to the non-radiaitve lifetime of S_1 states with possible contribution from inter-system crossing and/or radiative part. However, further detailed transient absorption studies are necessary to identify the exact contributions to this lifetime.

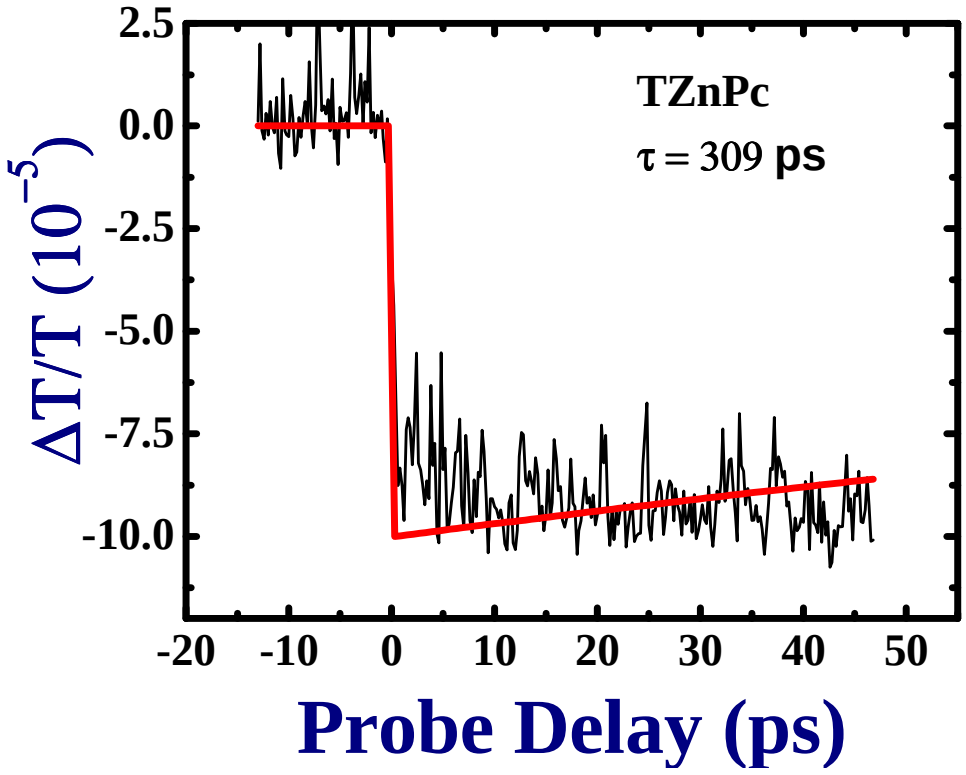

Figure 11 Degenerate pump-probe data of **Pc-3** recorded with ~70 fs pulses at 600 nm. The fit (solid, red line) depcits a single exponential decay of ~309 ps.

Jarota et al. [62] have also investigated tetrasulfonated Pc's (again similar molecules to ours) and observed lifetimes in the 150-500 ps range. They have assigned it to the S_1 to S_0 non-radiative decay mechanism. Howe et al. [63] investigated Pc and zinc Pc tetrasulfonate using ultrafast pump-probe spectroscopy slow life time of ~370 ps for the free base (PcS_4) and ~460 ps for the Zn substituted compound ($ZnPcS_4$). We had observed S_1 state lifetimes of <200 ps in similar organic molecules in some our earlier studies on porphycenes, corroles [64] and naphthobipyrroles. Furthermore, in a few of our earlier works on Pc's [65] and porphyrins [66,67] we did observe sub-100 ps lifetimes (assigned to the S_1 state non-radiative decay) achived using incoherent laser spectroscopy. Fita et al. [68] observed <50 ps lifetimes for ester-alkyloxy substituted zinc Pcs. They also osberved ~ns lifetimes and assigned them due to the combination of inter-system crossing, radiative and non-radiative mechanisms. In our case the radiative lifetimes were >2 ns as seen in figure 12 and, therefore, can safely assume miminal conrtibution from this.

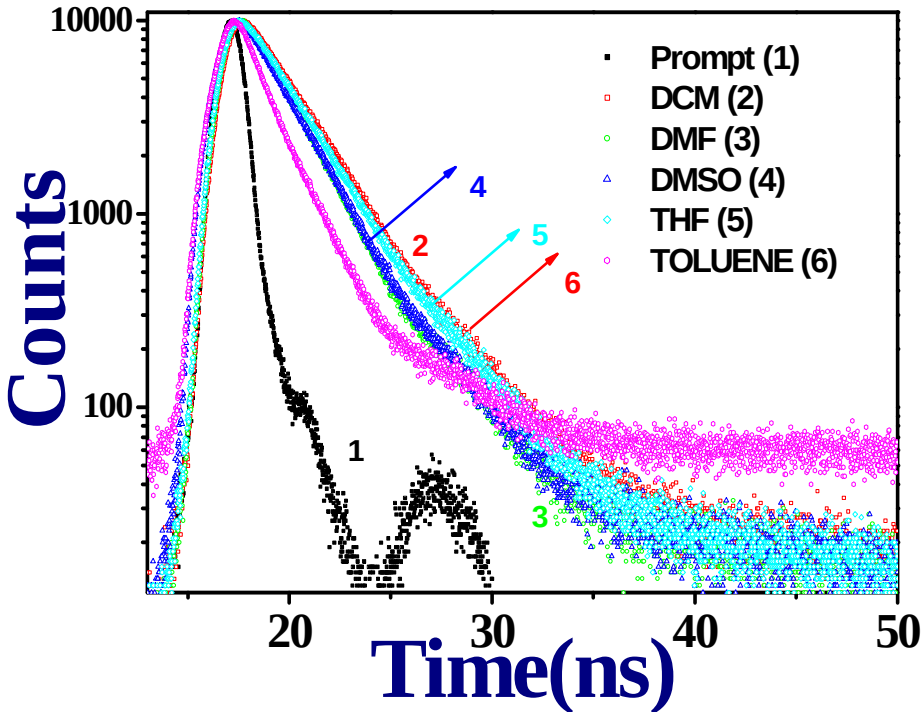

Figure 12 Fluorescence decay signals of **Pc-3** in different solvents.

Sample	Solvent	λ_{max}, nm (log ε) $M^{-1}cm^{-1}$	$\lambda_{em,\ max}$, nm	ϕ_f	τ_f (ns)
Zn-Thio-Pc (Pc-3)	DCM	803 (5.04)	823	0.020	1.23
	DMF	782 (5.13)	813	0.022	1.25
	DMSO	793 (4.84)	822	0.020	1.22
	THF	787 (5.45)	809	0.022	1.26
	Toluene	792 (4.99)	812	0.024	1.25

Table 2 Summary of absorption, emission data of **Pc-3**

5.5 NLO studies of Pc-1,Pc-2 and Pc-3

There have been reported several novel Pc-based sensitizers, including efforts from our group, and explored their interesting nonlinear optical (NLO) properties [69-76]. Several modifications such as substituents on the central metal core, peripheral attachments, incorporation into graphene, doping with polymer, preparing nanoparticles etc. [77-87] were embarked upon with the intention of understanding the structure-property relationship towards tailoring their NLO properties. However, the significant aspects missing amongst these studies are (a) spectral dependence (dispersion studies) of the optical nonlinearity (b) time resolution of the optical nonlinearity (c) pulse width dependent studies. Nonlinear optical absorption (NLA) studies with nanosecond (ns) pulses (in solution and doped in polymers/glasses) will

assist identification materials for optical limiting applications. For such applications time-response of the nonlinearity is not important. NLA studies with ps/fs pulses will help finding suitable saturable absorbers for mode-locking applications in ultrafast lasers. Nonlinear refractive index studies with ps/fs pulses will provide information of material properties useful for signal processing, all-optical switching applications. Desired characteristics for applications include small linear absorption, low nonlinear absorption, and strong nonlinear refractive index with sufficiently fast response (ps/fs time scales).

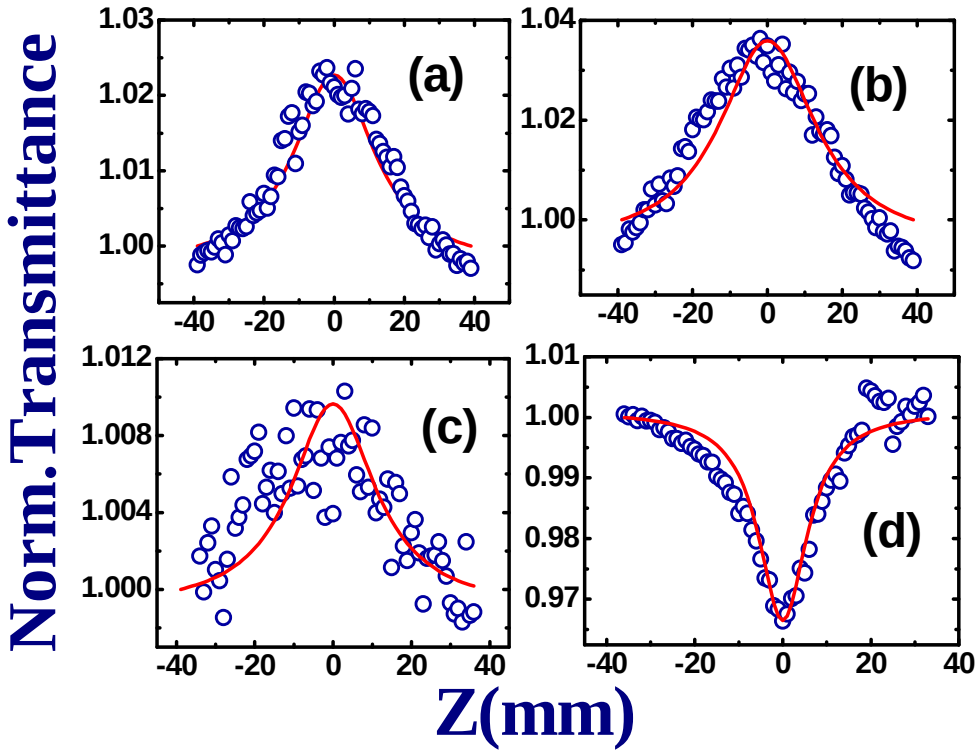

Figure 13 Ps open aperture Z-scan data of Pc-1 showing SA at **(a)** 640 nm **(b)** 680 nm and **(c)** 700 nm and RSA at **(d)** 800 nm. Pc-1 shows RSA for 800 nm. The peak intensities used were ~60 GW/cm^2. Solid lines are theoretical fits to the experimental data.

We have performed detailed studies on the optical, electrochemical, and emission properties in different solvents. Figures 13 (a-d) illustrate the open aperture data of Pc-1 obtained using ~1.5 ps pulses at wavelengths of 640 nm, 680 nm, 700 nm, and 800 nm, respectively. Typical peak intensities used were ~60 GW/cm^2. In all the figures open, blue circles represent the experimental data while the solid, red lines represent the theoretical fits. Below 700 nm we did observe strong linear absorption for Pc-1 and, therefore, nonlinear absorption mechanism was more of saturable absorption (SA) type. However, at 800 nm we do see RSA and this is due to the absence of any linear absorption and associated large peak intensities leading to an

effective 2PA (either 1+1 or instantaneous two-photon absorption). Solvent (DCM) contribution was neglected since no transmittance change was observed when the Z-scan was performed with solvent alone. Independent intensity dependent measurements confirmed the dominance of instantaneous 2PA. However, there could be minor contribution from 1+1 type of 2PA. Figures 14(a-d) depicts the closed aperture data for Pc-1 at 640 nm, 680 nm, 700 nm, and 800 nm, respectively. The solvent contribution again was minimal. The peak intensities used for closed aperture data were typically ~25 GW/cm^2. The asymmetry in figures 14a and 14c could be due to the poor spatial beam profile. Figures 15(a-d) illustrates the open aperture data of Pc-2 recorded at wavelengths of 640 nm, 680 nm, 700 nm, and 800 nm, respectively. It is evident that except at 700 nm we observed RSA for the peak intensities used and the data fitted well for 2PA. At 700 nm, though, we observed SA and this can be explained from the linear absorption spectra which indicated a strong absorption peak near 700 nm. However, harder pumping could lead to 2PA/ESA as was observed in our earlier studies [88-93].

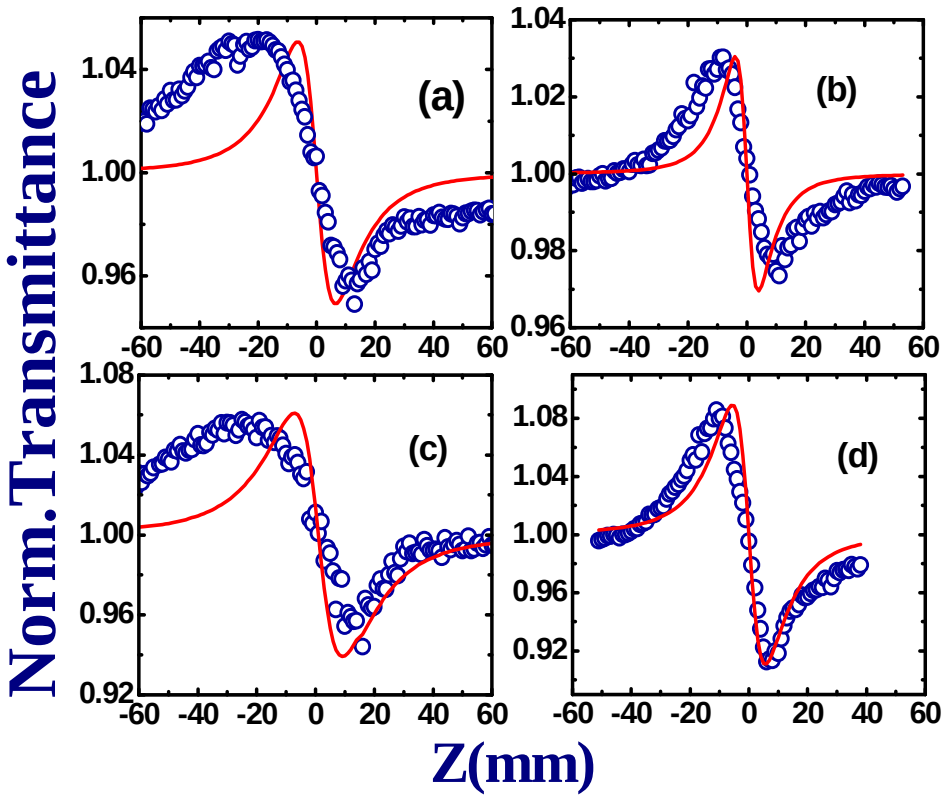

Figure 14 Ps closed aperture Z-scan data of **Pc-1** showing negative nonlinearity at **(a)** 640 nm **(b)** 680 nm **(c)** 700 nm and **(d)** 800 nm. The peak intensities used were ~25 GW/cm^2. Solid lines are theoretical fits to the experimental data.

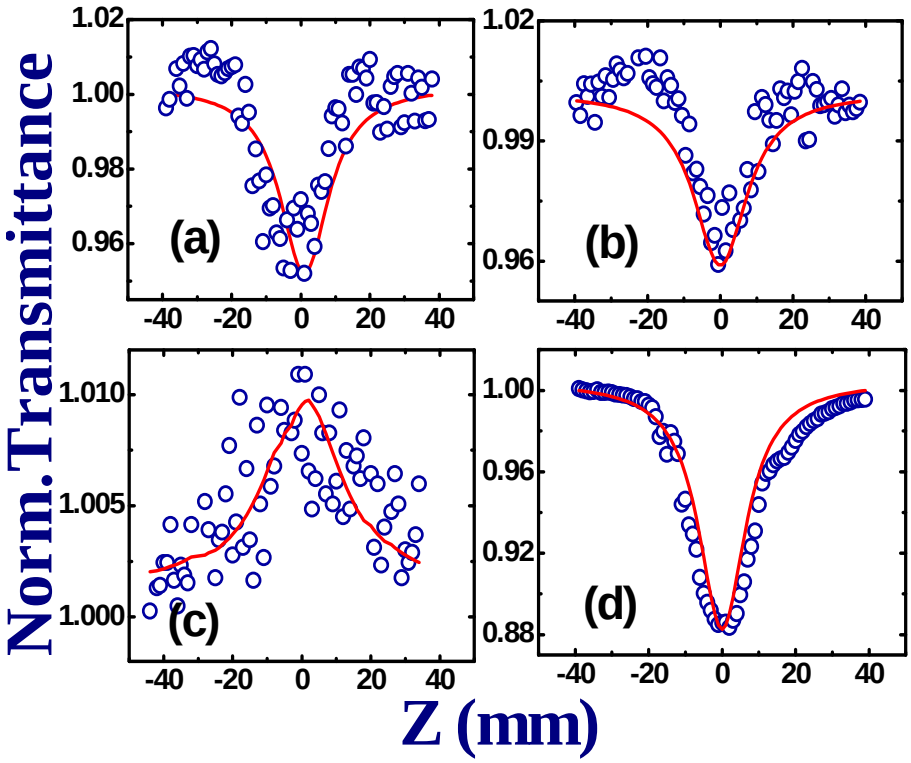

Figure 15 Ps open aperture Z-scan data of **Pc-2 (a)** 640 nm **(b)** 680 nm **(c)** 700 nm **(d)** 800 nm. At 700 nm PC-2 shows maximum linear absorption and SA. The peak intensities used were ~60 GW/cm^2. Solid lines are theoretical fits to the experimental data.

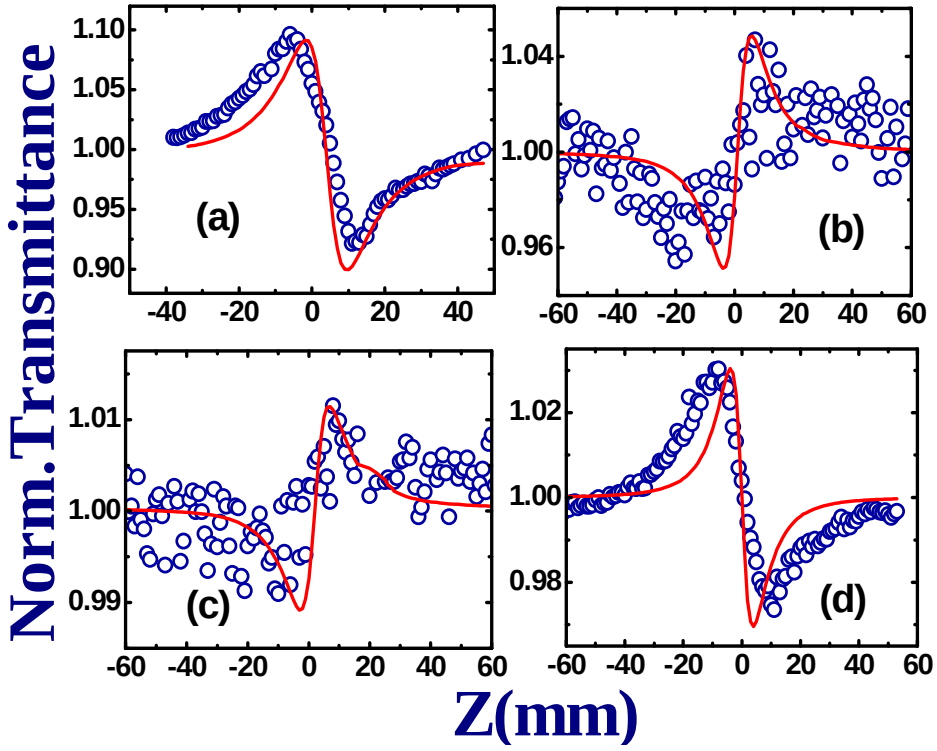

Figure 16 Ps closed aperture Z-scan data of Pc-2 **(a)** 640 nm (negative n_2) **(b)** 680 nm (positive n_2) (c) 700 nm (positive n_2) (d) 800 nm (negative n_2). The peak intensities used were ~25 GW/cm^2. Solid lines are theoretical fits to the experimental data.

Figures 16(a–d) demonstrate the closed aperture Z-scan data of Pc-2 obtained at all the four wavelengths where open aperture data was recorded. Interestingly, the sign of nonlinearity was positive at 680 and 700 nm whereas the sign was negative at 640 and 800 nm. Tables 3 and 4 summarize the NLO coefficients extracted from various fits to the data for both **Pc-1** and **Pc-2**. Figures of merit were also evaluated for these molecules and they were found to be comparable with some of the recently, successfully reported molecules [88-93].

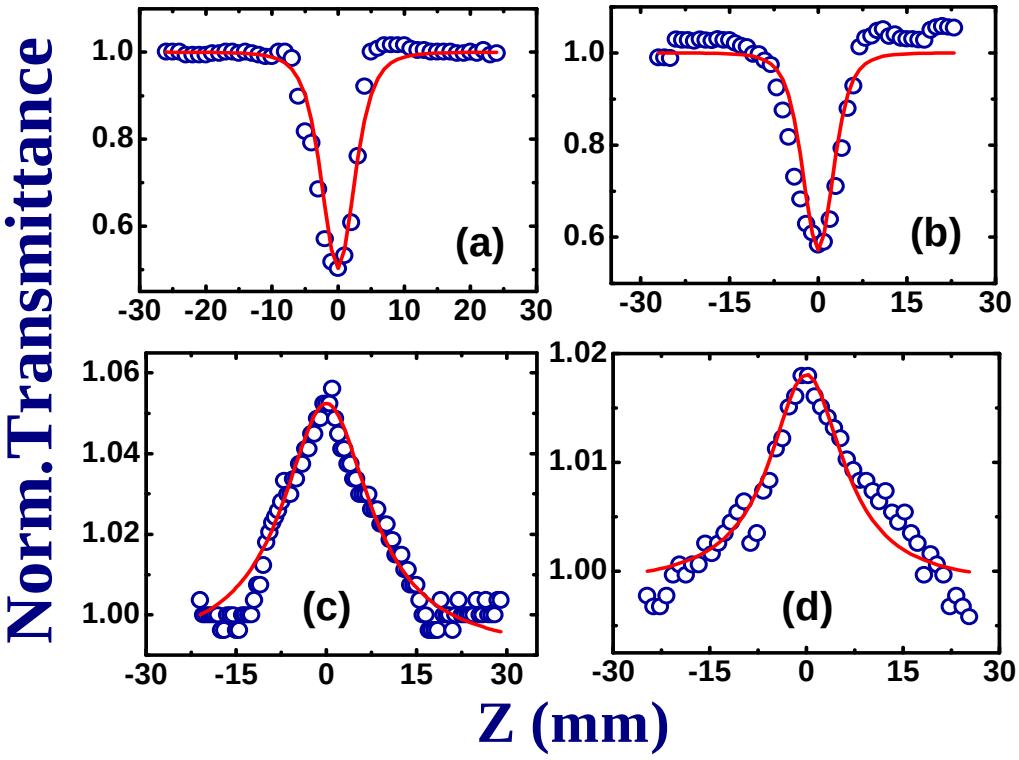

Figure 17 Fs open aperture Z-scan data shows 2PA for **Pc-1** (a) 800 nm, 80 MHz, 35 mW (b) 760 nm, 1 kHz, 30 mW. SA observed for fs open aperture data of **Pc-2** (c) 800 nm, 32 mW, 80 MHz (d) 800 nm, 12 mW and 1 kHz. Typical peak intensities used were 10^{8}-10^{9} W/cm^{2}. Solid lines are theoretical fits to the experimental data.

λ (nm)	n_2 (cm^2/W)	β (cm/W)	σ_2 (GM)	$\lvert Re[\chi^{(3)}] \rvert$ e.s.u.	$\lvert Im[(\chi^{(3)})] \rvert$ e.s.u.	Total($\chi^{(3)}$) e.s.u.	FOM (W)
640	2.1×10^{-16}	-0.2×10^{-11}	464	1.1×10^{-14}	4.7×10^{-16}	1.1×10^{-14}	0.39
680	1.5×10^{-16}	-0.4×10^{-11}	873	7.7×10^{-15}	10.0×10^{-16}	7.7×10^{-15}	0.23
700	3.3×10^{-16}	-0.2×10^{-11}	518	1.7×10^{-14}	6.3×10^{-16}	1.7×10^{-14}	0.47
800	7.1×10^{-16}	1.6×10^{-11}	3297	1.2×10^{-14}	5.2×10^{-15}	1.3×10^{-16}	0.70

Negative sign of β indicates saturable absorption (SA)

Table 3 Summary of NLO coefficients of Pc-1 recorded with ~1.5 ps pulses

λ (nm)	n_2 (cm^2/W)	β (cm/W)	σ_2 (GM)	$\lvert Re[\chi^{(3)}] \rvert$ e.s.u.	$\lvert Im[(\chi^{(3)})] \rvert$ e.s.u.	Total $\chi^{(3}$ e.s.u.	FOM (W)
640	5.4×10^{-16}	2.3×10^{-11}	5925	2.8×10^{-14}	6.0×10^{-15}	2.8×10^{-14}	1.03
680	2.4×10^{-16}	2.2×10^{-11}	5325	1.2×10^{-14}	6.0×10^{-14}	1.4×10^{-14}	0.38
700	6.0×10^{-17}	-0.05×10^{-11}	118	3.1×10^{-15}	1.4×10^{-16}	3.1×10^{-15}	0.08
800	2.4×10^{-16}	6.5×10^{-11}	13395	1.2×10^{-14}	2.1×10^{-14}	2.5×10^{-14}	0.23

Negative sign of β indicates saturable absorption (SA)

Table 4 Summary of NLO coefficients of Pc-2 recorded with ~1.5 ps pulses.

Figure 17a depicts the nonlinear absorption behavior (data fitted again with 2PA) for fs pulse excitation with ~35 mW average input power. The behavior was similar when excited with 1 kHz chopped pulses and at 760 nm, the data of which is presented in figure 17b for Pc-1. However, the behavior of Pc-2 was found to different with SA obtained at similar average powers for both 80 MHz and 1 kHz excitation and the data is presented in figure 17c and 17d, respectively. Typical peak intensities used in this case were in the range of ~10^8 W/cm^2. The observed behavior, again, can be attributed to the linear absorption. Closed aperture fs Z-scan of Pc-1 shows negative nonlinearity at 800 nm with an input power = 10 mW, 80 MHz repetition rate and n_2 = 2.05×10^{-12} cm^2/W. CA fs Z-scan of Pc-2 shows positive nonlinearity at 800 nm with an input power = 3.3 mW, 80 MHz repetition rate and n_2 = 0.51×10^{-12} cm^2/W as shown in figure 18(a-b). The n_2 value of Pc-1 is higher than Pc-2 at 800 nm. The power and concentrations were different in Pc-1 and Pc-2.

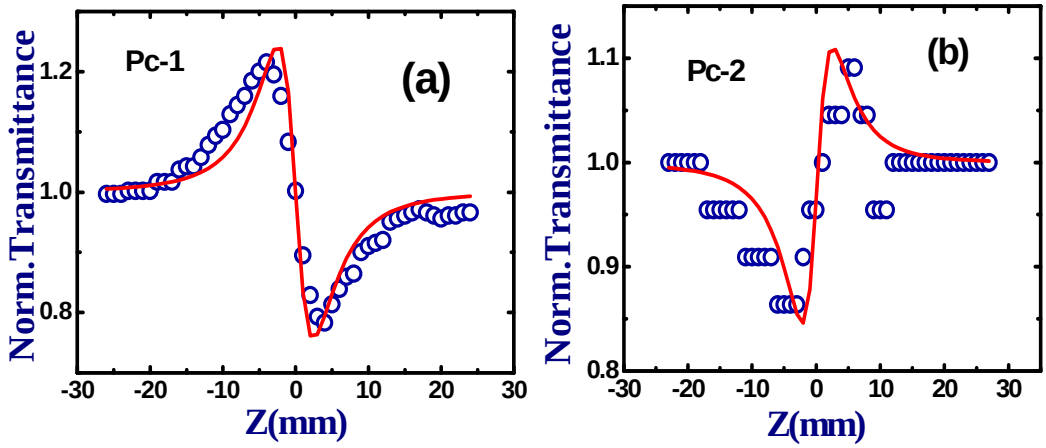

Figure 18 (a) CA Z-scan of Pc-1 (shows negative nonlinearity) at 800 nm with an input power = 10 mW, 80 MHz repetition rate. n_2 = 2.05×10^{-12} cm^2/W **(b)** CA Z-scan of Pc-2 (shows positive nonlinearity) at 800 nm with an input power = 3.3 mW, 80 MHz repetition rate. n_2 = 0.51×10^{-12} cm^2/W.

The different between fs and ps excitation is the spectral bandwidths associated with them. In fs case the bandwidth was ~ 11 nm (FWHM) whereas with ps excitation the bandwidth was ~1 nm. Therefore, with fs excitation we observed SA even at 800 nm, probably, due to the residual absorption resulting from the weak absorption peak near 800 nm (see figure 4b, for DCM). However, in the ps case due to large peak intensities (an order of magnitude higher than that used in the fs case) 2PA dominated over linear absorption.

We do expect a switchover from SA to RSA kind of behavior with stronger pumping (higher peak intensities) in the fs case. The only difference between the chemical structures of Pc-1 and Pc-2 is the peripheral groups attached [3,4-dimethoxy phenyl (Pc-1) and 2,6-dimethoxy phenyl (Pc-2) groups]. The NLO coefficients obtained were significantly different even with this slight difference. The 2PA cross-sections presented in Tables 3 and 4 clearly suggest the highest σ_2 values were obtained at 800 nm for both these molecules. Pc-2 σ_2 value was ~4 times higher than that of Pc-1 σ_2 value and this could possibly be attributed to strong linear absorption of Pc-2 at 800 nm compared to Pc-1. Furthermore, at 640 nm and 680 nm of (Pc-2) σ_2 values were at least 5-10 times stronger than those of (Pc-1) σ_2 values. We had earlier performed detailed studies on a variety of phthalocyanines using cw, ns, ps, and fs pulses. The values of n_2 obtained in Pc-1 and Pc-2 were slightly lower in magnitude to that of unsymmetrical alkoxy and alkyl substituted Zinc phthalocyanines [70]. We had investigated (a) alkoxy and alkyl phthalocyanines [12-19, 39] using cw, ns, ps, and fs pulses (b) phthalocyanine thin films [76] using ps pulses (c) phthalocyanine nanoparticles [15] using ns and fs pulses (d) symmetrical and unsymmetrical phthalocyanines [13] using ps pulses for evaluating their NLO properties. The summary of our meticulous NLO studies performed earlier on different phthalocyanines is as follows: (a) Unsymmetrical phthalocyanines had superior NLO properties compared to symmetrical counterparts. It has been established that the optical nonlinearity of a molecule increases with asymmetry if the excited states transition moments dominate (b) Alkoxy phthalocyanines had improved NLO properties compared to alkyl counterparts (c) Thin films possessed superior NLO properties compared to solutions (d) Nanoparticles demonstrated enhanced NLO properties compared to bulk solutions (e) Metal phthalocyanines NLO performance was superior to free-base phthalocyanines. These studies suggest that (i) doping these

molecules in thin polymer films (ii) creating nanoparticles out of these phthalocyanines and (c) an unsymmetrical substitution could enhance the NLO properties further.

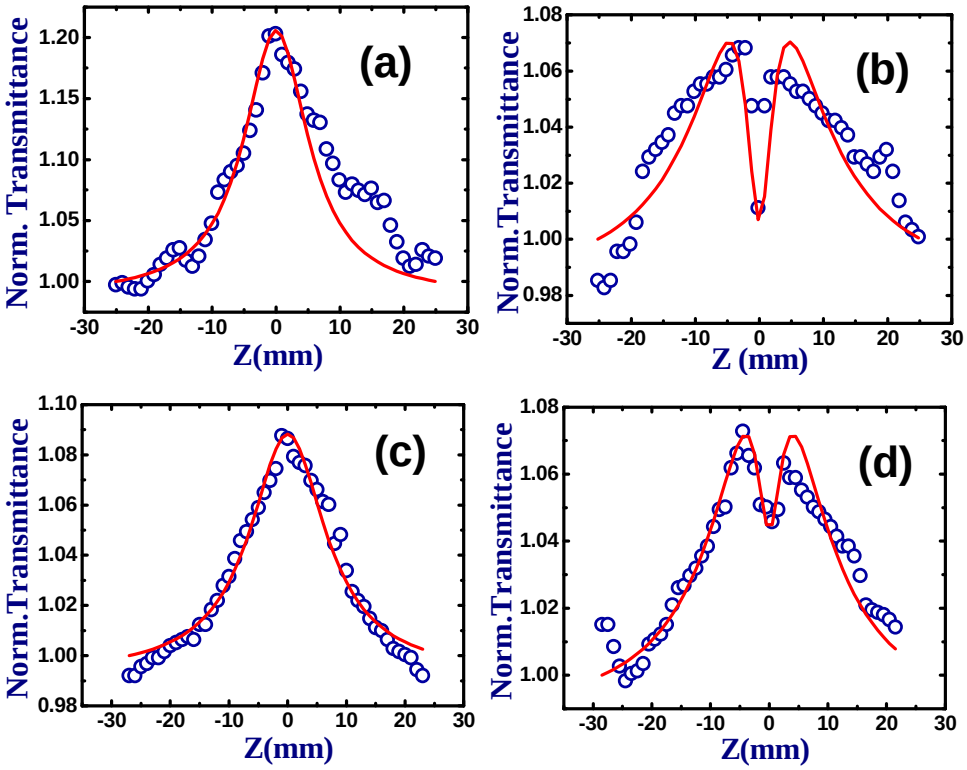

Figure 19 Fs open aperture Z-scan data of Pc-2 at 680 nm with (a) power = 9.0 mW and **(b)** power = 46 mW with **80 MHz.** Nonlinear absorption of Pc-2 680 nm with **(c)** power =10.7 mW (d) power =16.6 mW. The data **(c)** and **(d)** was acquired with a chopper at **1 kHz.**

The 2PA cross-sections presented in tables 3 and 4 clearly suggest the highest value was obtained at 800 nm for both these molecules. The above data clearly suggests that using the same molecule one could achieve SA, RSA, or RSA in SA using (a) same wavelength excitation but different pulse widths (b) same pulse width excitation but at different wavelengths. Therefore, one could easily tune the nonlinear absorption mechanism by slightly changing the peripheral substitutions of a Pc molecule. That these molecules do not aggregate even at higher concentrations combined with the strong NLO coefficients make them potential candidates for photonic applications. In the case of aggregation the energy level structure is generally modified thereby altering the optical and NLO properties and furthermore aggregation effects are not desirable for most of the device applications. Complete details of the experimental setup, equations used for fitting the experimental data (SA/2PA) for both fs 80 MHz and 1 kHz excitations can be found in chapter 2.

The higher peak intensity response of Pc-1 showed negative nonlinearity (figure 19a) same as that of solvent but with low peak intensity response of Pc-2 showed positive nonlinearity (figure 19b) opposite to that of solvent (DCM). The data was obtained using ~140 fs, 80 MHz pulses with 10 cm lens focusing. At lower peak intensities open aperture data behavior was pure SA type [figures 20(a) for 80 MHz and 20(c) for 1 kHz] but as the intensity increased it switched to RSA in SA as shown in figures 20(b) and 20(d). The peak intensities were 0.2-0.4 GW/cm^2 for both 80 MHz and 1 kHz excitation. These are **NOT** truly 1 kHz pulses as obtained in a typical ultrafast amplifier. A chopper was used (1 kHz; original repetition rate 80 MHz) indicating that we obtained bunches of pulses at repetition rate of 1 kHz. From OA, CA graphs, nonlinear absorption coefficient β and $|\chi^{(3)}|$ were calculated and summarized in tables 5 and 6.

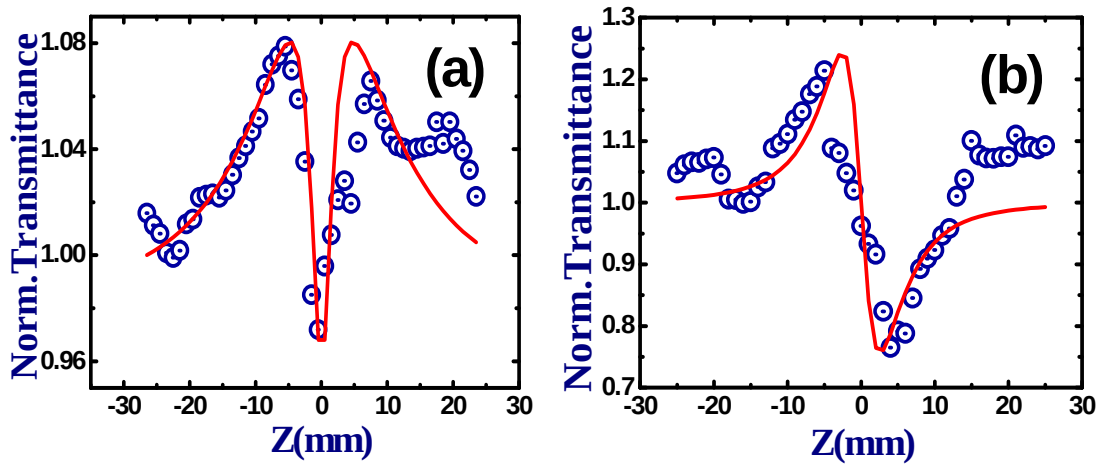

Figure 20 Fs open aperture data of Pc-2 at 850 nm with (a) power = 26.70 mW with chopper 1 kHz (b) Closed aperture behavior of Pc-1 at 850 nm with power = 5 mW at 80 MHz. Solid lines are fits while scattered data (open circles) are experimental data.

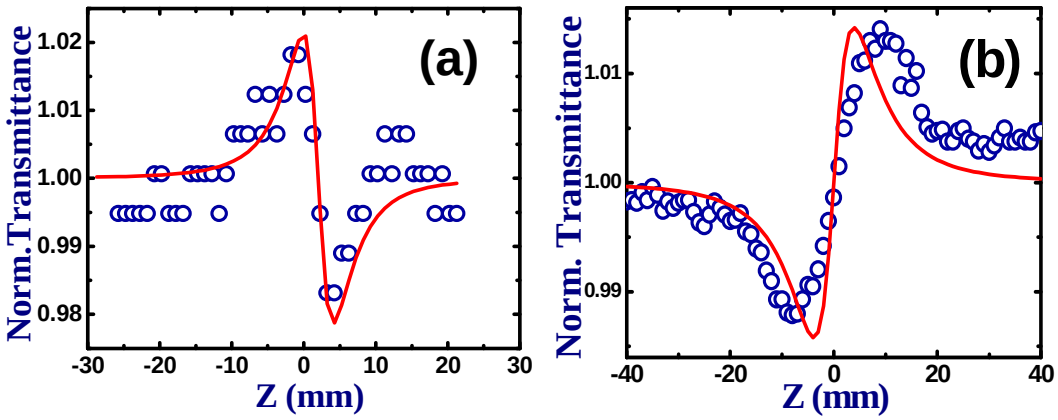

Figure 21 Closed aperture behavior of solvent DCM at 800 nm (a) fs pulses, 80 MHz (b) ps pulses, 1 kHz (1000 pulses/sec). Solid lines are fits while scattered data (open circles) are experimental data.

For calculating $|\chi^{(3)}|$ values the equations explained in chapter 2 were used. The fitting was performed using MATLAB and Sheik-Bahae et al. model. At 700 nm wavelength with power 14.5 mW we found that $I_s > I_{oo}$, this shows this is a 3rd order nonlinear process [97]. The nonlinear absorption coefficient was calculated using, $\beta = \frac{-\alpha_0}{I_s}$ where α_0 is the linear absorption coefficient and I_s is the saturation intensity.

Wavelength (nm)	$\mathbf{n_2}$ $(\mathbf{m^2/W}) \times \mathbf{10^{-16}}$	$\beta(\mathbf{m/W}) \times \mathbf{10^{-11}}$	$\mathbf{Re}\lvert\chi^{(3)}\rvert$ $(\mathbf{esu}) \times \mathbf{10^{-10}}$	$\mathbf{Im}\lvert\chi^{(3)}\rvert$ $(\mathbf{esu}) \times \mathbf{10^{-13}}$	$\lvert\chi^{(3)}\rvert$ $(\mathbf{esu}) \times \mathbf{10^{-10}}$	$\lvert\chi^{(3)}\rvert$ $(\mathbf{m^2/V^2}) \times \mathbf{10^{-18}}$
680	-5.2	2.6*	-2.7	7.2	2.7	3.9
700	-5.5	1.4*	-2.8	4.0	2.8	4.0
800	0.5	--	0.27	--	0.27	0.37

*** in β values indicates the presence of saturable absorption (SA)**

Table 5 NLO coefficients (fs regime) of **Pc-2** at different wavelength retrieved from **80 MHz** repetition rate data.

Wavelength (nm)	$\mathbf{n_2}$ $(\mathbf{m^2/W}) \times \mathbf{10^{-16}}$	$\beta(\mathbf{m/W}) \times \mathbf{10^{-11}}$	$\mathbf{Re}\lvert\chi^{(3)}\rvert$ $(\mathbf{esu}) \times \mathbf{10^{-10}}$	$\mathbf{Im}\lvert\chi^{(3)}\rvert$ $(\mathbf{esu}) \times \mathbf{10^{-12}}$	$\lvert\chi^{(3)}\rvert$ $(\mathbf{esu}) \times \mathbf{10^{-10}}$	$\lvert\chi^{(3)}\rvert$ $(\mathbf{m^2/V^2}) \times \mathbf{10^{-18}}$
680	-2.9	4.4*	-1.5	1.2	1.5	2.1
700	-4.7	11.1*	-2.4	3.2	2.4	3.4
750	-2.1	--	-1.0	--	1.0	1.4
850	-5.2	9.9*	-2.6	3.4	2.7	3.8

*** in β values indicates the presence of saturable absorption (SA)**

Table 6 NLO susceptibility (fs regime) of **Pc-2** at different wavelength with **1** k**Hz** repetition rate (using chopper)**.**

We observed RSA in SA for Pc-2 at 850 nm [data is presented in figure 20(a)] recorded with 1 kHz pulses. As the input intensity increased the excited state absorption could have dominated compared to the ground state absorption leading to RSA in SA. This type of switching behavior can be utilized for optical signal processing applications provided one can achieve such a behavior with low peak

powers. Closed aperture data [presented in figure 20(b)] demonstrated negative nonlinearity at low peak intensity when the data was recorded at the same wavelength. The solvent contribution was minimal in this case and was confirmed by recording the closed aperture data of solvent separately. Figure 21(a) depicts the solvent contribution with fs, MHz pulses while figure 21(b) depicts the contribution with ps, 1 kHz pulses. The magnitude of n_2 was much lower (at least an order of magnitude) than that of the solutions studied. With the intention of justifying the potential of these molecules we calculated the figures of merit (FOM). The merit factor W is defined as $W = \frac{n_2 I_{sat}}{\alpha_1 \lambda}$ where λ is wavelength, and I_{sat} is the light intensity at which n_2 saturates. The pre-requisite for superior FOM is $W > 1$. The corresponding FOM for nonlinear absorption is $T^{-1} = \frac{n_2}{\lambda \alpha_2}$. For photonics device applications $T < 1$ is desirable.

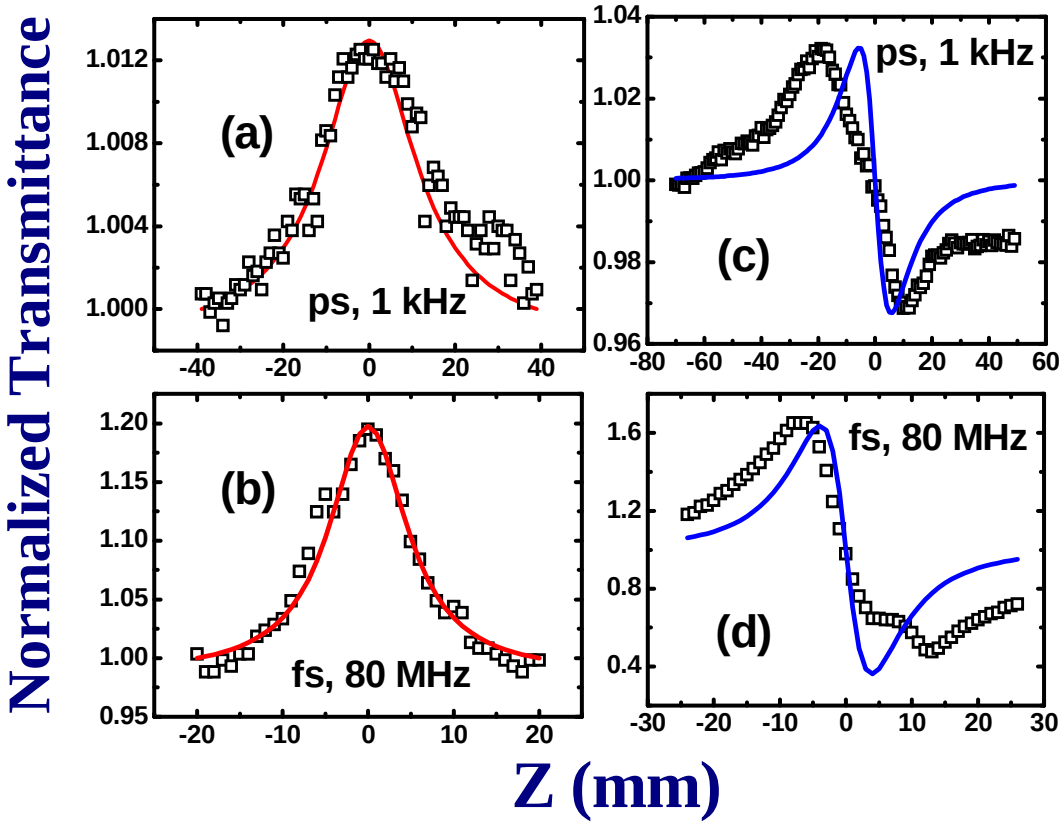

Figure 22 OA behavior of **Pc-3** (in THF) at 800 nm depicting (a) SA with ~2 ps, 1 kHz excitation and (b) ~150 fs, 80 MHz excitaiton **($I_s << I_{00}$)**. Closed aperure data depicting negative nonlinearity in (c) ~2 ps, 1 kHz excitation (d) ~150 fs, 80 MHz excitation.

Wavelength (nm)	$\mathbf{n_2}$ $(\mathbf{m^2/W})$ $\times \mathbf{10^{-16}}$	$\boldsymbol{\beta}$ $(\mathbf{^m/_W})$ $\times \mathbf{10^{-9}}$	$\mathbf{Re\lvert\chi^{(3)}\rvert}$ **(esu)** $\times \mathbf{10^{-10}}$	$\mathbf{Im\lvert\chi^{(3)}\rvert}$ **(esu)** $\times \mathbf{10^{-11}}$	$\mathbf{\lvert\chi^{(3)}\rvert}$ **(esu)** $\times \mathbf{10^{-10}}$	$\mathbf{\lvert\chi^{(3)}\rvert}$ $(\mathbf{m^2/V^2})$ $\times \mathbf{10^{-18}}$
800 nm, 80 MHz	-2.1	1.6	-1.1	5.2	1.2	1.2
760 nm, 1 kHz	-2.6	25.2	-1.3	79.2	8.0	11.2

Table 7 NLO coefficients (fs regime) of **Pc-1.**

Figures 22(a) and 22(b) illustrate the open aperture Z-scan data of Pc-3 (~0.1 mM concetration) recorded at 800 with ~2 ps pulses nm (1 kHz repetition rate) and ~150 fs pulses (80 MHz repetition rate), respectively. Both the data depicted saturable absorption (SA), which is due to the presence of strong linear absorption at that particular wavelength.

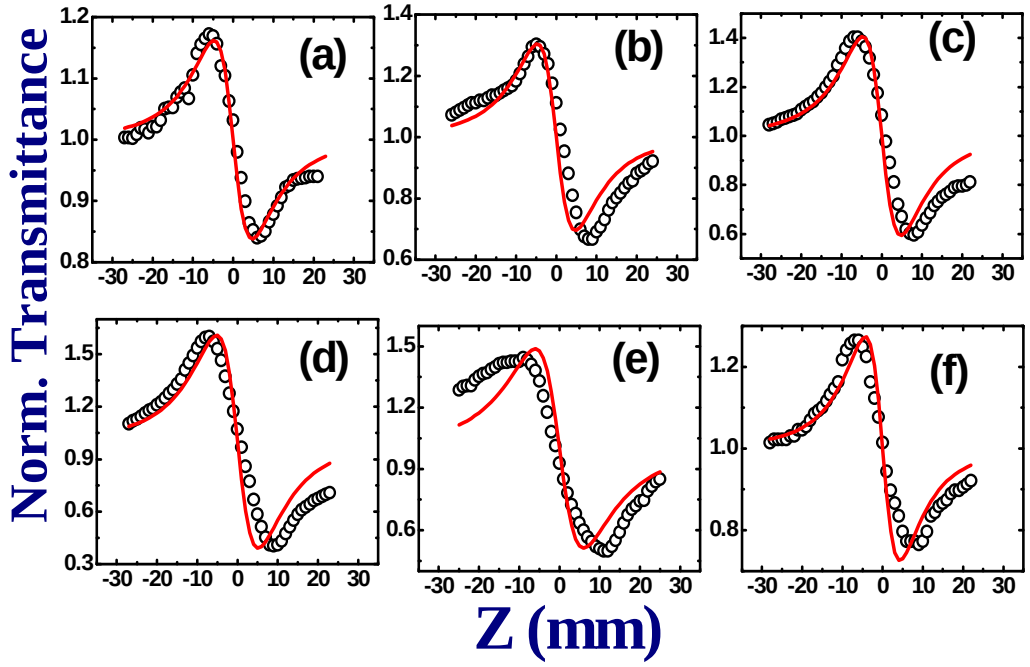

Figure 23 Closed aperture data of **Pc-3** demonstrating negative nonlinearity at (a) 700 nm (b) 720 nm (c) 740 nm (d) 760 nm and (e) 780 nm and (f) 820 nm with 80 MHz, fs pulse excitaiotn. n_2 values extracted from the fits were ~1.66×10^{-12} cm^2/W, ~2.10×10^{-12} cm^2/W, ~2.30×10^{-12} cm^2/W, ~6.95×10^{-12} cm^2/W, 4.36×10^{-12} cm^2/W and ~2.11×10^{-12} cm^2/W at respective wavelengths. The sign of n_2 was negative (self-defocusing).

Closed aperture Z-scan data is presented in figures 22(c), 22(d) for ps and fs excitaitons, respectively. It is evident that in both the case the nonlinearity was negative. The magnitudes of n_2 were ~10^{-12} cm^2/W in fs (MHz repetition) case and

~10^{-16} cm^2/W in the ps (1 kHz repetition rate) case. The magnitudes of $\chi^{(3)}$ were large (~10^{-11} e.s.u.) in the fs case and moderate (~10^{-14} e.s.u.) in the ps case. Figures 23(a)-23(f) depicts the fs closed aperture data of Pc-3 recorded at different wavelengths in the 700 nm–820 nm spectral range and the data clearly suggests negative nonlinearity with magnitudes of ~10^{-12} cm^2/W with a largest value of ~6.95×10^{-12} cm^2/W recorded at 760 nm. Figures 24(a) and 24(b) illustrate the typical open aperture data of Pc-3 at 600 nm recored with ~2 ps pulses at lower (~60 GW/cm^2) and higher (~120 GW/cm^2) peak intensities, respectively.

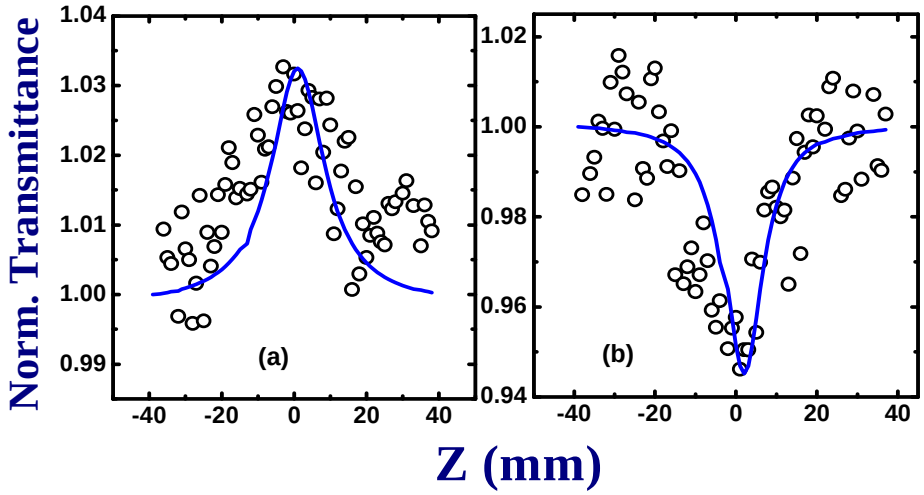

Figure 24 (a) Open aperture Z-scan data of **Pc-3** at 600 nm with ~2 ps, 1 kHz excitation depicting (a) SA at 60 GW/$cm^2$with $I_s > I_{00}$. I_s=170 GW/$cm^2$and (b) RSA at 120 GW/cm^2 with β ~1×10^{-11} cm/W. Solvent (THF) contribution was negligible in both cases.

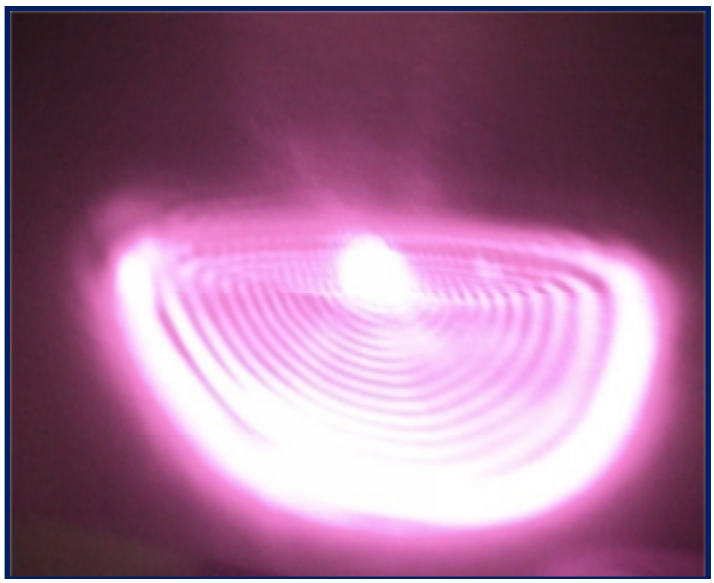

Figure 25 Spatial rings observed on a screen placed in far field for **Pc-3** at high input powers (fs, MHz excitation) due to self phase modulation/thermal lensing effect.

In such type of molecules depending on the excitation wavelength and the input peak intensity SA or RSA or switching behavior (SA to RSA and vice-versa) prevails [14-20, 36-39]. For Z-scans performed away from resonance (strong linear absorption) we have observed switching mechanism from SA to RSA (see supporting information) with both MHz, fs and kHz, ps excitation. The NLO coefficients extracted from the Z-scan studies are presented in table 2 for both ps and fs excitation.

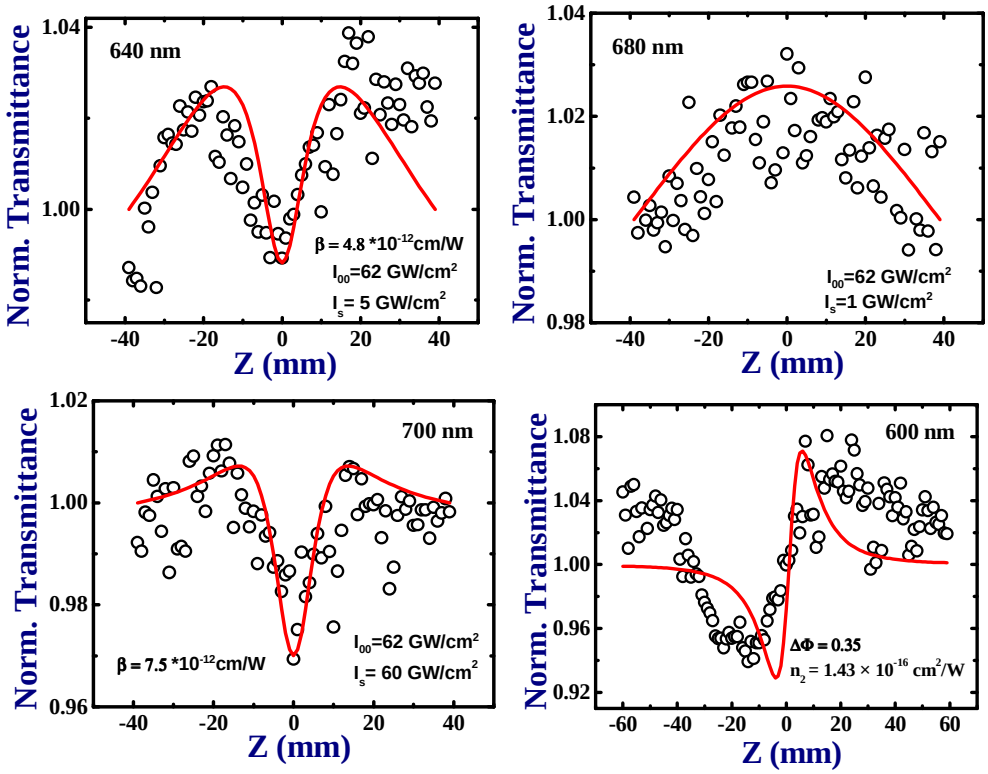

Figure 26 Open aperture Z-Scan of **Pc-3** at (a) 640 nm using ~2 ps, 1 kHz pulses showing RSA in SA with $I_s < I_{00}$ (62 GW/cm^2). I_s = 5 GW/cm^2. β ~4.8×10^{-12} cm/W. (b) 680nm SA with $I_s < I_{00}$. (c) RSA in SA with $I_s < I_{00}$ (62 GW/cm^2) β = 7.5×10^{-12} cm/W (d) at 600 nm (positive $n_2$of ~1.43×10^{-16} cm^2/W).

Sample	Solvent	λ_{max}, nm (log ε) $M^{-1}cm^{-1}$	$\lambda_{em,\ max}$, nm	ϕ_f	τ_f (ns)
Pc-3	DCM	803 (5.04)	823	0.020	1.23
	DMF	782 (5.13)	813	0.022	1.25
	DMSO	793 (4.84)	822	0.020	1.22
	THF	787 (5.45)	809	0.022	1.26
	Toluene	792 (4.99)	812	0.024	1.25

Table 6 Absorption, emission data of **Pc-3** from [98].

λ(nm)	n_2 (cm^2/W)	I_s(W/cm^2)	$\lvert Re[\chi^{(3)}] \rvert$ e.s.u.	Total[$\chi^{(3)}$] e.s.u.
800 nm (~2 ps, 1 kHz)	-2.6×10^{-16}	5×10^{11}	1.3×10^{-14}	1.3×10^{-14}
800 nm (~150 fs, 80 MHz)	-9.3×10^{-13}	1×10^{7}	4.7×10^{-11}	4.7×10^{-11}

Table 7 Summary of NLO coefficients of **Pc-3** ($I_s<I_{00}$)

5.6 Excited State Dynamics

Based on the nonlinear absorption data obtained at various wavelengths in the visible region we tried to analyze the fs pump-probe data. Figure 23 shows a simplified energy level diagram indicating the excitations and decay times for these molecules. Excitation with focused 600 nm photons (16600 cm^{-1}) and the peak intensities used enables 2PA resulting in population reaching the S_2 states.

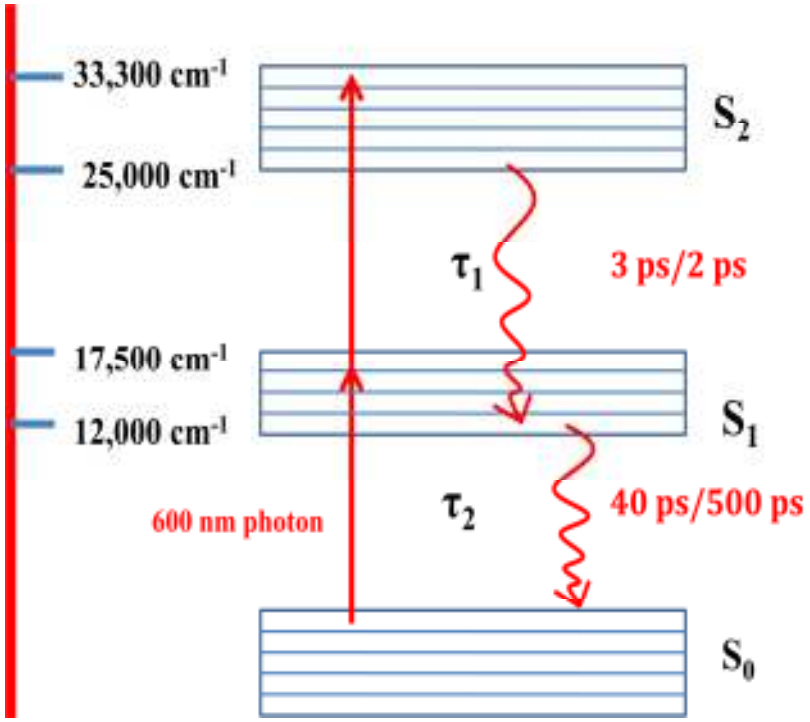

Figure 27 Typical energy level diagram of **Pc-1**, **Pc-2**

Once excited into the high lying states of S_2 the de-excitation mechanism could be from (a) lowest vibrational state of S_2 manifold to highest vibrational states of S_1 manifold (Internal Conversion, IC) followed by intra-molecular vibrational relaxation (IVR) from highest states of S_1 to lowest states of S_1). These are typically fast

processes (<1 ps for IC, 1–2 ps for IVR) and, therefore, the shorter lifetimes (2–3 ps) could be attributed to this relaxation and (b) from the lowest vibrational states of S_1 states the molecules relax to ground state via non-radiative mechanism by releasing the energy to solvent. This process typically occurs in few tens to hundreds of ps in such molecules. The longer lifetime can be associated with such a process as depicted in figure 23. The longer lifetime cannot be due to radiative processes since the radiative lifetimes measured in different solvents were typically few ns.

The lifetimes observed in Pc-1 and Pc-2 were comparable to those obtained in similar molecules such as Porphycenes and Corroles which were recently investigated by our group. But in Pc-3, relaxation is from S_1 state to S_0 showing only single non - radiative exponential recovery of magnitude 309 ps. Radiative decay times are expected to be few ns. Pc-1 has a short-lived non-radiative lifetime from S_1 states whereas Pc-2 has a long-lived lifetime. However, the radiative lifetimes of both Pc-1 and Pc-2 were similar in magnitude (2-3 ns). The long-lived lifetime could, possibly, have played a role in the observation of stronger NLO coefficients for Pc-2.

5.7 Conclusions

In summary two novel sterically hindered Pc's (Pc-1, Pc-2) and Thio-Zinc Pc (Pc-3) were synthesized and characterized. Their optical and electrochemical properties have been investigated in detail. Nonlinear optical (NLO) properties were also evaluated at different in the visible spectra region using picosecond (~1.5 ps) pulses and further studies with femtosecond (~140 fs) pulses at 800 nm have been performed. Excited state dynamics in Pc-3 molecule investigated using fs degenerate pump-probe spectroscopy revealed a single exponential of ~309 ps, which has been assigned to the S_1 state non-radiative lifetime and the radiative lifetime are few ~ns. 2PA and saturable absorption were the dominant nonlinear absorption mechanisms observed with ps excitation while 3PA was observed with fs excitation. NLO coefficients were extracted from ps/fs closed and open aperture Z-scan measurements. Large two-photon absorption cross sections in the range of 400-14000 GM and n_2 values in the range of $1\text{-}7\times10^{-16}$ cm^2/W were recorded for these samples. The excited state decay dynamics were investigated using degenerate pump-probe experiments with femtosecond pulses near 600 nm. Double exponential fits of the pump-probe data suggested two decay times. The shorter lifetime was 2-3 ps while the longer

lifetime was ~40 ps in Pc-1 and ~500 ps in Pc-2. Our studies suggest that these molecules can be tailored for potential applications in photonics.

By appropriate tuning of the input wavelength, pulse duration, peak intensities with a fixed concentration of the molecules in solution one could obtain all the nonlinear absorption behavior with these molecules. For example, with ns pulse excitation at 532 nm we could envisage RSA/ESA kind of behavior while with 800 nm ps/fs excitation we observed SA. For ps/fs excitation in the 600 nm-900 nm one can observe the switching mechanism of SA to RSA and with stronger and selective pumping one could achieve pure RSA (due to 2PA as was observed in the case at 600 nm). Though there are a number of reports on NLO studies of various Pc's it is imperative that (a) a database of NLO properties of all novel Pc's is created to facilitate establishing a structure-property relationship [94-96] useful for synthesis of novel molecules and devices (b) nonlinearities are measured with short pulses (ps and fs) excitation in an attempt to identify the true electronic nonlinearities and their time response (c) congregate information on the spectral dependence of nonlinearities indispensable for identifying the spectral region of interest for various applications of n_2 and nonlinear absorption. Some of our recent efforts [97, 98] have focused on understanding the nonlinearities and ultrafast dynamics in novel Pc's. Some recent results [99] have investigated the complete photophysical and photochemical phenomena in a Zinc-Pc. Furthermore, NLO measurements with MHz pulses is also required since the repetition rates of lasers to be used in optical signal processing will be of similar magnitude to achieve high-speed data transmission rates (for example Gigabits/s to Terabits/s). It is well understood and established that MHz repetition rate pulses induce thermal nonlinearities in open aperture Z-scan measurements. However, one needs to discover mechanisms to identify the magnitudes of both electronic and thermal nonlinearities and separate them. One of the certain ways of reducing the thermal nonlinearities is to incorporate these molecules in media (e.g. polymers or glasses) possessing higher thermal diffusion coefficients. Detailed investigations of dispersion studies (in the NIR spectral region) of NLO properties with both ps and fs pulses will be a subject of our future investigations.

5.8 References

1. (a) J. J. Miasik, A. Hooper, B. C. Tofield, J. Chem. Soc., Faraday Trans. **82** (1986) 1117 (b) F. I. Bohrer, C. N. Colesniuc, I. K. Schuller, J. Park, A. C. Kummel, M. E. Ruidiaz, W. C. Trogler, J. Am. Chem. Soc. **131** (2009) 478 (c) Y. J. Bae, N. J. Lee, A. Hirohata, T. H. Kim, H. Cho, C. Lee, L. Fleet, Nanoscale Res. Lett., **7** (2012) 650.
2. (a) S. Heutz, C. Mitra, W. Wu, A. J. Fisher, A. Kerridge, M. Stoneham, T. H. Harker, J. Gardener, H. Tseng, T. S. Jones, C. Renner, and G. Aeppli, Adv. Mater. **19** (2007) 3618 (b) N. Tsukahara, K. Noto, M. Ohara, S. Shiraki, N. Takagi, Y. Takata, J. Miyawaki, M. Taguchi, A. Chainani, S. Shin, and M. Kawai, Phys. Rev. Lett. **102** (2009) 167203 (c) H. Zollinger, Color Chemistry, Third edition, Wiley-VCH, (2001) (d) L. Li, Q. Tang, H. Li, W. Hu, X. Yang, Z. Shuai, Y. Liu, D. Zhu, Pure Appl. Chem.**80** (2008) 2231.
3. (a) R. Minnes, H. Weitman,Y. You, M. R. Detty, B. Ehrenberg, J. Phys. Chem. B **112** (2008) 3268 (b) Z. Sun, L. Jin, S. He, Y. Zhao, M. Wei, D. G. Evans and X. Duan, Green Chem. **14** (2012) 1909 (c) S. Nagel, M. Lerner, C. Keil, R. Gerdes, L. Lapok, S. M. Gorun and D. Schlettwein, J. Phys. Chem. C **115** (2011) 8759. (d) T. Nyokong, Pure Appl. Chem. **83** (2011)1763 (e) G. de la Torre, P. Vázquez, F. Agulló-López and T. Torres, Chem. Rev.**104** (2004) 3723 (f) Y. H. Gursel, B. F. Senkal, M. Kandaz and F. Yakuphanoglu, Polyhedron, **28** (2009) 1490 (g) C. G. Claessens, U. Hahn and T. Torres, The Chem. Record, **8** (2008) 75 (h) M. E. Ragoussi, M. Ince, T. Torres, Euro J. Org. Chem. **2013** (2013) 6475.
4. A.B. Sorokin. Chem. Rev. **113** (2013) 8152.
5. L. Giribabu, R. K. Kanaparthi, V. Velkannan, The Chem. Record **12** (2012) 306.
6. D. Wohrle, G. Schnurpfeil, S.G. Makarov, A. Kazarin, O.N. Suvorova, Macroheterocycles **5** (2012) 191.
7. T. Nyokong, Coord. Chem. Rev. **251** (2007)1707.
8. T. Nyokong, Pure Appl. Chem. **83** (2011)1763.
9. K. Ishii, N. Kobayashi, K.M. Kadish, K. M. Smith, R. Guilard The Porphyrin Handbook, Vol. **16**, Academic Press/Elsevier, New York, (2003); (Chapter 102):1-40.

10. F. Dumoulin, M. Durmuş, V. Ahsen, T. Nyokong. Coord. Chem. Rev. **254** (2010) 2792.
11. (a) V. K. Singh, P. Salvatori, A. Amat, S. Agrawal, F.D. Angelis, M.K. Nazeeruddin, N. V. Krishna, L. Giribabu, Inorg. Chim. Acta **407 (**2013) 289 (b) C. A. Strassert, G.M. Bilmes, J. Awruch, L.E. Dicelio, Photochem. Photobiol. Sci. **7** (2008) 738 (c) E. M. Maya, P. Vazquez, T. Torres, Chem. Eur. J. **5** (1999) 2004.
12. S. Venugopal Rao, Proc. SPIE **7728** (2010) 77281N.
13. S. Venugopal Rao, P.T. Anusha, L. Giribabu, S.P. Tewari, Pramana - J. Phys.; **75** (2010) 1017.
14. R. S. S. Kumar, S. Venugopal Rao, L. Giribabu, D. N. Rao, Opt. Mat. **31** (2009) 1042.
15. S. Venugopal Rao, L. Giribabu, N. Venkatram, D.N. Rao. J. Appl. Phys. **105** (2009) 053109.
16. N. Venkatram, L. Giribabu, D.N. Rao, S. Venugopal Rao. Appl. Phys. B **91** (2008) 149.
17. N. Venkatram, L. Giribabu, D.N. Rao, S. Venugopal Rao. Chem. Phys. Lett. **464** (2008) 211.
18. R. S. S. Kumar, S. Venugopal Rao, L. Giribabu, and D.N. Rao. Proc. SPIE **6875** (2008) 68751D.
19. S. J. Mathews, C.S. Kumar, L. Giribabu, S. Venugopal Rao. Mater. Lett. **447** (2007) 274.
20. G. Torre, P .Vazquez, F. Aqullo-Lopez, and T. Torres. J. Mater. Chem.**8 (**1998)1671.
21. M. D. Maree, T. Nyokong, K. Suhling, D. Phillips, J. Porphy. Phth.**6** (2002) 373.
22. J. Britton, M. Durmuş, S. Khene, V. Chauke, T. Nyokong, J. Porphy. Phth. **17** (2013) 691.
23. S. O. Sanusi, E. Antunes, T. Nyokong, J. Porphy. Phth. **17** (2013) 920.
24. F. Henari, A. Davey, W. Blau, P. Haisch, M. Hanack, J. Porphy. Phth. **3** (1999) 331.
25. L.C. Liu, C.H. Tai, A.T. Hu, T.H. Wei, J. Porphy. Phth. **8** (2004) 984.
26. E. Agar, S. Samaz, N. Akademir, L. Keskin, Dalton Trans. **12** (1997)2087.
27. I. Gurol, M. Durmus, V. Ashen, T. Nyokong, Dalton Trans. **34** (2007) 3782.

28. J.W. Owens, R. Smith, R. Robinso, Robins M. Inorg. Chimica Acta **279** (1998) 226.
29. D. A. Fernández, J. Awruch, L. E. Dicelio, Photochem. Photobiol. **63** (1996) 784.
30. B. Ertem, A. Bilgin, Y. Gok, H. Kanteki, Dyes and Pigments **77** (2008) 537.
31. S. Unlu, M.N. Yarasir, M. Kandaz, A. Koca, B. Salih, Polyhedron **27** (2008) 2805.
32. A. Bilgin, Y. Gok. Supramol. Chem. **18** (2006) 491.
33. K. P. Unnikrishnan, J. Thomas, V. P. N. Nampoori, C. P. G. Vallabhan, Appl. Phys. B **75** (2002) 871.
34. J. Savolainen, D.V.D. Linden, N. Dijkhuizen, J.L. Herek. J. Photochem. Photobiol. A: Chem. **196** (2008) 99.
35. I. A. C. García, A. M. Sevim, A. de la Escosura, T. Torres. Org. Biomol. Chem. **11** (2013) 2237.
36. K. Sakamoto, E. Ohno-Okumura, T .Kato, H. Soga. J. Porphy. Phth. **14** (2010) 47.
37. P.M. Burnham, M.J. Cook, L.A. Gerrard, M.J. Heeney, D.L. Hughes. Chem. Commun. **16** (2003) 2064.
38. M. J. Cook, I. Chambrier, S.J. Cracknell, D.A. Mayes, D. A. Russell. Photochem. Photobiol. **62** (1995) 542.
39. R. S. S. Kumar, S. Venugopal Rao, L. Giribabu and D. N. Rao, Chem. Phys. Lett. **447** (2007) 274.
40. P. Gregory, J. Porphy. Phth. **4** (2000) 432.
41. K. M. Smith, A. R. Katritzky, C.W. Rees (Eds.), Comp. Heter. Chem., vol. **4**, Pergamon, Oxford, (1984), 377.
42. J. Simon and J. Vacus, Adv. Mater. **7 (**1995) 797.
43. E. M. Maya, A. W. Snow, J. S. Shirk, R. G. S. Pong, S. R. Flom and G. L. Roberts, J. Mater. Chem. **13** (2003)1603.
44. I. Szymczyk and H. Abramczyk, Pure Appl. Chem.**76** (2004) 183.
45. K. M. Kadish, K. M. Smith, R. Guilard, The Porphyrin Handbook, Academic Press, San Diego, CA, 2003, Vol.**17**: Phthalocyanines: Properties and Materials.
46. M. Brewis, B. M. Hassan, H. Li, S. Makhseed, N.B. McKeown and N. Thompson, J. Porphy. Phth. **4** (2000) 460.

47. M. Brewis, G. J. Clarkson, A. M. Holder, N. B. McKeown, Chem. Commun. (1998) 969.
48. L. Giribabu, R. K. Kanaparthi, Curr. Sci. **104** (2013) 847.
49. L. Giribabu, V. K. Singh, T. Jella, Y. Soujanya, A. Amat, F. De Angelis, A. Yella, P. Gao, M.K. Nazeeruddin, Dyes and Pigments **98** (2013) 518.
50. L. Giribabu, V. K. Singh, Ch. V. Kumar, Y. Soujanya, P. Y. Reddy, M. L. Kantam, Sol. Ener. **85** (2011) 1204.
51. P. Y. Reddy, L. Giribabu, C. Lyness, H. J. Snaith, Ch. Vijaykumar, M. Chendrasekheram, M. L. Kantam, J. Hum, K. Kalyanasundaram, M. Gratzel, M. K. Nazeeruddin, Angew. Chem. Int. Ed. Eng. **46** (2007) 373.
52. L. Giribabu, Ch. Vijaykumar, V. G. Reddy, P. Y. Reddy, S.R. Jang, J.H. Yum, M. K. Nazeeruddin and M. Gratzel, Solar Energy Mater. Solar Cells, **91** (2007) 1611.
53. S. Eu, T. Katoh, T. Umeyama, Y. Matano, H. Imahori, Dalton Trans. **40** (2008) 5476.
54. G. Pozzi, S. Quici, M.C. Raffo, C.A. Bignozzi, S. Caramori, M. Orlandi, J. Phys. Chem. C **115** (2011) 3777.
55. M. E. Ragoussi, M. Ince, T. Torres, Euro J. Org. Chem. **2013** (2013) 6475.
56. C. Ozturk, A. Erdogmus, M. Durmus, A.L. Ugur, F.A. Kilicarslan, I. Erden. Spectrochimica Acta A **86** (2012) 423.
57. M. J. Stillman, T. Nyokong, C.C. Leznoff. A.B.P. Lever (Eds.), Phthalocyanines: Properties and Applications, Vol. **1**, VCH Publishers, New York, 1989 (Chapter 3).
58. A.B. Anderso, T.L. Gorden, M.E. Kenney J. Am. Chem. Soc.**107** (1985)192.
59. M. Konami, M. Hatano, and A. Tajiri, Chem. Phys. Lett.**166** (1990) 605.
60. H. Enkelkamp, R.J.M. Nolte, J. Porphy. Phth. **4** (2000) 454.
61. D. D. Dominguez, A.W. Snow, J.S. Shirk, R.G.S. Pong, J. Porphy. Phth. **5** (2001) 582.
62. X. Jarota, M. Tondusson, G. Galle, E. Freysz, H. Abramczyk, J. Phys. Chem.A **116** (2012) 4000.
63. L. Howe, J.Z. Zhang, J. Phys. Chem. A **101** (1997) 3207.
64. P. T. Anusha, D. Swain, S. Hamad, L. Giribabu, T.S. Prashant, S.P. Tewari, S. Venugopal Rao, J. Phys. Chem. C **116** (2012) 17828.
65. S. Venugopal Rao, D.N. Rao, J. Porphy. Phth. **6** (2002) 233.

66. D. N. Rao, S. Venugopal Rao, F. J. Aranda, D. V. G. L. N. Rao, M. Nakashima, J. A. Akkara, J. Opt. Soc. Am. B **14** (1997) 2710.
67. S. Venugopal Rao, N.K.M. Naga Srinivas, D.N. Rao, L. Giribabu, B.G. Maiya, R. Philip and G.R. Kumar, Opt. Commun.**192** (2001) 123.
68. P. Fita, T. Osmalek, T. Goslinski, M. Wierzchowski, J. Mielcarek, J. Photochem. Photobiol. A: Chem. **232** (2012) 44.
69. S. J. Mathews, S. C. Kumar, L. Giribabu, S. Venugopal Rao, Opt. Commun. **280** (2007) 206.
70. P.T. Anusha, P.S. Reeta, L. Giribabu, S.P. Tewari, S. Venugopal Rao, Mater. Lett. **6** (2010) 1915.
71. X. Chen, J. Zhang, W. Wei, Z. Jiang, Y. Zhang, Eur. Polymer J. **53** (2014) 58.
72. K. Sanusi, E. Antunes, T. Nyokong, Dalton Trans. **43** (2014) 999.
73. J. Britton, E. Antunes, T. Nyokong, J. Mol. Struct. **1047** (2013) 143.
74. M. B. M. Krishna, L. Giribabu, D. Narayana Rao, J. Porphy. Phth. **16** (2013) 1015.
75. Z. Chen, C. Zhong, Z. Zhang, Z. Li, L. Niu, Y. Bin, F. Zhang, J. Phys. Chem. B **112** (2008)7387.
76. S. Venugopal Rao, P.T. Anusha, T.S. Prashant, D. Swain, S. P. Tewari, Mater. Sci. Applns. **2** (2011) 299.
77. X. Zhao, X.Q. Yan, Q. Ma, J. Yao, X.L. Zhang, Z. B. Liu, J.G. Tian, Chem. Phys. Lett. **577** (2013) 62.
78. S. Tekin, U. Kürüm, M. Durmuş, H.G. Yaglioglu, T. Nyokong, A. Elmali, Opt. Commun. **283** (2010) 4749.
79. C. Yao, Y. Zhang, W. Sun, C. Yu, J. Li, P. Yuan, Opt. Express **21** (2013) 2212.
80. H. Gu, S. Li, J. Wang, W.J. Blau, Y. Chen, Mater. Chem. Phys. **137** (2012) 188.
81. A. B. Karpo, V.E. Pushkarev, V.I. Krasovskii, L.G. Tomilova, Chem. Phys. Lett. **554** (2012) 155.
82. H. Manaa, A. Tuhl, J. Samuel, A. Al-Mulla, N.A. Al-Awadi, S. Makhseed, Opt. Commun. **284** (2011) 450.
83. Y. Chen, S.M. O'Flaherty, M. Hanack, W.J. Blau, J. Mater. Chem. **13** (2003) 2405.
84. T. Ceyhan, M. Yuksek, H. G. Yaglioglu, B. Salih, M. K. Erbil, O. Bekaroglu, Dalton Trans. **18** (2008) 2407.

85. A. Auger, W.J. Blau, P.M. Burnham, I. Chambrier, M.J. Cook, B. Isare, F. Nekelson, S.M. O'Flaherty, J. Mater. Chem. **13** (2003) 1042.
86. A. Tuhl, H. Manaa, S. Makhseed, N. Al-Awadi, J. Mathew, H.M. Ibrahim, T. Nyokong, H. Behbehani, Opt. Mater. **34** (2012)1869.
87. T. Goslinski, T. Osmalek, K. Konopka, M. Wierzchowski, P. Fita, J. Mielcarek, Polyhedron **30** (2011) 1538.
88. T. Sarma, P.K. Panda, P.T. Anusha, S. Venugopal Rao, Org. Lett.**13** (2010)188.
89. D. Swain, P.T. Anusha, T.S. Prashant, S.P. Tewari, T. Sarma, P.K. Panda, S. Venugopal Rao, Appl. Phys. Lett. **100** (2012) 141109.
90. S. Venugopal Rao , T. S. Prashant, T. Sarma, P. K. Panda, D. Swain, S. P. Tewari, Chem. Phys. Lett. **514** (2011) 98.
91. D. Swain, T. Sarma, P.K. Panda, S. Venugopal Rao, Chem. Phys. Lett. **580** (2013) 73.
92. S. Hamad, S. P. Tewari, L. Giribabu, S. Venugopal Rao, J. Porphy. Phth. **16** (2012) 140.
93. B. S. Singh, H.R. Lobo, G. K. Podagatlapalli, S. Venugopal Rao, G.S. Shankarling, Opt. Mater. **35** (2013) 962.
94. G. de la Torre, P. Vázquez, F. Agulló-López and T. Torres. Chem. Rev. **104** (2004) 3723.
95. J. M. Hales, S. Barlow, H. Kim, S. Mukhopadhyay, J. L. Brédas, J. W. Perry, S. R. Marder, Chem. Mater. In Press, (2013) dx.doi.org/10.1021/cm402893s.
96. M.G. Kuzyk, K.D. Singer, G.I. Stegeman, Adv. Opt. Phot.**5** (2013) 4.
97. D. Swain, R. Singh, V.K. Singh, N.V. Krishna, L. Giribabu, S. Venugopal Rao, J. Mater. Chem. C **2** (2014) 1711.
98. D. Swain, V.K. Singh, N.V. Krishna, L. Giribabu, S. Venugopal Rao, J. Porphy. Phth. In press**,** (2014). DOI: 10.1142/S1088424614500035
99. G. Gümrükçü, G.K. Karaoğlan, A. Erdoğmuş, A. Gül, U. Avcıata, J. of Chem. Vol. 2014, Article ID 435834, 11 pages, 2014. DOI:10.1155/2014/435834

Chapter 6

Study of ultrafast excited state dynamics and NLO properties of Porphyrins

6.1 Introduction

The process of photosynthesis in plants has driven many researchers to investigate phenomena, which mimic this natural event [1-3]. Porphyrins play a major role in attracting the scientific community because of its use inartificial photosynthesis and respiration. The origin of name porphyrin came from ancient Greece with the word *porphura* meaning purple. Porphyrin is the name given to a class of intensely colored molecules all sharing a macrocycle of twenty carbon atoms and four nitrogen atoms. This macrocycle contains four pyrrole rings joined by methine bridges. Porphyrin is a nearly flat molecule though it may be distorted by certain ligand binding or by various substituent groups bound to the periphery. These family of compounds provides a compelling motivation to study and design new chromophores analogues with improved functions. The central cavity of the porphyrin can bind metals such as Fe, Zn, Cu, Ni, Mg, Ag, Au, and Co[4].Porphyrins have also been extensively used in a wide range of materials for sensing applications [5,6].The interesting absorbance or fluorescence properties of porphyrins make them suitable for sensing applications. Porphyrins can be modified by changing peripheral substituent's and/or centrally coordinated metal ion, to achieve binding specificity allowing for their application in amperometric or potentiometric protocols or for use with acoustical devices such as quartz crystal microbalances [7]. Some interesting works have been performed using porphyrin arrays as electronic noses and electronic tongues. Electronic noses are used for detection of vapors and electronic tongues are used for detection of compounds in the solution [8,9]. Amico's group has demonstrated the identification and quantification of fourteen different volatile organic compounds (VOCs) using an array of eleven metalloporphyrins [10]. They have also shown that the system can be used to classify unknown compound swhich are similar to others in library. The system used for this demonstration consisted of an HP flat-bed scanner as the spectrometer/light source and Adobe Photoshop for data analysis [10,60].Several other protocols using porphyrin arrays had employed quartz crystal microbalances. Porphyrins have also been used in amperometric and potentiometric detection protocols due to their ability to catalyze oxidation/reduction reactions. Most of the detection protocols are based on changes in the porphyrin absorbance spectra. One could gain by focusing on the Soret region of absorption

spectrum since very large extinction coefficients in that spectral region permits the detection of very small amounts of analyte.

Porphyrins are understood as a class of important biological pigments, endowed with rich photophysical properties owing to their conjugated 18π-electron aromatic system. Further, the properties of this macro cyclic tetra pyrrolic system can be easily modulated *via* substitution at one or more of the peripheral *meso*- and/or β-positions [11]. In the last two decades many porphyrin derivatives have been designed to study their utility as nonlinear optical (NLO) materials [12-37]. Porphyrin based oligomers, in association with other chromophores and polymers derived from porphyrins demonstrate interesting nonlinear optical behavior and hence hold great promise as second and third order NLO materials, as broadband optical limiters, in all optical switching, and in two-photon photodynamic therapy (PDT) [35-37].The basis of design in most of these systems for better NLO response is to have suitable donor and acceptor functionalities at the periphery of the aromatic porphyrin ring or the extended multi-porphyrinic systems. In this regard, monomeric porphyrin units were also studied as either reference for designing more accomplished systems or as standalone systems to gain understanding about their nonlinear optical response. Presence of multiple donor and acceptor functional groups at the porphyrin periphery is achieved either through direct link or through phenyl bridge or a combination of both. Also, it is known that direct linkage of functional groups at the porphyrin periphery impart a greater influence on the electronic properties of the macro cyclic ring. β-octa substituted porphyrins which could be synthesized quite conveniently could emerge as attractive target systems. However, there are very few reports containing substituents other than alkyl groups at all the β-positions of porphyrin[38-43].In particular, pyrroles with simultaneous single electron donating and single electron withdrawing substituents at their adjacent β-pyrrole positions are rare[44,45].

Detection and analysis of various types of explosives has been primary targets of many research groups for defense and security applications [46]. Trace detection of explosives has attracted attention for preventing terrorist activities [47]. Explosives are successfully detected by trained canines owing to its high vapor pressure [48]. However, some of the new explosive detecting techniques recently developed include Laser Induced Breakdown Spectroscopy (LIBS),Coherent Anti-stoke Raman

Spectroscopy (CARS), ion mobility spectroscopy (IMS),X-ray scanning, terahertz spectroscopy/imaging[49,50] etc. Fluorescence quenching method is also anemerging, sensitive low cost technique for on field detection[47]. Several polymer-based fluorophores, fluorescent dendrimers have been recently explored for superior results [51-52].Molecular imprinted polymer, coordination polymer, quantum dots, graphene, nano particles [53-57] were also used recently for sensing of high energy materials. There is scarce literature available to depict experimental work on detection of single molecule fluorophores [58].

Sensors based on porphyrin derivatives evoke particular interest owing to their superior photo-stability, ease of synthesis and capability of explosive molecules detection such as TNT [59,60]. There is limited literature existingon the sensing ability of differently substituted porphyrins with respect to different nitrated explosives. Ghosh and coworkers recently reported a fluoro-substituted organogelator, which demonstrated attogram level sensing of TNT [61]. Pradeep et al. recently reported selective visual detection of TNT at subzepto-molar level (i.e. almost in the regime of single molecule detection) in solution [62].These types of molecules may possess interesting NLO properties owing to special arrangement of multiple donor and acceptor substituents. These ideas are implemented in our recently reported symmetrical type 3,8,13,18-tetrachloro-2,7,12,17-tetramethoxyporphyrin (H_2TCTMP) [63].This molecule is unique, in the sense it contains an electron donating methoxy and electron withdrawing chloro group on the adjacent *β*- positions of each pyrrole moiety. Therefore, we studied its nonlinear optical behavior along with its Zn(II) and Ni(II) derivatives .

Porphyrins have also been evaluated in the context of PDT since they strongly absorb light, which can be converted to energy for storage. We have recently demonstrated the efficacy of β-octa-methoxy porphyrin (H_2OMP) and also their corresponding Zn(II)-derivatives as fluorophores in fluorescence quenching[63-66].Phthalocyanines, which are structurally related to porphyrins, are used in commerce as dyes and catalysts as described in chapter 5. Synthetic porphyrin dyes that are incorporated in the design of solar cells are the subject of ongoing research. Recent applications of porphyrin dyes for dye-sensitized solar cells (DSSC) have

shown solar conversion efficiencies approaching silicon based photovoltaic devices[4].

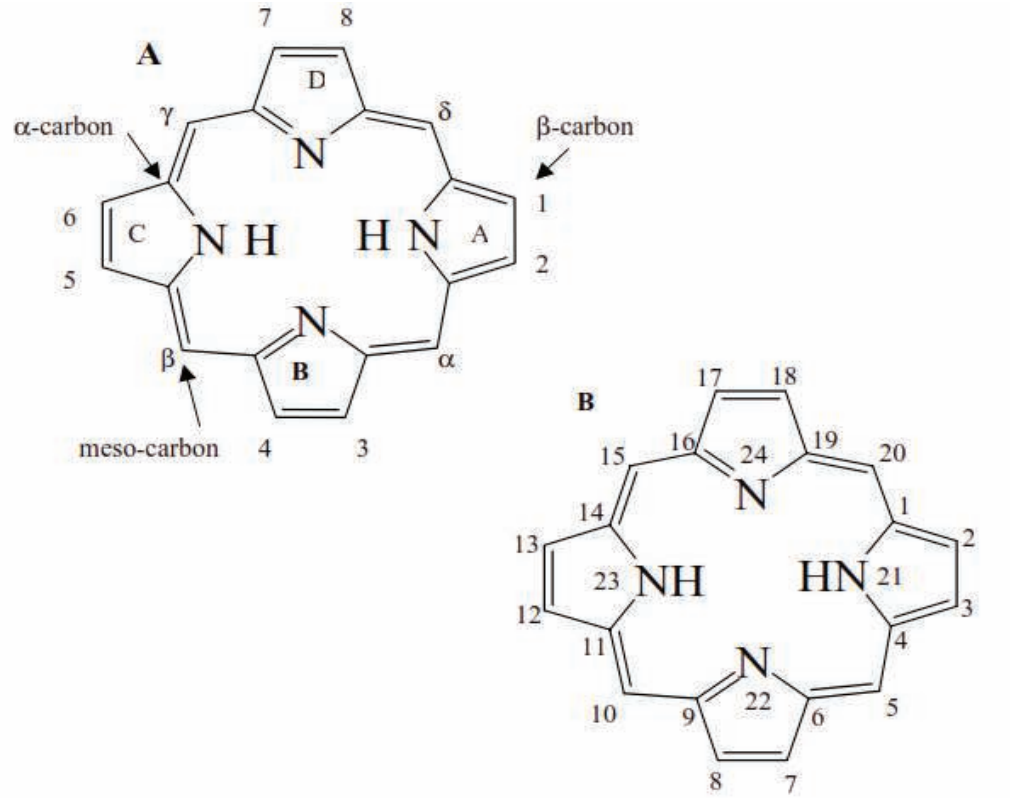

Figure1 Porphyrin macrocycle consisting of twenty carbon atoms and four nitrogen atoms. (A) Fischer numbering system (B) IUPAC numbering system as adapted from [4].

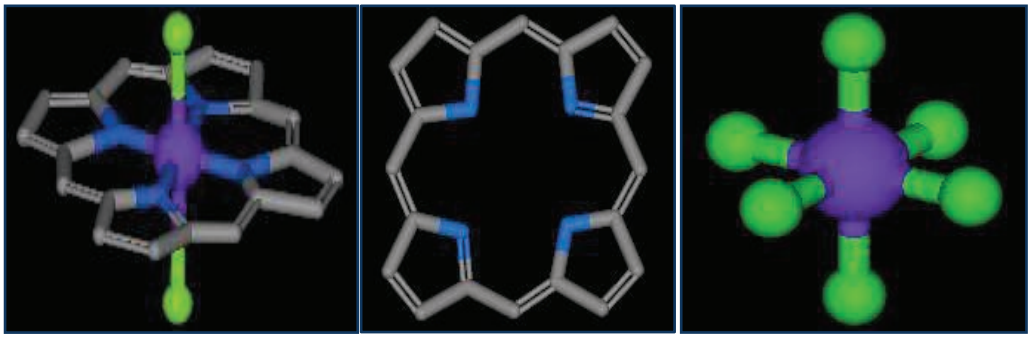

Figure 2 Structure of porphyrin molecule**.** Adapted from http://www.org-chem.org/yuuki/porphyrin/porphyrin.html

The molecule is stabilized by aromatic character which extends over its entire structure. A porphyrin has four of its nitrogen atoms facing the center, which can capture a metal ion to form a very stable organo metallic complex. This property of molecule is closely linked with the way it is used in living systems. When forming a complex, many metal ions accept six coordinating ligands to assume an octahedral configuration. The nitrogen atoms of a porphyrin occupy the four sites on the square

plane of an octahedron, leaving two empty sites on the top and the bottom (see figure 2). These two sites are then filled by the axial ligands, which are known to react in special ways. By using them, biological systems carry out a wide range of chemical reactions.

6.2 Structure, Absorption and emission data of porphyrins

1. M = H_2, R = OMe; H_2OMP
2. M = H_2, R = Cl; H_2TCTMP
3. M = Zn, R = OMe; ZnOMP
4. M = Zn, R = Cl; ZnTCTMP
5. M = Ni, R = Cl; NiTCTMP

Figure 3 Structure of novel porphyrins investigated in the present study.

Five porphyrins [H_2OMP (2,3,7,8,12,13,17,18-octamethoxyporphyrin), H_2TCTMP (3,8,13,18-tetrachloro-2,7,12,17-tetramethoxyporphyrin), ZnOMP, ZnTCTMP, NiTCTMP] were synthesized according to reported procedures [63]. The structure of the five porphyrins investigated is presented in figure 3. Porphyrin ground state absorption is sensitive to the surrounding environment. Changes in acidity, hydrophobicity, ion content, etc. can result in increased ordecreased absorbance at any/all of the bands as well as changes in the exact wavelength position of any/all of the bands [64-66]. The absorption spectra showed a relatively higher red shift of Soret band upon insertion of Zn, whereas Ni insertion led to only minor red shift of absorption bands than freebase H_2TCTMP. The high degree of conjugation in porphyrin ring results in several absorbancebands. A very intense band is observed around 400 nm referredto as Soret band. In addition to Soret band, there are several weaker absorbance bands in the spectral region from 450 nm to 700 nm, the Q-bands. Porphyrins are, in general, intensely fluorescent with emission bands in the spectral region of 600 nm-750 nm. Absorbance, fluorescence spectra of porphyrins are sensitive to binding of metal in the central ring position, addition of substituent groups to the macrocycle, solvent conditions, and presence of other analytes.

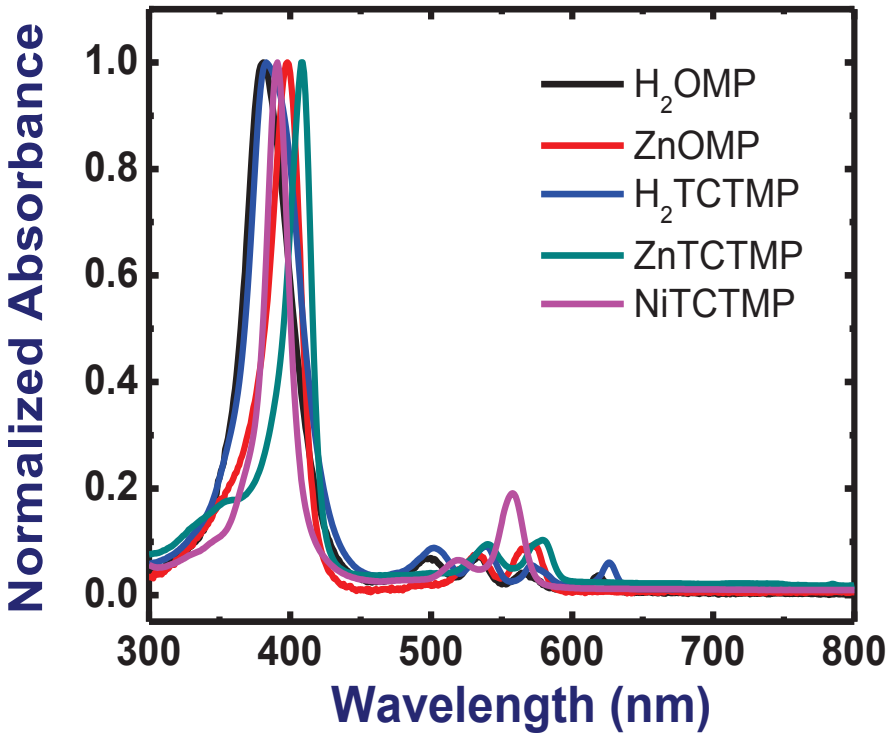

Figure 4 Absorption spectra of H_2OMP, ZnOMP, H_2TCTMP, ZnTCTMP, Ni-TCTMP.

UV-Visible and fluorescence spectral data for freebase porphyrins display strong near-UV Soret absorption bands in 377 nm–418 nm spectral region accompanied with four weaker Q-bands in the visible region, whereas corresponding Zn(II)-porphyrin derivatives possess strong Soret absorption bands in 398 nm–423 nm spectral region with two characteristic weaker Q-bands. Porphyrins depict two emission bands (574 nm–714 nm) when excited at Soret bands with large Stokes shift (180 nm–308 nm). UV-Visible spectral data for compounds H_2OMP, Zn-OMP, H_2TCTMP, Zn-TCTMP and Ni-TCTMP are presented in figure 4. Freebase porphyrin H_2OMP and H_2TCTMP displayed strong near-UV Soret absorption bands at 381 and 383 nm respectively. These are accompanied with four weaker Q-bands in the visible region, whereas the corresponding Zn(II)-complex of H_2OMP,H_2TCTMP and Ni-TCTMP derivatives possessed strong Soret absorption bands at 403 nm, 409 nm and 391nmrespectively, with characteristic of two weaker Q-bands in visible regions. The presence of metal ion (such as Zn, Ni) in the center of porphyrin molecule adds 4 weak absorption bands that is used prominently as sensitizers in PDT therapy Among these derivatives H_2OMP, Zn-OMP, H_2TCTMP and Zn-TCTMP emits in red regions with emission maxima at 622 nm, 578 nm, 629 nm, 584 nm respectively as depicted

in figure 5.Table 1 summarizes the absorption and emission data of all the compounds investigated.

The emission spectra of all the above porphyrin except Ni derivative shows (data presented in figure 5)two prominent peaks 575nm and 630nm for Zn-OMP and Zn-TCTMP and these are blue shifted as compared to the freebase porphyrins. H_2OMP and H_2TCTMP depicted two peaks 625nm and 680nm respectively.Ni-TCTMP did not show any florescence. These two emission peaks are significance of a typical porphyrin molecule. Fluorescence lifetime measurements were carried out using a time correlated single-photon counting (TCSPC) spectrometer (Horiba Jobin Yvon IBH). Pico Brite diode laser source was used as the excitation source and an MCP photomultiplier (Hamamatsu R3809U-50) as detector. The repetition rate of laser source was 10 MHz. The width of instrument response function, which was limited by the FWHM of the exciting pulse, was ~55 ps. The lamp profile was recorded by placing a scatterer (dilute solution of Ludox in water) in place of the sample. The time resolved emission decay profiles were collected at steady state emission spectrum maxima.

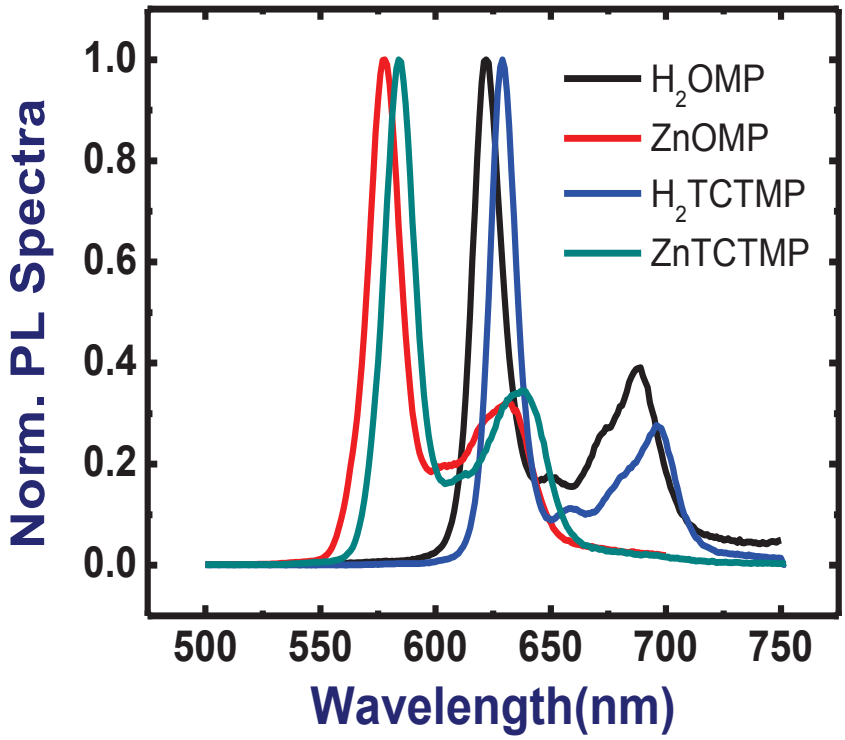

Figure 5 Emission spectra of H_2OMP, ZnOMP, H_2TCTMP, ZnTCTMP and NiTCTMP.

Porphyrins	UV-Vis (nm, logε)	Fluorescence in nm(Φ)
H_2OMP	377 (5.19), 494 (3.98), 530 (4.09), 564 (3.76), 618 (3.78)	622, 647, 688 (0.061)
ZnOMP	398 (5.34), 533 (4.24), 565 (4.29), 573 (4.33)	578, 632 (0.031)
H_2TCTMP	383(4.85), 502(3.80), 539(3.81), 571(3.60), 626(3.64)	629, 659,696(0.045)
ZnTCTMP	409(5.02), 540(3.99), 579(4.03)	584, 638 (0.032)
NiTCTMP	391(5.06), 519(3.88), 558(4.34)	

Table 1 UV-Vis and Emission studies of the porphyrins in chloroform at 25 °C. [63, 88]

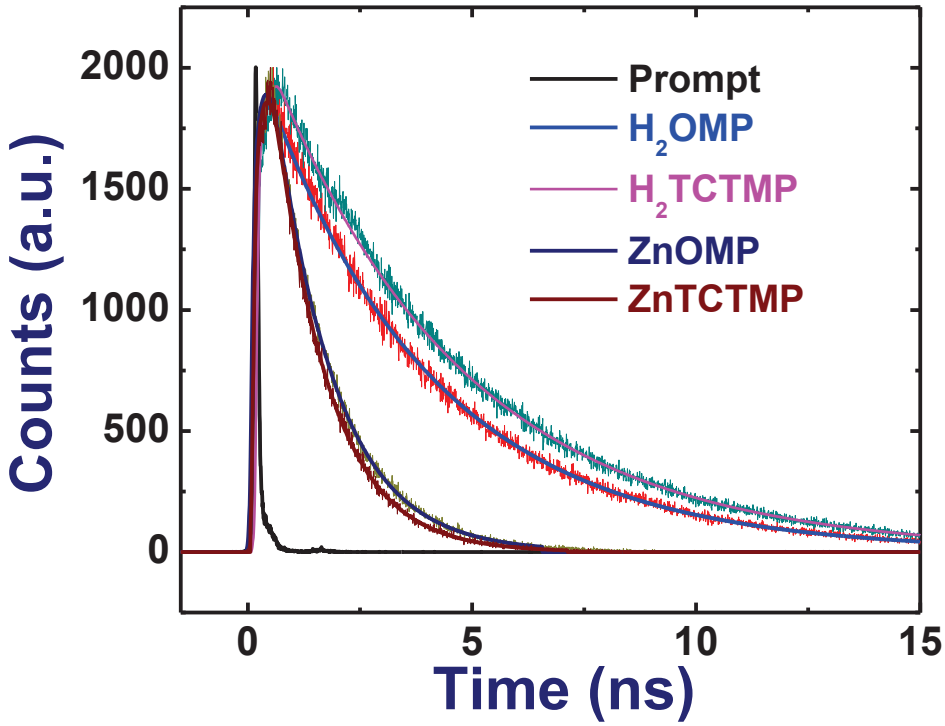

Figure 6 Fluorescence decay profile of H_2OMP, H_2TCTMP and their Zn(II) derivatives in chloroform.

Decay curves were analyzed by nonlinear least-squares iteration procedure using IBH DAS6 (version 2.2) decay analysis software. The quality of the fit was

assessed by inspection of the χ^2 values and the distribution of the residuals. The fluorescence lifetime data of H_2OMP, TCTMP, and their Zn(II) derivatives are tabulated in table 1, whereas their life time decay profiles are depicted in figure 6. Freebase porphyrins H_2OMP and H_2TCTMP both demonstrated shorter lifetimes of 3.77 and 4.54 ns respectively as compared to its octa ethyl analogue [50]. Whereas, Zn(II) complexes of H_2OMP and H_2TCTMP exhibited dual lifetimes, however, relatively shorter compared to their freebase analogues. The reduced singlet life time of these molecules may be attributed to efficient deactivation by oxygen and/or chloro groups present at the periphery.

6.3 Excited State Dynamics of porphyrins

The complete experimental details of fs pump probe experiments have been explained in sections 2.12 (figure 17). Figure 7 shows the triple exponential decay of H_2TCTMP, H_2OMP and ZnOMP near 600nm. We attempted fitting the data using two exponentials [67] but the fits were poor, especially at the initial time scales (<30 ps). The three lifetimes obtained (τ_1, τ_2, and τ_3) are summarized in table 1.The first lifetime (τ_1) which is in the ultrafast time scale (300-600 fs) could be attributed to the intra-molecular vibrational relaxation from S_2 states to the highest lying S_1 states. The shorter lifetime (τ_2) could be the vibrational relaxation within the S_1 vibrational manifold. The longest lifetime could be assigned to the non-radiative relaxation from S_1 states to the ground state.

These lifetimes are similar to the ones measured in porphycenes and corroles, recently investigated by our group [68, 69]. Figure 8shows a typical energy level diagram considering the various absorption peaks for the molecules investigated. Ha-Thi et al.[70] observed ultrafast dynamics of copper tetra-phenyl porphyrin (CuTPP), copper octa-ethyl porphyrin (CuOEP), and the free base tetra-phenyl porphyrin (H_2TPP)in the gas phase. The first two molecules exhibit a sequential four-step decay ending on a slow evolution in the nanosecond range $2S_2 \rightarrow {}^2CT \rightarrow {}^2T \rightarrow {}^2$Ground state. For the free-base case, the first ultrafast time scale of ~110 fs was attributed to an extremely rapid S_2-S_1 internal conversion.

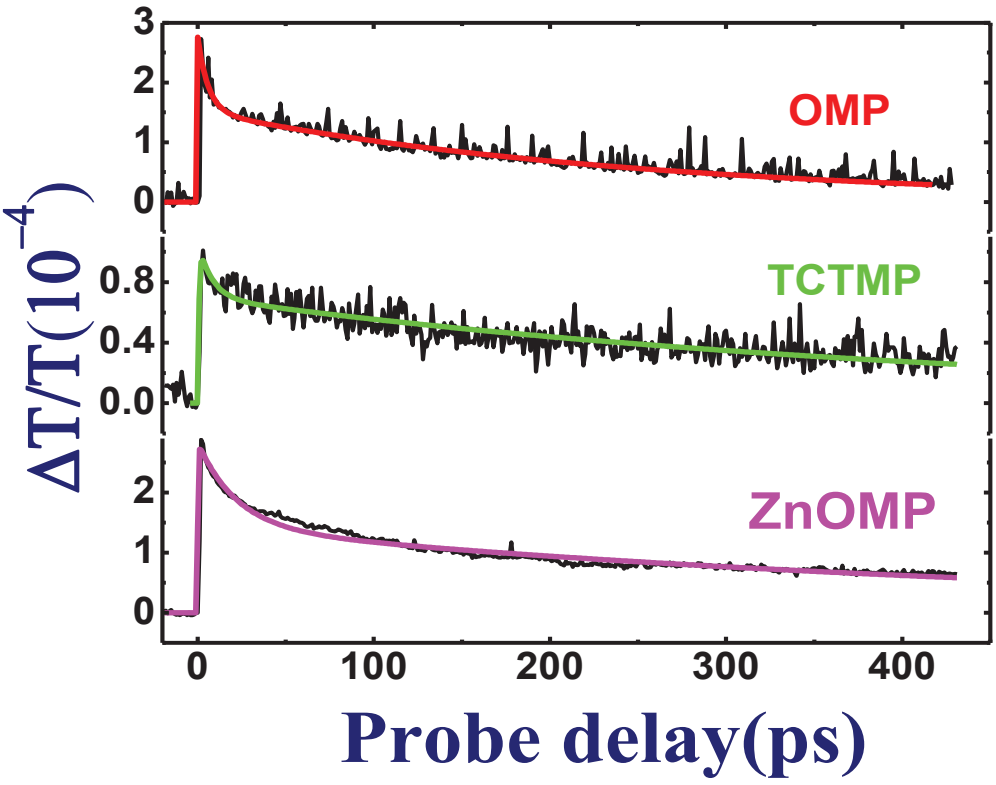

Figure 7 Pump-probe data of H_2TCTMP,H_2OMP and ZnOMP near 600nm

Okhrimenko et al. [71] measured a slow component with lifetime of ~690 psin a Ni(II)-porphyrin derivative, which was independent of probe wavelength.This process was established to be an electronic deactivation from the metal $d_{x^2-y^2}$ excited state to its d_{z^2}ground state.Three lifetimes were observed in the measurements of another set of porphyrins viz. Ni(II)TPPF, Ni(II)TNPP, and Ni(II)TPrF_7P [72-74]. The first lifetime (<1.2 ps) was assigned to **(ππ*)→(d,d)** transition while the second lifetime (few ps) was assigned to vibrational relaxation within the (d,d) states and the longest lifetime of 450-690 ps was assigned to the **(d,d)** → ground state transition. Dogan et al. [75] investigated the pump-probe dynamics of 5,10,15,20-tetrakis(4-hydroxyphenyl)porphyrin with different central metal ions (Zn^{2+}, Ni^{2+}, Co^{2+}, Fe^{3+}) using 532 nm excitation and observed three components in the data. They attributed the observed three lifetimes to (S_2→S_1), (S_1→ISC), (T_1→S_0) transitions for filled **'d'** shell metal and free base porphyrins, on the other hand those were attributed to (S_2→S_1), (S_1→**d**), (**d**→S_0) for unfilled **'d'** shell metal porphyrins. When these molecules are pumped at 600 nm with fs pulses we expect 2PA driving them to higher lying states (S_2). Z-scan data obtained at 600 nm with ps pulses confirmed this (data presented in next section). In our case we expect the fast lifetime (300-600 fs) to be due to internal conversion from S_2 states to the highest vibrational state of S_1

manifold. The slower component of 6-22 ps could be attributed to the vibrational relaxation within the S_1 states and the longest component to the S_1 to S_0 non-radiative transition. These molecules are fluorescent but the lifetimes are in the few ns regime (table 1). Therefore, the contribution of radiative decay to the longest component could be neglected.

Sample	Lifetime 1 (τ_1), ps	Lifetime 2 (τ_2), ps	Lifetime 3 (τ_3) ps
TCTMP	0.6	8.0	430
ZnOMP	0.3	22.0	480
H_2OMP	0.6	6.0	250

Table 2 Summary of various lifetimes of TCTMP, ZnOMP, H_2OMP retrieved from the pump-probe data.

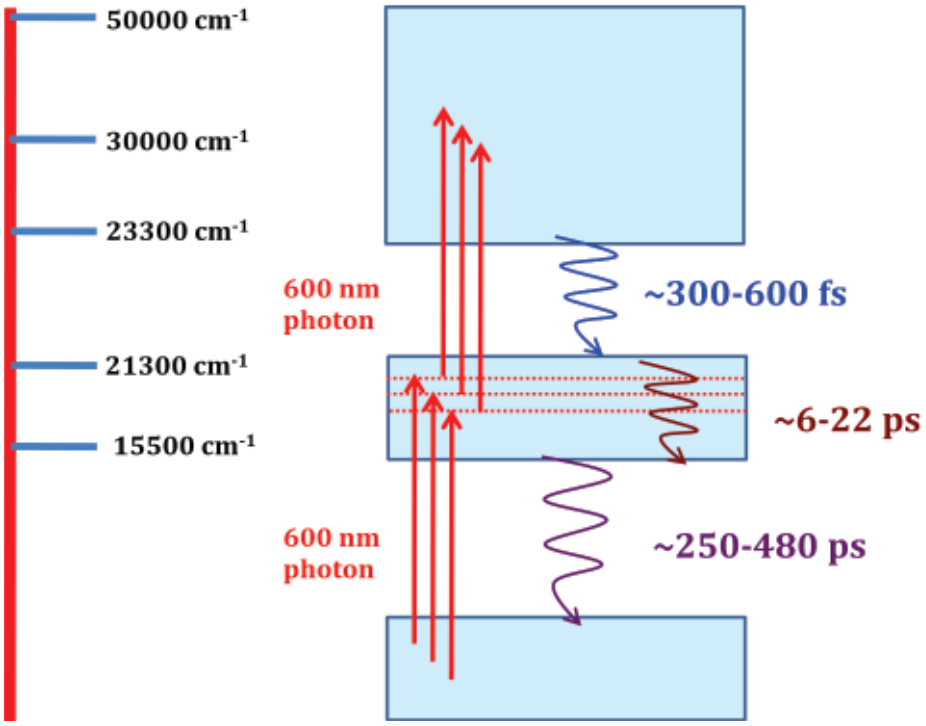

Figure 8 A simple energy level diagram to demonstrate the excited state dynamics .

6.4 NLO properties of Porphyrins

The NLO coefficients (β)and cross-sections (σ_2) were extracted from the open aperture data presented in figure 9 while n_2 was calculated from the closed aperture data presented in figure 10 using the Sheik-Bahae formulation [51]. Table 2 depicts the n_2 values of the molecules investigated indicating a positive nonlinearity (~10^{-16} cm^2/W). Two photon absorption (2PA) coefficients were obtained from experimental

data and the magnitudes were ~10^{-11} cm/W.2PA cross-sections (σ_2) were also estimated from 2PA coefficients and the magnitudes were in the range of 10^3-10^4 GM. The complete summary of NLO coefficients and cross-sections along with third order NLO susceptibilities are presented in table 2. The effect of introduction of electron withdrawing chloro- groups to an electron rich porphyrin core, hence a donor-acceptor characteristic to the resultant macrocycles, could be clearly perceived in these porphyrins, with large enhancement in σ_2 values in case of H_2TCTMP and its metallo-derivatives (containing four electron donating methoxy and four electron withdrawing chloro- groups), as compared to H_2OMP and its metallo-derivatives (containing only eight electron donating methoxy groups).

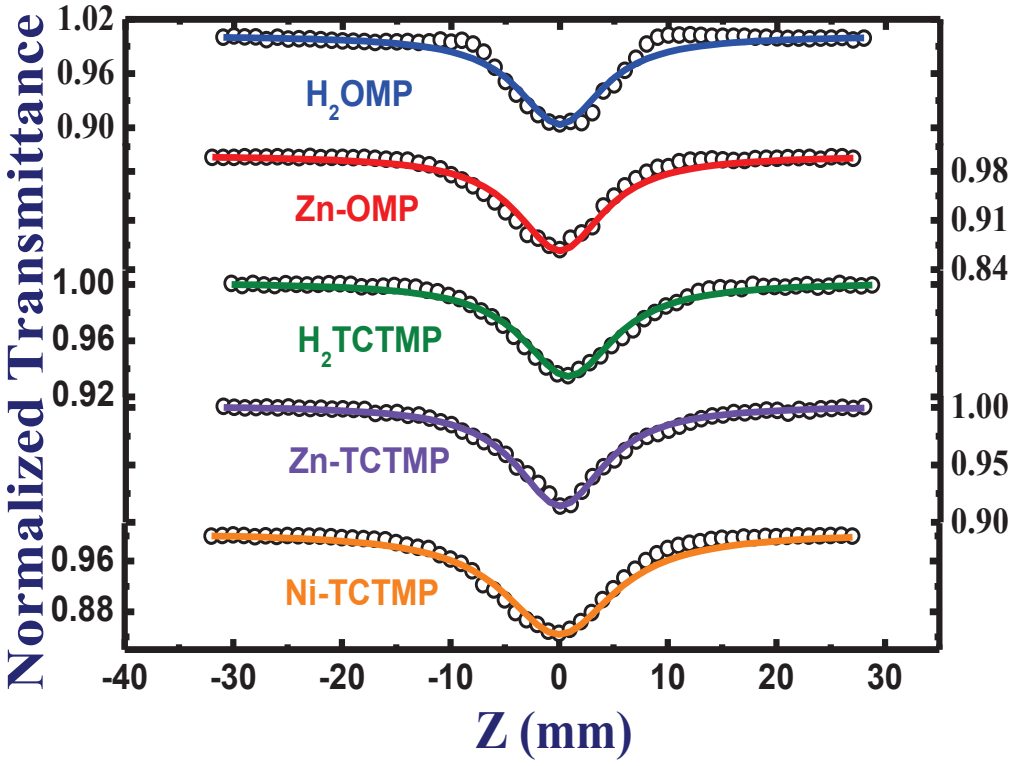

Figure 9 Open aperture Z-scan data of (a)H_2OMP (b)Zn-OMP(c)H_2TCTMP(d)ZnTCTMP (e) NiTCTMP inchloroformnm. Peak intensity used was ~100 GW/cm^2.

The largest σ_2 value was obtained for NiTCTMP (~5×10^4 GM). Interestingly, Zn-TCTMP and NiTCTMP molecules show strong 2PA coefficients and cross-sections compared to H_2TCTMP which, probably, could be attributed to the effect of central metal ion [37]. H_2OMP and ZnOMP molecules exhibited two times larger values of the nonlinear absorption when compared to H_2TCTMP and ZnTCTMP molecules. However, the n_2 value of H_2OMP was stronger compared to TCTMP and

ZnOMP. The closed aperture scans were performed with peak intensities <50 GW/cm^2 where we expect minimal contribution from nonlinear absorption and higher order nonlinearities. The solvent contribution was negligible and was confirmed through open aperture data of solvent alone.

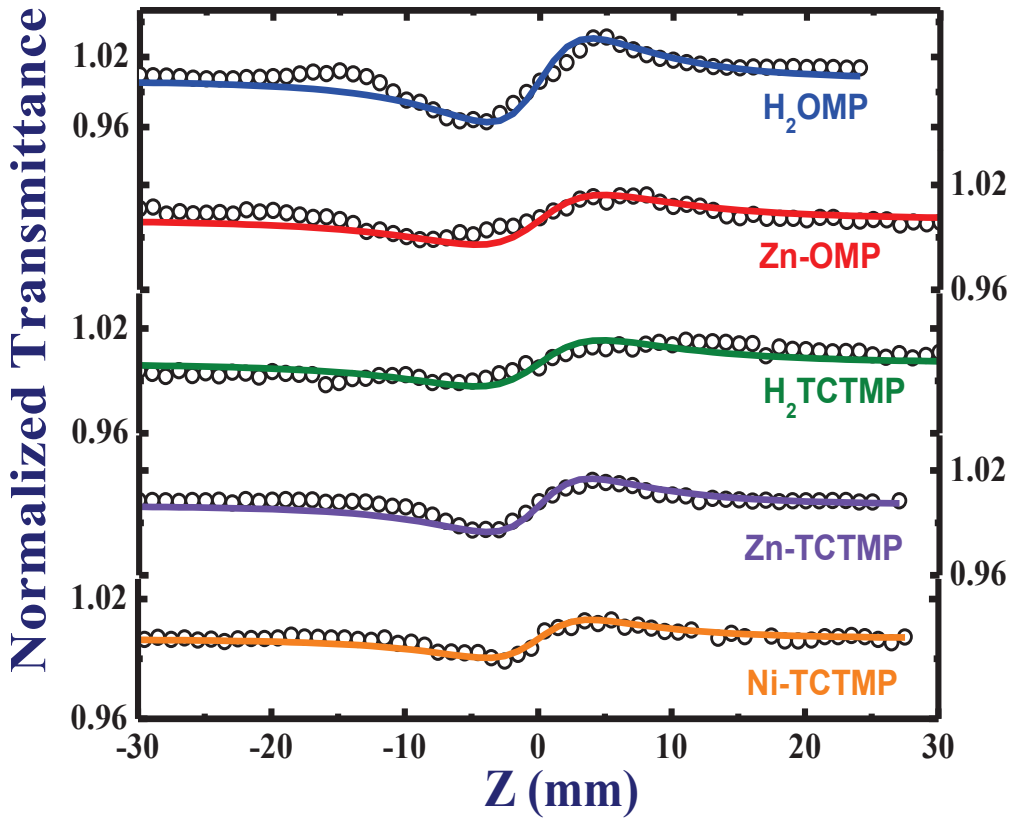

Figure 10 Closed aperture Z-scan data of H_2OMP, ZnOMP, H_2TCTMP, ZnTCTMP, NiTCTMP at 800nm.The solvent used was chloroform and peak intensity of <50 GW/cm^2 was used.

Drouet et al. [76] recently reported new Zn(II) tetraphenylporphyrin derivatives functionalized with electron-rich d^6-transition metal alkynyl complexes at periphery. They retrieved strong 2PA cross-sections (σ_2) of 10^3-10^4 GM for their molecules. Wang et al. [77] using nanosecond (ns) and picosecond (ps) pulses investigated a novel porphyrin derivative bearing one D–π–A–π–D pyrimidine chromophore at the periphery. They demonstrated that appropriate coupling of the chromophore to a porphyrin moiety with reverse saturable absorption was an efficient way for preparing molecules with superior nonlinearities. Senge's group has investigated several push-pull type of porphyrins [78-81] using ns laser pulses. Drobizhev et al. [82] studied double stranded conjugated porphyrin arrays and reported 10^3-10^4 GM cross-sections. Collini et al. [83] reported strong 2PA cross-

section of ~4000 GM measured by Z-scan technique for a push–pull A–π–D Zn(II) porphyrin complex di-substituted in the meso position with strong donor and acceptor moieties. Dogan et al.[75] studied nonlinear absorption behavior in 5,10,15,20-tetrakis(4-hydroxyphenyl)porphyrins with different central metal ions (Zn^{2+}, Ni^{2+}, Co^{2+}, and Fe^{3+})using open aperture Z-scan technique with 65 ps/ 4 ns excitation. Table 3 summarizes the NLO coefficients, cross-sections and $\chi^{(3)}$ of all the five porphyrins studied using 2 ps, 1 kHz pulses. The basis of design in most of these systems for better NLO response is to have suitable donor and acceptor functionalities at the periphery of aromatic porphyrin ring or extended multi-porphyrinic systems. In this regard, monomeric porphyrin units were also studied as either reference for designing more accomplished systems or as standalone systems to gain understanding about their NLO response.

Sample	n_2 (cm^2/W) $\times 10^{-16}$	β (cm/W) $\times 10^{-11}$	σ_{2PA} (GM)	$Re\lvert\chi^{(3)}\rvert$ (esu) $\times 10^{-14}$	$Im\lvert\chi^{(3)}\rvert$ (esu) $\times 10^{-14}$	$\lvert\chi^{(3)}\rvert$ (esu) $\times 10^{-14}$	$\lvert\chi^{(3)}\rvert$ (m^2/V^2) $\times 10^{-22}$
H_2OMP	2.90	2.85	1960	1.52	0.95	1.80	2.50
Zn-OMP	1.20	4.20	4000	0.63	1.40	1.52	2.10
H_2TCTMP	1.10	1.85	6440	0.57	0.61	0.85	1.20
Zn-TCTMP	1.25	2.50	14740	0.65	0.83	1.06	1.50
Ni-TCTMP	0.80	5.20	53690	0.41	1.74	1.80	2.50

Table 3 Summary of NLO coefficients of five compounds studied using ~1.5 ps pulses.

The presence of multiple donor and acceptor functional groups at the porphyrin periphery is achieved either through direct link or through phenyl bridge or a combination of both. Furthermore, it is known that direct linkage of functional groups at the porphyrin periphery impart a greater influence on the electronic properties of the macrocyclic ring. In this regard, *β*-octa substituted porphyrins which could be synthesized quite conveniently could emerge as attractive target systems. Towards this, symmetrical type, H_2TCTMP appears very promising [84-86]. In particular, the uniqueness of this molecule arises from the presence of orderly arrangement of pyrrole molecules in a cyclic fashion, where each pyrrole moiety is

endowed with an electron donating methoxy- and an electron withdrawing chloro-group on its adjacent *β*-positions. Therefore, we studied the fs NLO behavior along with its Zn(II)-and Ni(II)-derivatives i.e. ZnTCTMP and NiTCTMP respectively.

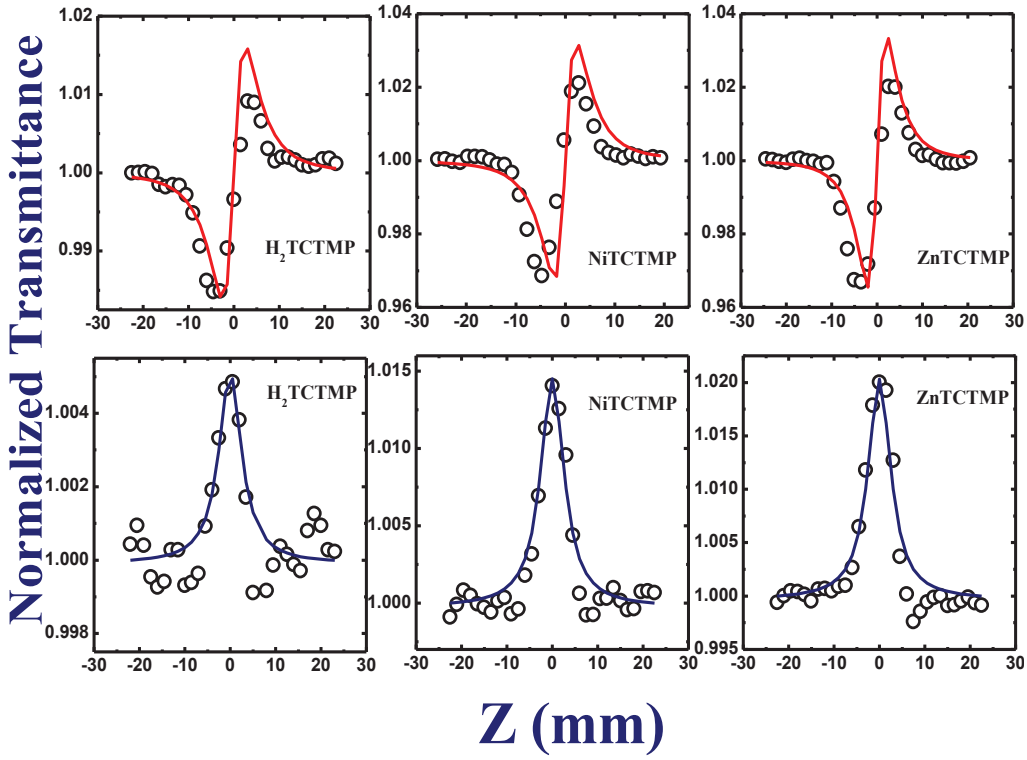

Figure 11 Fs closed aperture (top) and open aperture (bottom) data of H_2TCTMP, NiTCTMP and ZnTCTMP in chloroform. Open circles are experimental data and solid lines are theoretical fits. Peak intensities were ~0.65 TW/cm^2 for closed aperture scans.

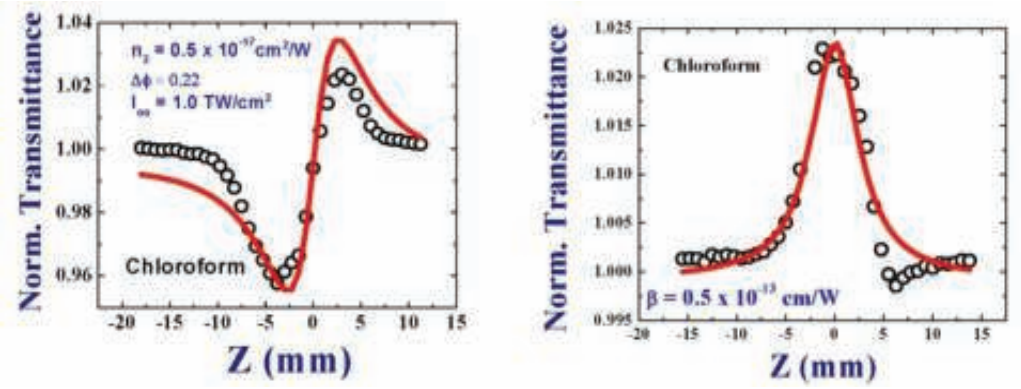

Figure 12 Closed aperture (left) and open aperture (right) data of solvent chloroform. Open circles are experimental data and solid lines are theoretical fits.

Experimental conditions for the fs Z-Scan studies of H_2TCTMP, NiTCTMP, and ZnTCTMP were as explained in chapter 2. Briefly, Z-scan measurements were performed using ~40 fs (FWHM), 800 nm, 1 kHz pulses. Typical concentrations of used in NLO measurements were 0.118 mM, 0.04 mM, and 0.07 mM respectively and

figure 11 illustrates the data. Closed aperture data revealed positive nonlinearity for all the samples.

Sample	**β (cm/W)×10^{-13}**	**n_2 (cm^2/W)×10^{-17}**
$CHCl_3$	0.50	0.50
H_2TCTMP	0.80	1.00
NiTCTMP	2.00	2.00
ZnTCTMP	2.25	2.00

Table 4 NLO coefficients extracted from fs Z-Scan data

The order of magnitude was ~10^{-17} cm^2/W. Open aperture scans revealed saturable absorption type of behaviour and the magnitude of nonlinear coefficients extracted were ~10^{-13} cm/W. Figure 12 shows the optical nonlinearity observed in solvent (chloroform). Saturable absorption has potential applications in mode-locking of ultrafast laser systems. Due to large peak powers associated with these short pulses, input energies play a significant role in their propagation through the sample. For pulse energies >1.5 μJ we could clearly observe the Supercontinuum being generated from the solvent (chloroform) affecting the transmission in open aperture data. Therefore, we restricted the input energies to a few hundred nJ for all the experiments and ensured that the transmittance changes were from the solute only. However, for similar energies, pure solvent in a similar cuvette was scanned and both closed aperture and open aperture data were obtained. The NLO coefficients of the porphyrins along with solvent are recorded in table 4. The sign of solvent nonlinearity was positive with magnitude of ≤0.5×10^{-17} cm^2/W and nonlinear absorption coefficient of ≤0.5×10^{-13} cm/W. It is evident that the solute contribution was higher than that of the solvent.

The linear absorption of these molecules near 800 nm is negligible and since these pulses possess extremely large bandwidth (~26 nm FWHM and a total width ~50 nm near 800 nm) and large peak intensities we strongly believe that the saturation could possibly be from the higher singlet states. The presence of two-photon states near 400 nm for all these molecules further suggests that this could be 2PA saturation.

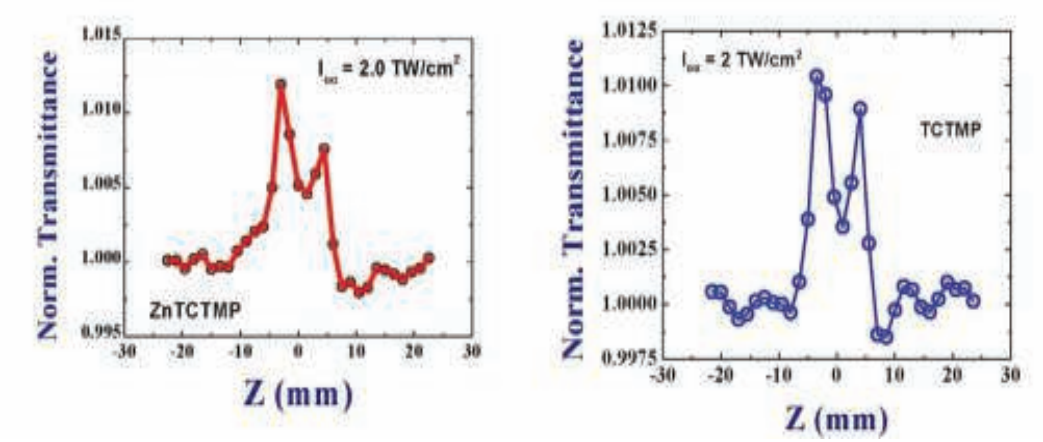

Figure 13 Open aperture data for large peak intensities (2 TW/cm^2) indicating a complicated behavior of nonlinear absorption in ZnTCTMP and TCTMP.

Figure 13 shows the open aperture scans of ZnTCTMP and H_2TCTMP recorded at a peak intensity of 2 TW/cm^2. It is obvious that the nonlinear absorption switches from saturable type to reverse saturable type indicating complicated behavior. Further increase in peak intensity resulted in Supercontinuum generation and the dip magnitude increased drastically. These measurements clearly suggest that at lower peak intensities saturable absorption is indeed the nonlinear absorption mechanism.

6.5 Conclusions

We have performed detailed studies for extracting the NLO coefficients and cross-sectionsfor five novel porphyrins. Fluorescence lifetimes measured for these molecules indicated radiative lifetimes of ~few ns. Ultrafast non-radiative decay dynamics were also investigated using fs pulses and the lifetimes of excited states were determined. NLO coefficients/cross-sections obtained with ps Z-scan technique suggests that these are potential molecules for photonic applications. NLO measurements performed with ~40 fs pulses revealed the electronic contribution to the nonlinearity. All the molecules exhibited saturable absorption with similar magnitude of nonlinear absorption coefficients.An estimated error of ±30%, in the nonlinear coefficients calculated, was deduced from the errors in (i) the estimation of beam waist and thereby the Rayleigh range and peak intensities (ii) pulse-to-pulse energy fluctuations (iii) calibration of neutral density filters (iv) fitting procedures (v) concentration measurements etc.

6.7 References

1. A. Kay and M. Griitzel, J. Phys. Chem. **97(**1993) 6272.
2. D. Gust, T.A. Moore, A.L. Moore,Acc. Chem. Research, **42**(2009)1890.
3. H. Imahori, Org. Biomol. Chem.**2**(2004)1425.
4. (a) B.J. White's Thesis, Oklahoma State University,July (2004)(b)L. Giribabu, R.K. Kanaparthi and V. Velkannan,The Chem. Rec.**12**(2012) 306.
5. A. Mills, A. Lepre, Anal. Chem.**69**(1997) 4653.
6. C. Zhang and K. S. Suslick, J. Am. Chem. Soc. **127**(2005) 11548.
7. P. Montméat, S. Madonia, E. Pasquinet, L. Hairault, C. P. Gros, J.M. Barbe, R. Guilard, IEEE Sensors **5**(2005) 610.
8. Anthony P.F. Turner and N. Magan, Nat. Rev. Microbiol.**2**(2004)161.
9. M. Peris,L. E. Gilabert, Anal. Chim. Acta **638** (2009) 1.
10. (a) C. D. Natale, D. Salimbeni,R. Paolesse, A. Macagnano, A. D. Amico, Sensors and Actuators B **65**(2000) 209(b) C. D. Natale, D. Salimbeni,R. Paolesse, A. Macagnano, A. D. Amico, Sens. Act. B **65** (2000) 220 (c) M. C. Drain, T. H. Joeseph, K. S. Suslick, M. R. Wasielewski, and X. Chen, J.Porphy.Phth. **6** (2002) 243.
11. K. M. Kadish, K. M. Smith, R. Guilard, The Porphyrin Handboo*k* Vol. **1-9**, Academic Press: San Diego, **2000**.
12. S. Venugopal Rao, N.K.M.N. Srinivas, L. Giribabu, B.G. Maiya, D. Narayana Rao, R. Philip, G.R. Kumar, Opt. Commun.**182** (2000) 255.
13. S. Venugopal Rao, N.K.M.N. Srinivas, L. Giribabu, B.G. Maiya, D. Narayana Rao, R. Philip, G.R. Kumar, Opt. Commun.**192** (2001) 123.
14. N.K.M.N. Srinivas, S. Venugopal Rao, D. Narayana Rao, J. Porphy. Phth. **5** (2001) 549.
15. S.J. Mathews, S. Chaitanya Kumar, L. Giribabu, S. Venugopal Rao, Mat. Lett.**61** (2007) 4426.
16. S.J. Mathews, S. Chaitanya Kumar, L. Giribabu, S. Venugopal Rao, Optics Commun. **280**(2007) 206.
17. N. Venkatram, L. Giribabu, D. Narayana Rao, S. Venugopal Rao, Appl. Phys. B **91** (2008) 149.
18. N. Venkatram, L. Giribabu, D. Narayana Rao, S. Venugopal Rao, Chem. Phys. Lett. **464**(2008) 211.

19. R.S.S. Kumar, S. Venugopal Rao,L. Giribabu, D. Narayana Rao, Chem. Phys. Lett. **447**(2007) 274.
20. R.S.S. Kumar, S. Venugopal Rao,L. Giribabu, D. Narayana Rao, Opt. Mat. **31**(2009)1042.
21. R.S.S. Kumar, S. Venugopal Rao,L. Giribabu, D. Narayana Rao, Proc. SPIE**6875**(2008) 68751D-1.
22. P.T. Anusha, P.S. Reeta, L. Giribabu, Surya P. Tewari, S. Venugopal Rao, Mat. Lett.**64**(2010) 1915.
23. S. Venugopal Rao, P.T. Anusha, L. Giribabu, Surya P. Tewari, Pramana - J. Phys.,**75**(2010) 1017.
24. S. Venugopal Rao, N. Venkatram, L. Giribabu, D. Narayana Rao, J. Appl. Phys.**105**(2009) 053109.
25. S. Venugopal Rao, P. Prem Kiran, L Giribabu, M. Ferrari, G. Kurumurthy, B.M. Krishna, H. Sekhar, D. Narayana Rao, Nonlin. Opt. Quant. Opt.**40**(2010) 183.
26. N.K.M. Naga Srinivas, S. Venugopal Rao, and D. Narayana Rao, J. Opt. Soc. Am. B **20**(2003) 2470.
27. D. Narayana Rao, S. Venugopal Rao, E. Blanco, F.J. Aranda, D.V.G.L.N. Rao, J.A. Akkara,J. Sci. Ind. Res.**57**(1998) 664.
28. S. Venugopal Rao, D. Swain, Surya P. Tewari, Organic Photonic Materials and Devices XII, edited by Robert L. Nelson, François Kajzar, Toshikuni Kaino, Proc. SPIE **7599**(2010) 75991P1.
29. S. Venugopal Raoand D. Narayana Rao, J. Porphy. Phth. **6**(2002) 234.
30. D. Narayana Rao, S. Venugopal Rao, F.J. Aranda, M. Nakashima, J.A. Akkara, J. Opt. Soc. Am. B**14**(1997) 2710.
31. M. Pawlicki, H. A. Collins, R. G. Denning, and H. L. Anderson, Angew. Chem.-Int. Ed. **48**(2009) 3244.
32. M. Drobizhev, Y. Stepanenko, A. Rebane, C. J. Wilson, T. E. O. Screen, H. L. Anderson, J. Am. Chem. Soc. **128**(2006)12432.
33. T. E. O. Screen, J. R. G. Thorne, R. G. Denning, D. G. Bucknall, and H. L. Anderson, J. Mater. Chem.**13** (2003)2796.
34. J.M. Hales, M. Cozzuol, T.E.O. Screen, H. L. Anderson, J.W. Perry,Opt. Expr.**17** (2009)18478.
35. K. Ogawa, H. Hasegawa, Y. Inaba, Y. Kobuke, H. Inouye, Y. Kanemitsu, E. Kohno, T. Hirano, S.T. Ogura, T. Okura, J. Med. Chem. **49** (2006) 2276.

36. D.Y. Kim, T.K. Ahn, J.H. Kwon, D. Kim, T. Ikeue, N. Aratani, A. Osuka, M. Shigeiwa, S. Maeda,J. Phys. Chem. A. **109**(2005) 2996.
37. M.O. Senge, M. Fazekas, E.G.A. Notaras, W.J. Blau, M. Zawadzka, O. B. Locos, E.M.N. Mhuircheartaigh, Adv. Mater. **19** (2007) 2737.
38. A. Merz, R. Scropp, E. Dotterl, Synthesis **26** (1995) 795.
39. M. O. Senge, O. Flögel, K. R. Senge,J. Porphy. Phth. **5** (2001) 503.
40. K. Sugiura, M. Ravikumar, T. K. Chandrashekar, Y. Sakata, Chem. Lett. **26** (1997)291.
41. N. Ono, K. Maruyama,Chem. Lett. **17** (1988)1511.
42. J. Takeda, T. Ohya, M. Sato,Chem. Pharm. Bull. **38**(1990)264.
43. J. Takeda, M. Sato, Chem. Lett.**23** (1994) 2233.
44. N. Ono, E Muratani, Y. Fumoto, T. Ogawa, K. Tazima,J. Chem Soc., Perkin Trans. I, **22** (1998) 3819.
45. N. Ono, H. Kawamura, K. Maruyama, Bull. Chem. Soc. Jpn. **62** (1989) 3386.
46. A.W.Czarnik,Nature **394**(1998) 417.
47. C.J.Cumming,C.Aker,M.Fisher,M.Fox,M.J.Grone,D.Reust, M. G. Rockley, T.M. Swager, E. Tower, V. William, IEEE Trans. Geosci. Remote Sens.**39** (2001) 1119.
48. S.W. Thomas III, J.P. Amara, R.E. Bjork, T.M. Swager, Chem.Commun. **36** (2005) 4572.
49. (a) P. Kolla, Anal. Chem. **67**(1995) 184A (b) J.S. Caygill, F. Davis, S.P.J. Higson, Talanta **88** (2012) 14.
50. (a) R.D.Luggar,M.J.Farquharson,J.A.Horrocks,R.J.Lacey,X-Ray Spectrom. **27**(1998) 87 (b) O. Katz,A. Natan,Y. Silberberg, S. Rosenwaks, Appl. Phys. Lett.**92** (2008) 171116 (c) J. F Federici, B. Schulkin, F. Huang, D. Gary, R. Barat, F. Oliveiraand D. Zimdars, Semicond. Sci. Technol. **20** (2005) S266.
51. J. S. Yang , T. M. Swager, J. Am. Chem. Soc.**120** (1998) 11864.
52. D.A.Olley, E.J.Wren, G.Vamvounis, M.J.Fernee, X.Wang, P.L. Burn, P. Meredith, P. E. Shaw, Chem. Mater.**23** (2011) 789.
53. J.Li, C.E.Kenclig, E.E.Nesterov,J. Am. Chem. Soc. **129** (2007) 15911.
54. A.Lan, K.Li, H.Wu, D.H.Olson, T.J.Emge,W.Ki, M.Hongand, J. Li, Angew. Chem. **48** (2009) 2334.
55. Y.Xia, L.Song, C. Zhu, Anal. Chem.**83** (2011) 140.
56. L. Tang, H. Feng, J. Cheng, J. Li, Chem. Commun. **46** (2010) 5882.

57. Y.Long, H.Chen, Y.Yang, H.Wang, Y.Yang, N.Li, K.Li, J. Pei, F. Liu, Macromolecules **42** (2009) 6501.
58. M. S.Meaney , V. L. McGuffin, Anal. Chim. Acta**610**(2008) 57.
59. S.Tao, Z. Shi, G. Li, P. Li, Chem. Phys. Chem.**7** (2006) 1902.
60. N.A.Rakow, K.S.Suslick, Nature **406** (2000) 710.
61. K.K. Kartha, S.S. Babu, S. Srinivasan, A. Ajayaghosh, J. Am.Chem. Soc.**134** (2012) 483.
62. A. Mathew, P. R. Sajanlal, T. Pradeep, Angew. Chem.**51** (2012) 9596.
63. A. Rana, P. K. Panda, TetrahedronLett. **52** (2011) 2697.
64. M. Gouterman, J. Molec. Spec. **6** (1961) 138163.
65. R. J. P. Williams, Chem. Rev.**56** (1956) 299.
66. M. Gouterman, J. Chem. Phys. **30** (1959) 1139.
67. D. Swain, P.T. Anusha, T. Sarma, P.K. Panda, S. Venugopal Rao, Chem. Phys. Lett. **580** (2013) 73.
68. D. Swain, P.T. Anusha, T. Shuvan Prashant, S.P. Tewari, T. Sarma, P.K. Panda, S. Venugopal Rao, Appl. Phys. Lett. **100**(2012) 141109.
69. P.T. Anusha, D. Swain, S. Hamad, L. Giribabu, T.S. Prashant, S.P. Tewari, S. Venugopal Rao, J. Phys. Chem. C. **116** (2012) 17828.
70. M.H. Ha-Thi, N. Shafizadeh, L. Poisson, B. Soep, J. Phys. Chem. A **117** (2013) 8111.
71. A.N. Okhrimenko, PhD. Thesis, Bowling Green State University, USA, 2005.https://etd.ohiolink.edu/ap:10:0::NO:10:P10_ACCESSION_NUM:bgsu1126888140.
72. H.S. Eom, S.C. Jeoung, D. Kim, J.H. Ha, Y.R. Kim, J. Phys. Chem. A**101** (1997) 3661.
73. J. Rodriguez, C. Kirmaier, D.J. Holten, J. Am. Chem. Soc. **111** (1989) 6500.
74. J. Rodriguez, D.J. Holten, Chem. Phys. **92** (1990) 5944.
75. N. Dogan, F.M. Dumanogullari, M. Hayvali, H. Yilmaz, U. Kurum, H.G. Yaglioglu, A. Elmali, Chem. Phys. Lett. **508** (2011) 265.
76. S. Drouet, A. Merhi, G. Grelaud, M.P. Cifuentes, M.G. Humphrey, K. Matczyszyn, M. Samoc, L. Toupet, C.O. Paul-Roth, F. Paul, NewJ. Chem. **36** (2012) 2192.
77. A. Wang, L. Long, S. Meng, X. Li, W. Zhao, Y. Song, M.P. Cifuentes, M.G. Humphrey C. Zhang, Org. Biomol. Chem. **11** (2013) 4250.

78. M. Zawadzka, J. Wang, W.J. Blau, M.O. Senge, Chem. Phys. Lett. **477** (2009) 330.
79. M. Zawadzka, J. Wang, W.J. Blau, M.O. Senge, Photochem. Photobiol. Sci. **12** (2013) 996.
80. M. Zawadzka, J. Wang, W.J. Blau, M.O. Senge, Photochem. Photobiol. Sci. **12** (2013) 1811.
81. M. Zawadzka, J. Wang, W.J. Blau, M.O. Senge, J. Porphy. Phth. **17** (2013) 1.
82. M. Drobizhev, Y. Stepanenko, A. Rebane, C.J. Wilson, T.E.O. Screen, H.L. Anderson, J. Am. Chem. Soc. **128** (2006)12432.
83. E. Collini, S. Mazzucato, M. Zerbetto, C. Ferrante, R. Bozio, M. Pizzotti, F. Tessore, R. Ugo, Chem. Phys. Lett. **454** (2008) 70.
84. A.Rana, P. K. Panda, RSC Adv.**2** (2012) 12164.
85. D. Swain, A. Rana, P.K. Panda, S. Venugopal Rao, Proc. SPIE **8258** (2012) 82581B.
86. D. Swain, A. Rana, P.K. Panda, S. Venugopal Rao, Communicated to Chem.Phys.Lett. (2014).

Chapter 7

Conclusions and Future Scope

7.1 Summary and Conclusions

After photo-excitation of excited molecules in liquids experience various relaxation processes, which can be broadly classified into four major categories: electronic relaxation, solvent relaxation, orientation relaxation and vibrational relaxation. We have investigated only the first two cases in this thesis. The excited state dynamics and nonlinear optical properties of these molecules (such as dinaphthoporphycenes, cyclo[4]naphthobipyrroles, phthalocyanines, porphyrins) with different wavelengths, pulse widths, repetition rates were the central theme of this thesis. Structure and absorption properties of these molecules were understood in detail, in particular the electronic transitions. The connection between multi-photon absorption and relaxation processes were well understood in the visible spectral regime. Internal conversion (IC) processes were studied in the above molecular systems. The dynamics of these fundamental photo-induced processes were investigated by fs/ps pump-probe spectroscopy and steady-state fluorescence techniques. Degenerate fs pump-probe results can be extended to non-degenerate and white light continuum (WLC) to have a complete insight of dynamics in the entire visible spectrum. We believe that we have achieved progress towards extending these experiments to IR region and study the dynamics in different high energy materials (HEMs).

Decomposition mechanism of various energetic materials is our focus at ACRHEM. Energetic materials, defined as controllable storage systems of chemical energy, have numerous military and industry applications as propellants, fuels, explosives, and pyrotechnics. They can release their entire chemical energy over a very short period of time, often within the fs/ps time scales. Due to this very rapid detonation, decomposition studies of these materials pose considerable challenge for physicists and physical chemists. Elucidation of detailed fundamental steps in the initiation of and the propagation phases of energetic material decomposition reactions is central for better understanding, controlling, and enhancing the performance of these materials for combustion and explosion, and to model the combustion behavior of either pure compounds or simple mixtures.

The photo-physics of diverse organic macromolecules with the different laser pulse durations [ps, fs], energy/intensity, wavelength, and repetition rates was the focal point of the thesis. High-energy materials (HEMs) are materials that store a huge amount of chemical energy, a majority of which gets converted into mechanical energy during decomposition. Ignition processes such as sparks, shocks, and heat can initiate decomposition of these materials through their excited electronic states. The direct applications of novel compounds (e.g. porphyrins) have found applications in sensing HEMs. Pump probe spectroscopy is the simplest experimental technique used to study ultrafast electronic dynamics. The use of real-time fs transient absorption spectroscopy to study molecular motions and photochemical reaction dynamics is relatively a young and rapidly growing field. Because of the limitations that the Heisenberg principle places on traditional pump-probe spectroscopy, transient absorption method [1,2] will become increasingly important as experimentalists take advantage of ever shorter optical pulses. For example, Dang et al. [1] response to ultrafast laser shock loading of nine liquids was monitored in an effort to reveal evidence of chemical changes occurring during the first 350 ps following the shock front. Significant transient absorption, attributed to chemical reaction, was observed for shocked phenylacetylene and acrylonitrile. Brown et al. [2] investigated the shock driven chemical reaction in Nitromethane(NM) and in NM sensitized with diethylenetriamine, using a laser-driven, sustained, 300 ps shock driven by fs pulses.

The basic idea behind multi-dimensional vibrational spectroscopy is to apply the elegant methods originally developed in NMR to study nonlinear excitations of nuclear spin transitions to nonlinear optical excitations of vibrational transitions. These vibrational transitions can be resonantly driven by excitation in the infrared (IR) wavelength region. Two-dimensional vibrational infrared (2D-IR) spectroscopy can be used to study both structure (by measuring couplings between vibrations) and structural fluctuations (by measuring relaxation processes). Fs pump-probe spectroscopy enables to follow in real time vibrational motions coupled to electronic transitions. Indeed, if the system is excited by a pulse shorter than the vibrational period, vibrational coherence is induced both in the ground and excited electronic states, providing information also on the excited state nuclear dynamics. Our aim is also to develop pump–probe techniques to evaluate the vibrational dynamics in HEMs. For example, nitromethane (CH_3NO_2) is the simplest member of a series of

energetic nitro-compounds that are of great interest to the HEMs community. Nitromethane (NM) has 15 vibrational degrees of freedom. If a particular mode of the molecule is excited, the de-excitation follows two ways: (1) energy relaxation and (2) phase relaxation. Energy relaxation is an incoherent process whereas phase relaxation is a coherent phenomenon. The energy relaxation dynamics can be obtained from coherent anti-Stokes Raman experiments through which vibrational energy re-distribution and its time evolution mechanisms can be investigated. These relaxation times and pathways play crucial roles in the process of detonation. However, there are limited literature is available other than Bernstein's group and Dlott's group [3, 4] regarding ultrafast excited state dynamics of HEMs. They have the common interest for understanding the critical role of non-adiabatic couplings in the initial steps of the excited electronic state decomposition of energetic materials. These experiments provide a potentially useful methodology for accurate and predictive determination, design, and synthesis of new energetic materials.

Little is known about the chemical evolution and states of matter found within an energetic material undergoing detonation. The short time scales of the chemical reactions (microseconds and less) and inherent danger of experimental work have been a major obstacle to understanding their microscopic nature. Recently, molecular dynamics simulations [5, 6] have been effectively utilized to shed light on the initial steps during detonation in secondary explosives, the less sensitive class of energetic materials. Significantly knowledge about detonation in primary explosives, those which are most easily detonated by external stimuli and are most dangerous to work with, is still in its infancy. Very recently Sun et al. [7] introduced a new type of three-dimensional (3D) spectroscopy to study vibrational energy transfer, where an IR pulse tunable through the CH-stretching and CD stretching regions was used to create parent vibrational excitations in liquids and a visible probe pulse was used to generate both Stokes and anti-Stokes Raman spectra as a function of delay time. The technique was used to study NM and acetonitrile (ACN) and their deuterated analogues at ambient temperature.

7.2 References

1. N.C. Dang, C.A. Bolme, D.S. Moore, and S.D. McGrane, J. Phys. Chem. A **116** (2012) 10301.
2. K.E. Brown, S.D. McGrane, C.A. Bolme, D.S. Moore, J. Phys. Chem. A, In press, (2014) DOI: 10.1021/jp4125793.
3. A. Bhattacharya, Y. Guo, E.R. Bernstein, Acc. Chem. Res. **43** (2010) 1476 and references therein
4. D.D. Dlott, Annu. Rev. Phys. Chem. **62** (2011) 575
5. A. Strachan, A.C.T. van Duin, D. Chakraborty, S. Dasgupta, W.A. Goddard, Phys. Rev. Lett. **91** (2003) 098301.
6. K. Nomura, R.K. Kalia, A. Nakano, P. Vashishta, A.C.T. van Duin, W.A. Goddard III, Phys. Rev. Lett. **99** (2007) 148303
7. Y. Sun, B.C. Pein, D.D. Dlott, J. Phys. Chem. B **117** (2013) 15444.

Appendix

The transmitted probe data was fitted using the equation given below. For the case of single decay observed only τ_1, for double decay τ_1 and τ_2, and for triple exponential decay τ_1, τ_2 and τ_3 were used.

$$\frac{\Delta T(t)}{T} = y_0 + A_1 e^{-(t-t_0)/\tau_1} + A_2 e^{-(t-t_0)/\tau_2} + A_3 e^{-(t-t_0)/\tau_3}$$

(1)

$\Delta T(t)$ is the time dependent change in probe transmission, induced by the pump at time 't' after the pump excitation and T is the probe transmission in the absence of pump.

The following tables provide the weightings of different fitted parameters (lifetimes)

Ps-pump probe data of porphycenes (chapter 3)

Sample	Y_0	X_0	A_1	τ_1 (ps)	A_2	τ_2 (ps)
Po1	1×10^{-5}	0	1.81×10^{-4}	2.0	2.1×10^{-4}	7.2
Po2	1×10^{-5}	0	3.85×10^{-4}	3.1	3.76×10^{-5}	7.6
Po3	1×10^{-5}	0	2.73×10^{-4}	2.0	8.07×10^{-5}	7.2
Po4	1×10^{-5}	0	-2.19×10^{-4}	1.8	5.89×10^{-4}	8.5
Po5	3×10^{-5}	0	5.53×10^{-4}	1.8	3.54×10^{-4}	7.0

Sample (Ps-PP)	τ_1 (%)	τ_2 (%)
Po1	46	54
Po2	91	9
Po3	77	23
Po4	27	73
Po5	60	40

Fs-pump probe data of porphycenes (chapter 3)

Sample	Y_0	X_0	A_1	τ_1 (fs)	A_2	τ_2 (ps)	A_3	τ_3 (ps)
Po1	1×10^{-6}	0	-8.4×10^{-5}	120	-8.86×10^{-6}	7.2	-4.54×10^{-5}	8
Po2	1×10^{-6}	0	-8.47×10^{-5}	105	-4.67×10^{-5}	7.6	-4.84×10^{-5}	7.3
Po3	0	-0.5	-2.5×10^{-6}	102	-2.2×10^{-5}	7.2	-2.99×10^{-5}	8.2
Po4	0	0	-1.52×10^{-6}	100	-3.37×10^{-5}	8.5	-2.86×10^{-5}	10
Po5	0	-0.5	2.94×10^{-5}	135	-3.48×10^{-5}	7.0	-1.16×10^{-5}	8.1

Sample (Fs-PP)	τ_1 (%)	τ_2 (%)	τ_3 (%)
Po1	60	6	34
Po2	47	26	27
Po3	4	40	56
Po4	4	50	46
Po5	38	46	26

Fs-pump probe data of naphthobipyrroles (chapter 4)

Sample	Y_0	X_0	A_1	τ_1 (ps)	A_2	τ_2 (ps)
5a	1×10^{-7}	0.1	7.1×10^{-5}	5	7.0×10^{-5}	37
5b	2×10^{-7}	0.1	7.6×10^{-5}	2.5	4.5×10^{-5}	20
5c	1×10^{-7}	0	7.5×10^{-5}	2	1.9×10^{-4}	33

Sample (Fs-PP)	τ_1 (%)	τ_2 (%)
5a	50	50
5b	62	38
5c	28	72

Fs-pump probe data of phthalocyanines (chapter 5)

Sample	Y_0	X_0	A_1	τ_1 (ps)	A_2	τ_2 (ps)
Pc1	1×10^{-7}	0	1.08×10^{-4}	40	-5.58×10^{-5}	3
Pc2	1×10^{-7}	0	4.23×10^{-5}	500	3.58×10^{-5}	2
Pc3	1×10^{-7}	0	-1×10^{-4}	309	---	---

Sample (Fs-PP)	τ_1 (%)	τ_2 (%)
Pc1	65	35
Pc2	54	46
Pc3	100	0

Fs-pump probe data of porphyrins (chapter 6)

Sample	Y_0	X_0	A_1	τ_1 (ps)	A_2	τ_2 (ps)	A_3	τ_3 (ps)
H_2OMP	1×10^{-5}	0	1.45×10^{-4}	250	4.53×10^{-5}	6	1×10^{-5}	0.6
TCTMP	1×10^{-6}	0	6.72×10^{-5}	430	2.69×10^{-5}	8	1.01×10^{-4}	0.6
ZnOMP	1.5×10^{-6}	0	1.42×10^{-4}	480	1.29×10^{-4}	22	2.78×10^{-4}	0.3

Sample (Fs-PP)	τ_1 (%)	τ_2 (%)	τ_3 (%)
H_2OMP	72	22	6
TCTMP	34	13	53
ZnTCTMP	25	23	52

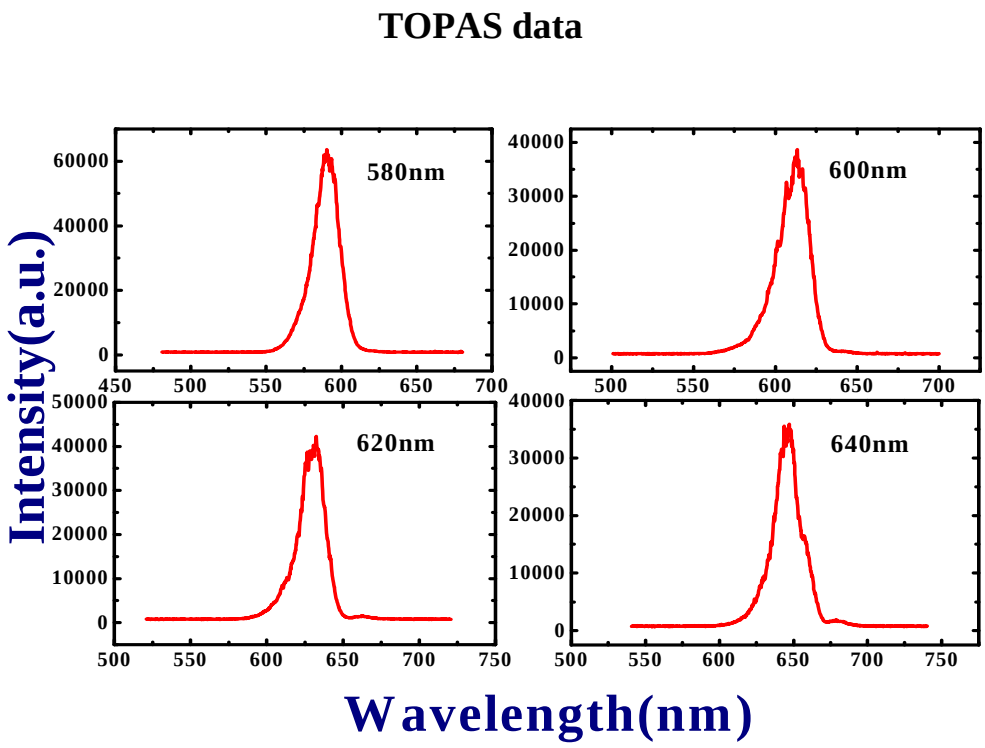

Figure 1 Typical spectra of the ps optical parametric amplifier (TOPAS) at different wavelengths.

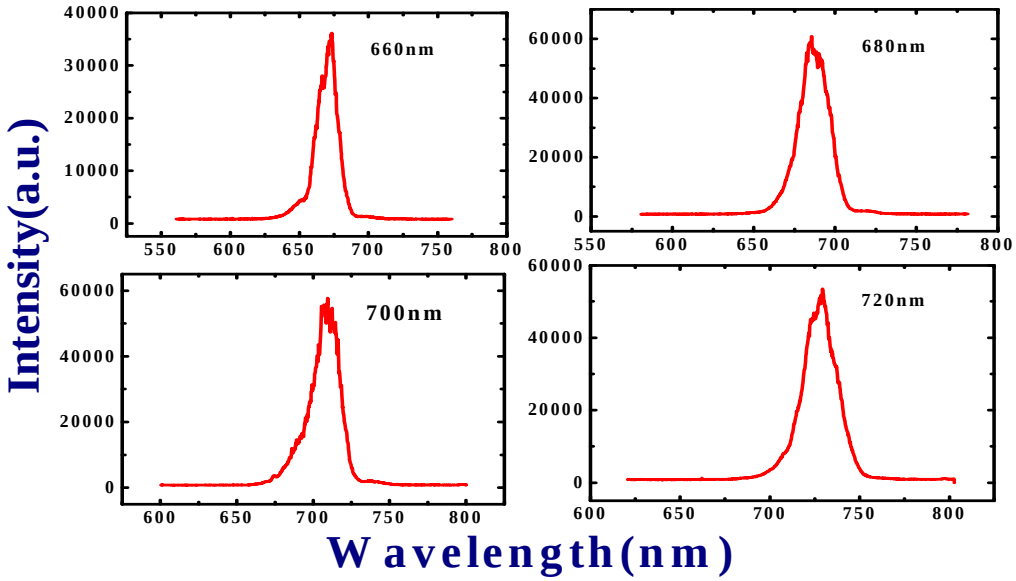

Figure 2 Typical spectra of the ps optical parametric amplifier (TOPAS) at different wavelengths.

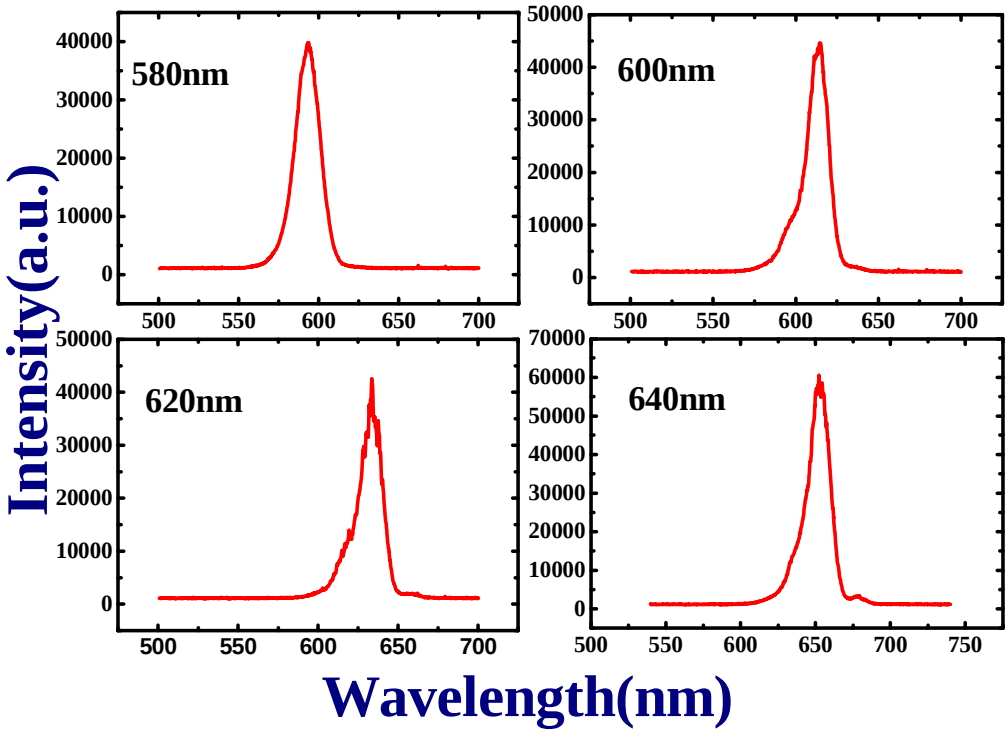

Figure 3 Typical spectra of the fs optical parametric amplifier (TOPAS) at different wavelengths.

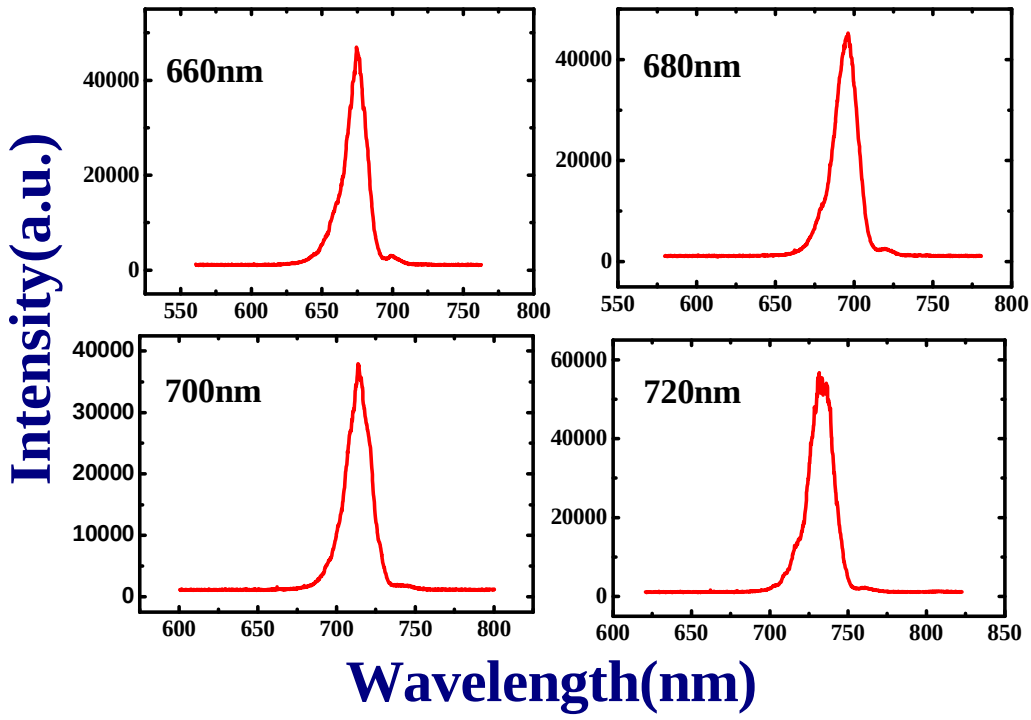

Figure 4 Typical spectra of the fs optical parametric amplifier (TOPAS) at different wavelengths.

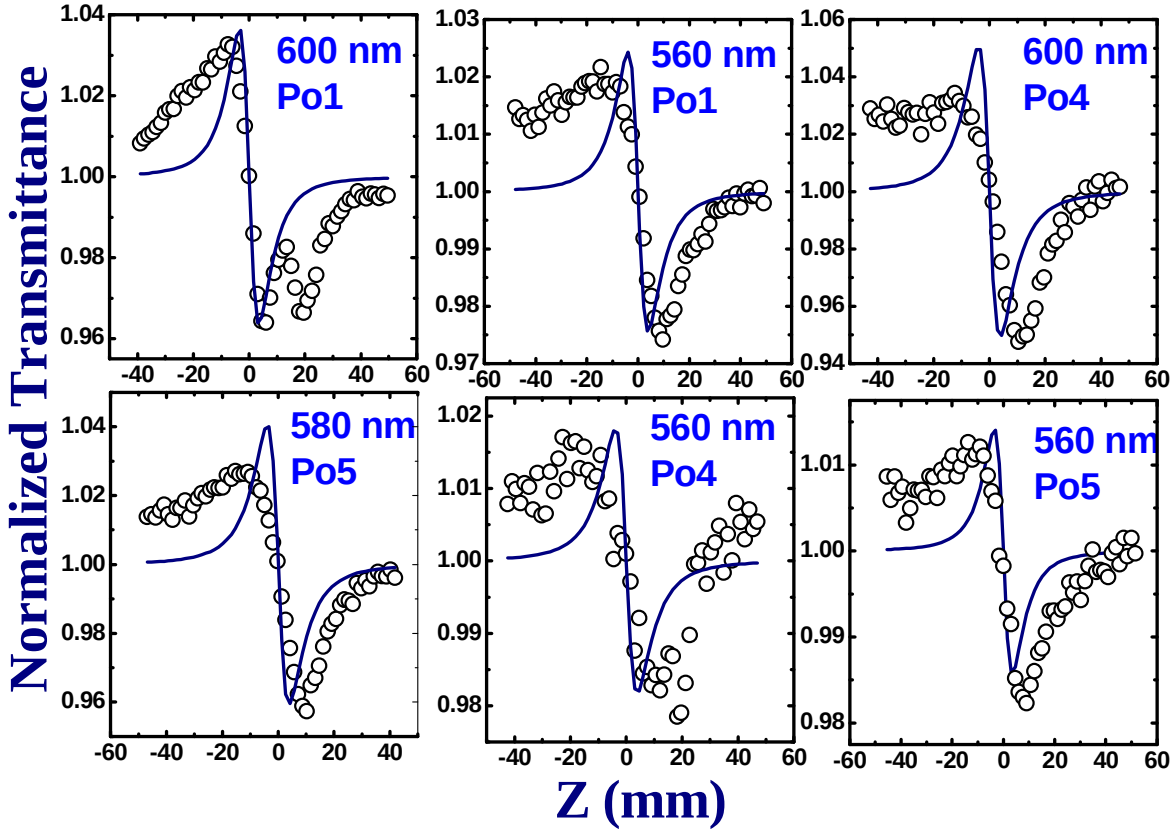

Figure 5 Typical ps closed aperture Z-scan data of porphycenes

Formulae for calculating $\chi^{(3)}$

$$Re|\chi^{(3)}|(in\ esu) = \frac{10^{-4}\varepsilon_0 n_0^2 c^2}{\pi} n_2 \left(\frac{m^2}{W}\right)$$

$$n_0 = solvent\ R.I$$

$$n_2 = nonlinear\ R.I$$

$$\varepsilon_0 = permittivity\ of\ free\ space$$

$$c = velocity\ of\ light$$

$$Im|\chi^{(3)}|(in\ esu) = \frac{10^{-2}\varepsilon_0 n_0^2 c^2 \lambda}{4\pi^2} \beta\left(\frac{m}{W}\right)$$

$$|\chi^{(3)}|(esu) = \sqrt{|Re|\chi^{(3)}||^2 + |Im|\chi^{(3)}||^2}$$

$$|\chi^{(3)}|(S.I) = 1.4 \times 10^{-8}|\chi^{(3)}|(esu)$$

List of Publication (2008-2014)

Book Chapter

1. **D. Swain**, S. Venugopal Rao**,** "Sub-100 femtosecond pulse propagation in nonlinear optical crystals," in Emerging Trends in Laser & Spectroscopy and Applications, **(ISBN # 978-81-8424-626-1),** Eds. A.K. Rai, I.M.L. Das, K.N. Uttam, Allied Publishers Pvt. Ltd., 272-276, 2010.

International Publications

1. **D. Swain**, A. Rana, Pradeepta K. Panda, S. Venugopal Rao**,** "Strong two-photon absorption properties and pump-probe studies of novel porphyrin derivatives," Submitted, Chem. Phys. Lett., 2014.(communicated)
2. **D. Swain**, R. Singh, V.K. Singh, N.V. Krishna, L. Giribabu, S. Venugopal Rao , "Sterically Demanded Zinc(II) Phthalocyanines : Synthesis, Optical, Electrochemical, Nonlinear Optical, Excite State Dynamics Studies," J. Mater. Chem. C, **2,** 1711, 2014.
3. **D. Swain**, V.K. Singh, N.V. Krishna, L. Giribabu, S. Venugopal Rao , "Optical, electrochemical, third-order nonlinear optical, excited state dynamics studies of Thio-Zinc Phthalocyanine," J. Porphy. Phth., In Press 2014, DOI: 10.1142/S1088424614500035.
4. **D. Swain**, P.T. Anusha, T. Sarma, Pradeepta K. Panda, S. Venugopal Rao, "Dispersion studies of optical nonlinearity and excited state dynamics in Cyclo[4]naphthobipyrroles," Chem. Phys. Lett., **580,** 73-77, 2013.
5. P.T. Anusha, **D. Swain**, T. Shuvan Prashant, L. Giribabu, Surya P. Tewari, S. Venugopal Rao, "Ultrafast excited state dynamics and third order optical nonlinearities of novel Corroles," J. Phys. Chem. C., **116**, 17828-17837, 2012.
6. S. Sreeja, B. Nityaja, **D. Swain**, V.P.N. Nampoori, P. Radhakrishnan, S. Venugopal Rao, "Nonlinear optical studies of DNA doped Rhodamine 6G PVA films using picosecond pulses," Optics and Photonics Journal, **2,** 135-139, 2012.
7. **D. Swain**, P.T. Anusha, T. Shuvan Prashant, Surya P. Tewari, Tridib Sarma, Pradeepta K. Panda, S. Venugopal Rao**,** "Ultrafast excited state dynamics and dispersion studies of nonlinear optical properties in Dinaphthoporphycenes," Appl. Phys. Lett., **100** , 141109, 2012.
8. S. Venugopal Rao , T. Shuvan Prashant, T. Sarma, Pradeepta K. Panda, **D. Swain**, Surya P. Tewari, "Two-photon and three-photon absorption in dinaphthaporphycenes," Chem. Phys. Lett., **514** , 98-103, 2011.
9. S. Venugopal Rao , P.T. Anusha, T. Shuvan Prashant, **D. Swain**, Surya P. Tewari, "Third order optical nonlinearities and optical limiting in phthalocyanine thin films," Materials Science and Applications, **2,** 299-306, 2011.
10. B. Anand, A. Kaniyoor, **D. Swain**, T.T. Baby, S. Venugopal Rao**,** S.S. Sankara Sai, S. Ramaprabhu, R. Philip, "Ultrafast Dynamics and Enhanced Optical Limiting in Metal Oxide-Hydrogen Exfoliated Graphene Hybrids," **Submitted, 2014**

International Conference Proceedings

1. P.T. Anusha, **D. Swain**, T. Sarma, Pradeepta K. Panda, S. Venugopal Rao**,** "Ultrafast nonlinear optical studies of Cyclo[4]naphthobipyrroles," in Nonlinear Optics and Applications VI, edited by Benjamin J. Eggleton, Alexander L. Gaeta, Neil G. Broderick, Proc. SPIE Vol. **8434** (SPIE, Bellingham, WA), 84341D 2012.
2. **D. Swain**, A. Rana, Pradeepta K. Panda, S. Venugopal Rao**,** "Ultrafast nonlinear optical studies of 3,8,13,18-Tetrachloro-2,7,12,17-tetramethoxyporphyrin," Proc. SPIE, **8258**, 82581B, 2012 .
3. S. Venugopal Rao**,** P.T. Anusha, T. Shuvan Prashant, **D. Swain**, Surya P. Tewari, "Ultrafast nonlinear optical properties and excited state dynamics of phthalocyanine thin films," in Organic Photonic Materials and Devices XIII, edited by Robert L. Nelson, François Kajzar, Toshikuni Kaino, Yasuhiro Koike, Proc. SPIE **7935** (SPIE, Bellingham, WA 2011) 793517.
4. S. Venugopal Rao, **Debasis Swain**, Surya P. Tewari, "Pump-probe experiments with sub-100 femtosecond pulses for characterizing the excited state dynamics of phthalocyanine thin films," Proc. SPIE, **7599** , 75991P, 2010.
5. **D. Swain**, P.T. Anusha, Syed Hamad, L. Giribabu, Surya P Tewari, S. Venugopal Rao, "Femtosecond pump-probe spectroscopy of novel Corroles," AIP Conf. Proc., **1461,** 363-366, 2012.
6. **D. Swain**, P.T. Anusha, T. Shuvan Prashant, Surya P. Tewari, Tridib Sarma, Pradeepta K. Panda, S. Venugopal Rao**,** "Multiphoton absorption studies in porphycenes using picosecond and femtosecond pulses," AIP conf. Proc. **1391,** 674-676, 2011.

National Conference Proceedings

1. **D. Swain**, P. T. Anusha, Tridib Sarma, Pradeepta K. Panda, S. Venugopal Rao, "Ultrafast Excited State Dynamics and Dispersion Studies of Cyclo[4]naphthobipyrrole",NLS-21,February 6-9,2013,BARC,Mumbai.
2. **D. Swain**, L. Giribabu, S. Venugopal Rao, "Ultrafast Nonlinear Optical Properties and Excited State Dynamics of Sterically Demanded Zinc(II) Phthalocyanines" DAE – BRNS Theme Meeting on Ultrafast Science October 25 - 26, 2013. Indian Institute of Technology Kharagpur, West Bengal**.(Poster)**
3. P.T. Anusha, **D. Swain**, Surya P. Tewari, S. Venugopal Rao**,** "Ultrafast Degenerate Pump-Probe Studies of SI-GaAs and LT-GaAs," Photonics West**,** 2-7 February 2013, San Francisco, California, USA. **(POSTER).**
4. **D. Swain**, P.T. Anusha, T. Shuvan Prashant, T. Sarma, Pradeepta K. Panda, Surya P Tewari, S. Venugopal Rao, "Femtosecond and picosecond dynamics in Dinaphthoporphycenes investigated using pump-probe technique," TC 2012, BRNS-ISAMP Topical conference on Interaction of lasers with atoms, molecules, and clusters, University of Hyderabad, Hyderabad, January 09-12, 2012. (POSTER).
5. **D. Swain**, P.T. Anusha, T. Shuvan Prashant, T. Sarma, Pradeepta K. Panda, Surya P Tewari, S. Venugopal Rao, "Ultrafast excited state dynamics of Dinaphthoporphycenes," MTIC-IV, Modern Trends in Inorganic Chemistry, University of Hyderabad, Hyderabad, December 10-13, 2011. (POSTER).

6. P.T. Anusha, **D. Swain**, Surya P. Tewari, S. Venugopal Rao, "Ultrafast degenerate pump probe studies of SI-GaAs." XXXVI OSI SYMPOSIUM on Frontiers in Optics and Photonics (FOP11), IIT Delhi, December 3-5, 2011. **(RECEIVED AWARD FOR EXCELLENCE IN POSTER PRESENTATION).**
7. P.T. Anusha, T. Shuvan Prashant, **D. Swain**, Surya P. Tewari, S. Venugopal Rao, "Ultrafast Nonlinear Optical Studies of Phthalocyanine Thin films Using the Z-scan and Pump-Probe Techniques," Photonics 2010, IIT Guwahati, December 11-15, 2010 (POSTER).
8. P.T. Anusha, **D. Swain**, Syed Hamad, L. Giribabu, Surya P. Tewari, S. Venugopal Rao, "Ultrafast excited state dynamics and third order optical nonlinearities of novel Corroles," DAE-BRNS National Laser Symposium, Anna University, Chennai, January 09-12, 2012. (POSTER).
9. **D. Swain**, P.T. Anusha, Shuvan Prashant, Tridib Sarma, Pradeepta K. Panda, Surya P. Tewari, S. Venugopal Rao, "Ultrafast relaxation dynamics of Dinaphthoporphycenes," DAE-BRNS National Laser Symposium, Anna University, Chennai, January 09-12, 2012. (POSTER).
10. **D. Swain**, P.T. Anusha, Tridib Sarma, Pradeepta K. Panda, Surya P. Tewari, S. Venugopal Rao, "Ultrafast relaxation of Dinaphthoporphycenes studied using pump-probe technique," First International OSA Network of students conference in Asia IONS-1, IIT Delhi, Delhi, December 1-2, 2011. (POSTER).
11. P.T. Anusha, **D. Swain**, L. Giribabu, Surya P. Tewari, S. Venugopal Rao, "Ultrafast excited state dynamics and third order optical nonlinearities of novel Corroles," Frontiers in Physics, University of Hyderabad, Hyderabad, October 28-29, 2011. (POSTER).
12. **D. Swain**, P.T. Anusha, Tridib Sarma, Pradeepta K. Panda, Surya P. Tewari, S. Venugopal Rao, "Ultrafast relaxation dynamics of Dinaphthoporphycenes studied using pump-probe techniques," Frontiers in Physics, University of Hyderabad, Hyderabad, October 28-29, 2011. (POSTER).
13. **D. Swain**, S. Venugopal Rao, "Sub-100 femtosecond pulse propagation in nonlinear optical crystals," Meghnad Saha memorial symposium on Emerging Trends in Lasers & Spectroscopy and applications, Allahabad, 23-25 March 2009. (POSTER) **AWARDED BEST FIRST POSTER**.